Technical Progress Report
Power Systems Development Facility

Kellogg Brown & Root
Transport Reactor Train and
Siemens Westinghouse
Particulate Control Device

GCT1: September 9 - December 15, 1999

DOE Cooperative Agreement Number
DE-FC21-90MC25140

SOUTHERN COMPANY
Energy to Serve Your World®

TECHNICAL PROGRESS REPORT
POWER SYSTEMS DEVELOPMENT FACILITY

KELLOGG BROWN & ROOT
TRANSPORT REACTOR TRAIN AND
SIEMENS WESTINGHOUSE
PARTICULATE CONTROL DEVICE

DOE Cooperative Agreement Number
DE-FC21-90MC25140

TEST RUN GCT1
SEPTEMBER 9 – DECEMBER 15, 1999

Prepared by:
Southern Company Services, Inc.
Power Systems Development Facility
P.O. Box 1069
Wilsonville, AL 35186

March 2001

POWER SYSTEMS DEVELOPMENT FACILITY

DISCLAIMER

Available to the public from the National Technical Information Service, U.S. Department of Commerce, 5285 Port Royal Road, Springfield, VA 22161. Phone orders accepted at (703) 487-4650.

ACKNOWLEDGEMENT

The authors wish to acknowledge the contributions and support provided by various project managers: Jim Longanbach (DOE), Neville Holt (EPRI), Gene Cover (KBR), Zal Sanjana (Westinghouse), and Vann Bush (SRI). Also, the enterprising solutions to problems and the untiring endeavors of many personnel at the site during commissioning of the transport reactor train in gasification mode of operation are greatly appreciated. The project was sponsored by the U.S. Department of Energy National Energy Technology Laboratory (NETL) under contract DE-FC21-90MC25140.

CONTENTS

This Page Intentionally Left Blank

Listing of Tables

Listing of Figures

1.0 EXECUTIVE SUMMARY

1.1 SUMMARY

This report discusses test campaign GCT1 of the Kellogg Brown & Root (KRB) transport reactor train with a Siemens Westinghouse Power Corporation (Siemens Westinghouse) particle filter system at the Power Systems Development Facility (PSDF) located in Wilsonville, Alabama. The transport reactor is an advanced circulating fluidized-bed reactor designed to operate as either a combustor or a gasifier using one of two possible particulate control devices (PCD). The transport reactor was operated as a pressurized gasifier during GCT1.

GCT1 was planned as a 250-hour test run to commission the transport reactor train in the gasification mode of operation and to characterize the limits of operational parameter variations. Due to the short-time duration of the test run the tests were exploratory in nature and the results of some of the test objectives outlined below were qualitative.

- *Transport Reactor Commissioning* – Complete precommissioning mechanical checks of process modifications and functional checks of safety interlocks and subsystems. Demonstrate stable and safe reactor, PCD, and other process operations using a Powder River Basin (subbituminous) coal and Plum Run dolomite sorbent.

- *Sulfator Commissioning* – Commission the sulfator preheat system, sorbent addition system, and solids removal and transport systems. Demonstrate stable operation of sulfator with char feed. Evaluate maintainability of operating temperature in the sulfator with varying char content in the feed, and the extent of sulfation and SO_2 emissions.

- *Other Subsystems Commissioning* – Commission the flare and recycle gas systems. Demonstrate stable reactor start-up burner operations with low-excess air. Demonstrate complete incineration of syngas in the thermal oxidizer.

- *Startup and Transition to Coal* – Vary start-up procedures as necessary to minimize oxygen concentration in the process gas to PCD during heat-up with the reactor start-up burner and during transition to coal gasification.

- *Operational Stability* – Characterize reactor loop and PCD operations with short-term tests by varying coal feed, air/coal ratio, riser velocity, solids circulation rate, system pressure, and air distribution.

- *Reactor Operations* – Study the devolatatilization and tar cracking effects from transient conditions during transition from start-up burner to coal. Evaluate effect of process operations on heat release, heat transfer, and accelerated fuel particle heat-up rates. Study effect of changes in reactor conditions on transient temperature profiles, pressure balance, and product gas composition.

- *Effects of Reactor Conditions on Syngas Composition* – Evaluate effect of air distribution, steam/coal ratio, solids circulation rate, and reactor temperature on CO/CO_2 ratio, gasification rates, carbon conversion, and cold and hot gas efficiencies.

- *Effects of Reactor Conditions on H_2S Emissions* – Study effect of Ca/S molar ratio, riser velocity, and solids-circulation rate on H_2S capture. Evaluate effects on limits of sulfur capture dynamics in relation to CaS-H_2O-H_2S-CaO reaction approach to equilibrium.

- *Forms of Sulfur From Reactor Operations* – Determine the effect of reactor operations on forms of sulfur (CaS, $CaSO_4$, and FeS) in the reactor standpipe solids and in the fines from PCD. Quantify the reactive sulfide concentration in these solids streams and at the sulfator solids outlet.

- *Bituminous Coal Feedstock* – Demonstrate stable operations using Illinois No. 6 and Calumet Mine coal from Mary Lee seam in Alabama and Plum Run dolomite and other sorbents.

- *Inspection* – Upon shutdown, perform thorough inspections of start-up burner, complete reactor loop, disengager, primary cyclone, primary gas cooler, sulfator cooling coils, and other process equipment for any signs of corrosion due to H_2S and other acid gases, deposit formation, and refractory and mechanical stability.

Test run GCT1 was started on September 9, 1999, and was completed December 15, 1999. This test run provided the data necessary to a preliminary analysis of reactor operations and to identify necessary modifications to improve equipment and process performance. Five different feed combinations were tested. The reactor temperature was varied between 1,500 and 1,810°F at pressures from 97 to 216 psig. In GCT1, 360 hours of solid circulation and 233 hours of coal feed were attained. The major accomplishments and observations during GCT1 include:

1. Transition from the start-up burner to coal feed was smooth without any incidents of oxygen breakthrough.

2. The thermal oxidizer operated well with syngas and during transitions from syngas with different heating values.

3. The circulation rate in the reactor loop consistently ran at about 50 percent of the design rate. Reactor operations were smooth without any incident of oxygen breakthrough or any temperature excursions.

4. The highest temperature could be maintained in the mixing zone. By increasing the coal feed rate the highest temperature would move from lower riser to mid-mixing zone.

5. As coal feed rate was increased the solids circulation rate increased, the standpipe level increased, and the PCD pressure drop (ΔP) increased due to high-solids loading.

6. After initial problems with line plugging with coal feed fines the coal feed system operated flawlessly. High coal-feed rates (up to 1.1 x design) were achieved with room to increase rates further to 1.2 x design.

7. With logic changes made to its programmable logic controller (PLC), the coarse char/ash removal system (FD0510) operated well without any line plugging during gasification.

8. PCD operated well during the short test runs at moderate conditions tested (i.e., at solids-circulation rates, gas flows, moderate coal-feed rates, lower solids loading).

9. The fines screw cooler (FD0502) and the fines depressurization and transport system (FD0520) operated well; however, there were problems at times when trying to remove solids from PCD cone. If further increases result in solids loading to the PCD the bottleneck in the fines removal system will be FD0502.

10. Separate level/temperature control system for steam condensate system worked well. There were no sulfator-related trips due to no- or low-steam flow.

11. Overall, the dipleg operated well with very high solids flow through the dipleg due to the inefficiency of disengager. However, there were small, brief cyclone dipleg upsets.

12. Both the coal-feed rate and reactor-circulation rate from a reactor standpipe can be increased with the existing design.

13. Due to the inefficiencies in the solids collection system the carbon content of circulating solids is just sufficient to maintain reactor temperature of 1,800°F at coal-feed rates tested.

14. Primary gas cooler operated well without any signs of plugging. However, there was a decrease in heat-removal rates over a period of time likely due to a tar film on the heat transfer area.

15. Heat-removal capacity in sulfator remains too high to achieve operating temperature of 1,600°F. Due to the inefficiencies in the transport reactor solids collection system much higher than designed char feed rates to the sulfator resulted in insufficient air flow to complete oxidation.

16. Flare-pilot-sensing reliability was better than previous run; however, there needs to be additional improvements made. Flow sensing of both propane and syngas flow to flare were more reliable.

17. In addition to the high-inlet loading to the PCD, high-outlet loadings were a presistent problem during GCT1. The higher outlet loading was attributed to leakage of several ceramic composite filters (both through the body and around the flange) and leakage through some instrumentation fittings.

18. Redesign of the filter holder and a new gasket for the fail-safe was tested on several filter elements with promising results and will be fully implemented during GCT2.

19. Another important observation was that the residual dust cake in the September portion of GCT1 was roughly half the thickness of a residual dust cake from the December portion of GCT1.

20. Operation of the char-removal system was a key factor during the run, especially during the December portion of GCT1. Due to the higher particulate loading to the PCD, as well as the lower bulk density of the material, this volumetric feeder was cycling almost continuously during the run. Ultimately, the inability of the char-removal system to remove char quickly enough ended GCT1.

1.2 FUTURE PLANS

During 2000, two 250-hour characterization tests with the transport reactor train operating in gasification mode are planned. Several large-scale modifications and repairs for the transport reactor and PCD will be completed before the last gasification test campaign in 2000. These activities include major refractory repairs to the primary cyclone and the PCD, redesigning and replacing the disengager, and modifying the dipleg leg with a loop seal.

2.0 INTRODUCTION

This report provides an account of the GCT1 test campaign with the Kellogg Brown & Root (KBR) transport reactor and the Siemens Westinghouse Power Corporation (Siemens Westinghouse) filter vessel at the Power Systems Development Facility (PSDF) located in Wilsonville, Alabama, 40 miles southeast of Birmingham. The PSDF is sponsored by the U. S. Department of Energy (DOE) and is an engineering-scale demonstration of two advanced coal-fired power systems. In addition to DOE, Southern Company Services, Inc. (SCS), Electric Power Research Institute (EPRI), and Peabody Holding Company are cofunders. Other cofunding participants supplying services or equipment include KBR, Foster Wheeler (FW), Siemens Westinghouse, and Combustion Power Company. SCS is responsible for constructing, commissioning, and operating the PSDF.

2.1 THE POWER SYSTEMS DEVELOPMENT FACILITY

SCS entered into an agreement with DOE/FETC for the design, construction, and operation of a hot-gas clean-up test facility for pressurized gasification and combustion. The purpose of the PSDF is to provide a flexible test facility that can be used to develop advanced power system components, evaluate advanced-turbine system configurations, and assess the integration and control issues of these advanced power systems. The facility was designed as a resource for rigorous, long-term testing and performance assessment of hot-stream clean-up devices and other components in an integrated environment.

The PSDF will consist of five modules for systems and component testing. These modules include:

- An advanced pressurized fluidized-bed combustion module (APFBC).
- A transport reactor module.
- A hot-gas clean-up module.
- A compressor/turbine module.
- A fuel cell module.

The APFBC module consists of FW technology for second-generation PFBC. This module relies on the partial conversion of the coal to fuel gas in a carbonizer, with the remaining char converted in a PFBC. Both the fuel gas and PFBC exhaust-gas streams are filtered to remove particulates, then combined to fire a combustion turbine. The advanced gasifier module includes KBR transport reactor technology for pressurized combustion and gasification to provide either an oxidizing or reducing gas for parametric testing of hot-particulate-control devices.

The filter systems that will be tested at PSDF include particulate control devices (PCDs) supplied by Combustion Power Company and Siemens Westinghouse.

2.2 TRANSPORT REACTOR SYSTEM DESCRIPTION

The transport reactor is an advanced circulating fluidized-bed reactor acting as either a combustor or as a gasifier, using one of two possible hot-gas clean-up filter technologies (particulate control devices or PCDs) at a component size readily scaleable to commercial systems. The transport reactor train operating in either the combustion or gasification mode is shown schematically in Figure 2.2-1. A tag list of all major equipment in the process train and associated balance-of-plant is provided in Tables 2.2-1 and -2. Two PCDs are shown in this flow diagram; however, only one PCD is tested with the transport reactor at a given time during operations. The intent is to be able to install, change out, or provide maintenance on a second PCD while one is being tested. This provides increased flexibility for the test facility and reduces downtime. The facility is sized to process nominally 2 ton/hour of coal. This size generates sufficient gas to test the PCDs at a nominal 1,000 ACFM of gas at the PCD inlet. Indirect cooling of the gas from the transport reactor allows testing of the PCD with inlet temperatures between 700 and 1,400°F and at pressures ranging from 150 to 305 psia. The PCD in this train receives particulate-laden gas from the transport reactor, which can operate in either gasification or combustion mode. In the gasification mode, the gas exiting the PCD is oxidized, cooled, and filtered, if necessary, in a baghouse before being discharged from a stack. The sulfides and char produced in the gasification mode are oxidized in a sulfator prior to disposal.

Coal and sorbent are ground to a nominal-average-particle diameter of 350 and 15 microns (Sauter mean), respectively. Using feeders to control the rates, both coal and sorbent are pneumatically fed continuously into the transport gasifier/combustor.

Air is compressed to about 350 psia in the main air compressor and fed directly to the transport reactor. For start-up purposes, a burner (BR0201) is provided at the reactor mixing zone. Liquefied propane gas (LPG) is used as start-up fuel. Fuel, sorbent, and gas feeds enter a mixing zone at the bottom of the reactor where they mix with recycled solids from the disengager cyclone. Coal conversion begins in this zone; the reaction mixture then flows upward into the narrower riser section at high velocity, and then flows to the disengager.

Gasification Operations

In gasification mode, the nominal transport reactor operating temperature is 1,800°F. The reactor system is designed to have a maximum operation pressure of 294 psig with a thermal capacity of about 41 million Btu/hr for gasification mode. The solids cooler (combustor heat exchanger, HX0203), which is necessary for combustion operations, is not used in gasification.

The gas leaves the transport reactor cyclone and goes to the primary gas cooler which cools the gas prior to entering the Siemens Westinghouse PCD barrier filter. The PCD uses ceramic or sintered metal elements to filter out dust from the reactor. The PCD removes almost all the dust from the gas stream to prevent erosion of a downstream gas turbine in a commercial plant. The operating temperature of the PCD is controlled both by the reactor temperature and by an upstream gas cooler. For test purposes, the gas from the transport reactor can flow through the gas cooler from zero to 100 percent. The PCD gas temperature can range from 700 to 1,600°F. The filter elements are back-pulsed by high-pressure nitrogen in a desired time interval or at a

given maximum pressure difference across the filter elements. There is a secondary gas cooler after the filter vessel to cool the gas before discharging to the stack or thermal oxidizer. In a commercial process, the syngas from the PCD would be sent to a combustion gas turbine. The syngas is sampled for on-line analysis immediately after the PCD and after traveling through the secondary gas cooler.

After exiting the secondary gas cooler the gas is then let down to about 2 psig through a pressure-control valve. The syngas is then sent to a thermal oxidizer (atmospheric syngas combustor) to burn the gas and oxidize all reduced sulfur compounds (H_2S, COS, CS_2) and reduced nitrogen compounds (NH_3, HCN). The thermal oxidizer uses less than 5-percent propane (by heating value) as a supplemental fuel. The gas from the thermal oxidizer is cooled and passes through a baghouse for any additional cleanup before discharging to a stack.

The transport reactor produces both fine ash/char mixture collected by the PCD and coarse ash/char mixture extracted from the transport reactor standpipe. The two solid streams are cooled using screw coolers, reduced in pressure in lock hoppers, and them combined. In gasification, any fuel sulfur captured by sorbent should be present as calcium sulfide (CaS). The gasification solids are processed in the sulfator to oxidize the CaS to calcium sulfate ($CaSO_4$) and burn any residual carbon in the ash/char mixture. The waste solids are then suitable for commercial use or disposal. Neither the sulfator nor the thermal oxidizer would be part of a commercial process. In a commercial process, the gasification solids could be burned in a pressurized fluidized bed combustor to recover the solids heat value.

Table 2.2-1

Major Equipment in the Transport Reactor Train

TAG NAME	DESCRIPTION
BR0201	Reactor Start-Up Burner
BR0401	Thermal Oxidizer
BR0602	Sulfator Start-Up/PCD Preheat Burner
CO0201	Main Air Compressor
CO0401	Recycle Gas Booster Compressor
CO0601	Sulfator Air Compressor
CY0201	Primary Cyclone in the Reactor Loop
CY0207	Disengager in the Reactor Loop
CY0601	Sulfator Cyclone
DR0402	Steam Drum
DY0201	Feeder System Air Dryer
FD0206	Spent Solids Screw Cooler
FD0210	Coal Feeder System
FD0220	Sorbent Feeder System
FD0502	Fines Screw Cooler
FD0510	Spent Solids Transporter System
FD0520	Fines Transporter System
FD0530	Spent Solids Feeder System
FD0602	Sulfator Solids Screw Cooler
FD0610	Sulfator Sorbent Feeder System
FL0301	PCD — Siemens Westinghouse
FL0302	PCD — Combustion Power
FL0401	Compressor Intake Filter
HX0202	Primary Gas Cooler
HX0203	Combustor Heat Exchanger
HX0204	Transport Air Cooler
HX0402	Secondary Gas Cooler
HX0405	Compressor Feed Cooler
HX0601	Sulfator Heat Recovery Exchanger
ME0540	Heat Transfer Fluid System
RX0201	Transport Reactor
SI0602	Spent Solids Silo
SU0601	Sulfator

Table 2.2-2 (Page 1 of 3)

Major Equipment in the Balance-of-Plant

TAG NAME	DESCRIPTION
BO2920	Auxiliary Boiler
BO2921	Auxiliary Boiler – Superheater
CL2100	Cooling Tower
CO2201A-D	Service Air Compressor A-D
CO2202	Air-Cooled Service Air Compressor
CO2203	High-Pressure Air Compressor
CO2601A-C	Reciprocating N_2 Compressor A-C
CR0104	Coal and Sorbent Crusher
CV0100	Crushed Feed Conveyor
CV0101	Crushed Material Conveyor
DP2301	Baghouse Bypass Damper
DP2303	Inlet Damper on Dilution Air Blower
DP2304	Outlet Damper on Dilution Air Blower
DY2201A-D	Service Air Dryer A-D
DY2202	Air-Cooled Service Air Compressor Air Dryer
DY2203	High-Pressure Air Compressor Air Dryer
FD0104	MWK Coal Transport System
FD0111	MWK Coal Mill Feeder
FD0113	Sorbent Mill Feeder
FD0140	Coke Breeze and Bed Material Transport System
FD0154	MWK Limestone Transport System
FD0810	Ash Unloading System
FD0820	Baghouse Ash Transport System
FL0700	Baghouse
FN0700	Dilution Air Blower
HO0100	Reclaim Hopper
HO0105	Crushed Material Surge Hopper
HO0252	Coal Surge Hopper
HO0253	Sorbent Surge Hopper
HT2101	MWK Equipment Cooling Water Head Tank
HT2103	SCS Equipment Cooling Water Head Tank
HT0399	60-Ton Bridge Crane
HX2002	MWK Steam Condenser
HX2003	MWK Feed Water Heater

Table 2.2-2 (Page 2 of 3)

Major Equipment in the Balance-of-Plant

TAG NAME	DESCRIPTION
HX2004	MWK Subcooler
HX2103A	SCS Cooling Water Heat Exchanger
HX2103C	MWK Cooling Water Heat Exchanger
LF0300	Propane Vaporizer
MC3001-3017	MCCs for Various Equipment
ME0700	MWK Stack
ME0701	Flare
ME0814	Dry-Ash Unloader for MWK Train
ML0111	Coal Mill for MWK Train
ML0113	Sorbent Mill for Both Trains
PG2600	Nitrogen Plant
PU2000A-B	MWK Feed Water Pump A-B
PU2100A-B	Raw Water Pump A-B
PU2101A-B	Service Water Pump A-B
PU2102A-B	Cooling Tower Make-Up Pump A-B
PU2103A-D	Circulating Water Pump A-D
PU2107	SCS Cooling Water Make-Up Pump
PU2109A-B	SCS Cooling Water Pump A-B
PU2111A-B	MWK Cooling Water Pump A-B
PU2300	Propane Pump
PU2301	Diesel Rolling Stock Pump
PU2302	Diesel Generator Transfer Pump
PU2303	Diesel Tank Sump Pump
PU2400	Fire-Protection Jockey Pump
PU2401	Diesel Fire Water Pump #1
PU2402	Diesel Fire Water Pump #2
PU2504A-B	Waste-Water Sump Pump A-B
PU2507	Coal and Limestone Storage Sump Pump
PU2700A-B	Demineralizer Forwarding Pump A-B

Table 2.2-2 (Page 3 of 3)

Major Equipment in the Balance-of-Plant

TAG NAME	DESCRIPTION
PU2920A-B	Auxiliary Boiler Feed Water Pump A-B
SB3001	125-V DC Station Battery
SB3002	UPS
SC0700	Baghouse Screw Conveyor
SG3000-3005	4160-V, 480-V Switchgear Buses
SI0101	MWK Crushed-Coal Storage Silo
SI0103	Crushed-Sorbent Storage Silo
SI0111	MWK Pulverized-Coal Storage Silo
SI0113	MWK Limestone Silo
SI0114	FW Limestone Silo
SI0810	Ash Silo
ST2601	N_2 Storage Tube Bank
TK2000	MWK Condensate Storage Tank
TK2001	FW Condensate Tank
TK2100	Raw-Water Storage Tank
TK2300A-D	Propane Storage Tank A-D
TK2301	Diesel Storage Tank
TK2401	Fire Water Tank
XF3000A	230/4.16-kV Main Power Transformer
XF3001B-5B	4160/480-V SS Transformer No. 1-5
XF3001G	480/120-V Miscellaneous Transformer
XF3010G	120/208 Distribution Transformer
XF3012G	UPS Isolation Transformer
VS2203	High-Pressure Air Receiver

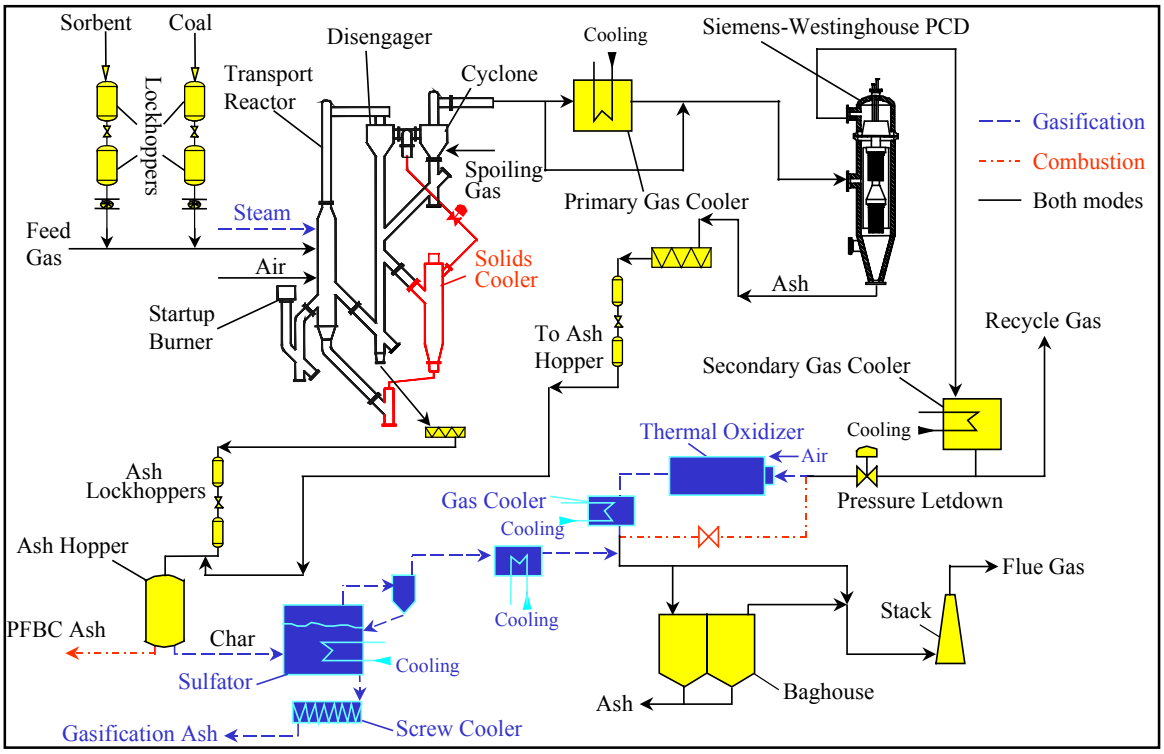

Figure 2.2-1 Flow Diagram of the Transport Reactor Train in Gasification Mode of Operation

2.3 SIEMENS WESTINGHOUSE PARTICULATE CONTROL DEVICE

Different PCDs will be evaluated on the transport reactor train. The first PCD that was commissioned in 1996 and has been used in all of the testing to date was the filter system designed by Siemens Westinghouse. The dirty gas enters the PCD below the tubesheet, flows through the filter elements, and the ash collects on the outside of the filter. The clean gas passes from the plenum/filter element assembly through the plenum pipe to the outlet pipe. As the ash collects on the outside surface of the filter elements the pressure drop across the filter system gradually increases. The filter cake is periodically dislodged by injecting a high-pressure gas pulse to the clean side of the filter elements. The cake then falls to the discharge hopper.

Until this first gasification test run, GCT1 in late 1999, the transport reactor had been operated only in the combustion mode. Initially, high-pressure air was used as the pulse gas for the PCD. However, the pulse gas was changed to nitrogen early in 1997. The pulse gas was routed individually to the two plenum/filter element assemblies via injection tubes mounted on the top head of the PCD vessel. The pulse duration was typically 0.1 to 0.5 seconds.

A sketch of the Siemens Westinghouse PCD is shown in Figure 2.3-1.

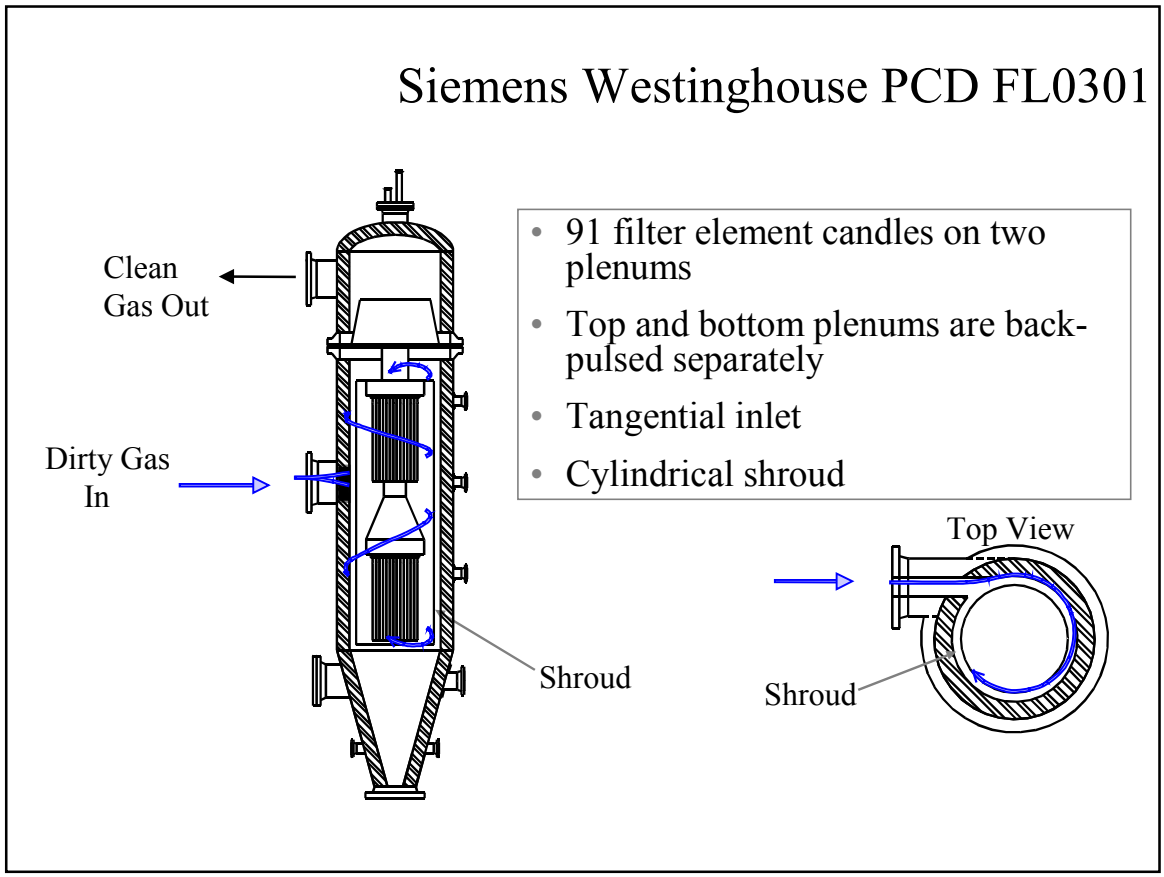

Figure 2.3-1 Siemens Westinghouse PCD

2.4 OPERATION STATUS

Commissioning activities began in September 1995 and proceeded in parallel with construction activities. Design and construction of the transport reactor and associated equipment was completed in early summer of 1996. All separate components and subsystems were fully operational by midsummer and commissioning work was focused on integration issues for the entire transport reactor train. The first coal fire was achieved on August 18, 1996. A series of combustion characterization tests was initiated to develop an understanding of reactor system operations. Test runs CCT1, CCT2, and CCT3 were completed by December 1996. Solids carryover from the reactor to the PCD was found to be excessive during these test runs. A number of start-up and design problems associated with various equipment were successfully addressed.

During 1997 three additional sets of characterization test runs—CCT4, CCT5, and CCT6—and one major test campaign—TC01—were undertaken. TC01 focused on exposing the PCD filter elements to process gas for 1,000 hours at temperatures from 1,350 to 1,400°F and achieving stable reactor operations. An Alabama bituminous coal from the Calumet Mine in the Mary Lee seam and Plum Run dolomite were used in these test runs.

Two test campaigns (TC02 and TC03) were successfully completed during 1998. TC02 was planned for reactor parametric testing to better quantify the effect of different variables on reactor and filter element operation. Test run TC02 was started on April 5, 1998, and was completed on May 11, 1998. Based on TC02 observations, TC03 was planned for additional reactor parametric testing to better quantify the effect of different variables on reactor and PCD operation and to evaluate operation with an Eastern Kentucky bituminous coal and a Gregg Mine limestone from Florida. The third major test campaign, TC03, was performed from May 31, 1998, to August 10, 1998. Stable operations were demonstrated using the Eastern Kentucky coal along with Plum Run, Bucyrus, and Longview limestone during TC03. There were, however, circulation problems using the Eastern Kentucky coal and Florida Gregg Mine limestone because of deposits resulting from excessive fines (segregated) in the Eastern Kentucky feed. One additional test run, TC04, was started on October 14, 1999, but was prematurely ended due to a temperature excursion in the PCD during the initial heat-up of the transport reactor system.

The final combustion test campaign (TC05) was started on January 10, 1999, in combustion mode of operation and was completed May 2, 1999. During TC05, steady-state operations with a variety of fuel and sorbent feed materials were demonstrated (including petroleum coke with two different sorbents) and reactor parametric testing with different feed combinations was performed. Overall, TC05 was a successful test run with 10 different feed combinations tested. Conversion of the transport reactor train to gasification mode of operations was performed from May to September 1999. The first gasification test run, GCT1, was a 250-hour test run to commission the transport reactor train in gasification mode of operation and to characterize the limits of operational parameter variations. GCT1 was started on September 9, 1999, with the first part completed on September 15, 1999 (GCT1A). The second part of GCT1 was started on December 7, 1999, and completed on December 15, 1999 (GCT1B through D).

This test run provided the data necessary for a preliminary analysis of reactor operations and to identify necessary modifications to improve equipment and process performance. Five different feed combinations were tested to gain a better understanding of the reactor solids collection system efficiency. Figure 2.4-1 gives a summary of operating hours and a transport reactor train operating history.

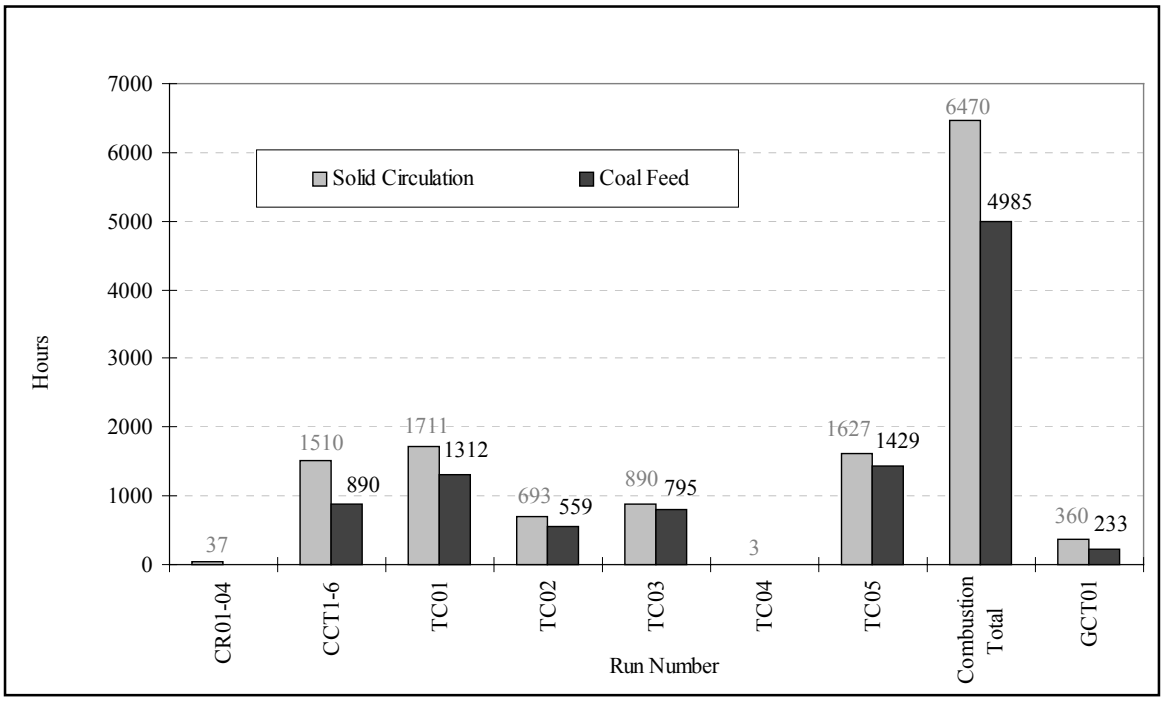

Figure 2.4-1 Operating Hours Summary for the Transport Reactor Train

3.0 PARTICLE FILTER SYSTEM

3.1 GCT1 OVERVIEW

GCT1 was the first series of tests for the KBR transport reactor in gasification mode of operation. Since it was a new experience for both the personnel and the equipment it was expected to be a learning experience. As reported by several facilities, filter cakes formed from gasification char have pressure drops much higher than filter cakes formed from combustion ash. This was certainly experienced in GCT1. Whereas in combustion the pressure drop ranged from roughly 80 to 120 inH_2O over 40 minutes, in gasification the pressure drop ranged from 120 to 250 inH_2O in less than 10 minutes. These higher gasification-pressure drops were partially due to higher than normal inlet particulate loadings and the possible formation of aerosol tars that may have prevented the efficient removal of the filter cake during pulse cleaning.

In addition to the high-inlet loading, high-outlet loadings were a persistent problem during GCT1. During the first test, GCT1A, the outlet loading was nominally 250 ppmw. During GCT1B through D, the outlet loading started at nominally 80 ppmw and decreased to about 10 ppmw during the run; but even this lower loading is much higher than permissible turbine-inlet-particulate loading. The higher outlet loading was attributed to leakage of several ceramic composite filters during GCT1A (both through the body and around the flange) and leakage through some instrumentation fittings during GCT1B through D. Redesign of the filter holder and a new gasket for the fail-safe was tested on several filter elements during GCT1B through D with promising results and will be fully implemented during GCT2.

This report on PCD issues contains four sections:

- GCT1 Run Report (section 3.2) – The operation of the PCD during the gasification testing is briefly described. The most notable concern was the uncontrollable baseline-pressure drop during the run. The rise in pressure drop was probably due to the increased drag of the char particulate (when compared to combustion ash), backside blinding due to the high-outlet loading, and the possibility of tar being collected by the filter cake.

- GCT1 Inspection Report (section 3.3) – Findings during the PCD disassembly and inspection are discussed. During GCT1A, metal filter elements as well as ceramic composite filters were used. Evidence of leakage through the body of several composite filter elements and around the flanges was observed. Another important observation was that the residual dust cake in GCT1A was roughly half the thickness of the residual dust cake from GCT1B through D.

- GCT1 Char Characteristics and PCD Performance (section 3.4) – Key to understanding the change in drag of the char particulate and the varying residual dust cake thickness is the change in fundamental properties of the char. Discussed in this section are the char chemistry, drag, and other fundamental properties, as well as

additional observations made during the inspections. Also discussed are the inlet- and outlet-particulate loadings taken by SRI during the run.

- Fines Handling System (section 3.5) – Operation of the char-removal system was a key factor during the run, especially during GCT1B through D. Due to the higher particulate loading to the PCD, as well as the lower bulk density of the material, this volumetric feeder was cycling almost continuously during the run. Ultimately, the inability of the char-removal system to remove char quickly enough ended GCT1B through D.

3.2 GCT1 RUN REPORT

3.2.1 GCT1A

3.2.1.1 Introduction

The GCT1A commissioning run was the first gasification startup at the PSDF. During this run two major incidents occurred which resulted in the shutdown of the process. The first incident occurred when an oxygen sensor was calibrated while the process was running. Since the system logic "thought" oxygen breakthrough had been detected, the process shut down. The second incident was a power outage.

The baseline pressure drop in the PCD was one of the major problems faced during GCT1A. Ultimately, the increase in the baseline pressure drop ended the run. Several reasons for the higher pressure drop were: (1) the gasification char had a higher drag, (2) back-side blinding of the filters due to leaks found in the composite filters and around the gaskets of the filters, and (3) possible tar deposition on the filters.

Maintaining the PCD temperature below 750°F was a major challenge. The majority of the filter elements used in GCT1A were Hastelloy X (a nickel-based alloy). One of the objectives for the test was to operate the PCD below 750°F since literature reports that the nickel can react with H_2S in the gas to form nickel-sulfide, which will blind the filter elements at higher temperatures. During gasification, tar production and higher particulate loading affected the primary gas cooler operation, causing the PCD temperature to exceed 750°F. Eight of the thirty tubes in the gas cooler were plugged, which significantly reduced the heat transfer area of the gas cooler.

3.2.1.2 Test Objectives

The primary test objectives for the run included the following:

- Test Metal and Composite Filter Elements – During TC04 the PCD experienced a thermal event that damaged many of the ceramic filters. One of the main concerns for the gasification run was that oxygen could enter to the PCD, causing the uncombusted char to burn, which could produce a thermal event similar to the one in TC04. Therefore, composite and metal filters with significantly better thermal properties than monolithic ceramic filters were installed for GCT1A.

- Maintain PCD Temperature at Around 750°F – There was a concern that the nickel found in many of the metal filters would react with the H_2S in the process gas to form nickel-sulfide, which could cause the filter to blind and increase the pressure drop across the PCD. This reaction occurs above 900°F. From the operating conditions in combustion runs it was projected that the PCD inlet temperature would be about 750°F.

- Monitor Filter Element Temperature – Thermocouples were placed in the PCD on the T-1, T-7, T-13, B-1, B-7, and B-13 filter elements. The thermocouples were wired to

the plant DCS system. This was done to monitor the PCD for any thermal events that might take place.

- Control the Pressure Drop – The gasification char was expected to present challenges in controlling the pressure drop in the PCD. This was based on the difference in physical characteristics between the combustion ash and the gasification char. Therefore, the back-pulse frequency and pressure were increased to control the pressure drop in the PCD. Also, the surface filtration area was approximately 232 ft^2 in order to maintain the face velocity between 4 to 5 ft/min. The lower face velocity would produce a lower pressure drop in the PCD.

3.2.1.3 Observations/Events – 9/09/99 Through 9/15/99

A. Test Started, 9/09/99 at 07:40 – The main air compressor (MAC) was started.

B. Start-Up Burner Lit, 9/09/99 at 09:45.

C. System Pressure Increased to 100 psig, 9/10/99 at 05:30.

D. Start-Up Burner Stopped, 9/10/99 at 07:00. It was relit and run until 9/12/99.

E. Back-Pulse Set at 10 Minutes and 500 psig, 9/11/99 at 17:25.

F. Coal Feed Began, 9/11/99 at 20:21 – Oxygen level was at zero percent, which marked the beginning of gasification. The coal and sorbent fed into the transport reactor were Powder River Basin and Plum Run dolomite. The start-up burner was stopped. Temperature and pressure drop began to increase in the PCD. During this time the actual back-pulse time was less than 10 minutes (due to the high peak-pressure drop triggering the back-pulse logic).

G. PCD Pulse Pressure Increased to 550 psig, 9/12/99 at 12:05.

H. Reactor Pressure Increased, 9/12/99 at 12:50 – The system pressure was increased by 10 psig to reduce the face velocity in the PCD.

I. High-O_2 Alarm Triggered, 9/12/99 at 15:13 – The high-oxygen alarm was tripped due to oxygen analyzer being calibrated while the process was running. During this event the DCS logic detected oxygen downstream of the reactor. Once oxygen was detected in the PCD the MAC was manually shut down.

J. Start-Up Burner Relit, 9/12/99 at 16:30. After the problems mentioned in item I were resolved a hot startup was attempted.

K. Coal Feed Restarted, 9/13/99 at 11:00.

L. PCD Baseline Began to Increase, 9/14/99 at 00:40.

M. Power Outage, 9/14/99 at 06:30 – This was due to a 230-kV-line loss. The MAC and coal feeder were shut down. This resulted in a PCD temperature decrease.

N. Power Returned, 9/14/99 at 10:00 – The MAC and start-up burner were restarted.

O. Coal Feeder Restarted, 9/14/99 at 15:43.

P. System Pressure Increased, 9/14/99 at 17:30 – The system pressure steadily increased by approximately 50 psig over a 6-hour span.

Q. PCD Trigger Increased From 225 to 250 inH_2O, 9/14/99 at 23:20.

R. System Pressure Increased to 140 psig, 9/15/99 at 00:30.

S. PCD Baseline Pressure Increased, 9/15/99 at 03:40.

T. System Pressure Increased to 165 psig, 9/15/99 at 07:40.

U. PCD Pulse Pressure Increased to 640 psig, 9/15/99 at 07:45.

V. System Pressure Increased to 170 psig, 9/15/99 at 08:10.

W. PCD Back-Pulsing Every 3 Minutes, 9/15/99 at 14:00.

X. Run Ended, 9/15/99 at 16:00.

3.2.1.4 Run Summary

The first gasification run began at 07:40 on September 9. Once the reactor temperature approached 1,200°F coal was fed to the reactor. At this point the PCD back-pulse pressure and frequency were changed to 500 psig and 10 minutes from 350 psig and 30 minutes. At 21:05 on September 11, the PCD temperature increased to 800°F from 570°F due to the coal feeder being started. During this time the baseline pressure drop increased to 100 inH_2O and the peak pressure drop increased to 170 inH_2O. At 12:50 on September 12, the system pressure was increased to 110 psig to decrease the face velocity in the PCD.

At 15:15 on September 12, the high-oxygen alarm went off during calibration, which shut the process down. During the calibration none of the system overrides were activated. The DCS logic was programmed to shut down the process in the event of an oxygen breakthrough to the PCD. The purpose of this logic was to prevent the uncombusted char in the PCD from catching on fire. During this time the coal feeder tripped, which caused the reactor and PCD temperatures to drop. The main air compressor was shut down to prevent combustion in the PCD. Once the problem had been identified the process was restarted at 16:30 on September 12.

At 11:00 on September 13 coal was fed to the reactor. At this time the temperature in the PCD increased to 800°F. The baseline and peak pressure drop increased to 90 and 180 inH_2O, respectively. In order to maintain control over the pressure drop in the PCD, the back-pulse frequency was changed to 10 minutes. However, due to the high-pressure drop triggering the pulse logic, the actual time between back-pulses was sometimes less than 10 minutes. At 06:30 on September 14 the power to the PSDF was cut due to the failure of a 230-kV line. Prior to the power outage the PCD temperature had increased to 850°F. Also, the baseline- and peak-pressure drop had increased to 163 and 225 inH_2O, respectively.

At 10:00 on September 14, power was returned to the PSDF. By 12:40 the process was started again. At 16:00 the coal feeder was started and immediately the PCD temperature increased to over 800°F. The baseline- and peak-pressure drops were approximately 140 and 225 inH_2O, respectively. At 23:20 the back-pulse trigger was increased from 225 to 250 inH_2O. At 06:00 on September 15 the actual back-pulse frequency had decreased to 3 minutes and the temperature in the PCD was over 850°F. Two reasons given for the higher than expected temperatures were:

- Increased particulate loading to the PCD – The inlet loading to the PCD was as high as 60,000 ppm, which may have contributed to the higher than expected temperatures.

- Inspection of the primary gas cooler yielded severe fouling – Eight of the thirty tubes were plugged, which decreased the heat duty of the gas cooler.

The PCD baseline- and peak-pressure drops were 180 and 250 inH_2O, respectively. The reasons given for the increased pressure drop in the PCD were:

1. The gasification char had a higher drag than that of combustion ash.

2. Leaks found in some of the composite filters and around the filter gaskets allowed the char to penetrate to the clean side of the filter. This resulted in the char being forced into the pores of the filter media on the inside during pulse cleaning, leading to back-side blinding.

3. Tar deposition on the filters. Since the PCD was several hundred degrees cooler than the reactor, high-molecular-weight tars could possibly condense between the gas cooler and the PCD, causing the char particles to bind tightly to each other.

At this time the control over the PCD was lost because the back-pulse frequency had reached the limit of the control logic. Also, there was no evidence that the pressure drop was going to stop increasing. Based on the extreme conditions in the PCD it was decided to terminate the run at 16:00 on September 15, 1999.

3.2.2 GCT1B Through D

3.2.2.1 Introduction

The GCT1B through D run was started on December 7, 1999. Three fuel sources were used during this run—Powder River Basin, Illinois No. 6, and Alabama coals. Unlike the GCT1A run, there were no major upsets that shut down the process and there were no incidents of oxygen breakthrough to the PCD. This was important since all the filters used in this run were monolithic ceramics. The outlet loading, which was as high as 547 ppm during GCT1A, started at 81 ppm and decreased throughout the run to 6 to 8 ppm.

As in GCT1A, maintaining the baseline- and peak-pressure drops at reasonable levels was a major challenge during GCT1B through D. The baseline-pressure drop reached 180 inH_2O and the peak-pressure drop was as high as 270 inH_2O. Every attempt to decrease the pressure drop across the PCD was unsuccessful (i.e., increase system pressure, increase back-pulse pressure, and vary back-pulse valve open time and frequency). Reasons given for the high-pressure drop are outlined in the char report (see section 3.4).

Another problem experienced during GCT1B through D was the accumulation of char in the cone of the PCD. The main reason for the char accumulation was the high-inlet loading to the PCD, which caused the ash removal system to operate at full capacity throughout most of the run. For most of the run the transport reactor operation was limited due to accumulation of char in the PCD cone.

3.2.2.2 Test Objectives

The primary test objectives for the run included:

- Monitor Element Temperature – In September, a total of six thermocouples were used to monitor temperature on the filters; for this run, fourteen thermocouples were placed on the filters, seven on the top plenum and seven on the bottom plenum. The main purpose of these thermocouples was to warn of burning solids that might be on the filters.

- Install Monolithic Ceramic Filter – Only monolithic ceramic filters were installed in the PCD for this run. The reasons for using monolithic ceramic filters were:

    1. The composite filters proved to be unreliable in GCT1A.

    2. At the time, it had not been determined if the metal filter elements used in GCT1A had blinded due to the nickel-sulfide reaction.

    3. Using metal filters in GCT1A restricted the temperature range in which the transport reactor could operate. Operating at lower temperatures may have led to the tar formation seen in GCT1A. Using monolithic ceramic filters in the PCD gave the transport reactor more operating flexibility.

- Test New Filter Holder Design – For GCT1B through D, 14 new filter holders were installed to see how they would perform. The new filter holder design was tested for two reasons:

    1. The original filter holder design did not provide appropriate sealing for the multi-gasket arrangement.

    2. Siemens Westinghouse provided a new sealing gasket that would fit around the fail-safe. The original gasket was made of fiberfrax. This material was too brittle for the process conditions. Therefore, Siemens Westinghouse provided a more robust gasket. The new filter holder design came in two separate sections which allowed separate compression on the two different gaskets.

3.2.2.3 Observation/Events – 12/07/99 Through 12/15/99

A. Main Air Compressor Started, 12/07/99 at 11:49 – System pressure increased to 50 psig.

B. Start-Up Burner Lit, 12/07/99 at 15:08.

C. System Pressure Increased to 75 psig, 12/07/99 at 16:40.

D. System Pressure Increased to 100 psig, 12/07/99 at 20:00 – PCD back-pulse pressure was increased to 350 psig.

E. Coal Feeder Started, 12/08/99 at 05:15 – The coal and sorbent fed to the transport reactor was Powder River Basin coal and dolomite. Back-pulse pressure and frequency were changed to 500 psig and 5 minutes, respectively. The start-up burner was tripped.

F. Coal Feed Rate Decreased, 12/08/99 at 08:45 – The coal feeder was decreased from 80 to 55 percent due to PCD solids not clearing.

G. PCD Temperature Increased, 12/09/99 at 06:30 – The PCD inlet temperature increased by 73°F within a 50-minute time range. During this time the coal feed was swinging from 45 to 70 percent. Also, the primary gas cooler heat duty decreased.

H. System Pressure Increased to 110 psig, 12/09/99 at 08:10.

I. System Pressure Increased to 150 psig, 12/09/99 at 13:45 – Back-pulse pressure increased to 540 psig.

J. System Pressure Increased to 175 psig, 12/10/99 at 04:40 – Back-pulse pressure increased to 570 psig.

K. System Pressure Increased to 185 psig, 12/10/99 at 11:35.

L. Started Feeding Alabama Limestone, 12/10/99 at 16:00.

M. Back-Pulse Pressure Increased to 580 psig, 12/10/99 at 23:30.

N. System Pressure Increased to 190 psig, 12/11/99 at 04:25.

O. Started Continuous Illinois No. 6 Coal-Feed Rate, 12/11/99 at 07:00 – PCD temperature increased by 133°F.

P. System Pressure Increased to 195 psig, 12/11/99 at 11:20.

Q. Baseline Pressure Drop Increased, 12/11/99 at 19:00 – The baseline pressure drop increased approximately 50 inH_2O over a 12-hr-time range.

R. System Pressure Increased to 200 psig, 12/12/99 at 01:55.

S. System Pressure Decreased to 195 psig, 12/12/99 at 04:25.

T. Started Feeding Ohio Limestone, 12/12/99 at 08:30.

U. Back-Pulse Pressure Increased to 650 psig, 12/12/99 at 17:53.

V. Back-Pulse Pressure Decreased to 600 psig, 12/12/99 at 22:25.

W. System Pressure Increased to 205 psig, 12/13/99 at 04:24.

X. Baseline-Pressure Drop Increased, 12/13/99 at 05:00 – The baseline pressure drop increased by approximately 50 inH_2O over a 15-hr-time range.

Y. System Pressure Increased to 210 psig, 12/14/99 at 09:00.

Z. Run ended, 12/15/99 at 07:00.

3.2.2.4 Run Summary

The second gasification run began on December 7, 1999. Once the reactor temperature reached ~1,000°F, coal was fed to the reactor. The coal feeder was started on December 8 at 05:15. The coal and sorbent fed to the reactor were Powder River Basin coal and Plum Run dolomite. During this time the PCD temperature began to increase. Initially, the coal feed to the reactor was ~3,600 lb/hr. Around 08:00 on December 8, the coal feed to the reactor was decreased below ~2,500 lb/hr due to char accumulation in the cone of the PCD.

There was an increase in coal-feed rate on December 9, 22:00 to 23:00, when the coal-feed rate increased from 2,600 to 4,000 lb/hr. There also was a minor coal-feed rate decrease at 02:00 on December 12.

There was no sorbent fed to the reactor during December 10 and none during the Alabama coal testing on December 14 and 15.

Removing char from the cone of the PCD was challenging during GCT1B through D. The inability of the ash removal system to remove char from the cone of the PCD required that the transport reactor be operated off-design throughout the run. The main reason for the char accumulation was the higher inlet loading to the PCD. Another contributing factor was that the nitrogen flow to the purge line on the outlet end of the screw cooler was higher than normal in responding to the required pressure drop across the seal. The excessive nitrogen flowed backwards into the cone of the PCD, affecting the char flow out of the PCD.

At 01:00 on December 10 the baseline and peak pressures were over 100 and 250 inH_2O, respectively. The system pressure was increased to 175 psig to lower the pressure drop. During this time the back-pulse pressure and timer was at 570 psig and 5 minutes, respectively. At 16:00 the sorbent feed to the reactor was changed to Alabama limestone.

The fuel source to the reactor was changed from Powder River Basin to Illinois No. 6 at 07:00 on December 11. After the Illinois No. 6 coal was fed to the reactor, the pressure drop and temperature in the PCD began to increase dramatically. The temperature rapidly increased by 130°F, probably due to tar deposition in the gas cooler. The baseline-pressure drop increased by 50 inH_2O over the next 12 hours. The reason for the increase in pressure drop is discussed in section 3.4. During this time the system pressure was increased to 200 psig in an attempt to the lower the pressure drop across the PCD.

The sorbent feed to the reactor was changed to Ohio limestone at 08:30 on December 12. Over the next 12 hours the baseline-pressure drop increased another 50 inH_2O. The back-pulse pressure was increased to 650 psig and the system pressure increased to 205 psig in an attempt to decrease the baseline-pressure drop. By 04:30 on December 13 the baseline- and peak-pressures were 180 and 250 inH_2O, respectively.

Late on December 14 the coal source was changed from Illinois No. 6 to Alabama. At 07:00 on December 15 the run was ended due to the accumulation of char in the PCD. It appeared that FD0502 was not transferring any char to FD0520.

Table 3.2-1

GCT1A Run Statistics
09/09/1999 Through 09/15/1999

Start Time:	9/9/99 07:40
End Time:	9/15/99 16:00
Coal Type/Sorbent Type:	
09/09/99 to 09/15/99	Powder River Basin/Plum Run Dolomite
Hours on Coal	Approx. 63.5 hrs
Number of Filter Elements:	85
Filter Element Layout No.:	14 (Figure 3.2-1)
Filtration Area:	231.9 ft^2 (21.5 m^2)
Pulse Valve Open Time:	0.2 sec (Experimented With 0.15 and 0.5 sec)
Pulse Time Trigger:	3 to 10 min
Pulse Pressure:	325 to 640 psig
Pulse DP Trigger:	200 to 250 inH_2O

Table 3.2-2

GCT1A Major Events
09/09/1999 Through 09/15/1999

Event	Description	Date at Time
A	Test Started	September 9 at 07:40
B	Start-Up Burner Lit	September 9 at 09:45
C	System Pressure Increased to 100 psig	September 10 at 05:30
D	Start-Up Burner Stopped	September 10 at 07:00
E	Back-Pulse Set at 10 Minutes and 500 psig	September 11at 17:25
F	Coal Feed Began	September 11 at 20:21
G	PCD Pulse Pressure Increased to 550 psig	September 12 at 12:05
H	Reactor Pressure Increased	September 12 at 12:50
I	High-O_2 Alarm Triggered	September 12 at 15:13
J	Start-Up Burner Relit	September 12 at 16:30
K	Coal Feed Restarted	September 13 at 11:00
L	PCD Baseline Began to Increase	September 14 at 00:40
M	Power Outage	September 14 at 06:30
N	Power Returned	September 14 at 10:00
O	Coal Feed Restarted	September 14 at 15:43
P	System Pressure Increase	September 14 at 17:30
Q	PCD Trigger Increased From 225 to 250 inWG	September 14 at 23:20
R	System Pressure Increased to 140 psig	September 15 at 00:30
S	PCD Baseline Pressure Increased	September 15 at 03:40
T	System Pressure Increased to 165 psig	September 15 at 07:40
U	PCD Pulse Pressure Increased to 640 psig	September 15 at 07:45
V	System Pressure Increased to 170 psig	September 15 at 08:10
W	PCD Back-Pulsing Every 3 Minutes	September 15 at 14:00
X	Run Ended	September 15 at 16:00

Table 3.2-3

GCT1B Through D Run Statistics
12/07/99 Through 12/15/99

Start Time:	12/7/99 11:49
End Time:	12/15/99 07:00
Coal Type/Sorbent Type:	
12/08/99 to 12/10/99	Powder River Basin/Plum Run Dolomite
12/10/99 to 12/11/99	Powder River Basin/Alabama Limestone
12/11/99 to 12/12/99	Illinois No. 6/Alabama Limestone
12/12/99 to 12/14/99	Illinois No. 6/Ohio Limestone
12/14/99 to 12/15/99	Alabama/Ohio Limestone
Hours on Coal	170
Number of Filter Elements:	89
Filter Element Layout No.:	15 (Figure 3.2-5)
Filtration Area:	252.8 ft^2 (23.5 m^2)
Pulse Valve Open Time:	0.2 sec
Pulse Time Trigger:	5 min
Pulse Pressure:	380 to 650 psig
Pulse DP Trigger:	250 to 275 inH_2O

Table 3.2-4

GCT1B Through D Major Events
12/07/99 Through 12/15/99

Event	Description	Date at Time
A	Main Air Compressor Started	12/07/99 at 11:49
B	Start-Up Burner Lit	12/07/99 at 15:08
C	System Pressure Increased to 75 psig	12/07/99 at 16:40
D	System Pressure Increased to 100 psig	12/07/99 at 20:00
E	Coal Feed Started	12/08/99 at 05:15
F	Coal-Feed Rate Decreased	12/08/99 at 08:45
G	PCD Temperature Increased	12/09/99 at 06:30
H	System Pressure Increased to 110 psig	12/09/99 at 08:10
I	System Pressure Increased to 150 psig	12/09/99 at 13:45
J	System Pressure Increased to 175 psig	12/10/99 at 04:40
K	System Pressure Increased to 185 psig	12/10/99 at 11:35
L	Started Feeding Alabama Limestone	12/10/99 at 16:00
M	Back-Pulse Pressure Increased to 580 psig	12/10/99 at 23:30
N	System Pressure Increased to 190 psig	12/11/99 at 04:25
O	Steady Illinois No. 6 Coal-Feed Rate	12/11/99 at 07:00
P	System Pressure Increased to 195 psig	12/11/99 at 11:20
Q	Baseline-Pressure Drop Increased	12/11/99 at 19:00
R	System Pressure Increased to 200 psig	12/12/99 at 01:55
S	System Pressure Decreased to 195 psig	12/12/99 at 04:25
T	Started Feeding Ohio Limestone	12/12/99 at 08:30
U	Back-Pulse Pressure Increased to 650 psig	12/12/99 at 17:53
V	Back-Pulse Pressure Decreased to 600 psig	12/12/99 at 22:25
W	System Pressure Increased to 205 psig	12/13/99 at 04:24
X	Baseline-Pressure Drop Increased	12/13/99 at 05:00
Y	System Pressure Increased to 210 psig	12/14/99 at 09:00
Z	Run Ended	12/15/99 at 07:00

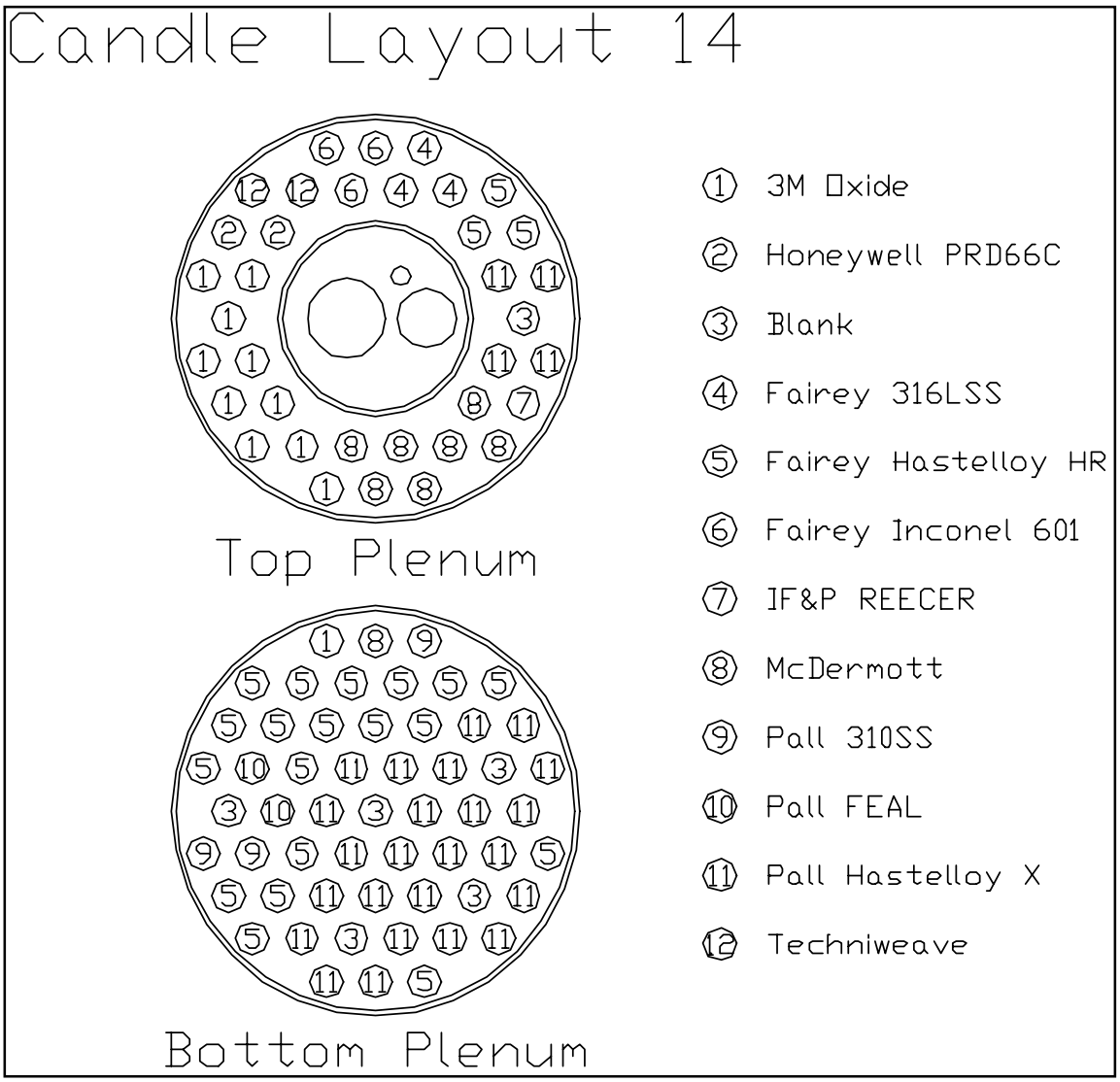

Figure 3.2-1 Filter Element Layout for GCT1A – September 9 Through September 15 (Layout 14)

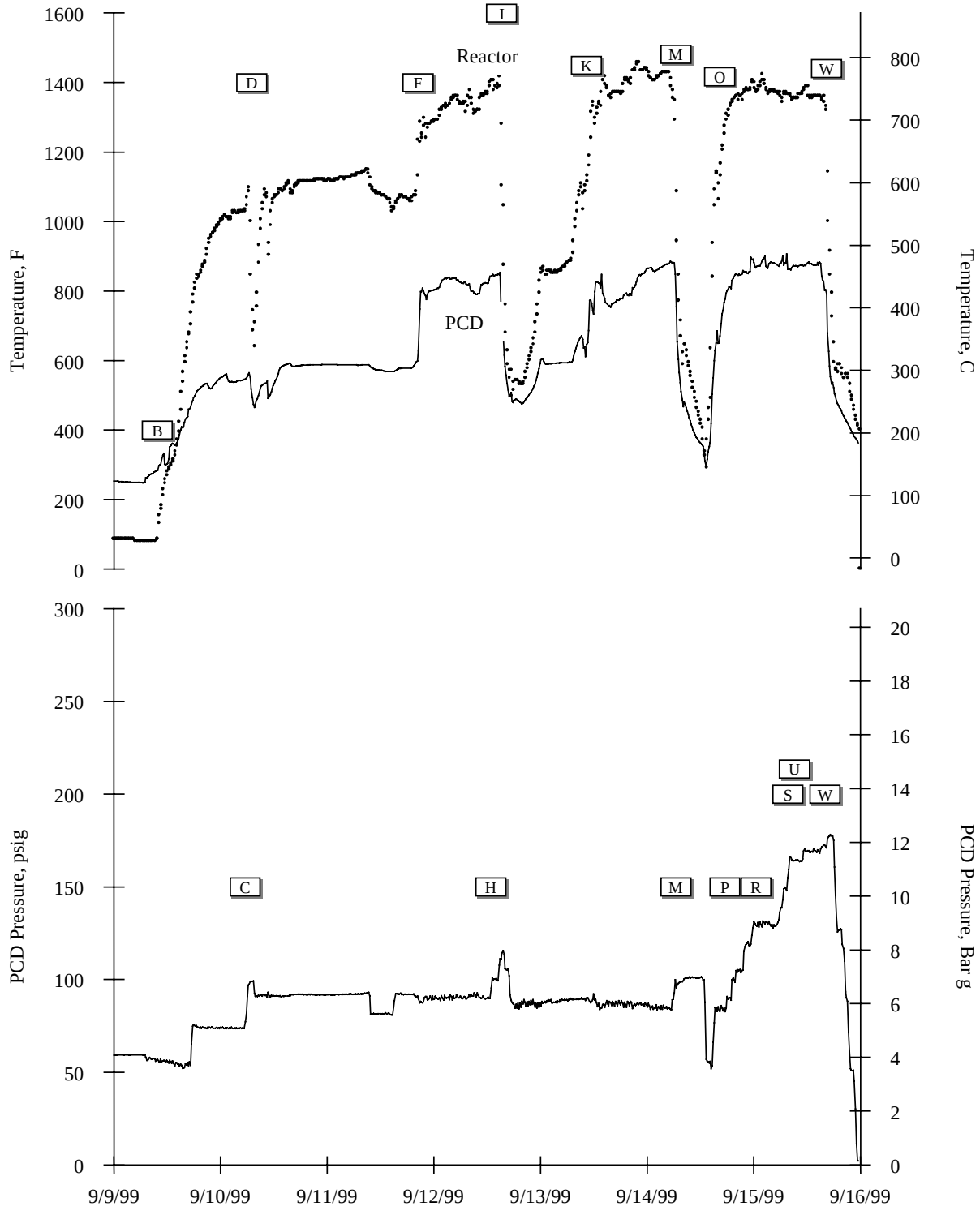

Figure 3.2-2 GCT1A Temperature and Pressure for September 9 Through September 16

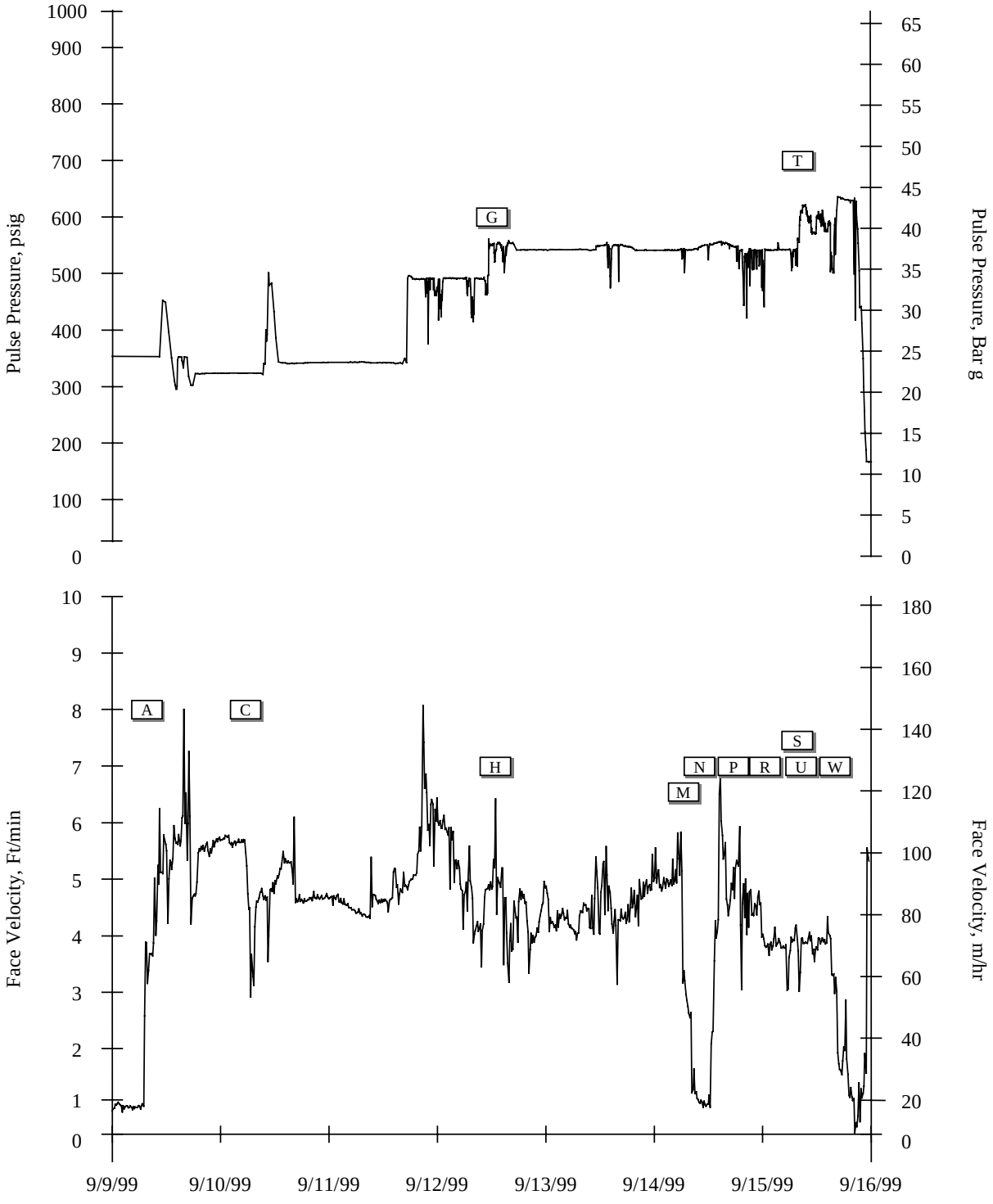

Figure 3.2-3 GCT1A Back-Pulse Pressure and Face Velocity for September 9 Through September 16

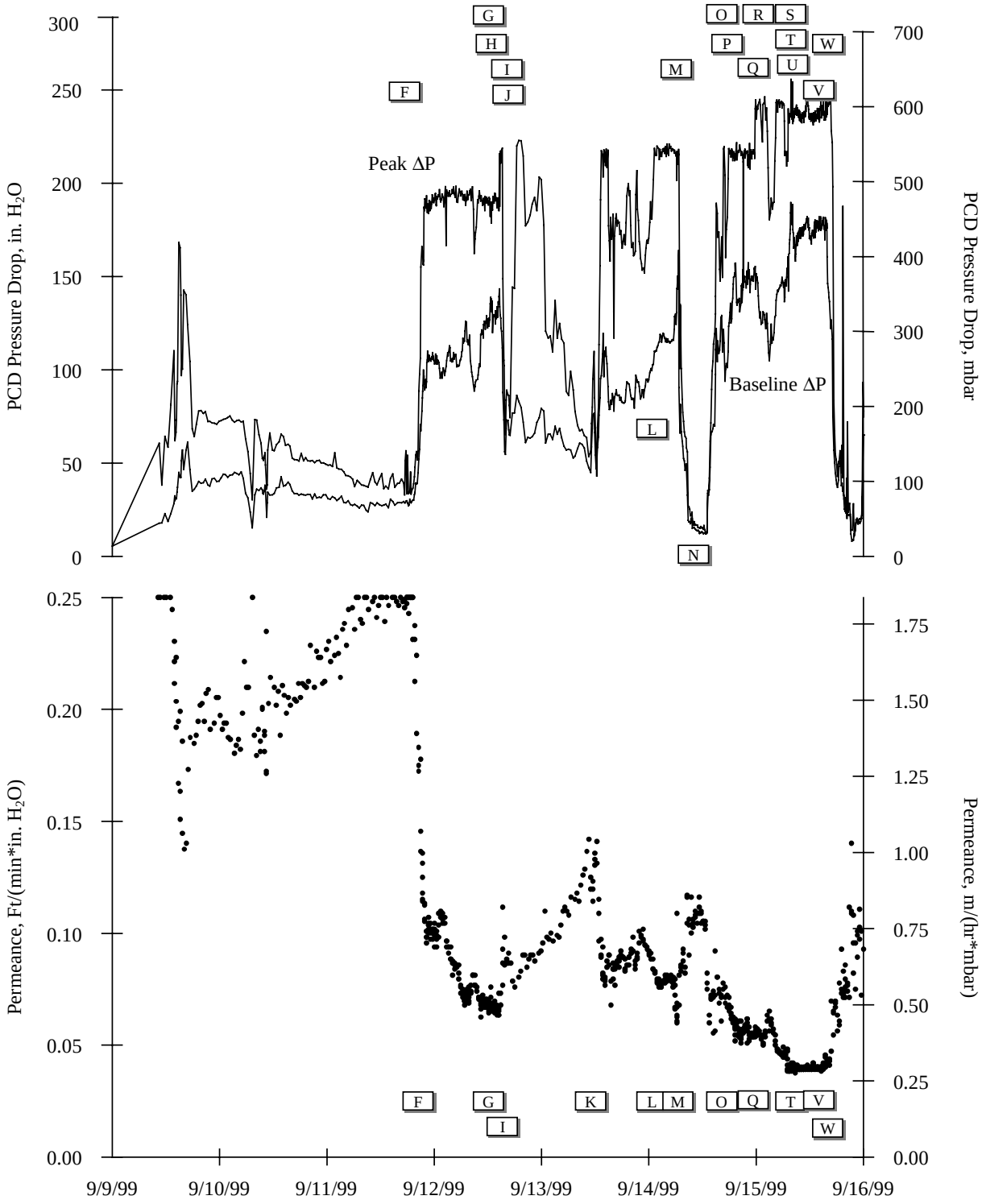

Figure 3.2-4 GCT1A Pressure Drop and Permeance for September 9 Through September 16

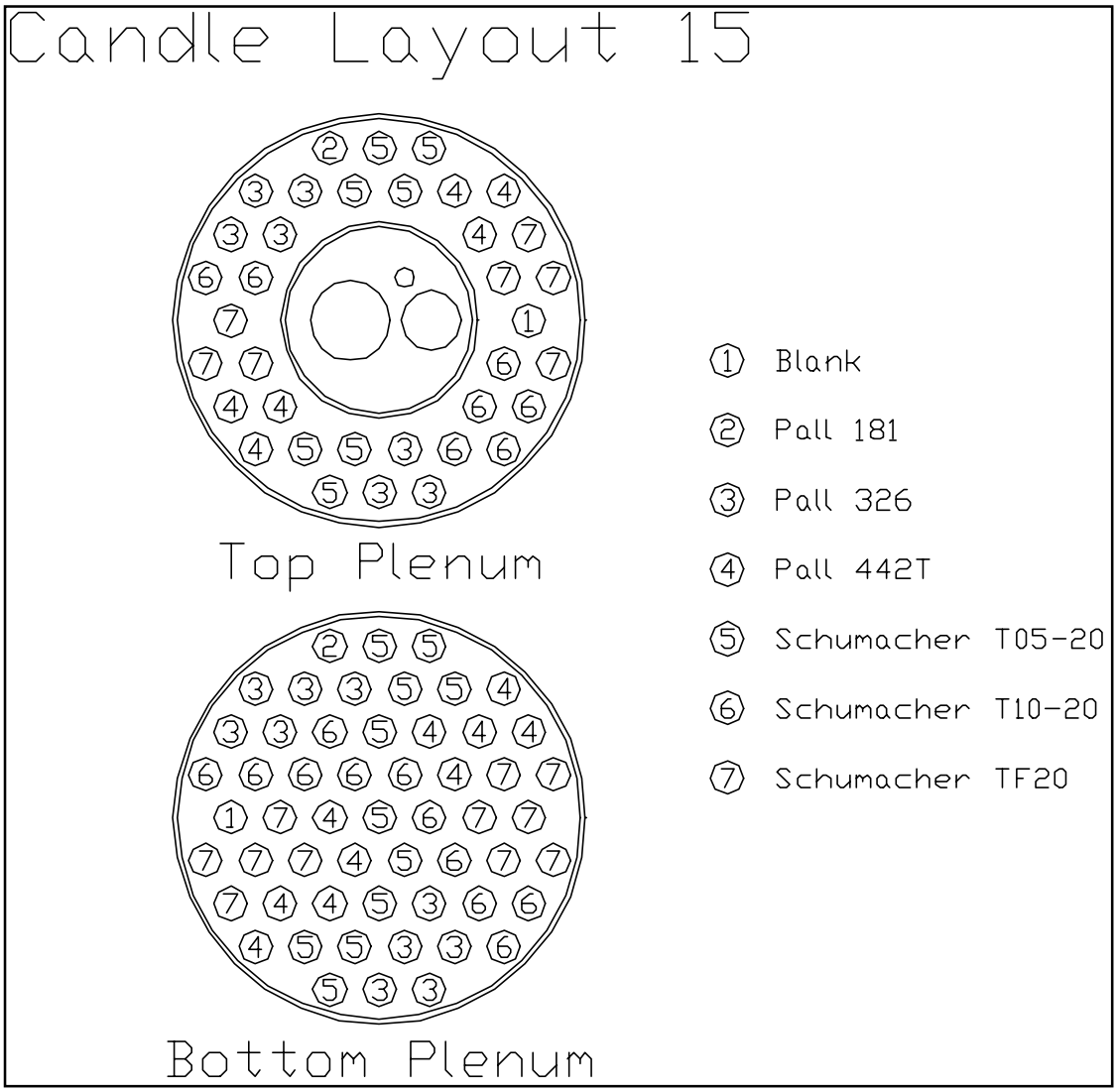

Figure 3.2-5 Filter Element Layout for GCT1B Through D – December 7 Through December 15 (Layout 15)

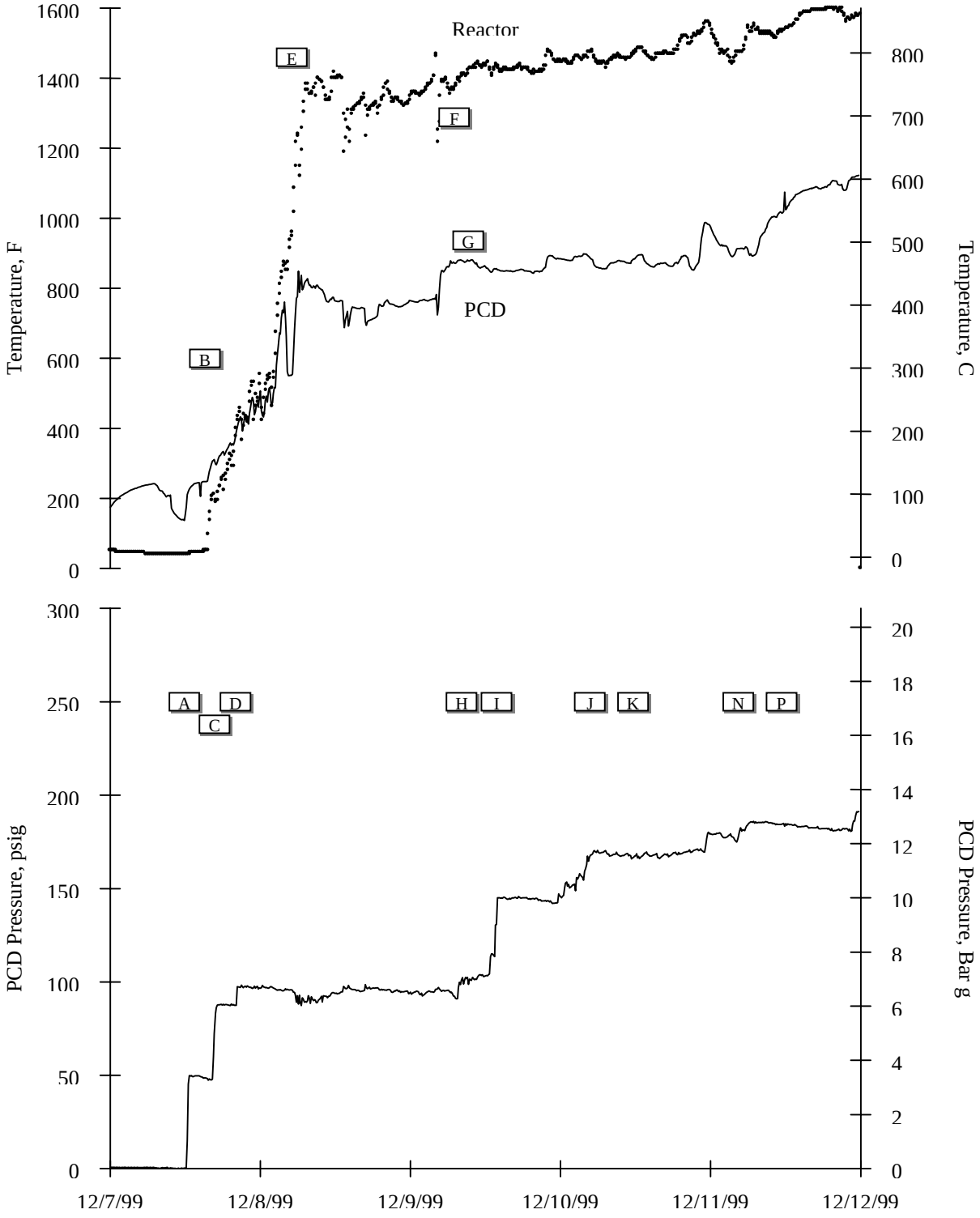

Figure 3.2-6 GCT1B Temperature and Pressure for December 7 Through December 12

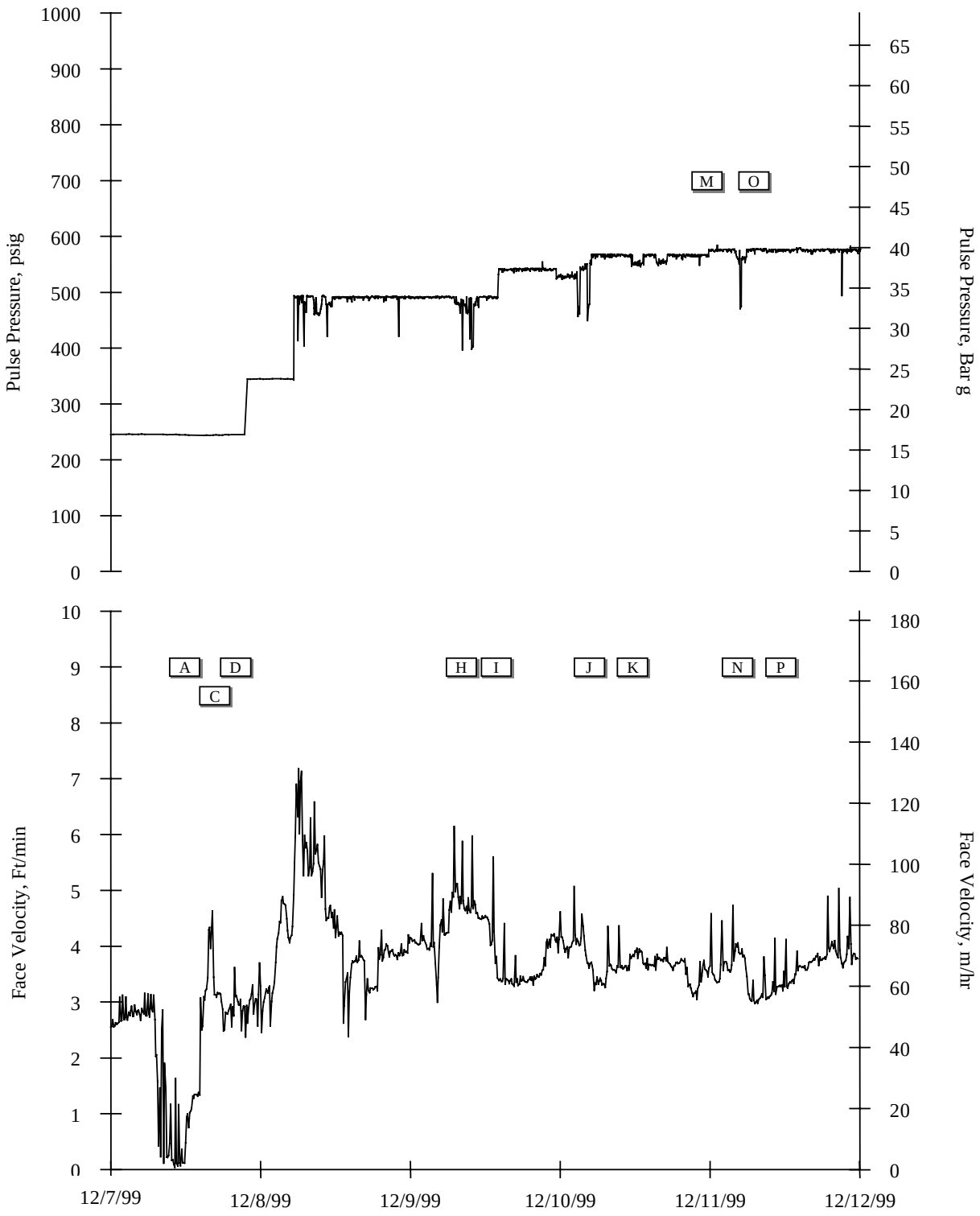

Figure 3.2-7 GCT1B Back-Pulse Pressure and Face Velocity for December 7 Through December 12

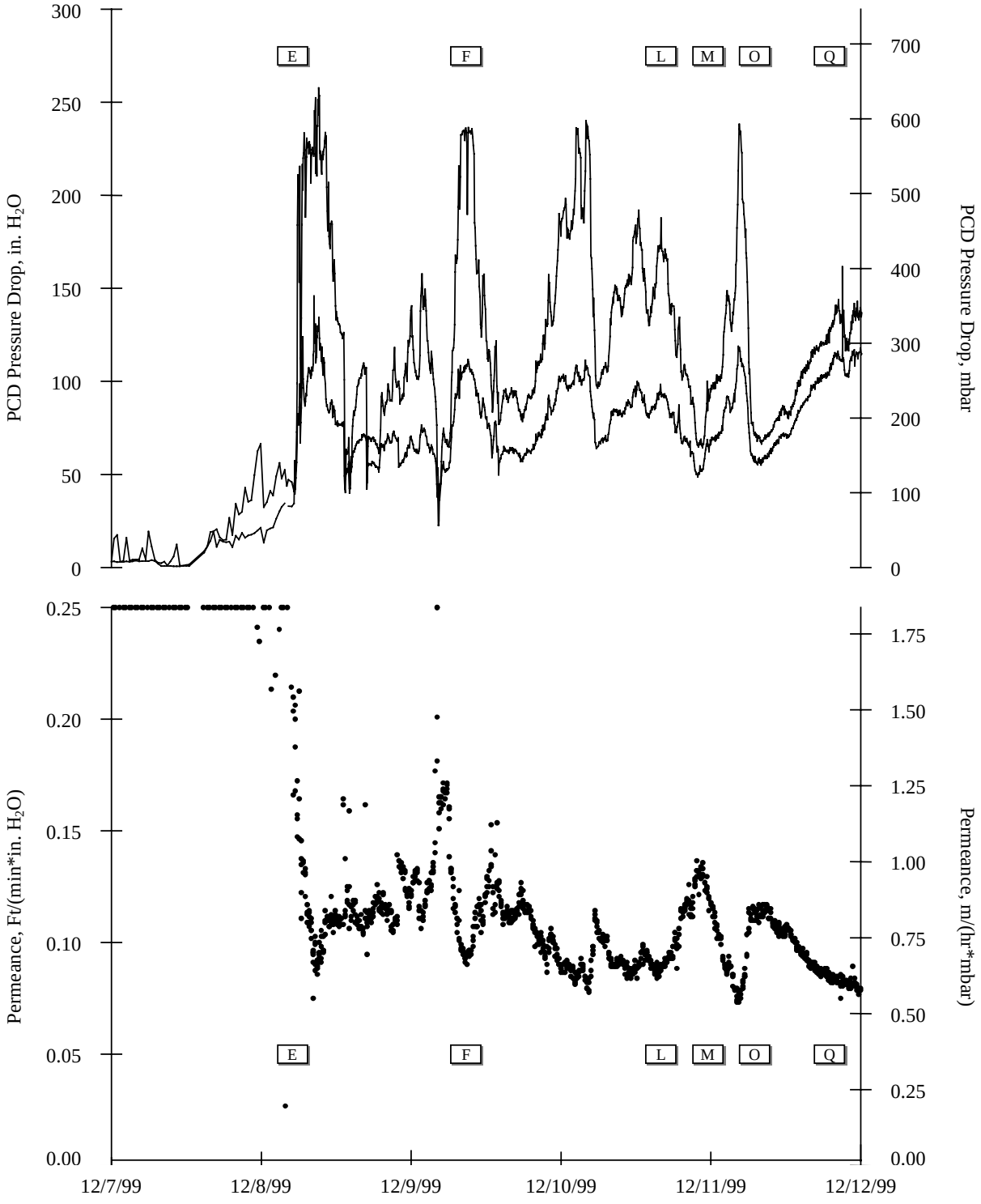

Figure 3.2-8 GCT1B Pressure Drop and Permeance for December 7 Through December 12

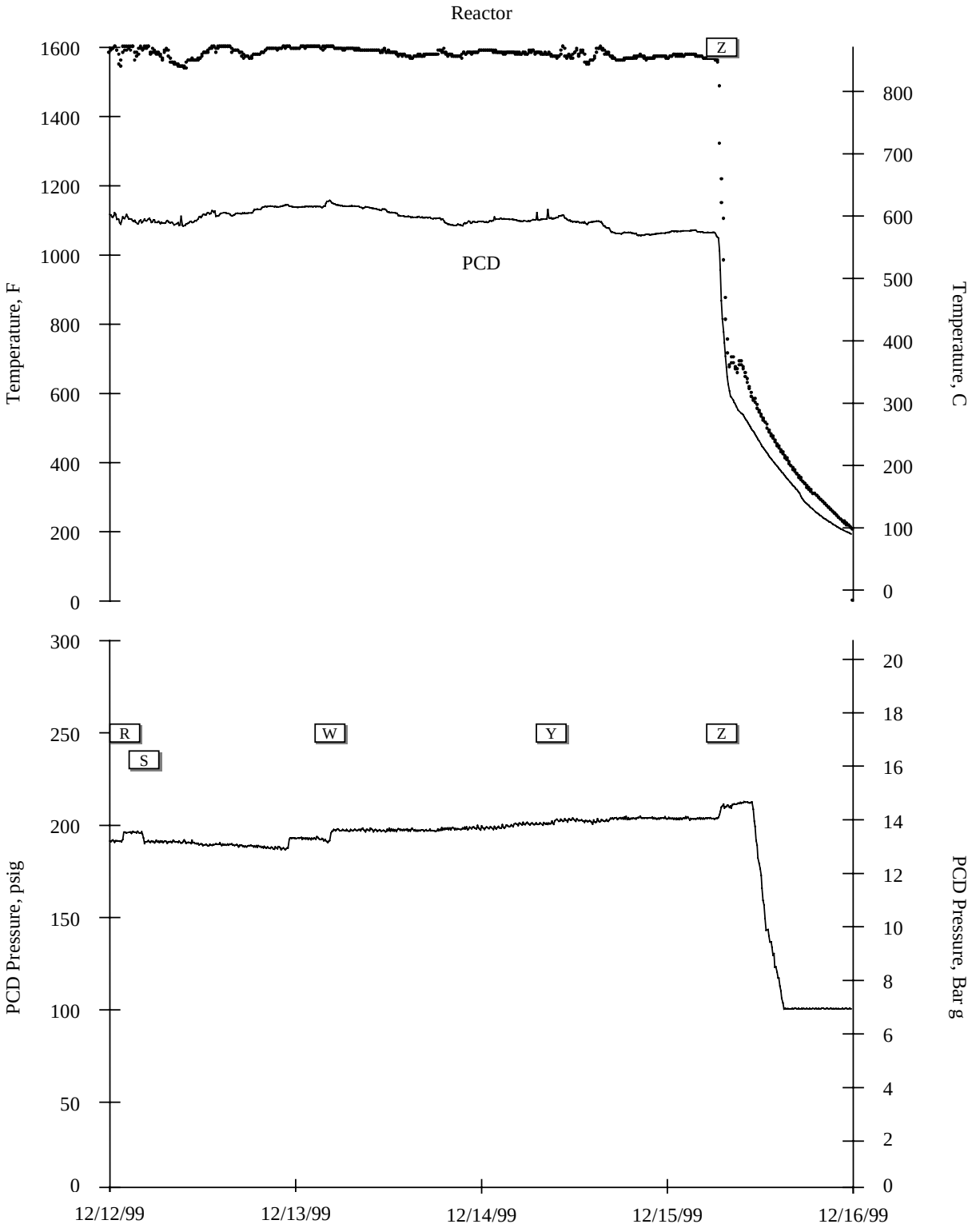

Figure 3.2-9 GCT1B Temperature and Pressure for December 12 Through December 16

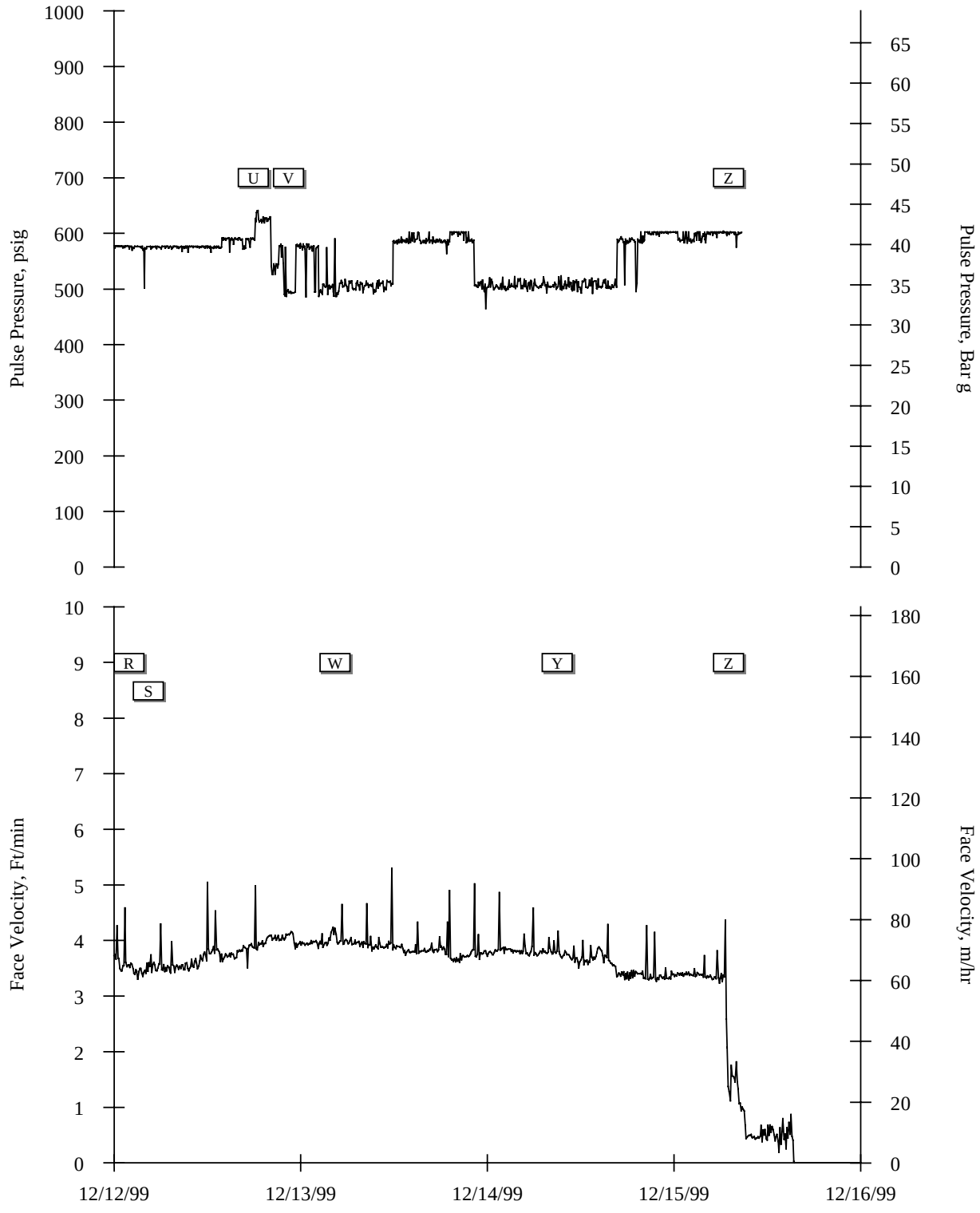

Figure 3.2-10 GCT1B Back-Pulse Pressure and Face Velocity for December 12 Through December 16

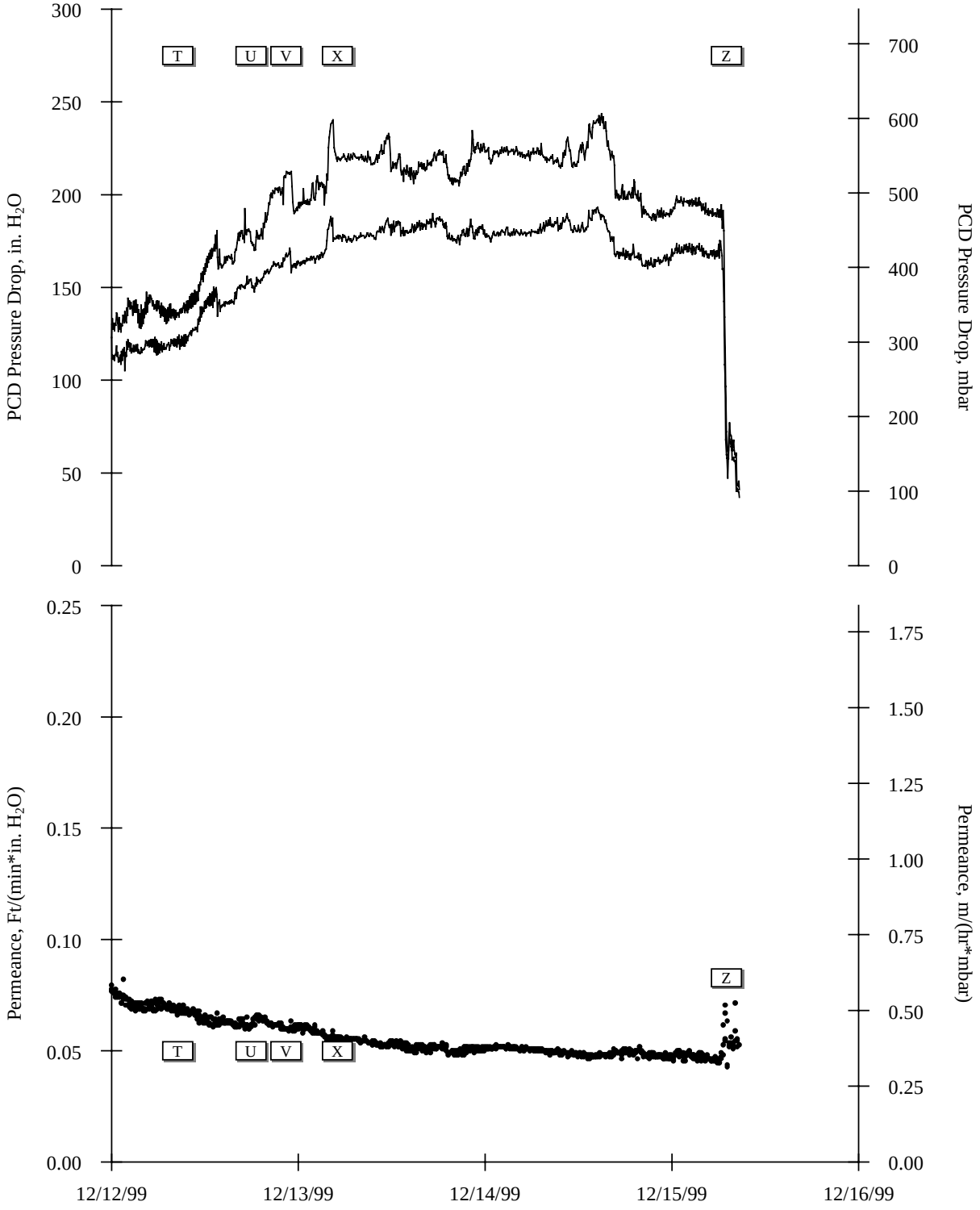

Figure 3.2-11 GCT1B Pressure Drop and Permeance for December 12 Through December 16

3.3 GCT1 INSPECTION REPORT

3.3.1 Introduction

The GCT1 test run was divided into two separate runs. The runs were categorized as GCT1A and GCT1B through D. The particulate control device (PCD) was inspected after each run. Generally, the inspections included visual examinations of the following:

- Char deposition.
- Filter element gaskets.
- Fail-safes.
- Filter elements.
- Filter element fixtures.
- PCD vessel and plenum assemblies.
- Auxiliary equipment.

After each GCT1 inspection the "lessons learned" were applied to determine what type(s) of filter elements would be installed in the subsequent run.

3.3.2 GCT1A Inspection

The PCD operated in gasification mode for a total of 63 hours on coal during the GCT1A run. During the operation the PCD experienced severe leakage and high-pressure drop (DP) across the tubesheet. On September 15, 1999, the DP reached the high-pressure-trigger point of 250 inH_2O before the back-pulse logic minimum-cycle time (3 minutes) could be completed. Had this trend continued the DP across the tubesheet would have reached unacceptable levels. Therefore, the system was shut down due to high DP and severe leakage through the PCD. The PCD was shut down in a clean state, which means that the back-pulse equipment continued to cycle after coal feed was stopped. The PCD was opened on September 30. GCT1A operating parameters are shown in Table 3.3-1. A tubesheet map and a filter element layout drawing (layout 14) are shown in Figures 3.3-1 and -2, respectively. The letters T and B preceding the numbers denote the top and bottom plenums, respectively.

3.3.2.1 Char Deposition

No char bridging was found and the char cake on the elements was generally thin—approximately 0.03 to 0.10 in. In some areas the cake was too thin to obtain meaningful thickness measurements. The char cake was the thickest on the Fairey microfiltrex metal elements. The outer screens on these elements appeared to be "plugged" with char. It was suspected that the char packed into the screens and caused the back-pulse cleaning to be less effective. There were slight char deposits on the filter holder flanges. The shroud and liner sections were generally clean (see Figure 3.3-3) and there was a shallow pile of char on the top plenum (see Figure 3.3-4).

3.3.2.2 Filter Element Gaskets

Evidence of leakage past and/or through the filter element gaskets was identified on almost every type of filter element. Potential leak paths were identified by first inspecting the area around the filter nut flanges for "gaps" or "holes" in the char cake that would indicate a localized higher velocity flow in the area (see Figure 3.3-5). After the filter elements were removed, each individual gasket was then visually inspected. Also, selected gaskets were cut open to visually inspect the internals of the gaskets. Gasket types are defined below.

Gasket Type	Gasket Location
Fiberfrax ring	Plenum-to-fail-safe (primary gasket)
Top donut	Fail-safe-to-element
Bottom donut	Filter nut-to-element
Sock gasket	Element-to-bottom donut gasket

All of the composite and ceramic filter elements except the 3M Oxide elements were installed using spacer nuts to avoid excessive compression of the gaskets and/or the filter element flanges. Since the metal elements could withstand higher forces during installation these elements were installed using a bolt torque of 100 in-lb, which corresponded to a higher compression on the gaskets. The bolts on the 3M Oxide elements were tightened without using a certain torque setting. (However, the bolt torque was below 100 in-lb.)

The top donuts were originally white. During the inspection it was noticed that the color of the gaskets had changed to light black and that the gasket fiber patterns could be seen on the flange sealing surfaces. The color of the gaskets used with the metal filter elements was a lighter color than the gaskets used with the composite or ceramic elements. The black color as well as the fiber patterns on the sealing surfaces, indicated that the very fine char particles penetrated through the structure of the gaskets. Since the top donuts were dust-tight rather than gas-tight seals this penetration of fine particles was expected. However, it appeared that the higher compression on the metal filter element gaskets minimized the particle penetration. It should be noted that some of the metal element top-donut gaskets showed signs of damage from the higher compression.

During inspection it was noticed that several of the fiberfrax gaskets were either completely missing or pieces of the gaskets were missing. The inspected fiberfrax rings were brittle, had a black color, and could easily be broken during disassembly. It appeared that the ring material had lost its resilience after exposure to the operating atmosphere and repeated back-pulse cycles, and did not continue to provide effective sealing. The rings that were "intact" generally had a clear indention caused by the initial compression between the fail-safe flange and the plenum, indicating that higher torques were used on these rings. All of the missing rings were from McDermott composite elements. The McDermott elements were installed with spacer nuts that limited the connecting bolt torque, and therefore limited the compression on the gaskets. However, it should be noted that even the higher-torqued fiberfrax rings used on the metal elements showed signs of leakage.

3.3.2.3 Fail-safes

Due to the high-outlet loadings the downstream end (top plates) of many of the fail-safes was dirty. Small fibers that appeared to be gasket material, and larger particles (1 to 5 mm) that appeared to be sand or a loose deposit layer, were found on the top plates of many of the bottom plenum fail-safes. On the top plenum, one of the fail-safes was damaged. The top plate broke loose from the fail-safe body and all of the contents were blown into the adjacent filter areas.

3.3.2.4 Filter Elements

Since GCT1A was the first gasification run there was concern that the PCD could be subjected to operational upsets that could lead to high-thermal transients. Therefore, element types that were proven to have high-thermal shock resistance and were mechanically robust were installed. A tubesheet map and a filter element layout drawing (layout 14) are shown in Figures 3.3-1 and -2, respectively. The letters T and B preceding the numbers denote the top and bottom plenums, respectively.

Despite the high-outlet loadings there were no broken filter elements. However, there was evidence of damage to several elements. Also, the inside (clean side) walls of all filter elements were dirty. Due to the severe leakage, char may have been entrained to the inside of the filter elements during back-pulse cleaning. Any char on the inside walls of the filter elements would have contributed to the higher pressure drop.

Specific observations regarding the filter elements are summarized below by element type. It should be noted that all observations are based only on visual inspections.

3M Oxide Composite – There were 11 3M Oxide filter elements installed. Evidence of possible leak paths was found on the body of several of the elements. Flow traces could be seen on the char cake of these elements (see Figure 3.3-6). Loose char was found inside five of the filter elements, which suggests that char passed through the element or beyond the element gaskets. The fail-safes on these 3M filter elements were generally dirty.

Honeywell PRD-66 Composite – Two PRD-66 filter elements were installed. Membrane spalling was found on both elements (see Figure 3.3-7). The spalling occurred in approximately 1-inch diameter "scales." The scales were aligned approximately 1 to 3 inches apart along the length of the filter element. No loose char was found inside these filter elements. However, the filter elements were loose prior to removal. This looseness indicated that the remaining compression on the gaskets may have been inadequate to seal against leakage.

Techniweave Composite – Two Techniweave filter elements were installed. Small "pinholes" (1 to 5 mm diameter) and several "clear spots" were found on the surface of one of the elements (see Figure 3.3-8). Very small openings could be seen between the fibers, when the char was brushed from the pinholes. There was also evidence of leakage around the fiberfrax ring, and loose char was found inside the damaged element. Both fail-safes installed above the Techniweave elements were dirty.

McDermott Composite – Eight McDermott filter elements were installed. Broken fibers were found on at least three of the elements (see Figure 3.3-9). McDermott has explained that the outer thin-fiber layer is not for filtration and that the filter element should not leak if the continuous fiber inside the body is not broken. All fiberfrax rings were either missing or broken. One of the fail-safes was dirty and one top donut was lightly covered with char. At least three of the filter elements were loose prior to removal.

IF&P REECER Monolithic Silicon Carbide (SiC) – One IF&P REECER filter element was installed. There was no evidence of damage to this element. However, the fiberfrax ring was missing and the element was loose prior to removal.

Fairey Microfiltrex Metal (316L SS, Inconel 601, Hastelloy HR) – Twenty-eight Fairey filter elements were installed. On at least two of the elements there was evidence of possible leakage at the weld between the filtration media and the solid metal hardware (see Figure 3.3-10). Loose char was found inside three of the filter elements.

Experiments have shown that nickel-based porous-metal filter elements may be subject to gaseous corrosion, mainly by sulfidation, in highly reducing, sulfur-bearing gasification atmospheres at temperatures above approximately 500°C (reference 1). Therefore, there was concern that the nickel-based metal elements may have "blinded" and contributed to the high-pressure drop. However, no determination could be made by visual inspection. Further testing will be required to confirm or deny the presence of the sulfidation reaction.

Pall Metal (310 SS, Iron Aluminide, Hastelloy X) – Thirty-three Pall filter elements were installed. Two of the elements showed evidence of possible leakage at the weld between the filtration media and the solid hardware. A small amount of loose char was found inside one of the iron aluminide filter elements. No determination has been made regarding the possibility that the nickel-based metal elements "blinded" due to sulfidation.

Per the manufacturer's recommendation, the Pall metal elements were rigidly supported to minimize vibration and to hold the elements in place in the event of a failure. The Pall elements were supplied with a pin at the bottom of the element. These pins were used to connect groups of elements to a common support post. The inspection showed that the support posts and support pins performed acceptably (see Figure 3.3-11).

3.3.2.5 PCD Vessel and Plenum Assemblies

With the PCD head removed, the shroud and liner sections were visually inspected from the top of the PCD vessel. Both the shroud and liner sections were generally clean (see Figure 3.3-3). The liner section repairs that were performed after the TC05 test campaign were still intact. There was no obvious change in the liner shape. The insulation on the outside diameter of the tubesheet was covered with char (see Figure 3.3-12). It appeared that there was circulation of gas on the outside of this insulation, which suggests that the insulation should have been thicker to minimize the gap between the insulation and the PCD head.

3.3.2.6 Auxiliary Equipment

There was concern initially that oxygen breakthrough could cause a fire in the PCD. Six thermocouples were installed on individual filter elements in order to monitor the local temperatures. During inspection, the thermocouples were found to be in acceptable condition.

In an attempt to characterize the vibration of the PCD plenums and filter elements, vibration equipment was installed at location B2. Two accelerometers and two strain gauges were mounted to the element, and two accelerometers were mounted to the bottom plenum above the element. During inspection it was determined that all of the accelerometers remained tightly connected to their respective mounts, but both strain-gauge lead-wire connections were found to be damaged.

The wires for the vibration and temperature measurement equipment were routed from the dirty side of the PCD to the clean side through the plenum. Conax fittings with lava sealant were used to seal these wires and maintain the pressure boundary inside the PCD. Each fitting was designed to seal seven individual 62-mil wires. Sixty-mil, solid-metal wire was used to fill two unused holes in one of the Conax fittings. It was assumed that the fitting could accommodate the smaller wire. However, a potential leak path was found in this particular Conax fitting. The smaller wire may have caused the leakage in this Conax fitting. Upon removal, it was noticed that loose char was inside the support post that contained this fitting.

Compared to previous combustion runs, the back-pulse equipment was cycled much more frequently during the GCT1A gasification run. Due to the high number of cycles, the back-pulse valves were removed and inspected for wear. It was determined that there was very little wear on the equipment. Certain seals were replaced while the equipment was broken down and the valves were then put back into service.

3.3.2.7. GCT1A Inspection Summary

No char bridging was found. The char cake on the filter elements was relatively thin.

There was evidence of leakage past and/or through the filter element gaskets on almost every type of element. Leakage past the fiberfrax primary gaskets may have caused the severe leakage in the PCD. Composite elements that were installed with spacer nuts, such as the McDermott elements, often had damaged or missing fiberfrax gaskets. The spacer nuts limited the amount of compression on these gaskets. To address this leakage problem, alternate primary gasket designs and alternate filter element fixture designs were tested during the subsequent GCT1B through D run.

All of the filter elements were dirty inside. Char on the inside walls of the filter elements may have contributed to the higher pressure drop.

The IF&P REECER monolithic SiC element did not show any signs of damage. The composite elements showed signs of surface damage and possible leak paths. There were potential leak paths on a few of the metal elements at the weld between the filtration media and the solid-metal

hardware. There was concern (not yet validated) that the nickel-based metal elements may have "blinded" due to a sulfidation reaction and contributed to the higher pressure drop. Also, the outer screens on the Fairey microfiltrex metal elements appeared to hold thicker residual char cake and may have contributed to the higher pressure drop. Therefore, it was decided that the composite elements, Fairey microfiltrex metal elements and other nickel-based metal elements would not be used in subsequent gasification runs until further tests could be performed on the GCT1A elements. Monolithic SiC elements were used for the GCT1B through D gasification run.

There was one broken fail-safe on the top plenum. The top plate broke loose from the fail-safe body and all of the contents were blown into the adjacent filter areas. To guard against this type failure, stiffener rings were added to the top plate of all fail-safes prior to the GCT1B through D gasification run.

The insulation on the outside diameter (OD) of the tubesheet was covered with char (Figure 3.3-12). It appeared that there was circulation of gas on the outside of this insulation, which suggests that the insulation should have been thicker to minimize the gap between the insulation and the PCD head.

The liner section repairs performed after the TC05 test campaign were still intact. There was no obvious change in the liner shape. It was decided to continue to use the existing liner sections and to delay the planned modifications to the PCD vessel refractory.

3.3.3 GCT1B Through D Inspection

The PCD operated in gasification mode for a total of 169 hours on coal during the GCT1B through D run. Compared to the GCT1A run, the PCD leakage was much lower. However, the outlet loadings continued to be above the target value of 1 ppmw. Due to possible plugging in the FD0502 fines screw cooler, the system was shut down on December 15, 1999. The PCD was shut down in a clean state, which means that the back-pulse equipment continued to be cycled after coal feed was stopped. The PCD was opened on January 19, 2000. GCT1B through D operating parameters are shown in Table 3.3-2.

In an attempt to limit the leakage past the fiberfrax primary gasket, the following changes were made prior to the GCT1B through D run:

- An alternate filter-element-fixture design called a modified filter holder was used on 14 of the elements. These modified filter holders are described below.

- Siemens Westinghouse supplied a "lapped-construction" gasket that was used to replace the original fiberfrax primary gasket on all of the filter elements.

3.3.3.1 Filter Element Fixtures

Each of the fixture gasket types potentially required different compression values to adequately seal. However, with the conventional filter nut design this was not possible since the gaskets

were compressed in series with one set of bolts. Therefore, the modified filter holder filter-element-fixture design was implemented to address this issue.

The modified filter holder design added an additional part called a "fail-safe holder" that allowed the primary gasket and the element flange gasket to be compressed separately. With this design the primary gasket was compressed by the fail-safe holder bolts and the element flange gasket was compressed by the "new filter nut" bolts.

During installation no spacer nuts were used that would have limited the compression on the filter element gaskets. All conventional filter nut bolts were torqued to 70 in-lb. The new filter nut bolts were also torqued to 70 in-lb. Since the fail-safe holder bolts could be torqued independently of the filter element they were torqued to 120 in-lb in order to get as much compression on the newly designed primary gaskets as possible without damaging the gaskets. During inspection the remaining bolt torque was checked on random conventional and modified fixture designs to determine if the modified filter holders continued to provide greater sealing compression. The remaining torques are shown in Figures 3.3-13, -14, and -15. The following observations were made:

- The remaining torque on the conventional filter nut bolts generally ranged from below 20 to 60 in-lb per bolt. This is the remaining torque that was available to compress both the primary gasket and the element flange gasket in series. (It should be noted that 20 in-lb was the lowest setting on the torque wrench. Several of the bolts had torques below 20 in-lb.)

- The remaining torque on the new filter nut bolts generally ranged from 40 to 60 in-lb. This is the remaining torque that was available to compress the element flange gasket.

- The remaining torque on the fail-safe holder bolts generally ranged from 60 to 80 in-lb. This is the remaining torque that was available to compress the newly designed primary gasket.

During the GCT1B through D disassembly two of the new filter nuts bound slightly on the fail-safe holders. Otherwise, there were no significant problems with the mechanical fit-up and operation of the modified filter holders.

3.3.3.2 Filter Element Gaskets

The conventional filter nut fixtures and the modified filter holder fixtures used two different gasket arrangements. The gasket types are defined below.

Gasket Type (Conventional Filter Nut)	Gasket Location
Lapped-construction	Plenum-to-fail-safe (primary gasket)
Top donut	Fail-safe-to-element
Bottom donut	Conventional filter nut-to-element
Sock gasket	Element-to-bottom donut gasket

Gasket Type (Modified Filter Holder)	Gasket Location
Lapped-construction	Plenum-to-fail-safe (primary gasket)
Top donut	Fail-safe-to-fail-safe holder
Bottom donut (No. 1)	Fail-safe holder-to-element
Bottom donut (No. 2)	New filter nut-to-element
Sock gasket	Element-to-bottom donut gasket (No. 2)

During the GCT1A inspection there was evidence that the fiberfrax gasket did not provide effective sealing after exposure to the operating atmosphere and repeated back-pulse cycles. Therefore, a lapped-construction gasket was used to replace the original fiberfrax primary gasket on all of the filter elements prior to the GCT1B through D run.

The new lapped-construction primary gasket provided better sealing than the original fiberfrax ring. There were no obvious leak paths in the area of the filter nut flanges that would have indicated leakage past the primary gaskets. The element flange gaskets and the new lapped-construction gaskets had changed from a white color to a light-black color, and the gasket-fiber patterns could be seen on the flange-sealing surfaces. The black color and the fiber patterns on the sealing surfaces indicated that the very fine char particles penetrated through the structure of the gaskets. Since the element flange gaskets and the new lapped-construction gaskets were dust-tight rather than gas-tight seals this penetration of fine particles was expected.

Five elements (T5, T8, T21, T22, and T27) showed signs of char in the area of the top-donut gasket. In each case, the top donut and/or the sealing surfaces were dirty. It should be noted that each of these elements was held with a conventional filter-nut fixture.

3.3.3.3 Filter Elements

Based on the experience gained during the GCT1A gasification run, monolithic SiC elements were installed for the GCT1B through D gasification run. A filter-element-layout drawing (layout 15) is shown in Figure 3.3-16.

The monolithic SiC elements performed well. There were no broken or damaged filter elements. No loose char was found inside any of the elements and all of the elements were considered to be "clean" inside by visual inspection.

3.3.3.4 Fail-safes

One of the fail-safe top plates was damaged during the GCT1A run. Therefore, in an effort to avoid this type of failure, a stiffener ring was added to the top plate of all fail-safes prior to the GCT1B through D run. There were no damaged fail-safes during this run.

Approximately half of the fail-safes had loose particles on the top plates. Fail-safe contents were found on the top plates of fail-safes T5, T6, T9, and T11. Since no fail-safes were damaged during the GCT1B through D run it was assumed that these contents came from the fail-safe that was damaged during the GCT1A run.

3.3.3.5 Char Deposition

Compared to the GCT1A char cake, the GCT1B through D char cake was approximately twice as thick (see Section 3.4).

The filter element char cake measured a 0.07- to 0.24-in. thickness. The char cake on the filter elements appeared to have two distinct layers. The top layer had a "fluffy" appearance and could generally be brushed from the element. The bottom layer was much more adherent and could not be removed by brushing (see Section 3.4). Looking at the elements on the outer periphery of each plenum, it was noticed that the build-up was generally thinnest on the leading edge of the elements. It was also common for these outer periphery elements to have build-up that was thicker in the middle of the element than on the ends of the element. Distinct "peaks" and "valleys" could be seen in the char cake on all of the elements (see Figures 3.3-17 and -18).

There was heavy char accumulation in the area of the top plenum as shown in Figures 3.3-19 and -20. It should be noted that the build-up was not as heavy on the bottom plenum wall and the bottom ash shed.

The accumulated char on the inside diameter (ID) of the shroud was approximately 1 in. thick and there were distinct flow "swirl patterns" in the char (see Figure 3.3-21). The deposits on the liner sections were also very heavy.

3.3.3.6 PCD Vessel and Plenum Assemblies

With the PCD head removed the shroud and liner sections were visually inspected from the top of the PCD vessel. The liner section repairs that were performed after the TC05 test campaign were still intact. There was no obvious change in the liner shape.

Compared to the GCT1A inspection, the tubesheet insulation was not as dirty (see Figure 3.3-22). Based on the GCT1A experience, additional insulation thickness had been added to the OD of the tubesheet prior to the GCT1B through D run. The additional insulation minimized the gap and limited the circulation of gas between the insulation and the PCD head.

Selected tubesheet welds were inspected to verify that there were no cracks and possible leak paths through the tubesheet. Each weld was dye-penetrant tested. No weld cracks and/or leaks were found.

There was concern that oxygen breakthrough could cause the accumulated char on the top plenum to ignite. Therefore, an "ash shed" was added to the top plenum prior to the GCT1B through D run (see Figure 3.3-20). During inspection it was noticed that there was some char build-up on the ash shed. However, the ash shed generally performed adequately.

Prior to the GCT1B through D run, the plasite coating on the upper manway nozzle and door was replaced to prevent corrosion in this area. After the run a visual inspection showed that the plasite coating was still intact.

3.3.3.7 Auxiliary Equipment

Fourteen thermocouples were installed on individual filter elements in order to monitor the local temperatures. Seven thermocouples were installed on both the top and bottom plenum elements. During the run all seven of the top plenum thermocouples and three of the bottom plenum thermocouples periodically gave errant readings. During disassembly it was noticed that several of the thermocouple wires may have been damaged inside the plenums.

The thermocouple wires were routed from the dirty side of the PCD to the clean side through the plenum. Conax fittings with lava sealant were used to seal these wires and maintain the pressure boundary inside the PCD (see Figure 3.3-23). One Conax fitting per plenum for a total of two Conax fittings were used. Each fitting was designed to seal seven individual 62-mil wires. There was evidence of leakage around four of the fourteen thermocouple wires.

There was tar accumulation on the back-pulse pipes (see Figure 3.3-24). The tar was removed to verify that there was no corrosion in this area and none was found.

Inspection showed that the 304 SS instrument tubing that was routed through Flange 12A into the PCD head was corroded and/or broken. These instrument tubing lines inside the PCD head were replaced with Hastelloy C-276 tubing during the outage.

3.3.3.8 GCT1B Through D Inspection Summary

The PCD leakage experienced during the GCT1B through D run was much lower than the GCT1A leakage. However, the outlet loadings continued to be above the target value of 1 ppmw.

There was heavy char build-up throughout the PCD. Compared to the GCT1A char cake, the GCT1B through D char cake was approximately twice as thick (see Section 3.4). The filter element char cake appeared to have two distinct layers, with the "bottom layer" being very adherent and difficult to remove (see Section 3.4).

The Conax fittings that were used to seal the filter element thermocouple wires continued to show signs of leakage. For subsequent runs it was decided that the thermocouple wires should not be routed through the clean side of the PCD.

Based on visual inspections the monolithic SiC elements performed well. There were no broken or damaged filter elements; the decision was made to install monolithic SiC elements for the GCT2 gasification run.

The new lapped-construction primary gasket supplied by Siemens Westinghouse provided good sealing compared to the original fiberfrax ring. It was decided that these lapped-construction gaskets would continue to be used on subsequent runs.

The modified filter holder element fixtures allowed the primary gasket and the element flange gasket to be compressed separately. This design also resulted in higher residual torques on both gaskets after repeated back-pulse cycles. Consequently, none of the elements supported by the modified filter holder fixtures showed signs of char in the area of the element flange gasket. It was decided that modified filter holders would be used throughout both plenums in the subsequent GCT2 gasification run.

The stiffener rings that were added to the top plates of all fail-safes performed well. It was decided that stiffener rings would be added to all fail-safes in subsequent runs.

The liner section repairs that were performed after the TC05 test campaign were still intact. There was no obvious change in the liner shape. It was decided to continue to use the existing liner sections and to delay the planned modifications to the PCD vessel refractory.

3.3.4 References

1. Nieminen, M., Kangasmaa, K., Kurkela, E., and, Stahlberg, P., "Durability of Metal Filters in Low-Sulphur Gasification Gas Conditions," High-Temperature Gas Cleaning, Institut fur Mechanische Verfahrenstechnik und Mechanik der Universitat Karlsruhe, 1996.

Table 3.3-1

GCT1A PCD Operating Parameters

Element Layout	Layout 14 (Figure 3.3-2)
Filtration Area	231.9 ft^2
Back-Pulse Pressure	400 to 450 psig Above Reactor Pressure (Approximate)
Back-Pulse Timer	Set to 10 Min (Varied Between 3 and 10 Min)
Back-Pulse High Pressure Trigger Point	200 to 250 inH_2O
Back-Pulse Valve Open Time	0.2 sec (Experimented With 0.15 and 0.5 sec)
Inlet Gas Temperature	800 to 925°F (Approximate)
Face Velocity	3.5 to 6.0 Ft/min (Approximate)
Baseline DP	50 to 180 inH_2O (Approximate)
Peak DP	170 to 250 inH_2O
Inlet Loading (SRI Sampling)	17,700 to 64,400 ppmw
Outlet Loading (SRI Sampling)	266 to 547 ppmw
Coal/Sorbent	PRB/Dolomite

Table 3.3-2

GCT1B Through D PCD Operating Parameters

Element Layout	Layout 15 (Figure 3.3-16)
Filtration Area	252.8 ft^2 (9% Increase Compared to GCT1A)
Back-Pulse Pressure	380 to 500 psig Above Reactor Pressure
Back-Pulse Timer	Set to 5 min
Back-Pulse High Pressure Trigger Point	250 to 275 inH_2O
Back-Pulse Valve Open Time	0.2 sec
Inlet Gas Temperature	700 to 1,150°F (Approximate)
Face Velocity	3.0 to 6.0 ft/min (Approximate)
Baseline DP	50 to 190 inH_2O (Approximate)
Peak DP	50 to 250 inH_2O (Approximate)
Inlet Loading (SRI Sampling)	11,000 to 70,700 ppmw
Outlet Loading (SRI Sampling)	6.3 to 81 ppmw
Coal/Sorbent	PRB/Dolomite PRB/Alabama Limestone Illinois No. 6/Alabama Limestone Illinois No. 6/Ohio Limestone Alabama Calumet (No Sorbent)

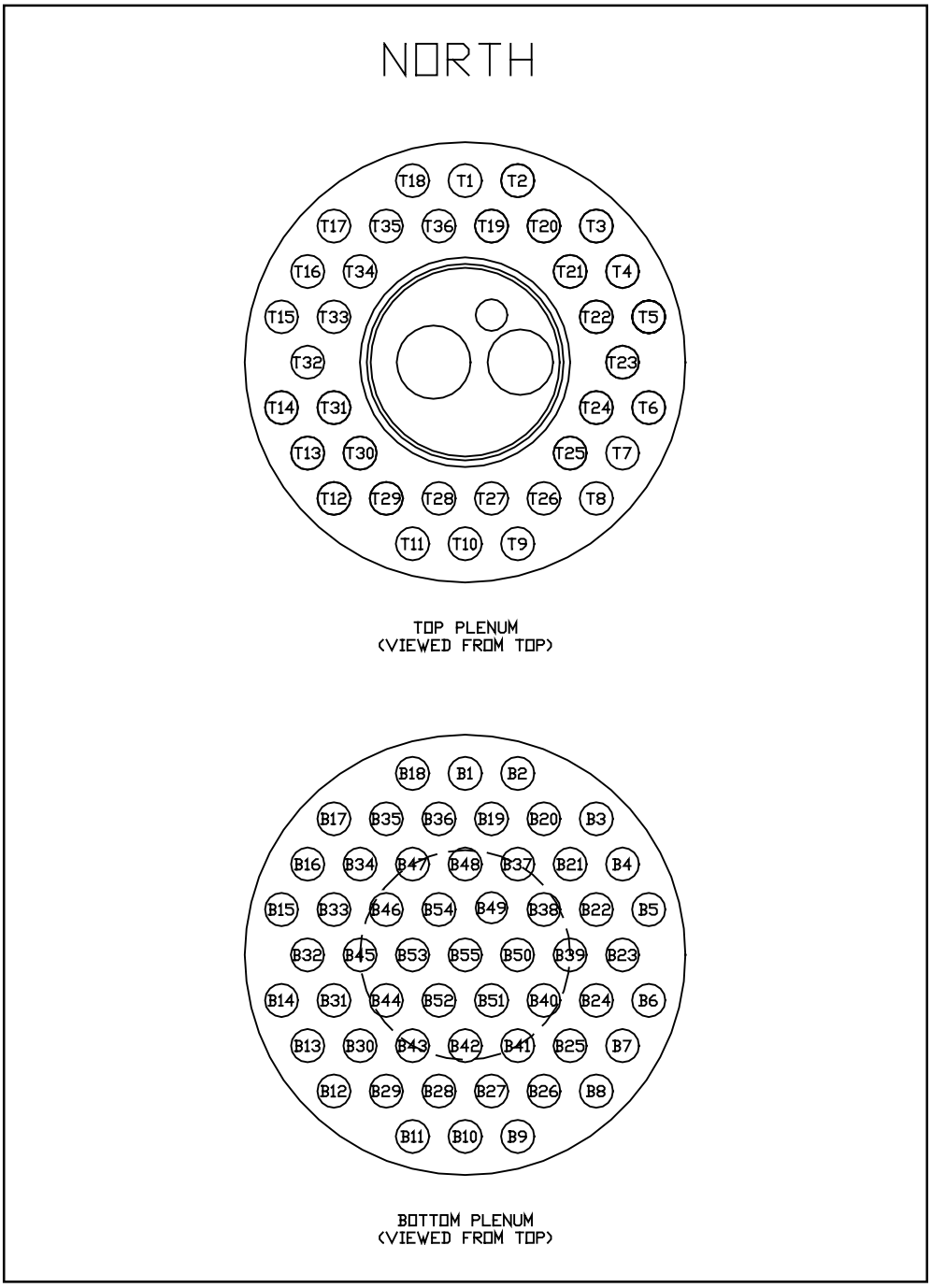

Figure 3.3-1 Tubesheet Layout

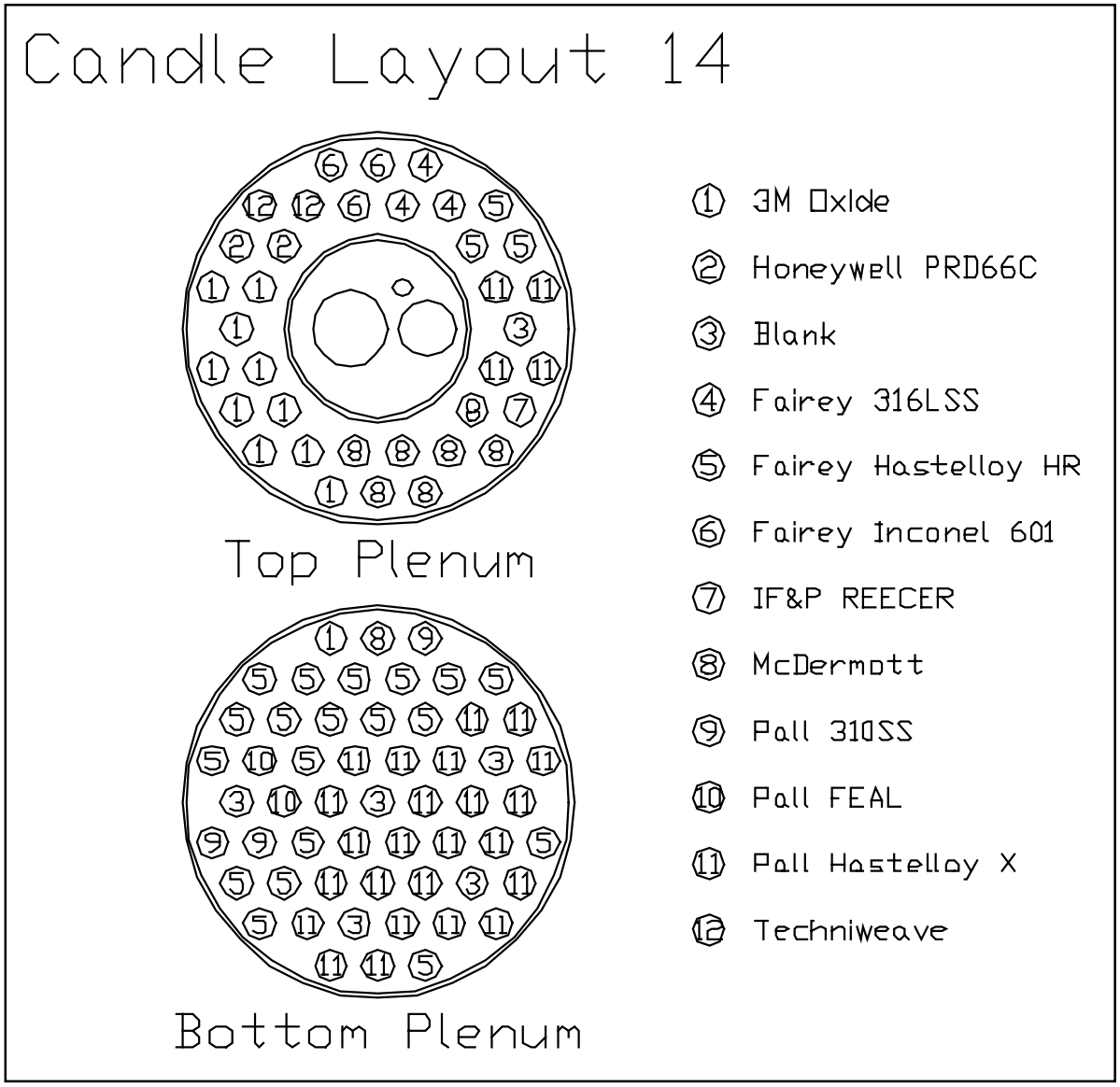

Figure 3.3-2 Filter Element Layout 14

Figure 3.3-3 Shroud and Liner (GCT1A)

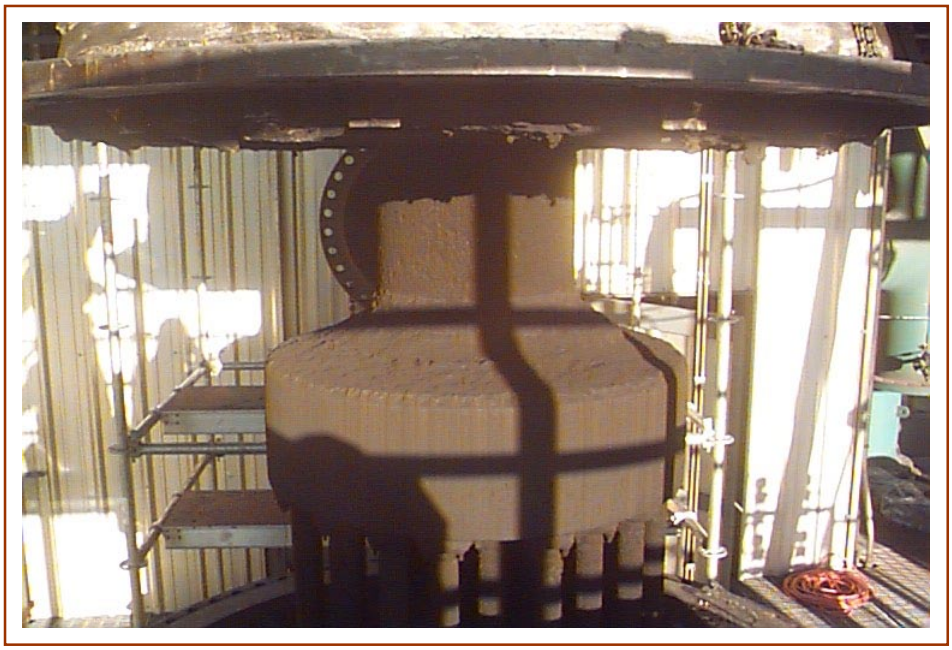

Figure 3.3-4 Char on Top Plenum (GCT1A)

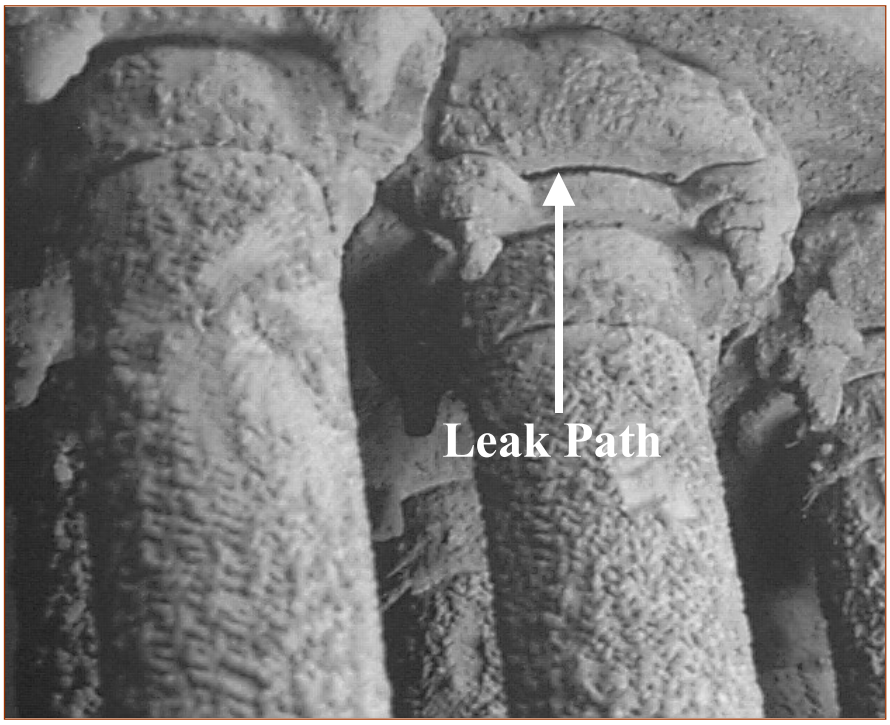

Figure 3.3-5 Potential Leak Paths Around Filter Nut Flanges

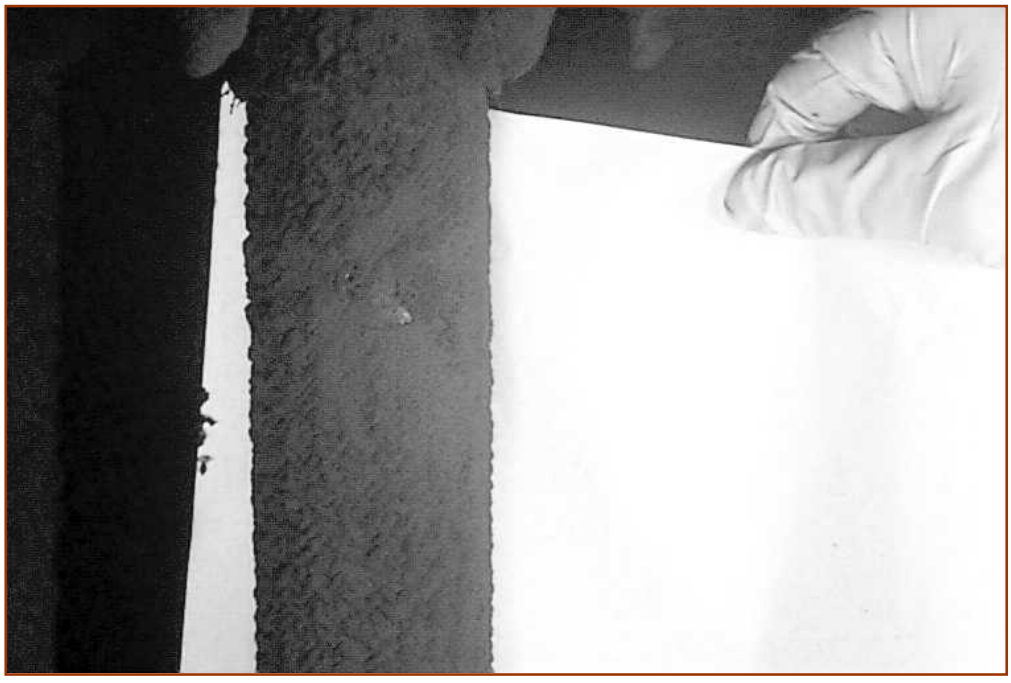

Figure 3.3-6 Potential Leak Paths on 3M Oxide Composite Filter Element (T14)

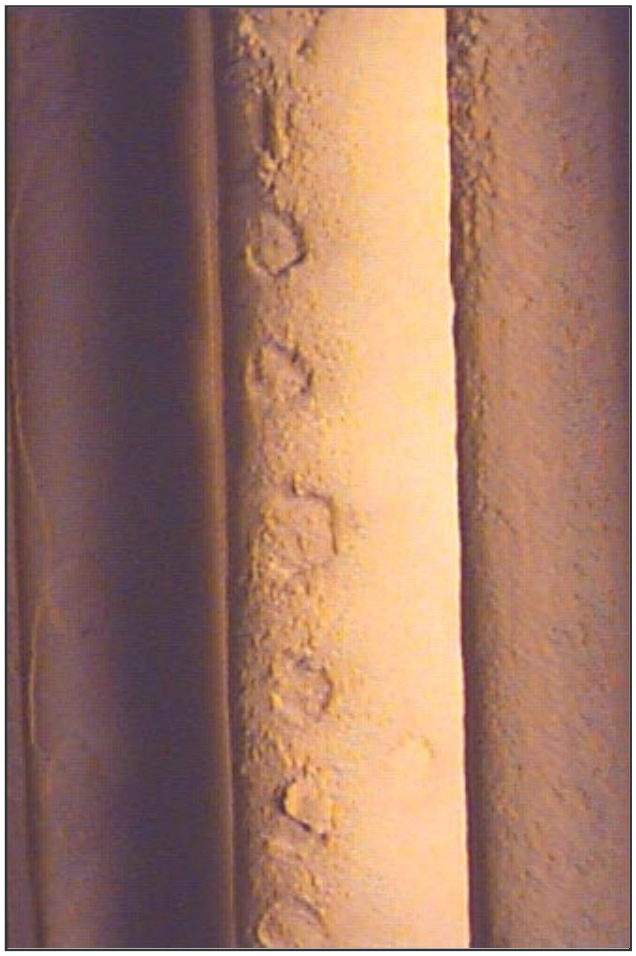

Figure 3.3-7 Membrane Spalling on Honeywell PRD-66 Composite Element (T16)

Figure 3.3-8 Possible Leaks on Techniweave Composite Filter Element (T17)

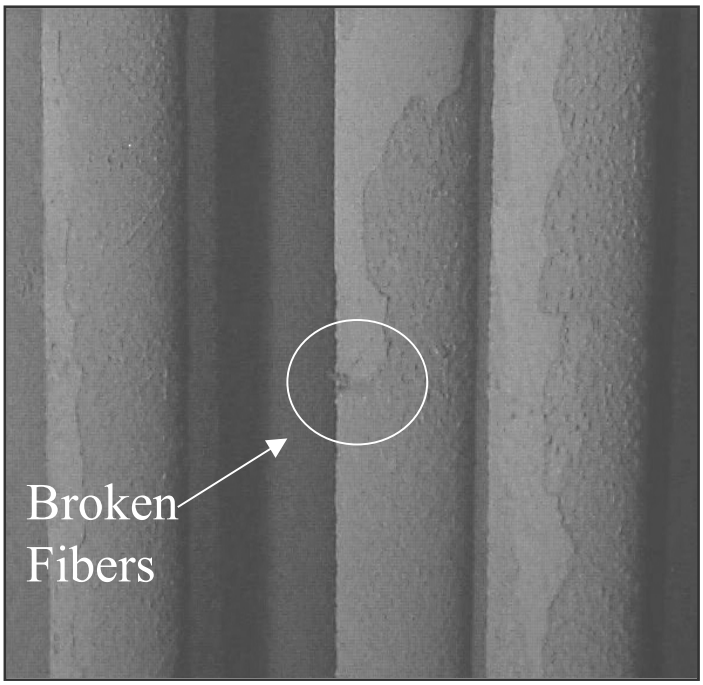

Figure 3.3-9 Broken Fibers on McDermott Composite Filter Element (T26)

Figure 3.3-10 Potential Leak Path on Fairey Microfiltrex Metal Element (B35)

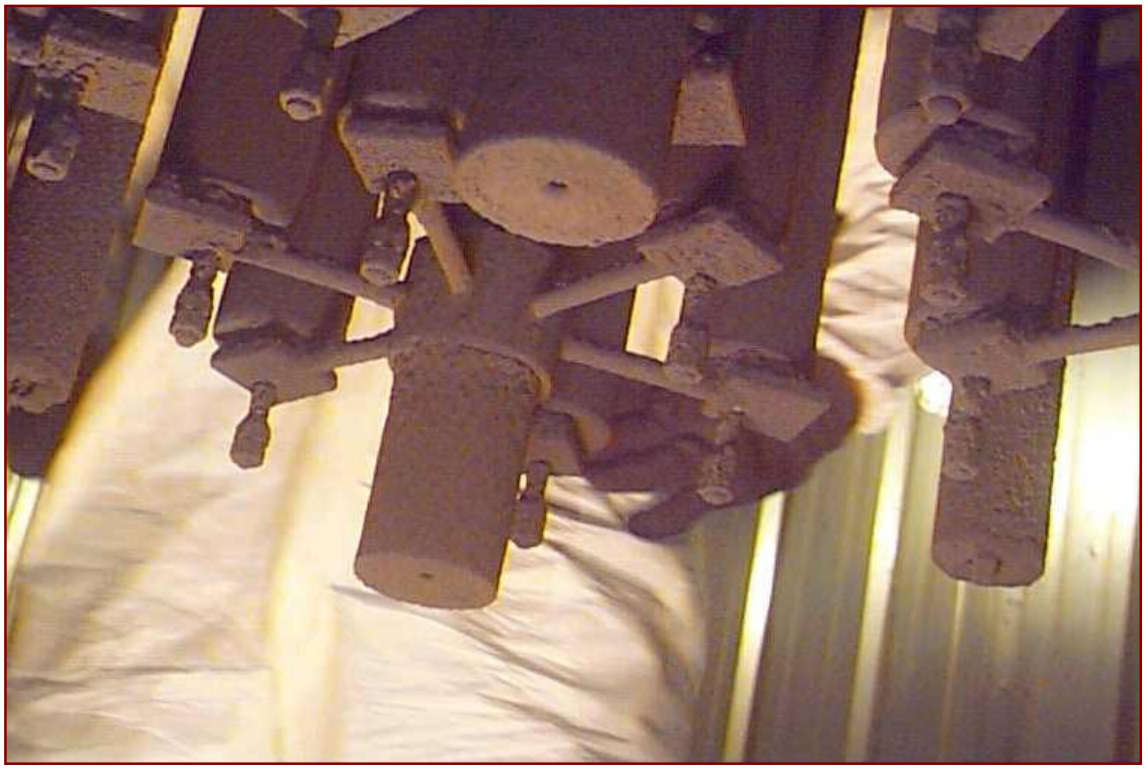

Figure 3.3-11 Rigid Supports for Pall Metal Elements (Bottom View)

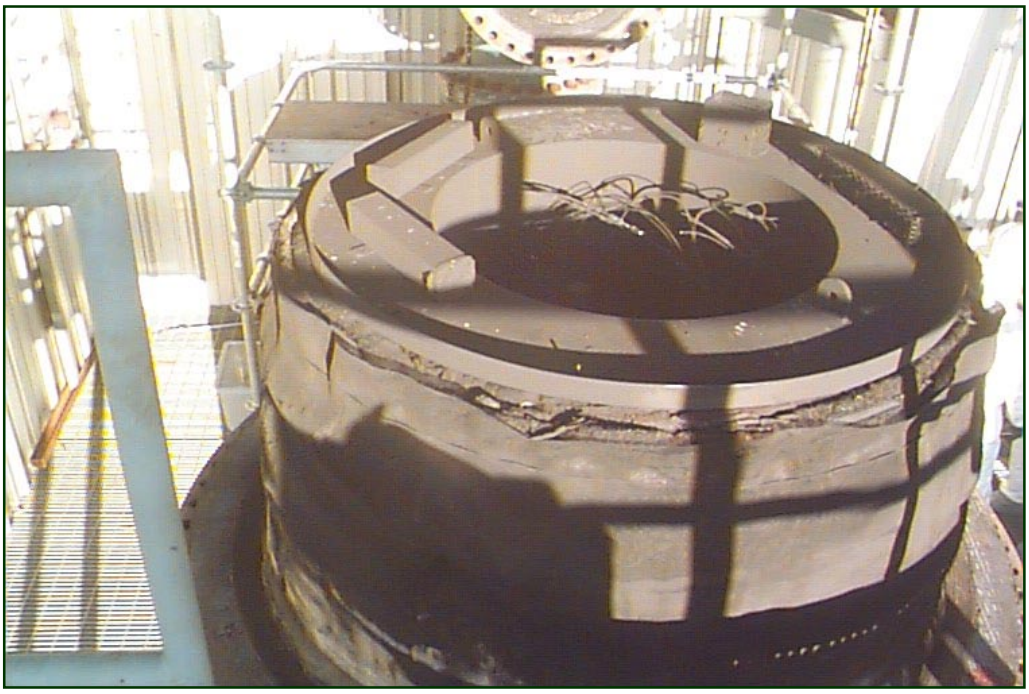

Figure 3.3-12 Tubesheet Insulation Covered With Char (GCT1A)

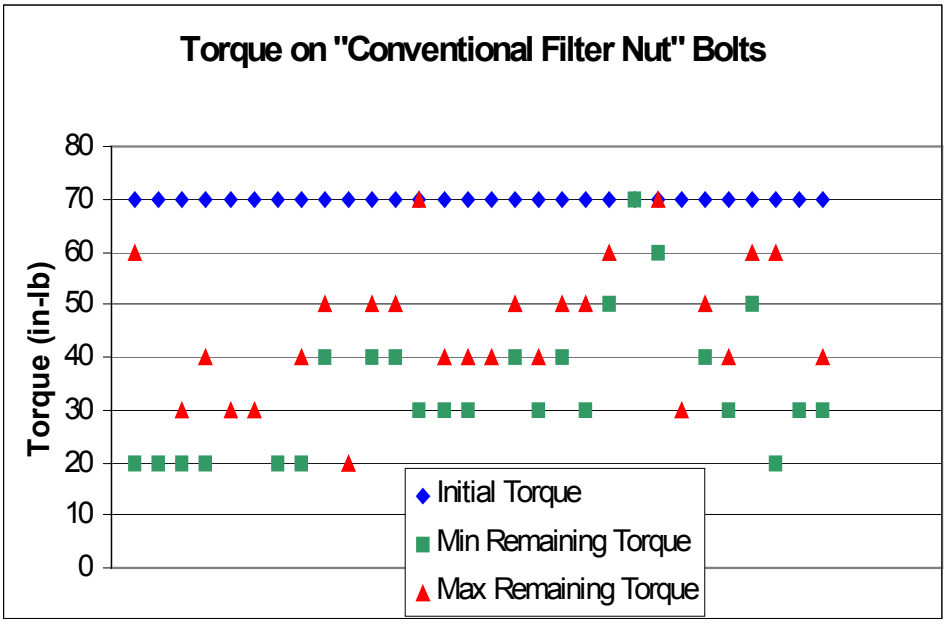

Figure 3.3-13 Remaining Torque on "Conventional Filter Nut" Bolts

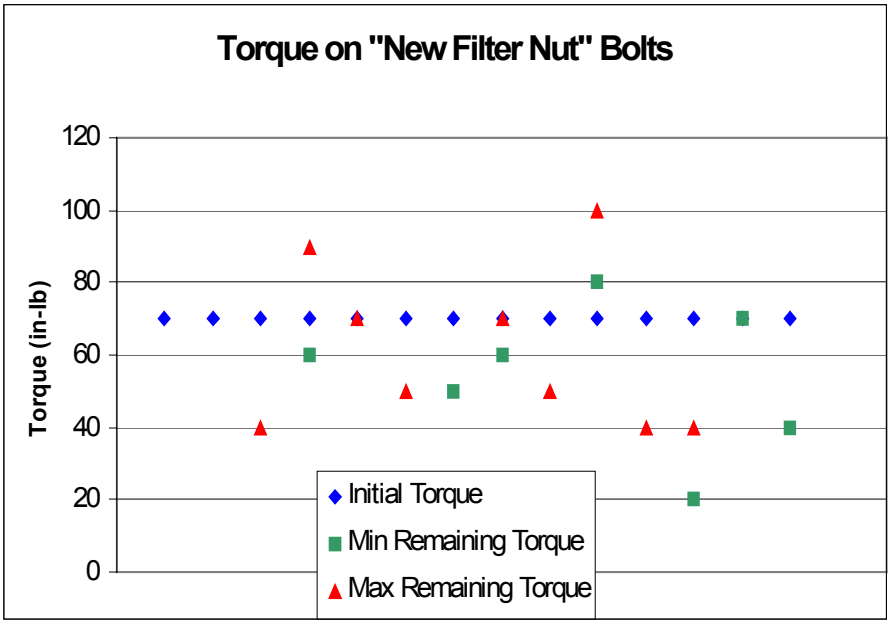

Figure 3.3-14 Remaining Torque on "New Filter Nut" Bolts

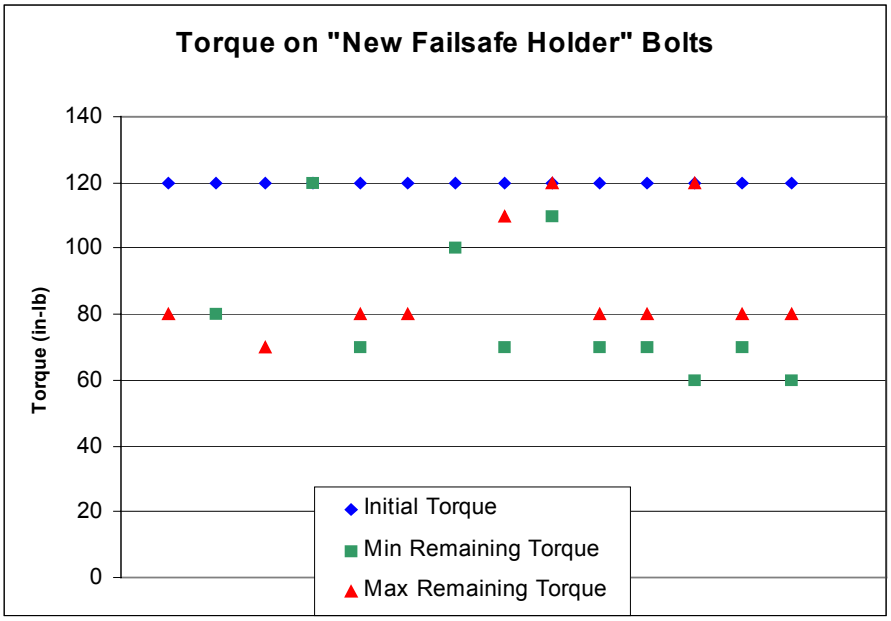

Figure 3.3-15 Remaining Torque on "New Fail-safe Holder" Bolts

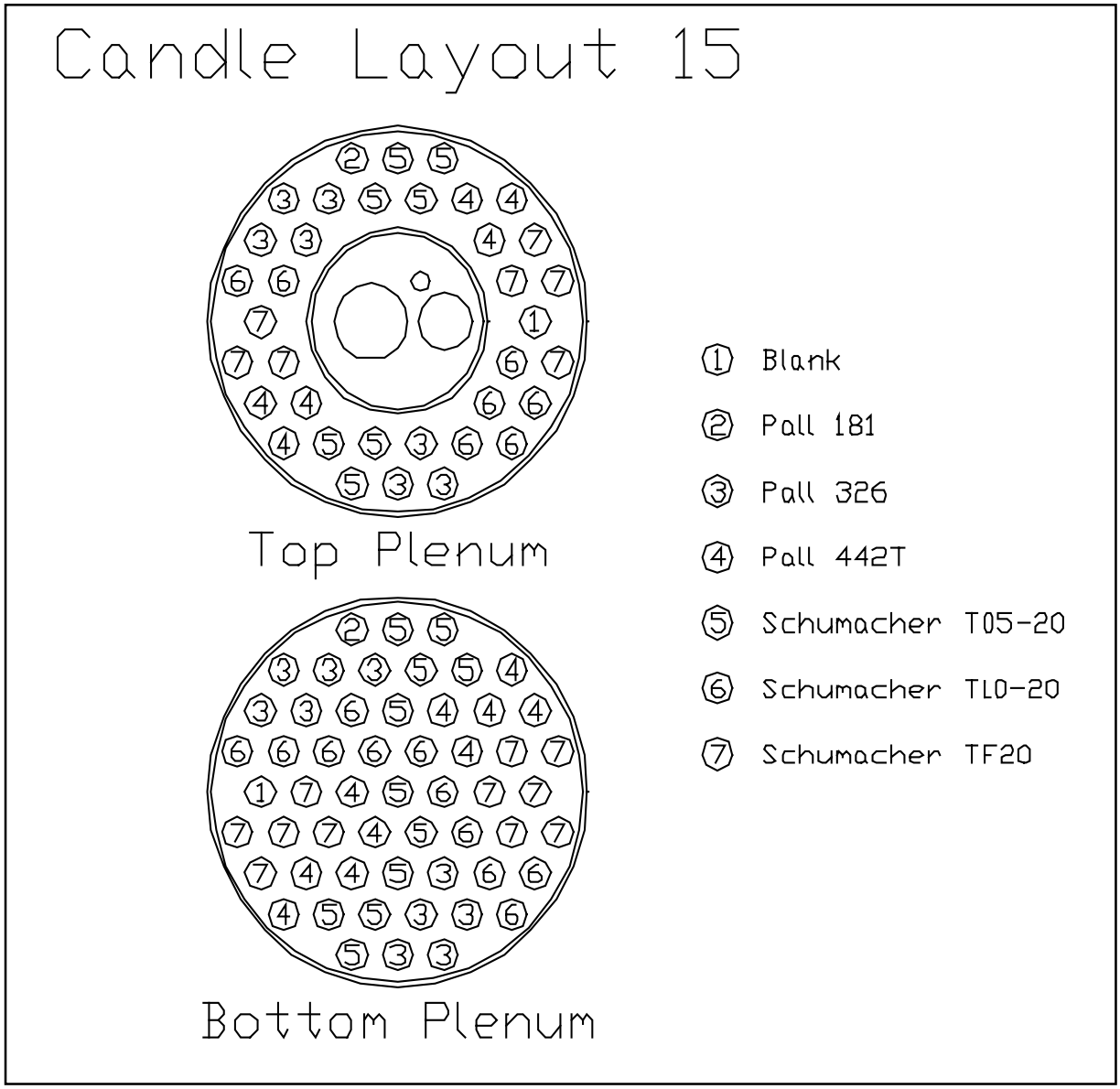

Figure 3.3-16 Filter Element Layout 15

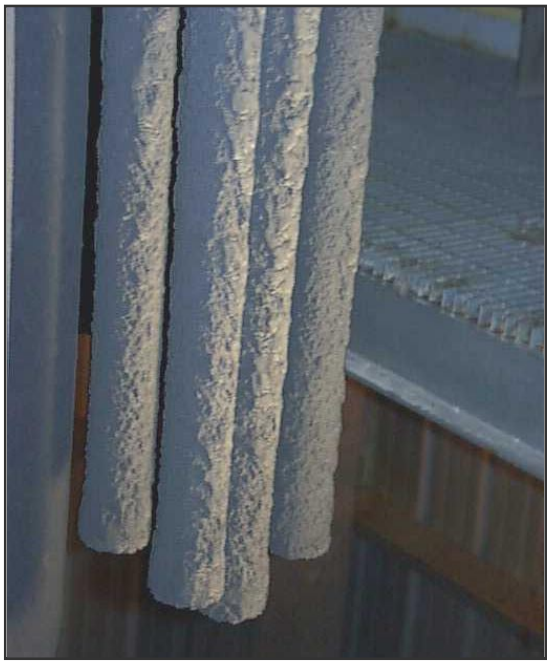

Figure 3.3-17 Top Plenum Filter Element Char Cake (GCT1B Through D)

Figure 3.3-18 Bottom Plenum Filter Element Char Cake (GCT1B Through D)

Figure 3.3-19 Char Accumulation on Top Plenum (GCT1B Through D)

Figure 3.3-20 Char Accumulation on Top Plenum, Top "Ash Shed," and Bottom of Tubesheet (GCT1B Through D)

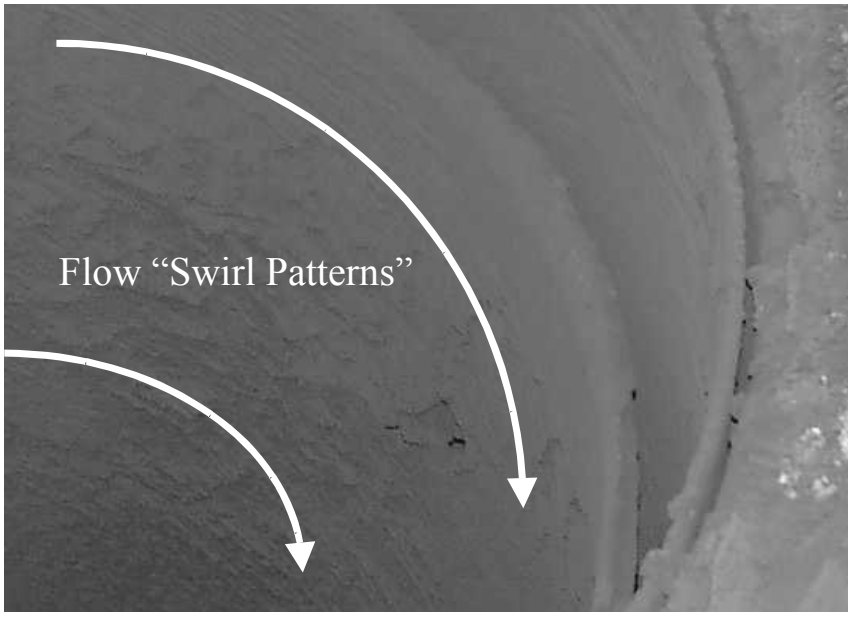

Figure 3.3-21 Shroud ID/Gas-Flow Patterns in Accumulated Char (GCT1B Through D)

Figure 3.3-22 Tubesheet Insulation (GCT1B Through D)

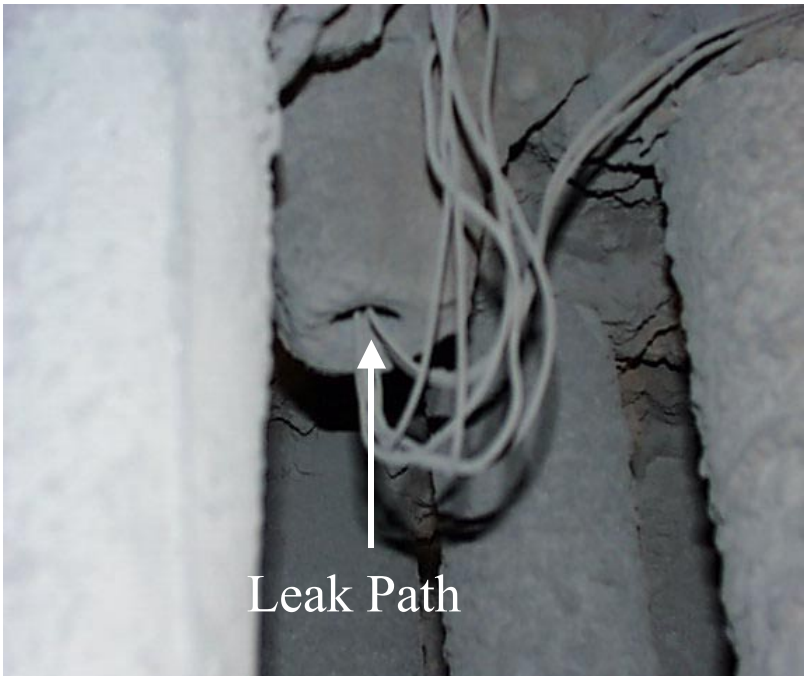

Figure 3.3-23 Potential Leak Paths on Conax Fittings

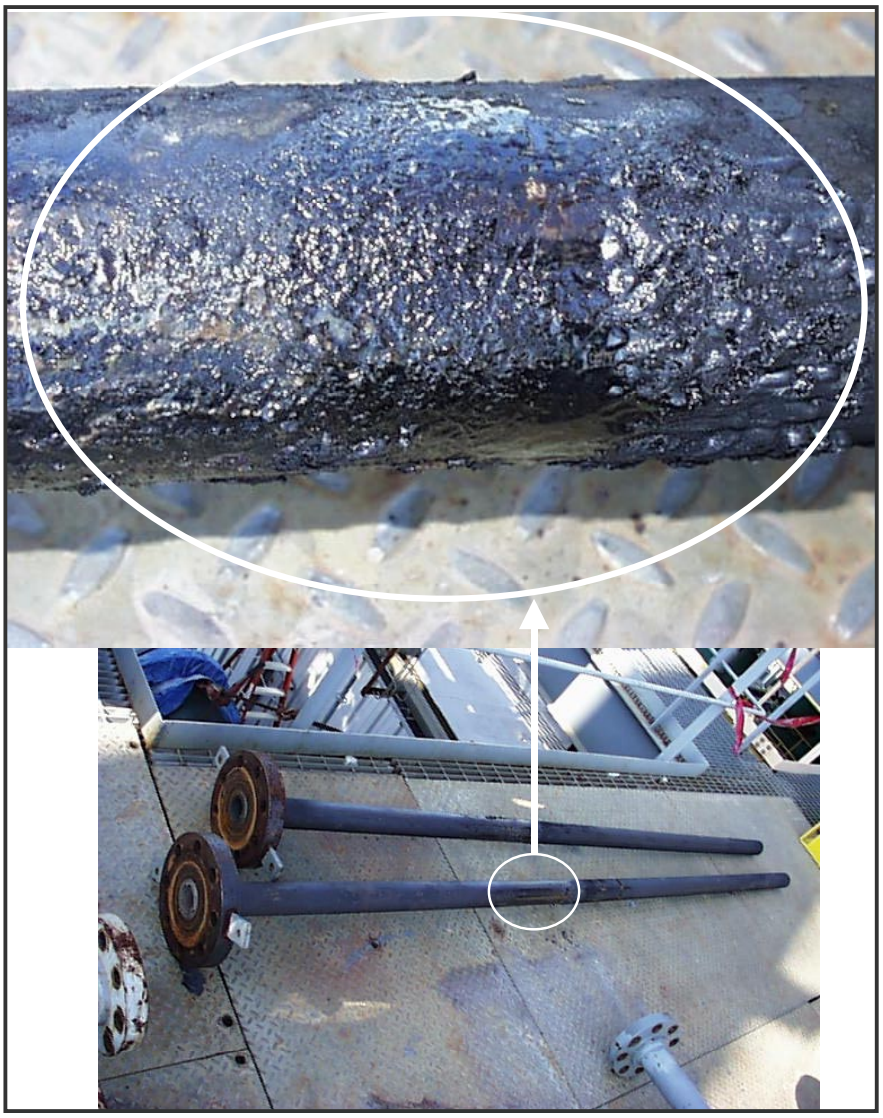

Figure 3.3-24 Tar Accumulation on Back-Pulse Pipes (GCT1B Through D)

3.4 GCT1 CHAR CHARACTERISTICS AND PCD PERFORMANCE

Tests performed at the PSDF and elsewhere have shown that the performance of a hot-gas filter is a strong function of the drag characteristics and other properties of the dust being collected. This section deals with the characteristics of the char produced in GCT1 and the relationship between char characteristics and PCD performance. In situ char samples and dustcake samples from GCT1 were thoroughly characterized in an effort to better understand the effects of the char characteristics on PCD performance. In situ char samples were collected at the PCD inlet and at the PCD outlet during both segments of GCT1 (GCT1A in September 1999 and GCT1B through D in December 1999). In addition to the in situ samples, residual dustcake samples were obtained after both test segments (in October 1999 and in January 2000). Characterization of these samples included: (1) chemical analysis; (2) particle-size analysis; (3) laboratory measurement of drag as a function of porosity; and (4) measurements of the true particle density, bulk density, uncompacted bulk porosity, and specific-surface area. These measurements were used to analyze the observed trends in baseline PCD pressure drop during the two GCT1 test segments.

In an effort to relate the GCT1 results to the experience at a similar facility, drag and particle-size characteristics of the GCT1A char were also compared to the characteristics of char produced from PRB coal in the Transport Reactor Development Unit (TRDU) at the University of North Dakota Energy and Environmental Research Center (UNDEERC). This comparison was of interest because the TRDU is basically a smaller version of the transport reactor system used at the PSDF except that the TRDU is equipped with a more efficient disengager/cyclone system. Since a more efficient disengager/cyclone system is being contemplated for the PSDF the comparisons with the TRDU char may give some indication of how the particle-size distribution and drag characteristics of the char would be affected by this change. Comparisons were also made between the GCT1 chars and combustion ashes produced from PRB and other coals during TC05. These comparisons were made to better understand the differences between the GCT1 results and previous experience with filtration of combustion ash.

This section also includes a brief discussion of water vapor and H_2S measurements that were performed in conjunction with some of the in situ particulate sampling runs. SCS and KBR process engineers requested the water vapor and H_2S measurements because the on-line moisture analyzer and H_2S analyzers failed to operate reliably, resulting in an ongoing need to periodically check H_2S and H_2O.

3.4.1 In situ Particulate Sampling

As in previous test campaigns, in situ particulate sampling runs were performed on a regular basis at the PCD inlet and outlet throughout both segments of GCT1. The system and procedures used for the in situ particulate sampling have been described in previous reports. During the first test segment (GCT1A), three particulate sampling runs were performed at the PCD inlet and two were performed at the PCD outlet. All of the GCT1A samples were produced from Powder River Basin (PRB) coal and Plum Run dolomite. During the second test segment (GCT1B through D) six particulate sampling runs were performed at the PCD inlet and five at the PCD outlet. Four of the GCT1B through D inlet samples were obtained with the same PRB coal and dolomite used in GCT1A and two of the GCT1B through D inlet samples

were obtained with Illinois No. 6 coal and Ohio (Bucyrus) limestone. Three of the GCT1B through D outlet samples were obtained with the PRB coal and dolomite and two of the outlet samples were obtained with the Illinois No. 6 coal and Ohio limestone. No samples were obtained during the operating periods on Alabama coal.

3.4.1.1 Sampling at PCD Inlet

Table 3.4-1 is a summary of the particulate loadings measured in the process-gas stream entering the PCD during GCT1. During the first seven sampling runs the transport reactor was gasifying PRB coal, Plum Run dolomite was added for in-bed sulfur capture. Illinois coal was gasified during the last two sampling runs and Ohio limestone was added for sulfur retention. As noted in the table, three of the PRB/dolomite sampling runs yielded abnormally high-particulate loadings because of unstable process operations. Based on the runs performed under stable-operating conditions the average inlet particulate loading was about 22,000 ppmw during the PRB/dolomite runs and about 54,000 ppmw during the Illinois coal/Ohio limestone runs. This result is consistent with the higher sorbent-addition rates used during the Illinois coal/Ohio limestone runs as required by the higher sulfur content of the Illinois coal.

The three stable PRB inlet particulate loadings were taken when there was no sorbent fed to the reactor while the one unstable point was taken with about 300 lb per hour of sorbent. The two Illinois coal inlet particulate loadings were taken with about 500 lb per hour of sorbent fed to the reactor.

3.4.1.2 Sampling at PCD Outlet

Table 3.4-2 is a summary of the particulate loadings measured in the process-gas stream leaving the PCD during GCT1 and the corresponding particulate collection efficiencies. The collection efficiencies were calculated using the average inlet loading for the corresponding coal/sorbent combination. As indicated in the table, the outlet-particulate loading declined steadily but remained unacceptably high throughout the test. As discussed in the section on PCD operations, the high-outlet loadings have been attributed to three mechanisms: (1) leaks around the fail-safe/filter element gaskets, (2) pinhole leaks in certain composite elements, and (3) leaks through a Conax fitting.

3.4.2 Sampling of Residual Dustcakes

In addition to the in situ particulate samples discussed above, residual dustcake samples were collected when the PCD filter cluster was removed after each test segment. At the conclusion of each test segment the PCD was pulsed extensively after the coal feed was terminated. Therefore, the dustcake samples should represent only the residual dustcake. There should be no significant contribution from the transient dustcake collected between pulse cycles.

The first set of residual dustcake samples was collected in October 1999 after the GCT1A test segment. This set of dustcake samples originated exclusively from the PRB coal and dolomite. The thickness of these dustcakes varied from about 0.03 to 0.10 in. and the average thickness was estimated to be about 0.065 in. The average-areal loading of the GCT1A dustcake was measured to be about 0.14 lb/ft^2.

The second set of residual dustcake samples was collected in January 2000 after the GCT1B through D test segment. This set of dustcake samples was the product of several different combinations of coal and sorbent, including: (1) PRB coal with dolomite, (2) Illinois No. 6 coal with Alabama (Longview) limestone, (3) Illinois No. 6 coal with Ohio limestone, and (4) Alabama (Calumet) coal with Ohio limestone. The thickness of these dustcakes varied from about 0.07 to 0.24 in. and the average thickness was estimated to be about 0.13 in., which was about twice as thick as the GCT1A dustcake. The average-areal loading of the GCT1B through D dustcake was measured to be about 0.28 lb/ft^2, which was about twice the areal loading of the GCT1A dustcake.

In addition to the residual dustcake samples described above, samples were collected after GCT1B through D from the PCD shroud, the tubesheet, and one of the filter holders. These samples were collected to determine how the properties of these "static" deposits differ from the properties of the "active" dustcakes. The dustcake sampling also included the collection of a separate, tightly adherent layer of the dustcake adjacent to the surface of the filter element. This tightly adherent layer was first noticed during efforts to clean the filter elements after they were removed from the PCD at the conclusion of GCT1A. Dustcakes from both test segments were found to comprise an easily removed outer layer and the aforementioned tightly adherent layer adjacent to the filter element surface. The adherent layer was quite thin, roughly 0.01 in. in average thickness, and could not be removed by vacuuming. The areal loading of the adherent layer was measured at about 0.033 lb/ft^2.

3.4.3 Chemical Analysis of In situ Samples and Dustcakes

As in previous test runs, chemical analyses were performed on selected in situ particulate samples and residual dustcake samples from GCT1A and from GCT1B through D. PCD hopper samples were also analyzed, but the compositions of the hopper samples were not used in the evaluation of PCD performance since previous tests have shown that hopper samples are generally not useful for this purpose. The samples were analyzed for carbon, hydrogen, nitrogen, sulfur, and ash; ashes from the ignited samples were subjected to a standard ash-minerals analysis. The standard ash-minerals analysis included: (1) aluminum (Al), (2) calcium (Ca), (3) iron (Fe), (4) magnesium (Mg), (5) phosphorous (P), (6) potassium (K), (7) silicon (Si), (8) sodium (Na), and (9) titanium (Ti). Only the results for Al, Ca, Fe, Mg, and Si are reported here since the concentrations of the other elements were generally less than 0.5-wt percent in the original sample. All of the analytical results reported here are expressed as weight percent of the element in the original sample on an as-received basis.

3.4.3.1 In situ Samples

Table 3.4-3 summarizes the analytical results for selected in situ particulate samples obtained during GCT1B through D. No analyses were done on in situ samples from GCT1A since all of the GCT1A samples were obtained under upset conditions. One of the GCT1B in situ samples (run no. GCT1IMT-5) was obtained under unstable conditions; the analytical results for that run were not included in the averages given in the table. As indicated in the table, the in situ samples collected during the PRB coal/dolomite testing contained less calcium and much less sulfur than did the in situ samples collected during the Illinois coal/Ohio limestone testing. This result was expected in view of the much lower sulfur content of the PRB coal compared to that of the

Illinois coal. The higher sorbent-addition rates required with the higher sulfur Illinois coal result in an increase in the calcium content and a corresponding reduction in the carbonaceous fraction of the solids, as indicated in the results. (Actually, some of the carbon occurs in the form of unsulfidized, uncalcined $CaCO_3$ but the net effect of higher sulfur and higher sorbent addition is to reduce the total carbon content of the solids, as discussed in section 4.1 on transport reactor operations.)

3.4.3.2 Dustcake Samples

Table 3.4-4 summarizes the analytical results obtained on the residual dustcake samples removed during the two GCT1 PCD inspections. Both sets of samples were obtained after a normal shutdown followed by substantial pulse cleaning of the PCD. Again, the primary difference between the two sets of samples appears to be in the sulfur content, which is higher in the GCT1B through D dustcakes due to the higher sulfur content of the bituminous coals used during GCT1B through D. Unlike the in situ samples, however, the dustcake samples do not show large differences in calcium and carbon content between GCT1A and GCT1B through D. It is interesting that the static deposits removed from the shroud, filter holder, and plenum appear to contain more sulfur than do the residual dustcake samples taken from the filter elements. One possible explanation for this difference in sulfur content is that it may reflect a difference in sorbent content associated with a difference in particle-size distribution. Another contributing factor is the apparent additional sulfidation of the sorbent fraction as indicated by the chemical analysis of the static deposits. It is also interesting that the average loss on ignition (LOI) of the dustcake samples was about 60 percent, which was originally greater than the sum of the carbon, hydrogen, nitrogen, and sulfur (about 54 percent on average). Some of this difference could be attributable to the loss of CO_2 that occurred when $CaCO_3$ was decomposed during the ashing of the sample. No such discrepancy is evident in the analytical results on the static deposits, where the LOI values are roughly equal to the sum of the carbon, hydrogen, nitrogen, and sulfur. This result suggests that most of the $CaCO_3$ in the static deposits has been converted to CaS during prolonged sulfidation of the deposits.

3.4.4 Physical Properties of In situ Samples and Dustcakes

Selected in situ particulate samples and dustcake samples were subjected to the standard suite of physical measurements used in previous tests. The measurements included: (1) true particle density, (2) bulk density, (3) uncompacted bulk porosity, (4) specific-surface area, (5) particle-size analysis, and (6) dustcake drag measurements as a function of dustcake porosity. The instruments and procedures used for making these measurements have been described in previous reports.

3.4.4.1 In situ Particulate Samples

Physical properties of the in situ particulate samples are summarized in Table 3.4-5. Samples GCT1IMT-1, -3, and –5 were collected during periods of unstable transport reactor operation; therefore, the properties of these samples may not be appropriate for the analysis of PCD performance. Excluding these samples, the properties of the PRB char from GCT1 are summarized below. For comparison, the range of properties of the Illinois coal char from

GCT1B as well as typical physical properties for combustion ashes generated from PRB coal and from Illinois coal during TC05 is also shown.

Physical Property	GCT1 PRB Char	GCT1 IL Char	TC05 PRB Ash	TC05 IL Ash
Bulk density (g/cc)	0.31-0.36	0.29-0.33	0.64-0.72	0.57-0.68
Skeletal particle density (g/cc)	1.9-2.1	2.2	2.8	2.9
Uncompacted-bulk porosity (%)	83-85	85-87	74-77	76-80
Specific-surface area (m^2/g)	87-104	18-20	0.5-1.0	1.8-2.6
Mass-median diameter (μm)	17-19	23-24	22-24	18-22

Based on the above comparison, the two chars produced from PRB coal and from Illinois coal seem to have fairly similar physical properties with the exception of specific-surface area, which is much higher in the case of the PRB char, and mass-median diameter (MMD), which is somewhat smaller in the case of the PRB char. Compared to the corresponding combustion ashes, both chars have relatively low-bulk densities, relatively high-bulk porosities, and relatively high specific-surface areas. Although there does not appear to be a large difference in MMD this result does not necessarily mean that there are not other significant differences in the particle-size distributions that are not reflected in the MMD. A more detailed comparison of the particle-size distributions of the char and ash will be presented in a subsequent section in the context of analyzing differences in the drag characteristics of char and ash.

3.4.4.2 Dustcake Samples

Table 3.4-6 is a summary of the physical properties of selected residual dustcake samples. As shown in the table, the GCT1A dustcake that was produced exclusively from PRB coal seems to have lower uncompacted-bulk porosity, higher specific-surface area, and smaller MMD than does the GCT1B dustcake that was produced primarily from the combination of various bituminous coals and sorbents. The properties of the two GCT1 residual char dustcakes are compared below to the properties of the residual ash dustcake from TC05.

Physical Property	GCT1A Dustcake	GCT1B Dustcake	TC05 Dustcake
Bulk density (g/cc)	0.31-0.37	0.25-0.30	0.47-0.55
Skeletal particle density (g/cc)	2.1-2.2	2.2-2.3	2.6-2.8
Uncompacted bulk porosity (%)	83-85	86-89	79-83
Specific surface area (m^2/g)	28-90	9-13	1.3-3.9
Mass-median diameter (μm)	5.5-7.4	7.4-11	11-18

Compared to the TC05 ash dustcake, both char dustcakes have relatively low-bulk density, relatively high-bulk porosity, relatively high specific-surface area, and relatively low MMD. These differences appear to be generally consistent with the differences observed in the in situ particulate samples. In addition, the residual dustcake samples suggest that the MMD of the char dustcake tends to be significantly smaller than the MMD of the ash dustcake. Again, it is

important to bear in mind that the MMD alone does not necessarily reflect what may be other significant differences in the particle-size distributions.

The different trends observed in comparing in situ samples and residual dustcake samples may be related to differences in particle dropout in the PCD vessel. Measurements of particle dropout have been made with combustion ash but not with char. It is possible that differences in the particle-size distributions of these two types of particulate matter may lead to differences in particle dropout in the PCD vessel, which might explain why the residual dustcakes show differences in MMD while the in situ particulate samples do not show as much difference.

In previous tests it has been noted that the residual dustcakes produced from combustion ash are typically finer than the in situ ash samples collected during the corresponding run. This result is to be expected based on the previous measurements of particle dropout in the PCD vessel. This difference in particle size can lead to differences in other physical properties such as bulk density, surface area, and drag. Listed below are the properties of the GCT1 residual dustcakes compared to the properties of the GCT1 in situ samples.

Physical Property	PRB Char In situ	GCT1A Dustcake	IL Char In situ	GCT1B Dustcake
Bulk density (g/cc)	0.31-0.36	0.31-0.37	0.29-0.33	0.25-0.30
Skeletal particle density (g/cc)	1.9-2.1	2.1-2.2	2.2	2.2-2.3
Uncompacted bulk porosity (%)	83-85	83-85	85-87	86-89
Specific surface area (m^2/g)	87-104	28-90	18-20	9-13
Mass-median diameter (μm)	17-19	5.5-7.4	23-24	7.4-11

Based on the above comparison, both dustcakes appear to be significantly finer than any of the corresponding in situ samples. This result suggests that there is significant dropout of the char in the PCD vessel. It is also interesting to note that the dustcakes have lower specific-surface areas than do the corresponding in situ samples. This result suggests that particles that drop out in the PCD vessel, presumably the larger particles, contain more surface area than the finer particles that are collected on the filter elements. Normally, one might expect the opposite trend (i.e., that specific-surface area would increase with decreasing particle size), but this is not necessarily the case when most of the surface area resides in pores inside the particles. In fact, since the external-surface area of a 1-μm sphere is only about 3 m^2/g it may be inferred that the preponderance of the char surface area originates from pores within the particles or from the surface texture of the particles. A rough surface texture may contribute to high drag but internal-surface area in the form of pores may not necessarily contribute to drag in the same way.

3.4.5 Particle-Size Analysis of In situ Samples and Dustcakes

3.4.5.1 In situ Samples

Figure 3.4-1 shows particle-size distributions of the in situ char samples generated from the PRB and Illinois coal during GCT1. The particle-size distribution of PRB char taken from the TRDU is included for comparison. The PRB char from the TRDU is obviously much finer than the

PRB char generated at the PSDF during GCT1. This difference is not surprising given that the TRDU is equipped with a more efficient disengager/cyclone than is the transport reactor at the PSDF.

The particle-size distribution of the Illinois char from GCT1B through D is interesting in that it contains an unusual submicron particle mode that is not evident in the PRB char samples. The source of this submicron mode is unknown. One possible explanation is that the submicron mode is composed of soot produced from the coking of tar or other hydrocarbons (L. Shadle, personal communication, April 7, 2000).

Particle-size differences are also evident in scanning electron microscope (SEM) photographs of the various char samples. Figure 3.4-2 shows comparative SEM photographs of the in situ char samples from PRB and Illinois coal; Figure 3.4-3 shows comparative SEM photographs of PRB char from GCT1 and the TRDU. In all cases the width of the photograph corresponds to a distance of 100 μm across the sample. The SEM photographs appear to confirm that the PRB char from the TRDU is indeed finer than the PRB char from GCT1.

3.4.5.2 Residual Dustcake Samples

Figure 3.4-4 shows particle-size distributions of residual dustcakes from GCT1A and from GCT1B through D. The particle-size distribution of the adherent layer adjacent to the filter element is included for comparison. The particle-size distribution of the adherent layer appears to be generally similar to that of the PRB dustcake from GCT1A. As discussed later, the porosity of the adherent layer was also about the same as that of the PRB dustcake from GCT1A, both of which were well below the porosity of the GCT1B dustcake. These similarities between the adherent layer and the GCT1A dustcake suggest that the adherent layer from GCT1B through D is primarily composed of PRB char that was laid down during the initial portion of GCT1B through D, prior to the introduction of the bituminous coal.

Figure 3.4-5 shows comparative SEM photographs of the two residual dustcakes from GCT1A and from GCT1B through D; Figure 3.4-6 shows comparative SEM photographs of the outer layer and adherent layer of the GCT1B through D dustcake. These photographs also suggest that the adherent layer is very similar to the PRB dustcake from GCT1A. The outer layer of the GCT1B through D dustcake, which accounts for over 90 percent of the total dustcake thickness, obviously contains more large particles than does the GCT1A dustcake or the adherent layer from GCT1B through D. Although the adherent layer accounts for only a small fraction of the total GCT1B through D dustcake thickness it is important in understanding the trend in baseline-PCD-pressure drop observed during the transition from PRB to bituminous coal (see section 3.4.7 on analyzing PCD pressure drop). This will be discussed in more detail after examining the drag characteristics of the residual dustcakes and of the adherent layer.

3.4.6 Drag Characteristics of In situ Samples and Dustcakes

The characteristic flow resistance of a dustcake may be expressed in terms of the normalized drag of the cake (R), which is the pressure drop across the cake (ΔP) per unit-face velocity (V) per unit-areal loading (L):

$$R = \Delta P/V/L \qquad \text{Equation 3.4-1}$$

The drag characteristics of various dust samples may be compared by plotting their normalized drag (R) as a function of dustcake porosity. Experience has shown that such curves of normalized drag versus porosity give a reasonably good indication of the inherent flow resistance of the dust, and the curves are, therefore, useful in understanding trends in PCD-pressure drop. As in previous tests, such characteristic curves of normalized drag versus porosity were generated for selected in situ char samples and residual-dustcake samples from GCT1A and from GCT1B through D. These measurements were made using the compressed ash permeability tester (CAPTOR), which has been described in previous reports.

For the first time, drag measurements were also made using a new resuspended ash-permeability tester (RAPTOR), which was developed under this project. The development and design of the RAPTOR has been discussed in various monthly reports. Basically, the RAPTOR provides a means of building up dustcakes under flowing conditions that simulate the dustcake development in the PCD. This simulation is accomplished by adjusting the RAPTOR face velocity to a value that simulates the drag of the PCD dustcake as hot-process gas passes through it. By building up dustcakes in this manner, the RAPTOR provides a measure of dustcake porosity that is not available from CAPTOR measurements. While RAPTOR provides an estimate of the actual dustcake porosity it does not provide the type of information that CAPTOR provides on the effect of porosity on drag. Therefore, the two methods are complimentary and should be used in conjunction with one another to improve the understanding of dustcake drag. Since RAPTOR requires a relatively large sample the RAPTOR measurements were made only on residual dustcake samples. (The in situ char samples were insufficient for RAPTOR measurements.)

3.4.6.1 In situ Samples

Because of particle dropout in the PCD vessel in situ samples collected upstream of the PCD do not accurately represent the dust arriving at the filter elements. Nevertheless, comparison of the drag-porosity curves of in situ samples is frequently a useful exercise to get an idea of how the dust drag varies with various coals and sorbents. Information of this type frequently cannot be gleaned from residual dustcake samples that are often the product of a number of different coal-sorbent combinations (as was the case in GCT1B through D).

Figure 3.4-7 shows a comparison of the CAPTOR drag characteristics of the PRB and Illinois char sampled during GCT1. This comparison clearly shows that the PRB in situ samples have inherently higher drag than do the Illinois in situ samples. The difference in drag may be related, at least in part, to the difference in the particle-size distributions (see Figure 3.4-1). Compared to the Illinois char the PRB char contains a higher concentration of particles in the 1- to 10-μm range and a lower concentration of particles larger than 10 μm. The Illinois char also contains the submicron mode mentioned earlier but the contribution of the submicron mode to drag may not be significant if the submicron particles are stuck to larger particles as suggested by the SEM photographs (see Figure 3.4-2).

In addition to the particle-size distribution another factor that contributes to drag is surface area. It is interesting to note that the PRB in situ samples had specific surface areas of 87 to 104 m^2/g,

while the Illinois in situ samples had specific surface areas of only 18 to 20 m^2/g. Some of this surface area may exist in the form of internal porosity that may not contribute to drag, but it is also possible that at least some of the additional surface area in the PRB samples is contributing to the higher drag of the PRB samples. (As discussed in previous reports, work done at the PSDF and elsewhere has shown that there is definitely a relationship between specific-surface area and normalized drag.)

3.4.6.2 Residual Dustcake Samples

Figure 3.4-8 shows a comparison of the drag characteristics of the residual dustcakes from GCT1A and GCT1B through D. This comparison clearly shows that the residual dustcake from GCT1B through D has inherently higher drag than does the residual dustcake from GCT1A. This result would not be expected based on the drag of the in situ samples, which showed that PRB char had higher drag than did the Illinois char. However, it is important to note that the GCT1B through D residual dustcake was not produced exclusively from Illinois coal, and the effects of particle dropout may not be the same with both coals. The difference in residual dustcake drag between GCT1A and GCT1B through D cannot be explained solely in terms of a difference in the particle-size distributions (see Figure 3.4-4). Compared to the GCT1B through D dustcake the GCT1A dustcake contains a higher concentration of particles in the 1- to 10-μm range and a lower concentration of particles larger than 10 μm. This was essentially the same difference that was noted in the particle-size distributions of the in situ char samples that produced the opposite trend in drag. This result may suggest that particle-size distribution is not the most important factor controlling drag. As mentioned earlier, surface area is another potentially important factor, but the GCT1B through D residual dustcake actually had a lower specific surface area than did the GCT1A residual dustcake (9 to 13 m^2/g versus 28 to 90 m^2/g).

The CAPTOR drag-porosity curves presented in Figure 3.4-8 are only useful in analyzing PCD pressure drop if the porosity of the dustcake can be determined. The porosity of the dustcake as it exists in the PCD cannot be measured directly but dustcake porosity can be estimated using the several different approaches discussed below.

1. The simplest and probably the least accurate estimate of dustcake porosity may be obtained by using the uncompacted bulk porosity (UBP) of a bulk-dust sample. This approach assumes that the process-gas flow and resulting pressure drop do not cause any compaction of the dustcake. Data from previous test programs suggest that the UBP is usually higher than the values of dustcake porosity estimated by other methods.

2. Dustcake porosity may be calculated from measurements of the residual dustcake thickness, areal loading, and particle density. This approach assumes that the residual dustcake that remains at the end of a run is representative of the dustcake that existed in the PCD during the run. This assumption may not be valid if the dustcake is altered by extensive back-pulsing, dewpoint excursions, dustcake spalling, or other anomalies associated with shutdown.

3. If the dustcake contains distinct nodules that can be removed intact the porosity of the nodules can be measured by absorption of isopropyl alcohol into the nodule. This approach assumes that the nodules are representative of the bulk dustcake. This

assumption may be questionable since the nodules can be removed intact and, therefore, may be different from the bulk dustcake in terms of other physical properties.

4. The porosity of the dustcake collected in the RAPTOR can be used as an estimate of the PCD-dustcake porosity. This approach assumes that the buildup of the dustcake in the RAPTOR accurately simulates the buildup of the dustcake in the PCD. The ability of the RAPTOR to accurately simulate dustcake buildup in the PCD may be compromised in situations in which dustcake properties vary substantially between laboratory and field conditions.

Dustcake porosities estimated using the above procedures are summarized below along with the corresponding CAPTOR drag values obtained from Figure 3.4-8. Also shown are porosity and drag values obtained from the RAPTOR measurements.

	GCT1A (PRB)	GCT1B Through D (Illinois)
Estimated porosity values (%)		
Uncompacted bulk porosity (UBP)	84	88
Porosity from areal loading (AL)	80	82
Porosity from isopropyl alcohol (IPA)	72*	80
Porosity from RAPTOR	82	84
Corresponding drag values (inWC/(ft/min)/(lb/ft^2))		
CAPTOR drag at UBP	15	12
CAPTOR drag at AL porosity	40	37
CAPTOR drag at IPA porosity	107*	55
RAPTOR drag	70	29

*Note that the IPA porosity of the GCT1A dustcake and the corresponding drag value are suspect because the dustcake nodules were too small to obtain accurate measurements of IPA absorption.

As expected, the UBP gives the highest estimate of porosity for both the GCT1A and GCT1B through D dustcake and the drag values obtained at the UBP are correspondingly low. With the exception of the suspect (IPA) values noted above all of the other data indicate that the dustcake porosity is in the range of 80 to 84 percent and the dustcake drag is in the range of 29 to 70 inWC/(ft/min)/(lb/ft^2). Although the various estimate methods yield different values of porosity and drag all of the procedures suggest that the GCT1A dustcake exhibits more drag than does the GCT1B dustcake. As will be discussed later, this result is consistent with the actual performance of the PCD observed during the two test segments.

Although the GCT1A dustcake exhibits more drag than does the GCT1B through D dustcake the GCT1B through D dustcake was about twice as thick and about twice as heavy as the GCT1A residual dustcake. This difference in dustcake thickness, or areal loading, will act to offset some of the difference in the dustcake drag between the two test segments. The net

effect of these differences will be examined in the following section on the analysis of PCD pressure drop.

In addition to the bulk residual dustcakes removed at the end of each test segment, the GCT1B through D dustcake also contained a distinct, thin adherent layer adjacent to the filter element surface (as mentioned previously). This layer was isolated, removed from the filter element, and subjected to drag measurements using the CAPTOR apparatus. RAPTOR measurements were not made on the adherent layer because the sample size was inadequate. Figure 3.4-9 data compares the drag characteristics of the bulk dustcakes with those of the adherent layer. The adherent layer appears to have drag characteristics that are more similar to the GCT1A dustcake than they are to the GCT1B through D dustcake, again suggesting that the adherent layer is primarily composed of PRB char laid down during the initial portion of GCT1B through D.

3.4.7 Analysis of PCD-Pressure Drop

Figure 3.4-10 illustrates the trends in baseline PCD-pressure drop (ΔP) that were observed during GCT1A and during GCT1B through D. The ΔP values plotted on this graph have been corrected for the effect of the ΔP increase between back-pulses of the upper and lower plenums. To allow direct comparison of the trends, all values have also been normalized to a PCD operating temperature of 1,000°F and to a face velocity of 3.5 ft/min. Comparing the normalized baseline ΔP trends in GCT1A and in GCT1B through D, the most interesting feature is the different trends observed during the PRB portion of the two test segments. During GCT1A the baseline ΔP rose much more rapidly than it did over an equivalent time period during the PRB portion of GCT1B through D. The sharp rise in baseline ΔP observed in GCT1A suggests that stable-PCD operation is not achievable under these conditions, while the relatively flat trend in baseline ΔP observed during the initial portion of GCT1B through D indicates a much more stable mode of PCD operation that could possibly be maintained indefinitely. The following discussion examines several possible causes for the steep rise in ΔP during GCT1A.

Some of the mechanisms that could account for the steep rise in ΔP include:

- Differences in dustcake thickness (areal loading), porosity, and drag. As discussed previously, the GCT1B through D dustcake was thicker and exhibited lower drag than did the GCT1A dustcake.

- Since there was significant leakage of dust through the PCD during GCT1A pulsing of dirty gas backwards into the filtering elements could result in plugging of PCD components. In the current PCD configuration the plugging of fail-safes and backside blinding of filter elements would cause increases in PCD ΔP that would be indistinguishable from dustcake buildup.

- Chemical reactions within the pores of the filter elements could also contribute to increased PCD ΔP. Since metal elements were in use during GCT1A there was a potential for sulfidation of the high-nickel alloys which could result in pore plugging. In addition, tar vapors that were generated during certain periods could have caused

plugging of filter elements with condensed tars or with soot from the coking of tar vapors.

The relative contributions of the various mechanisms mentioned above were estimated for both GCT1A and GCT1B through D using the following procedures: (1) the contribution of the dustcake drag was estimated using the drag data discussed in the previous section along with measured areal loadings and face velocities and (2) flow-ΔP measurements were made on fail-safes and cleaned filter elements from both test segments to assess the contributions of fail-safe and filter element plugging. Listed below is an estimated breakdown of the various contributions to PCD pressure drop using results from the flow-ΔP measurements mention in (2) above.

	GCT1A	GCT1B Through D
Average Dustcake Thickness (in.)	0.065	0.13
Average Area Loading (lb/ft²)	0.14	0.28
Normalized Baseline PCD ΔP (inWC*)	190	168
Correction for Vessel Losses (inWC*)	34	36
Nonrecoverable Filter Element ΔP (inWC*)	39	2.5
Fail-safe ΔP (inWC*)	40	0.8
Corrected Baseline PCD ΔP (inWC*)	77	129
Corrected Baseline PCD Drag (inWC/ft/min)/lb/ft²))	157	131

*Normalized to 1,000°F and to 3.5 ft/min

The dustcake thicknesses and areal loadings (see above) are the average values based on measurements made on selected filter elements at the end of each test segment. The values of normalized baseline PCD ΔP were taken from the data shown in Figure 3.4-10 at a point just prior to shutdown. This assumes that this ΔP corresponds to the dustcake thicknesses and areal loadings found in the PCD. However, this value of ΔP also includes contributions from vessel losses, filter element blinding, and fail-safe plugging. Vessel losses include all pressure drops through the clean PCD internals including the clean filter elements and fail-safes. Based on flow-ΔP measurements made just prior to coal feed and corrected to 1,000°F and 3.5 ft/min the vessel losses were estimated to be approximately equal for both test segments (~35 inWC). However, increased nonrecoverable pressure drop across the filter elements and fail-safes was not the same for the two test segments. The combined effects of filter element blinding and fail-safe plugging accounted for about 80 inWC of ΔP in GCT1A and about 3 inWC of ΔP in GCT1B through D. (These figures represent the difference between the ΔP in the used condition and the ΔP in the virgin condition. The ΔP of the clean elements and fail-safes is taken into account in the vessel losses.) When all of these effects are taken into account the remaining drag, which should be attributable solely to the dustcake, is higher for GCT1A than for GCT1B through D. This is consistent with the laboratory drag measurements presented earlier.

Only limited measurements have been made of the increased nonrecoverable ΔP of the filter elements and fail-safes. For example, the filter element ΔP value for GCT1A was based on measurements made on only two Hastelloy X elements. Measurements were also made on 310 stainless steel and iron aluminide elements which had only about half of the increased flow

resistance of the Hastelloy X elements. Therefore, the value used in the table for GCT1A may be conservative. The filter element ΔP value given for GCT1B is based on a single measurement made on a Schumacher T10-20 element. This measurement indicated that the increase in filter element ΔP was quite low, but this ΔP value may not be representative of the other GCT1B through D elements. However, there was much less particle leakage through the PCD during GCT1B through D so there should be much less potential for backside blinding. Given these uncertainties in the measurements, the values of filter element ΔP and fail-safe ΔP given above should be viewed as only rough estimates. Nevertheless, this analysis suggests that a significant portion of the GCT1A baseline-pressure drop may be attributed to blinding of filter elements and fail-safes while this is apparently not the case for GCT1B through D.

As discussed previously, the increased nonrecoverable ΔP of the filter elements can be the result of several different mechanisms, including: (1) particulate blinding, (2) pore plugging due to chemical reactions, or (3) condensation of tar vapor in the pores of the filter elements. At the present time it is not possible to precisely distinguish between these various mechanisms. However, one can infer from the relative behavior of the metal filters, ceramic filters, and fail-safes that the high-nonrecoverable ΔP during GCT1A is most likely related to the backside blinding and plugging caused by high-particulate leakage. SEM studies are planned to confirm that pore plugging due to chemical reaction did not contribute significantly to the pressure drop.

In summary, the pressure losses attributable to nonideal effects (blinding, etc.) were not insignificant during GCT1A. However, even after accounting for these nonideal effects there is still a difference in PCD drag that is attributable to differences in the dustcakes. The difference in dustcake drag determined from actual PCD performance is qualitatively consistent with the difference in dustcake drag determined from laboratory measurements. Drag values determined from various laboratory methods are not in perfect agreement, which indicates a need for further work in this area.

3.4.8 Comparison of Char With Combustion Ash

The drag-porosity curves shown in Figure 3.4-11 suggest that gasification char produced from PRB coal has substantially higher flow resistance than does combustion ash from PRB coal. The same trend also seems to apply to gasification char and combustion ash from Illinois No. 6 coal. These comparisons show that the drag imposed by the char is significantly higher than the drag imposed by the corresponding ash when the comparison is made at the same porosity. However, it is important to realize that the porosity of a char dustcake is not necessarily the same as the porosity of an ash dustcake. For example, the char dustcake samples from GCT1 had uncompacted-bulk porosities of 83 to 89 percent, while the ash dustcake samples from TC05 had uncompacted-bulk porosities of 79 to 83 percent. Actual dustcake porosities measured by absorption of isopropyl alcohol were in the range of 71 to 80 percent for the GCT1 char dustcakes and in the range of 69 to 76 percent for combustion ash dustcakes. From these results it appears that gasification char tends to produce a more porous dustcake than does combustion ash. The higher porosity of the char dustcake tends to partially offset the inherent difference in drag characteristics.

To show the differences in both dustcake porosity and inherent drag characteristics Table 3.4-7 compares the actual drag determined from PCD ΔP and areal loading to lab-measured drag

values determined at two different porosities: (1) the uncompacted bulk porosity (UBP) and (2) the flow-compacted porosity (FCP). The latter is determined as part of the procedure for laboratory drag measurements.

Figure 3.4-12 shows plots of the actual PCD drag versus the drag measured at the UBP and the actual PCD drag versus the drag measured at the FCP. As shown in the plot, the drag measured at the UBP is in reasonably good agreement with the actual drag at very low values of drag (< 10 inWC/(ft/min)/(lb/ft^2)). As drag increases, however, it is apparent that the drag measured at the UBP under-predicts the actual drag, and the error increases with increasing drag. The drag measured at the FCP overpredicts the actual drag at relatively low values of drag (< 50 inWC/(ft/min)/(lb/ft^2)) and appears to be in relatively good agreement with the actual drag at relatively high values of drag (> 100 inWC/(ft/min)/(lb/ft^2)). These results suggest that there is a compaction effect that must be taken into account to predict drag accurately (i.e., as drag increases the porosity of the dustcake is reduced due to the compacting force exerted by the ΔP across the cake). Under high-drag conditions (e.g., with gasification char) it may be more appropriate to use laboratory drag measurements made at the FCP if the true porosity of the dustcake is unknown. With low-drag combustion ashes (R < 10) it may be more appropriate to use laboratory drag measurements made at the UBP. For higher drag combustion ashes (R > 10) some intermediate value of porosity may be required to give good agreement with actual drag values.

3.4.9 Measurements of Water Vapor

The only three measurements of water vapor made during the PRB portion of GCT1B through D yielded values of 4.2 to 4.6 weight percent. The two measurements made during the Illinois coal portion yielded values of 7.2 to 8.1 weight percent. Based on calculations performed by the KBR process engineer these values of water vapor concentration appear to be within a reasonably close approach to equilibrium with respect to the water-gas shift reaction ($CO + H_2O \leftrightarrow CO_2 + H_2$).

3.4.10 Conclusions

The residual dustcake remaining at the end of GCT1B through D consisted of an outer layer that was easily removed and an adherent inner layer that was very difficult to remove. Based on the comparisons of physical properties and drag characteristics presented here, the inner adherent layer appears to have originated from the PRB portion of the run while the outer layer appears to have originated from the bituminous coal portion of the run. Measurements of the flow-ΔP characteristics of the filter elements from GCT1A show that the metal elements cannot be restored to their original flow resistance by simply scraping off the residual dustcake. This increase in filter element ΔP was much less pronounced in an element from GCT1B through D. The most likely explanation of these results appears to be that the increased particle leakage during GCT1A resulted in backside blinding of the filters and plugging of the fail-safes. Even after considering the effects of vessel losses, filter element blinding, and fail-safe plugging, the dustcake from GCT1A had higher drag than the dustcake from GCT1B. This result is in agreement with the laboratory drag measurements made on these dustcakes.

The chars produced during both GCT1A and GCT1B through D appear to be coarser and offer less flow resistance than char produced from PRB coal at the TRDU. The most likely explanation for the difference appears to be the higher particle collection efficiency of the disengager/cyclone system used on the TRDU, which could have implications on the installation of a more efficient disengager/cyclone system at the PSDF. The GCT1 chars offer more flow resistance than do any of the combustion ashes generated at the PSDF. The difference cannot be explained solely by differences in the particle-size distributions, and specific-surface area appears to be a contributing factor in the high drag of the char. Future PCD testing in a gasification mode should focus on demonstrating a stable-baseline ΔP while minimizing the production of tars. To facilitate the analysis of PCD performance the next gasification test should be limited to one fuel/sorbent combination.

Table 3.4-1

Summary of Inlet Particulate Loadings Measured During GCT1

SRI Run No.	Date	Start Time	End Time	Coal	Sorbent	Test Condition	Loading, ppmw
GCT1A With PRB Coal							
GCT1IMT-1	09/13/99	14:55	15:00	PRB	Dolomite	Unstable[1]	65,000
GCT1IMT-2	09/15/99	09:15	09:45	PRB	Dolomite	Stable[1]	Blown[2]
GCT1IMT-3	09/15/99	14:20	14:35	PRB	Dolomite	Unstable	55,400
Average for GCT1A							**60,200**
GCT1B With PRB Coal							
GCT1IMT-4	12/08/99	12:35	13:05	PRB	Dolomite	Stable	28,400
GCT1IMT-5	12/09/99	09:35	09:50	PRB	Dolomite	Unstable	69,900
GCT1IMT-6	12/10/99	09:45	10:00	PRB	Dolomite	Stable	10,800
GCT1IMT-7	12/10/99	12:50	13:05	PRB	Dolomite	Stable	27,000
Average for GCT1B With PRB Coal (Under Stable Conditions Only)							**22,100**
GCT1C With Illinois Coal							
GCT1IMT-8	12/13/99	09:45	10:00	Illinois	Ohio LS	Stable	55,800
GCT1IMT-9	12/14/99	08:50	08:55	Illinois	Ohio LS	Stable	52,700
Average for GCT1C With Illinois Coal							**54,300**
End of GCT1							

1. "Stable" means measurements were taken during a period when operating consistently at conditions chosen for tests. "Unstable" means measurements were taken at conditions which varied from the chosen test conditions.
2. Particulate filter in sampler was blown out during run.

Table 3.4-2

Outlet Particulate Loadings Measured During GCT1

SRI Run No.	Date	Start Time	End Time	Outlet Loading (ppmw)	Collection Efficiency (%[1])
GCT1A					
GCT1OMT-1	09/13/99	14:40	15:40	552	99.1
GCT1OMT-2	09/15/99	09:10	10:10	263	99.6
Average for GCT1A				408	99.3
GCT1B Through D With PRB Coal					
GCT1OMT-3	12/08/99	10:10	11:10	82.4	99.6
GCT1OMT-4	12/09/99	09:00	10:40	24.3	99.9
GCT1OMT-5	12/10/99	09:10	10:40	12.1	99.95
Average for GCT1B Through D With PRB Coal				39.6	99.8
GCT1B Through D With Illinois Coal					
GCT1OMT-6	12/13/99	09:15	10:15	6.6	99.99
GCT1OMT-7	12/14/99	10:05	11:05	8.8	99.98
Average for GCT1B Through D With Illinois Coal				7.7	99.99

Note:

1. Collection efficiency calculated using the average-inlet loading for the corresponding test segment, coal, and sorbent.

Table 3.4-3

Analytical Results on In situ Particulate Samples From GCT1
Weight %

Lab ID	SRI Run No.	Date	C	H	N	S	Al	Ca	Fe	Mg	Si
GCT1A with PRB Coal											
No analyses performed on GCT1A samples due to process upsets.											
GCT1B with PRB Coal											
AB06236	GCT1IMT-4	12/08/99	66.43	0.98	0.74	0.81	2.41	4.10	1.09	0.82	4.71
AB06237	GCT1IMT-5	12/09/99	32.86	0.41	0.30	0.53	2.32	20.37	1.20	0.01	6.28
AB06238	GCT1IMT-6	12/10/99	54.64	0.72	0.54	0.86	2.93	4.49	1.15	1.08	9.09
AB06239	GCT1IMT-7	12/10/99	54.55	0.72	0.55	0.87	2.51	6.04	1.54	1.37	7.12
Average with PRB Coal*			58.54	0.81	0.61	0.85	2.62	4.88	1.26	1.09	6.97
PRB Char from TRDU			45.11	0.36	0.37	0.17	N.M.	N.M.	N.M.	N.M.	N.M.
GCT1C with Illinois Coal											
AB06240	GCT1IMT-8	12/13/99	40.80	0.41	0.54	4.22	3.12	12.08	2.77	2.34	6.27
AB06241	GCT1IMT-9	12/14/99	41.99	0.44	0.60	4.07	2.82	13.21	2.43	1.68	5.96
Average with Illinois Coal			41.40	0.43	0.57	4.15	2.97	12.65	2.60	2.01	6.11

* Run No. GCT1IMT-5 not included in average, because sample was obtained under unstable conditions.
*Note: Carbon includes both elemental carbon and CO_2 carbon.

Table 3.4-4

Analytical Results on Residual Dustcake Samples From GCT1
Weight %

Lab ID	Element No.	Date Collected	C	H	N	S	Al	Ca	Fe	Mg	Si
GCT1A											
AB05820	T-6	10/01/99	54.18	0.80	0.54	0.48	2.78	7.39	1.42	1.93	3.94
AB05821	T-12	10/01/99	53.63	0.79	0.55	0.31	N.M.	N.M.	N.M.	N.M.	N.M.
AB05822	T-17	10/01/99	48.27	0.73	0.52	0.44	N.M.	N.M.	N.M.	N.M.	N.M.
AB05823	T-18	10/01/99	53.95	0.75	0.50	0.38	2.63	7.68	1.45	2.08	4.03
AB05824	B-4	10/01/99	49.29	0.76	0.55	0.44	N.M.	N.M.	N.M.	N.M.	N.M.
AB05825	B-14	10/01/99	48.95	0.74	0.55	0.45	N.M.	N.M.	N.M.	N.M.	N.M.
Average for All Elements			51.38	0.76	0.54	0.41	2.93	8.17	1.56	2.17	4.32
AB05826	Bulk/Top	10/01/99	52.48	0.76	0.55	0.41	N.M.	N.M.	N.M.	N.M.	N.M.
AB05827	Bulk/Bottom	10/01/99	50.69	0.75	0.53	0.35	N.M.	N.M.	N.M.	N.M.	N.M.
Average for Bulk Samples			51.59	0.76	0.54	0.38	N.M.	N.M.	N.M.	N.M.	N.M.
GCT1B-D											
AB06291	B-4	01/19/00	55.67	0.29	0.76	1.98	3.73	5.67	1.85	1.05	6.60
AB06292	B-6	01/19/00	55.44	0.42	0.72	1.99	3.62	5.74	1.88	1.03	6.60
AB06293	B-16	01/19/00	26.35	0.05	0.32	2.05	3.87	6.14	1.96	1.19	7.22
AB06294	B-29	01/19/00	25.91	0.06	0.31	2.10	3.48	6.26	1.93	1.15	6.78
AB06295	T-5	01/19/00	55.69	0.43	0.72	1.67	3.97	5.24	1.80	1.01	6.76
AB06296	T-10	01/19/00	54.40	0.44	0.70	1.81	3.78	5.47	1.81	1.05	6.68
AB06297	T-17	01/19/00	56.01	0.45	0.73	1.62	4.27	4.84	1.79	0.97	6.97
AB06298	T-32	01/19/00	54.31	0.47	0.68	1.85	4.07	5.33	1.80	1.02	6.71
Average for All Elements			47.97	0.33	0.62	1.88	3.85	5.59	1.85	1.06	6.79
AB06299	Shroud	01/19/00	48.69	0.31	0.56	2.77	3.58	8.19	2.03	1.81	6.67
AB06300	Holder	01/19/00	53.86	0.46	0.66	2.35	3.43	6.39	1.69	1.41	7.00
AB06301	Plenum	01/19/00	49.39	0.31	0.55	2.63	3.03	9.24	2.20	1.80	6.77
Average for Static Deposits			50.65	0.36	0.59	2.58	3.35	7.94	1.97	1.68	6.81

Table 3.4-5

Physical Properties of GCT1 In situ Samples

Lab ID	SRI Run No.	Date	Bulk Density, g/cm^3	True Density, g/cm^3	Uncompacted Bulk Porosity, %	BET Surface Area, m^2/g	Mass-Median Diameter, μm
GCT1A with PRB Coal							
AB05815	GCT1IMT-1	09/13/99	0.46	2.25	79.6	47.8	27.2
None	GCT1IMT-2	09/15/99	*Sample Unrecoverable Because Filter Was Blown Out*				
AB05809	GCT1IMT-3	09/13/99	0.55	2.20	75.0	107.0	127.2
Average for GCT1A			0.51	2.23	77.3	77.4	77.2
GCT1B with PRB Coal							
AB06236	GCT1IMT-4	12/08/99	0.33	1.92	82.8	88.0	18.3
AB06237	GCT1IMT-5	12/09/99	0.61*	2.38*	74.4*	75.8*	13.8*
AB06238	GCT1IMT-6	12/10/99	0.36	2.08	82.7	86.7	26.6
AB06239	GCT1IMT-7	12/10/99	0.31	2.05	84.9	104.0	16.9
Average with PRB Coal			0.33	2.02	83.5	92.9	20.6
PRB Char from TRDU			0.29	2.35	87.7	N.M.	4.7
GCT1C with Illinois Coal							
AB06240	GCT1IMT-8	12/13/99	0.33	2.23	85.2	20.3	23.6
AB06241	GCT1IMT-9	12/14/99	0.29	2.22	86.9	17.7	23.0
Average with Illinois Coal			0.31	2.23	86.1	19.0	23.3

* Not included in average, because sample was obtained under unstable conditions.

Table 3.4-6

Physical Properties of GCT1 Dustcake Samples

Lab ID AB0-	Element No.	Date Collected	Bulk Density, g/cm^3	True Density, g/cm^3	Uncompacted Bulk Porosity, %	Surface Area, m^2/g	MMD, μm
GCT1A							
5820	T-6	10/01/99	0.31	2.12	85.4	76.5	5.5
5821	T-12	10/01/99	0.32	2.09	84.7	43.1	5.9
5822	T-17	10/01/99	0.33	2.22	85.1	45.2	5.9
5823	T-18	10/01/99	0.31	2.06	85.0	90.4	5.9
5824	B-4	10/01/99	0.35	2.06	83.0	44.5	6.6
5825	B-14	10/01/99	0.37	2.13	82.6	27.7	7.4
Average for All Elements			0.33	2.11	84.3	54.6	6.2
5826	Bulk/Top	10/01/99	0.32	2.12	84.9	50.2	5.9
5827	Bulk/Bottom	10/01/99	0.36	2.15	83.3	45.2	7.1
Average for Bulk Samples			0.34	2.14	84.1	47.7	6.5
GCT1B-D							
6291	B-4	01/19/00	0.29	2.34	87.6	9.44	9.6
6292	B-6	01/19/00	0.28	2.32	87.9	10.6	7.8
6293	B-16	01/19/00	0.26	2.24	88.4	9.79	11.2
6294	B-29	01/19/00	0.26	2.26	88.5	8.72	10.2
6295	T-5	01/19/00	0.30	2.21	86.4	13.3	8.4
6296	T-10	01/19/00	0.29	2.23	87.0	11.1	8.1
6297	T-17	01/19/00	0.25	2.20	88.6	12.2	7.4
6298	T-32	01/19/00	0.29	2.22	86.9	11.3	7.6
Average for All Elements			0.28	2.25	87.7	10.8	8.8
6299	Shroud	01/19/00	0.28	2.28	87.7	6.9	20.0
6300	Holder	01/19/00	0.15	2.32	93.5	7.3	10.4
6301	Plenum	01/19/00	0.25	2.37	89.5	3.9	20.2
Average for Inactive Deposits			0.23	2.32	90.2	6.0	16.9
6302	Adherent	01/19/00	0.30	2.04	85.3	N.M.	5.4

Table 3.4-7

Average Drag Characteristics of Char and Ash Samples From Various Tests

(In situ Dust Samples)

					Drag, inwc/(ft/min)/(lb/ft^2)		
Test	**Dust**	**Fuel**	**Sorbent**	**DED, μm**	**Lab/UBP**	**Lab/FCP**	**Actual**
TC01	Ash	AL Coal	Dolomite	2.5	10	38	11
TC02	Ash	AL Coal	Dolomite	NM	NM	NM	11
TC03	Ash	AL Coal	Dolomite	2.8	7.8	73	12
TC03	Ash	E. Ky Coal	Dolomite	3.6	6.7	49	16
TC03	Ash	E. Ky Coal	OH LS	2.6	12	80	24
TC03	Ash	E. Ky Coal	AL LS	3.2	8.0	51	15
TC05	Ash	AL Coal	OH LS	2.8	9.4	34	21
TC05	Ash	AL Coal	AL LS	5.2	10	22	3.0
TC05	Ash	IL Coal	OH LS	3.7	7.5	15	5.3
TC05	Ash	IL Coal	AL LS	3.0	5.8	18	3.6
TC05	Ash	Pet Coke	Dolomite	9.9	1.8	3.6	0.1
TC05	Ash	PRB	OH LS	4.2	4.6	14	4.2
TC05	Ash	PRB	None	5.2	4.4	12	4.1
GCT1	Char	PRB	Dolomite	1.1	43	173	166
GCT1	Char	IL Coal	OH LS	1.8	6.1	27	30

Residual Dustcakes

					Drag, inwc/(ft/min)/(lb/ft^2)		
Test	**Dust**	**Fuel**	**Sorbent**	**DED, μm**	**Lab/UBP**	**Lab/FCP**	**Actual**
TC01	Ash	AL Coal	Dolomite	1.7	16	67	26
TC02	Ash	AL Coal	Dolomite	1.8	20	51	35
TC03	Ash	Various	Various	2.3	10	29	22
TC05	Ash	Various	Various	1.8	15	75	28
GCT1A	Char	PRB	Dolomite	0.85	37	151	247
GCT1B-D	Char	Various	Various	0.75	24	131	134

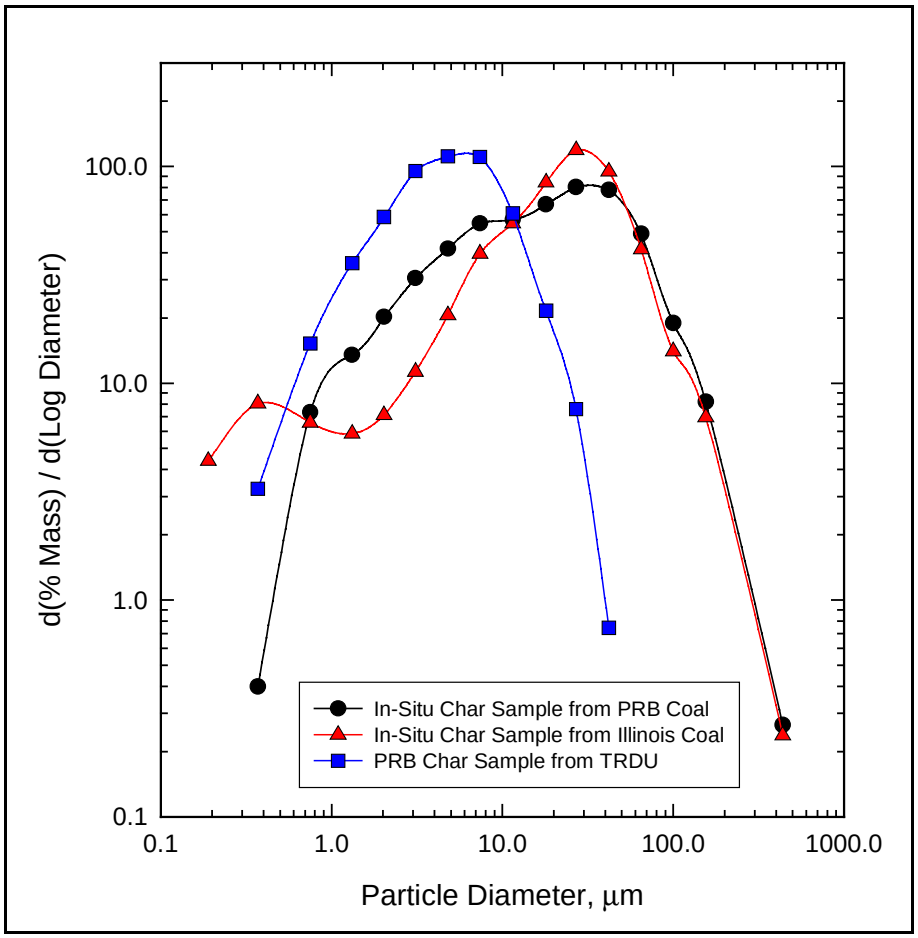

Figure 3.4-1 Particle-Size Distributions of In situ Char Samples

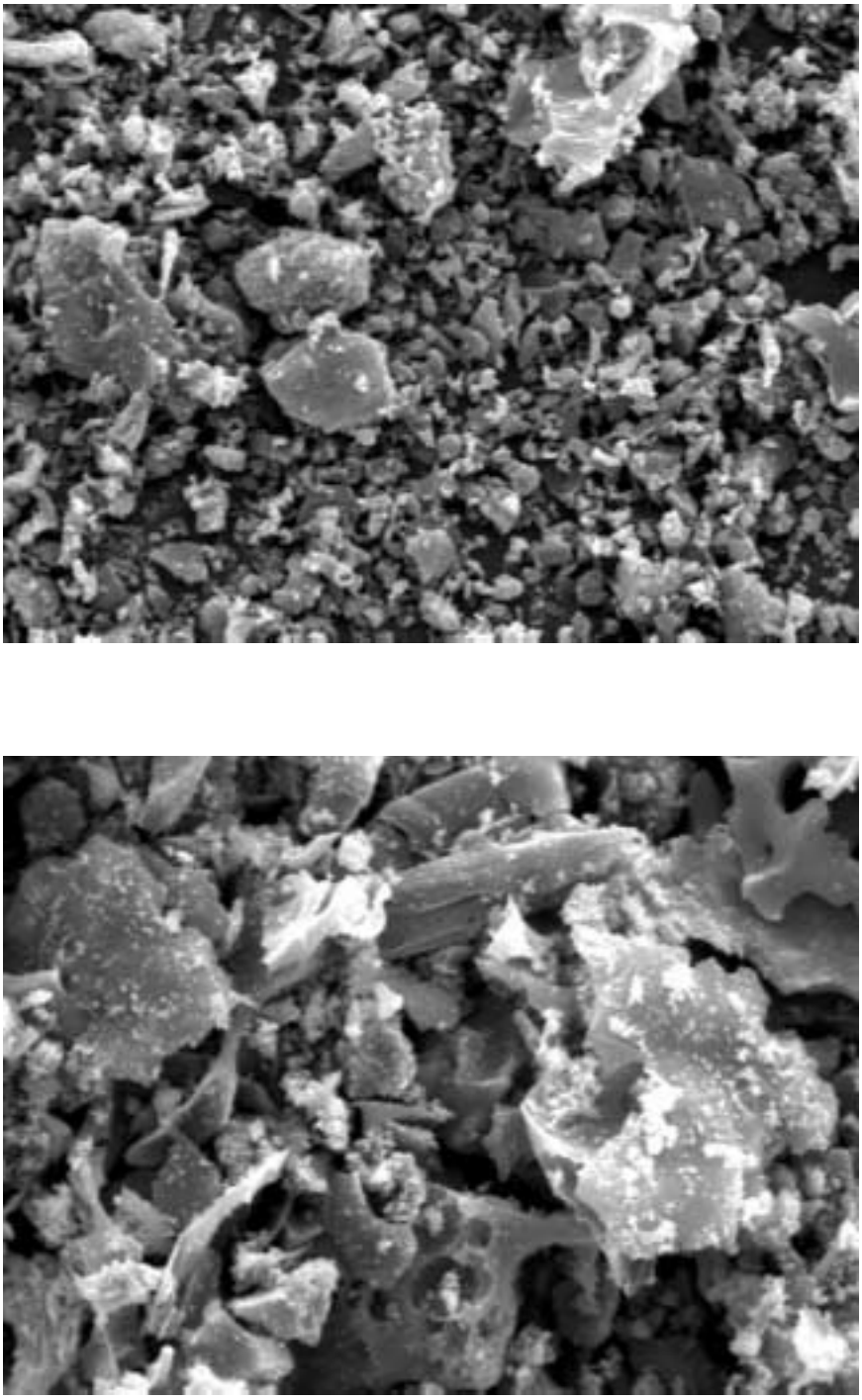

Figure 3.4-2 SEM Photographs of In situ Char Samples Collected During GCT1
Top Photo: Char From PRB Coal
Bottom Photo: Char From Illinois Coal
(Width of Photograph = 100 μm)

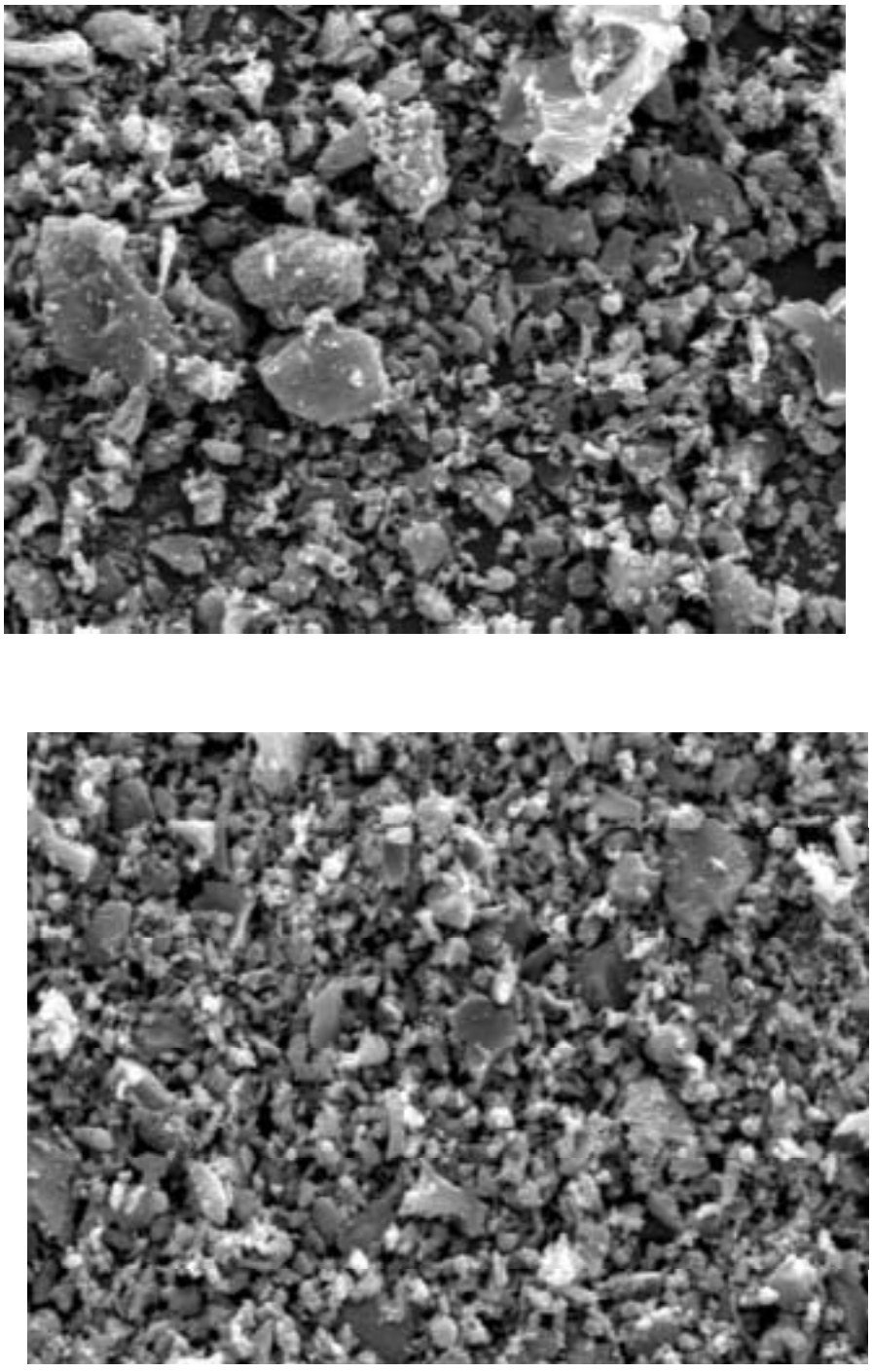

Figure 3.4-3 SEM Photographs of Char Produced From PRB Coal
Top Photo: In situ Sample From GCT1
Bottom Photo: Hopper Sample From TRDU
(Width of Photograph = 100 μm)

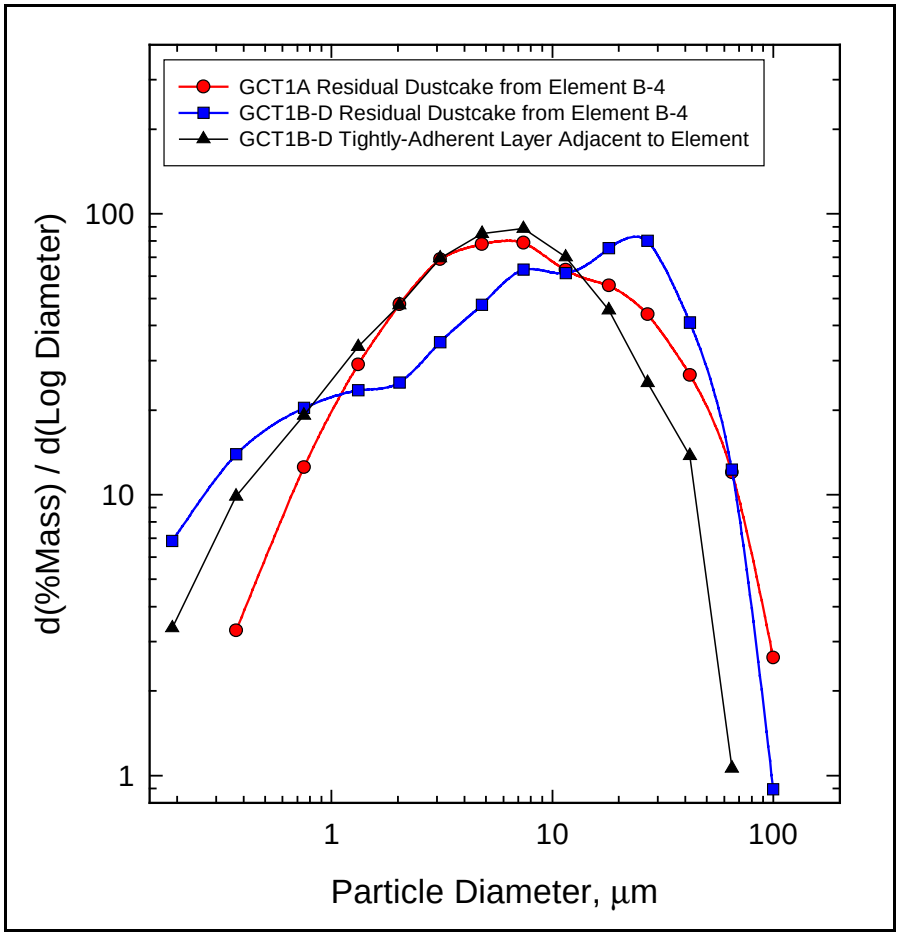

Figure 3.4-4 Particle-Size Distributions of Residual Dustcake Samples and Tightly Adherent Layer

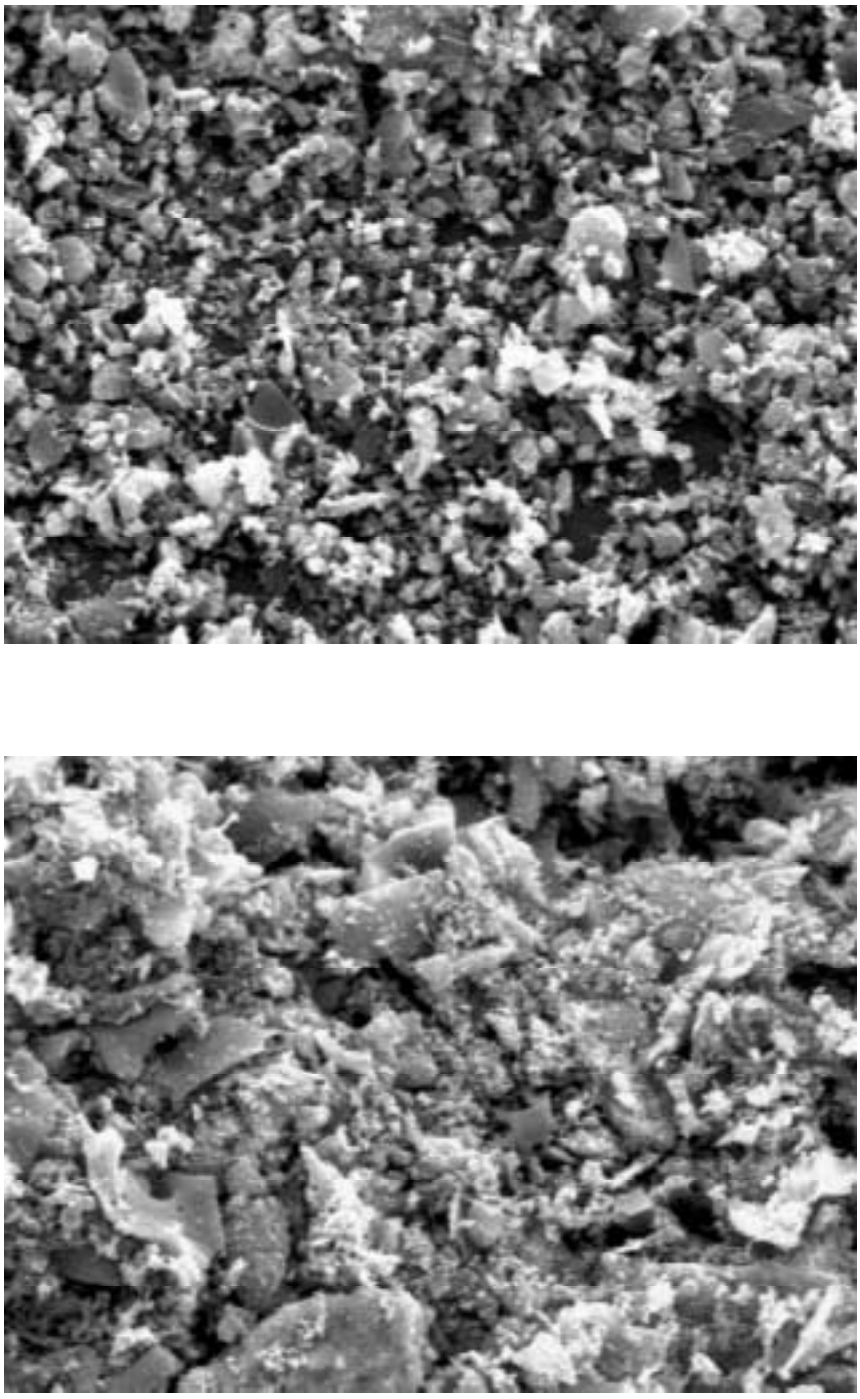

Figure 3.4-5 SEM Photographs of Residual Dustcake Samples
Top Photo: GCT1A
Bottom Photo: GCT1B Through D
(Width of Photograph = 100 μm)

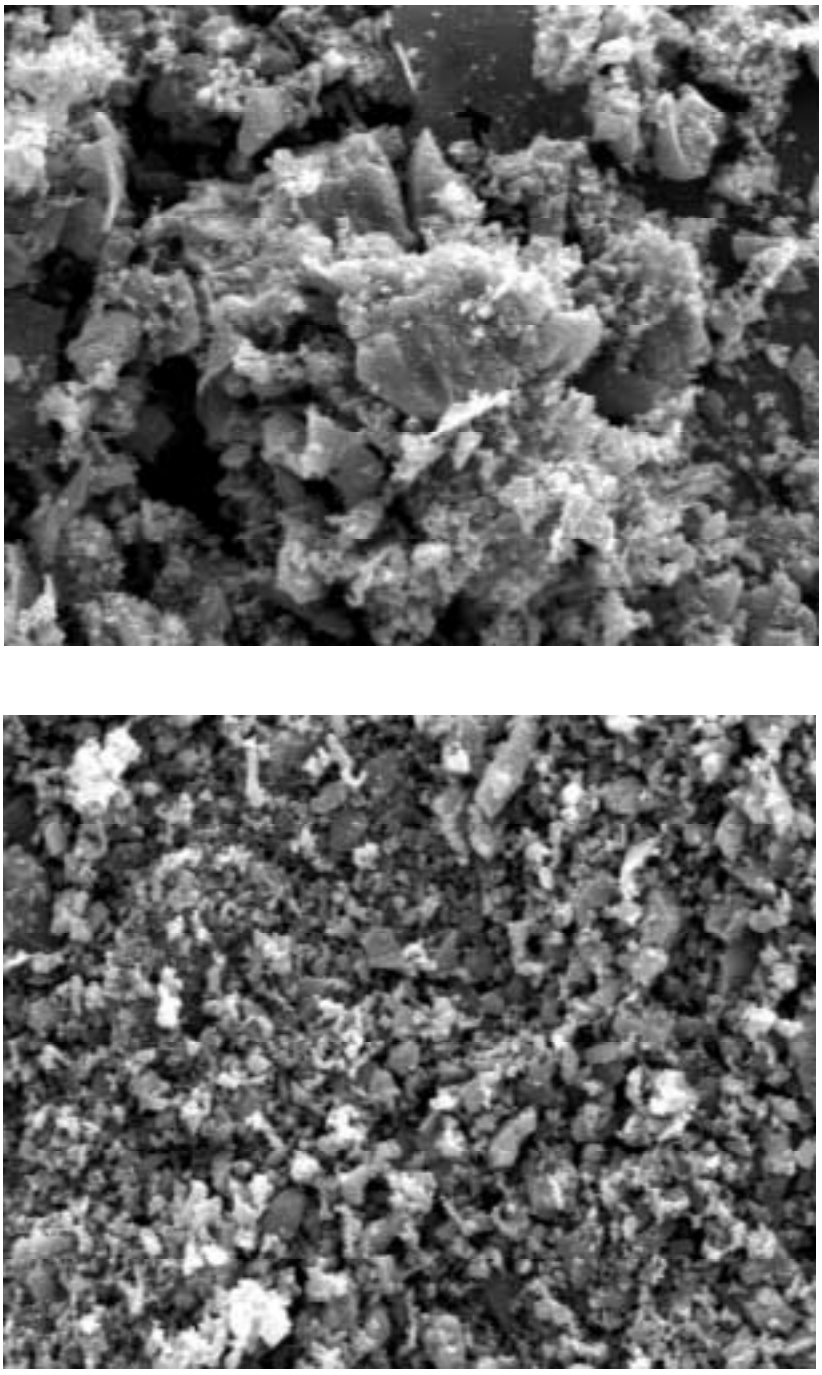

Figure 3.4-6 SEM Photographs of Residual Dustcake Layers
Top Photo: Outer Layer of Residual Dustcake
Bottom Photo: Adherent Layer Adjacent to Filter Element
(Width of Photograph = 100 μm)

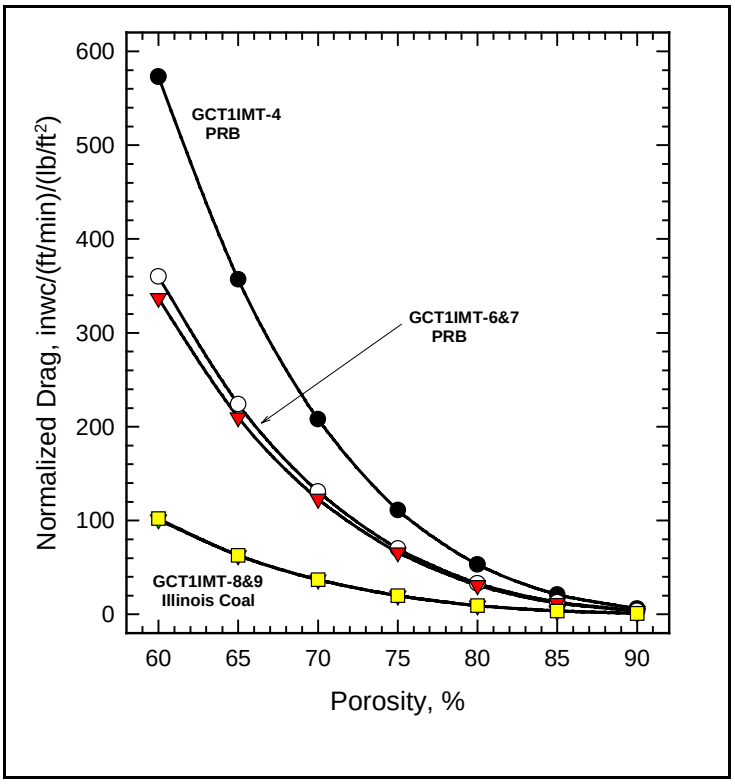

Figure 3.4-7 Drag-Porosity Characteristics of In situ Char Samples Collected During GCT1

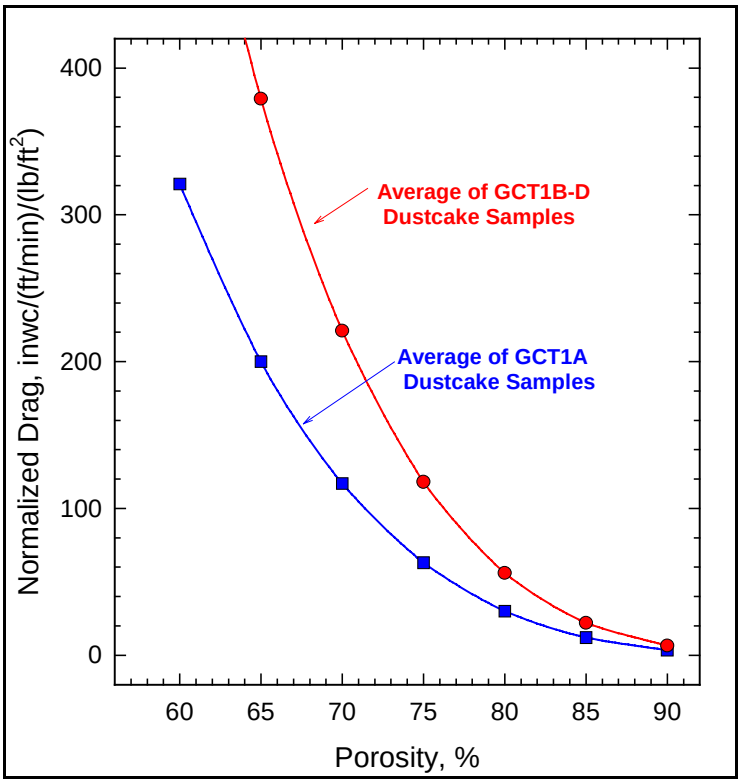

Figure 3.4-8 Drag-Porosity Characteristics of Residual Dustcakes From GCT1A and GCT1B Through D

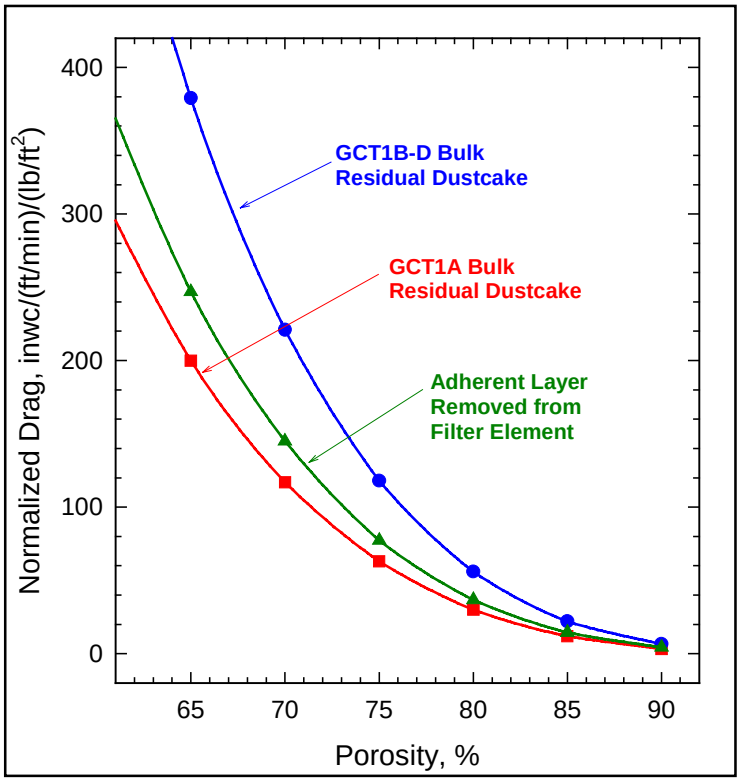

Figure 3.4-9 Drag-Porosity Characteristics of Adherent Layer Compared to Bulk-Residual Dustcakes From GCT1A and From GCT1B Through D

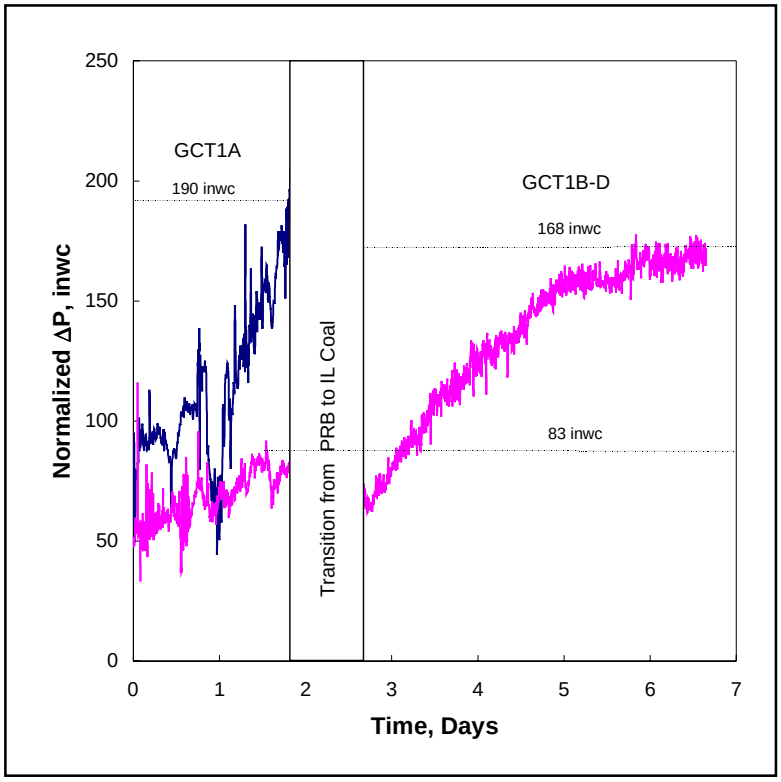

Figure 3.4-10 Trends in Baseline-PCD ΔP During GCT1A and GCT1B Through D

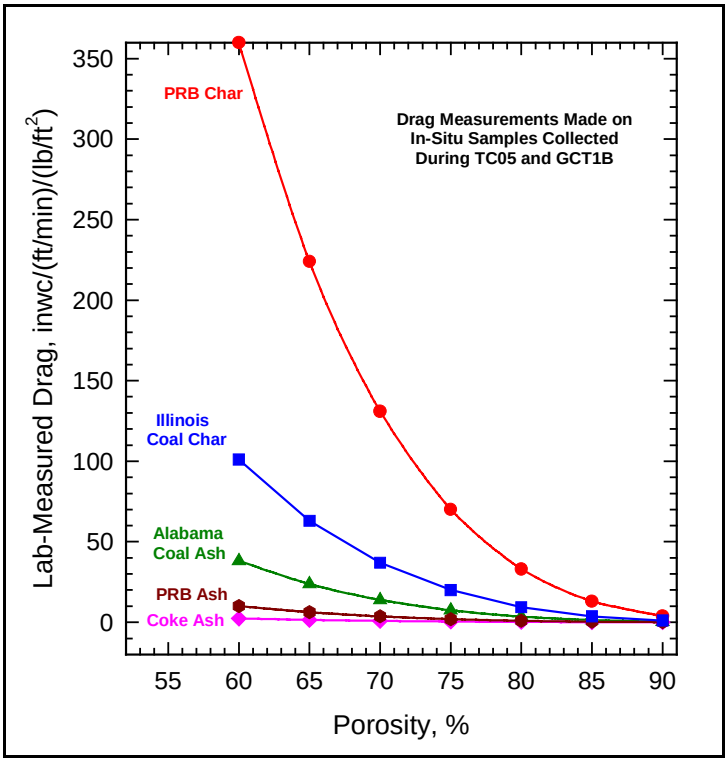

Figure 3.4-11 Comparison of Drag-Porosity Characteristics of In situ Char Samples From GCT1 and In situ Ash Samples From TC05

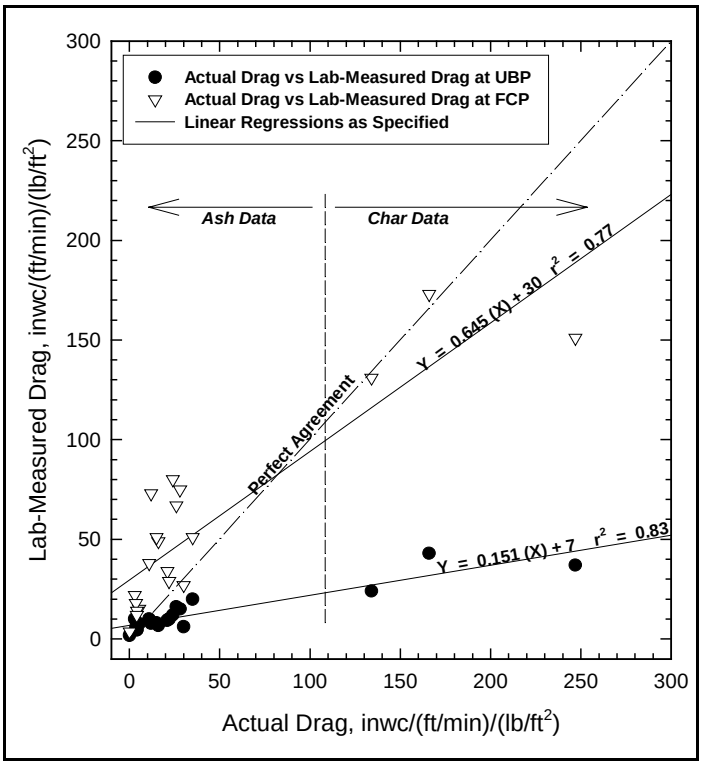

Figure 3.4-12 Comparison of Actual PCD Drag With Lab Drag Values Determined at Uncompacted-Bulk Porosity and at Flow-Compacted Porosity

3.5 FINES HANDLING SYSTEM

3.5.1 Run GCT1A Operational Summary

The operation of the spent fines ash removal system during run GCT1A was relatively uneventful when compared to the problems experienced during the early combustion runs. The increase in reliability can be attributed to the lessons learned and modifications made during the combustion runs. One of the problems experienced during the combustion runs was that the vent valve between the lock vessel and the dense-phase vessel would wear and lose the ability to seal (see Figure 3.5-1). To rectify this problem a second vent line was added to the FD0520 system (see Figure 3.5-2). Therefore, when one valve would wear the other valve could be activated without shutting down the process while the first valve was repaired.

Prior to run GCT1A a HAZOP meeting was held to discuss changes to the process when going from combustion to gasification. From this meeting came changes to the ash removal system including:

- The control gas for the ash-removal system was changed from air to nitrogen. This was done to prevent the possibility of char combusting in the ash-removal system.
- A second 10-in. ball valve was added to the drop pipe (the block valve was installed above FD0520 for personnel safety).
- During combustion the vent lines of the ash removal system were unplugged by connecting 100-psig air to the lines. For gasification it was determined to use low-pressure nitrogen to clear the lines.
- Due to the hazardous nature of the syngas and gasification char it was determined to pipe all vent discharge to FD0530. (During combustion all pressure relief valves associated with the ash-removal system were vented to the atmosphere.)

In spite of the increase in the ash removal system reliability there were still several problems associated with the system. The problems experienced by the screw conveyor (FD0502) included:

1. On a couple of occasions the seal-purge pressure dropped below the system pressure. When the seal-purge pressure is less than the system pressure the process gas and char is forced through the seal packing, which eventually erodes the packing and shaft.
2. On several occasions the drive-side shaft rider seal leaked. The drive-side seal packing follower is a four-bolt design (see Figure 3.5-3). However, the inlet-side seal packing, which is an eight-bolt design, did not leak (see Figure 3.5-4). Therefore, prior to GCT1B through D an eight-bolt design was implemented on the drive-side seal-packing follower. The addition of the eight-bolt design should improve the

sealing because (1) there will be uniform compression on the seal and (2) there will be less stress on a single bolt (which will allow more room for adjustments).

The problems with the FD0520 system were:

1. The level probe designed by Drexelbrook proved to be unreliable (see Figure 3.5-5). The level probe was too sensitive to the char movement in the lock vessel, causing the system to continuously cycle. Therefore, the lock vessel sequence was controlled by a timer, which resulted in frequent cycling. Prior to GCT1B through D Drexelbrook was contacted to properly calibrate the probe for the process conditions.

2. Slow venting of the lock vessel was experienced on several occasions during the run. Between the lock vessel and dense phase vessel is a vent line (see Figure 3.5-1) that allows the lock vessel to depressurize to the dense-phase vessel pressure. If this pressure vents off too slowly the performance of the ash-removal system is affected. In order to speed up the vent time the orifice gate valve had to be opened wider.

3. On one occasion the o-rings surrounding the top spheri valve leaked. This resulted in an unplanned shutdown of the process. Due to this leak the sealing pressure, which was set at 325 psig, could only maintain 290 psig.

The ash-removal rate of the FD0502/FD0520 system was higher during gasification than combustion. SRI reported the inlet loading to the PCD was as high as 60,000 ppm. In order to keep char from accumulating in the cone of the PCD the ash-removal-cycle timer ranged from 30 seconds to 5 minutes. Also, frequent-cycle-timer adjustments were made which required a considerable amount of attention from the operators and process engineers.

The GCT1A operational experience suggests that the ash-removal-system reliability has increased. However, the drive-side seal continues to be an operational challenge. By adding the eight-bolt design to the drive-side seal-packing follower future leaks on the screw conveyor should be eliminated. To further improve reliability the level probe in the lock vessel should be modified or replaced.

3.5.2 Run GCT1B Through D Operational Summary

The spent fines ash removal system required a significant amount of attention during the GCT1B through D run. The ash-removal system was the "bottle-neck" of the entire process because char accumulation in the cone of the PCD was unmanageable. Other problems associated with the ash removal system were poor level-probe performance and slow lock-vessel venting.

During the GCT1B through D run char accumulation in the cone of the PCD was a reoccurring problem. This limited the flexibility of the transport reactor operation. The transport reactor would have to reduce the coal-feed rate every time the cone would fill up. Figure 3.5-6 shows the frequency of char accumulation. TI3022 and TI3021 are thermocouples in the cone of the PCD. As the char level rises and covers the thermocouple the temperature drops. The accumulation of char in the cone of the PCD was a result of higher inlet loading to the PCD.

Another factor that contributed to the char accumulation was the nitrogen purge on the outlet seal of the screw conveyor. It has been determined that the nitrogen purge was too high, hindering char from flowing out of the cone. Figure 3.5-7 shows a simplified diagram of the PCD and the ash-removal system. The high-nitrogen flow essentially "fluffed" the cone and pushed char up the walls of the PCD. As the char built up on the walls of the PCD the thermocouples were covered giving the impression that char was accumulating in the cone of the PCD. Prior to GCT2 some type of flow restriction will be added to the outlet-side seal purge. At approximately 06:15 on December 15 the run ended when it appeared that the screw cooler "plugged" and was no longer conveying solids (as shown in Figure 3.5-7).

The FD0520 system failed on one occasion during GCT1B through D. The lock-vessel spheri valve failed due to fouling of the shuttle valve associated with the limit switch. The valve starting working correctly when lubricated.

Just as in GCT1A, the level probe proved to be unreliable. The probe was too sensitive to the char movement in the lock vessel; the probe was disabled early in the run and the ash-removal cycle was placed on a timer. Based on the condition of the PCD cone the cycle timer ranged anywhere from 15 seconds to 2 minutes. Also, without a functional level probe a large amount of attention was given to the system to ensure char was not accumulating in the cone of the PCD. For future runs an alternative level device is being explored.

On several occasions the lock vessel had trouble depressurizing. In the vent line there is a gate valve that has a hole drilled in the plate to act as an orifice and this orifice did not allow proper discharge. Therefore, the gate valve was partially opened to allow the line to vent. Also, it was believed that the 1-in. vent line below the vent valve could have been limiting the flow of gas, so prior to GCT2 this portion of the vent line will be increased to a 2-in. line.

After the GCT1A run it was decided to replace the four-bolt (see Figure 3.5-3) drive-side seal-packing follower with a new eight-bolt design as shown in Figure 3.5-8. The new design significantly reduced leakage by applying uniform compression on the seal packing and placing less stress on a single bolt, which allowed more room for adjustments.

The GCT1B through D operational experience suggests that the addition of the eight-bolt design improved the problems associated with leakage on the drives side of the screw conveyor. By adding flow restriction to the nitrogen-seal purge the overall process performance should improve. In order to prevent excessive valve wear in the FD0520 system a functional level probe needs to be found and installed that will ensure that the system will cycle only when required.

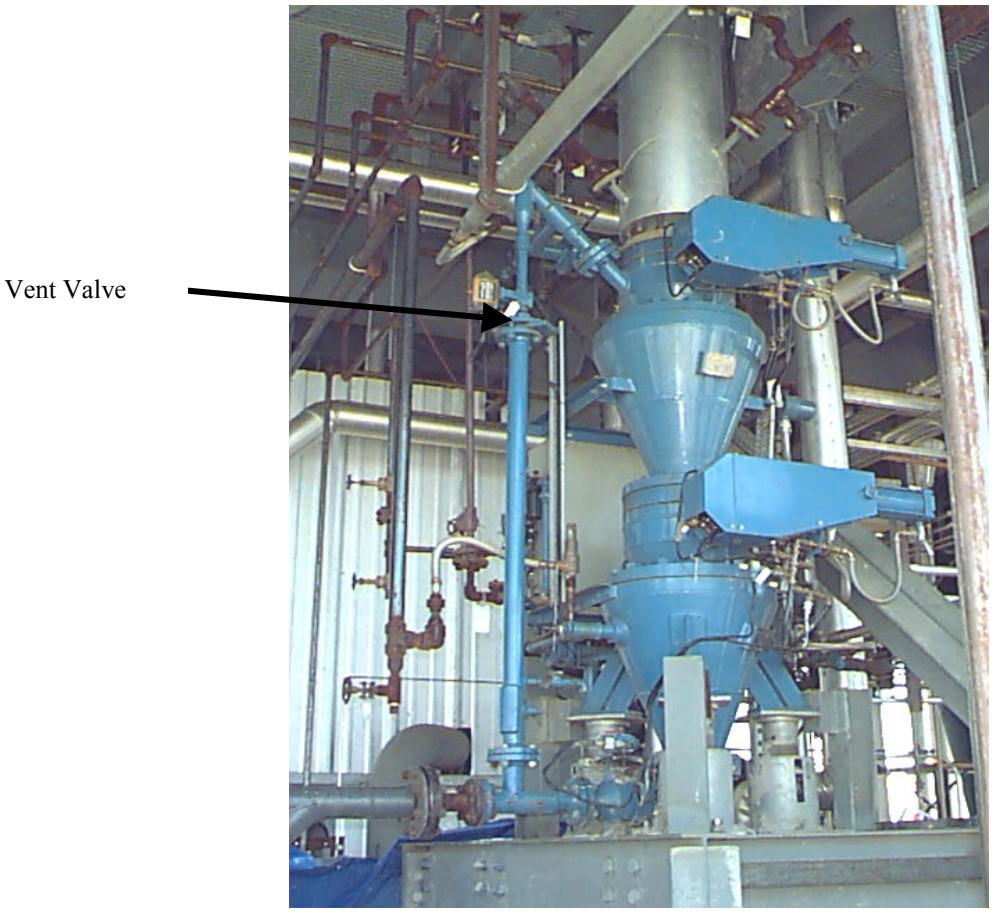

Figure 3.5-1 Spent Fines Transport System (FD0520)

Figure 3.5-2 FD0520 Vent Line Addition

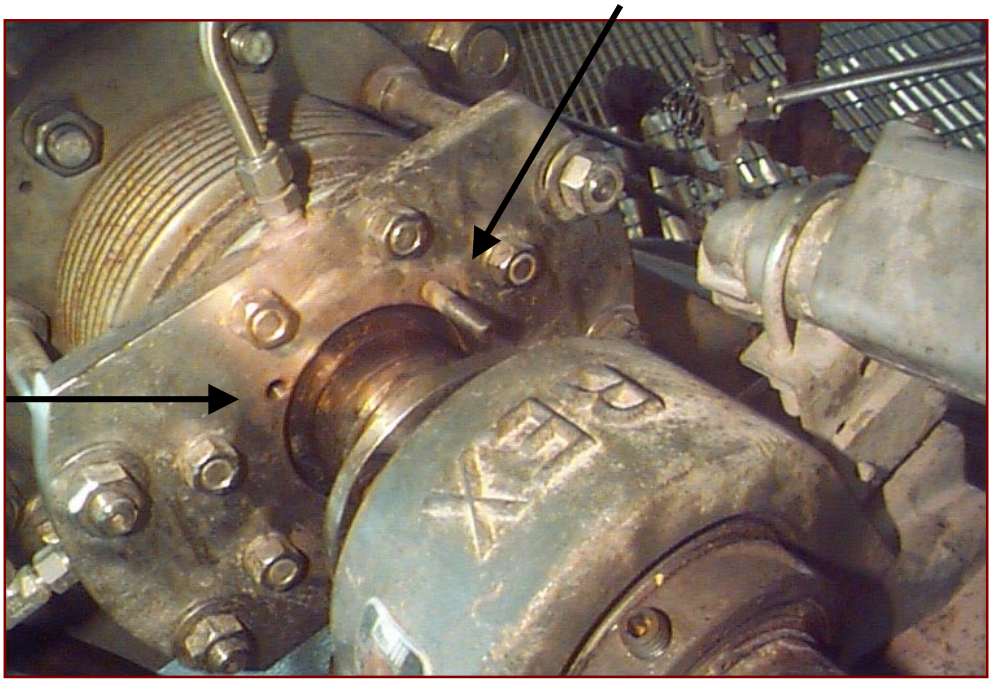

Figure 3.5-3 Drive-Side Seal Packing Follower (Four-Bolt)

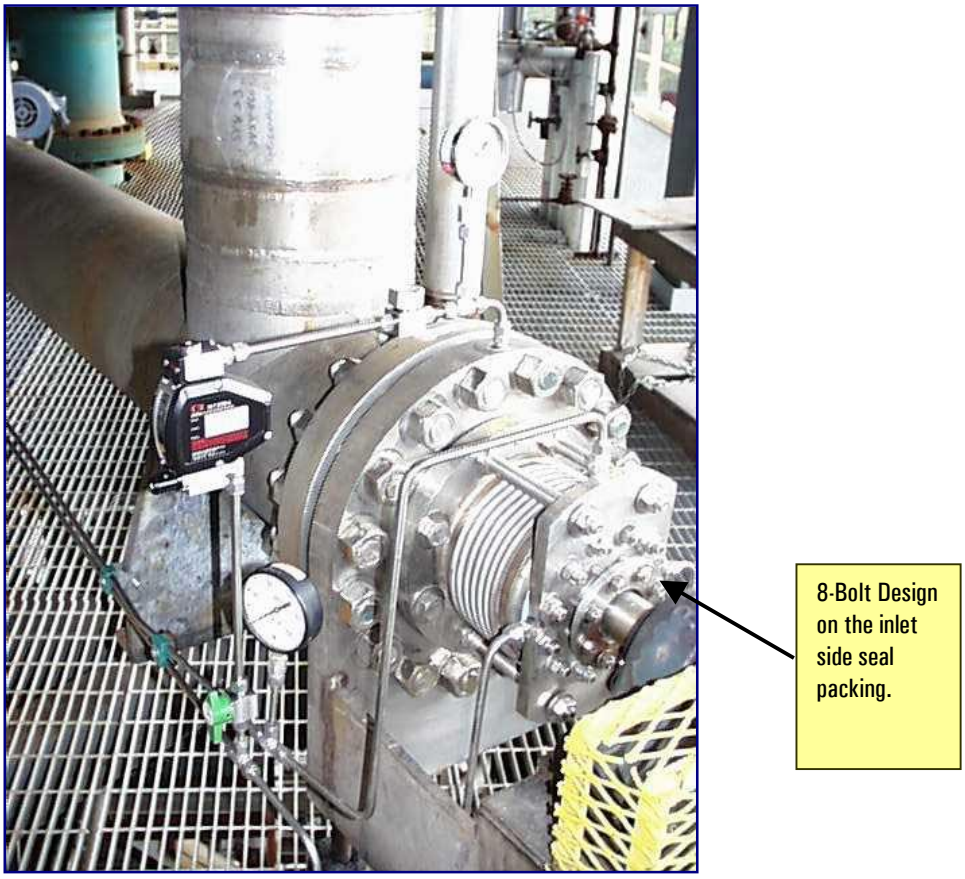

Figure 3.5-4 Inlet-Side Seal Packing Follower (Eight-Bolt)

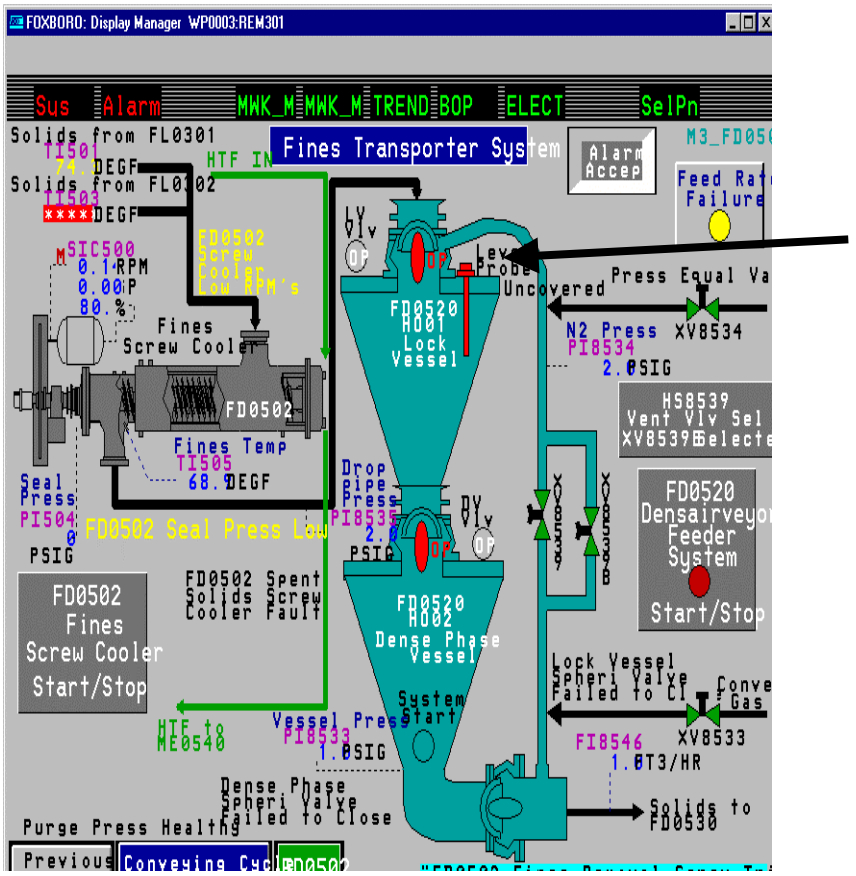

Lock-Vessel-Level Probe

Figure 3.5-5 FL0301 Ash Removal System

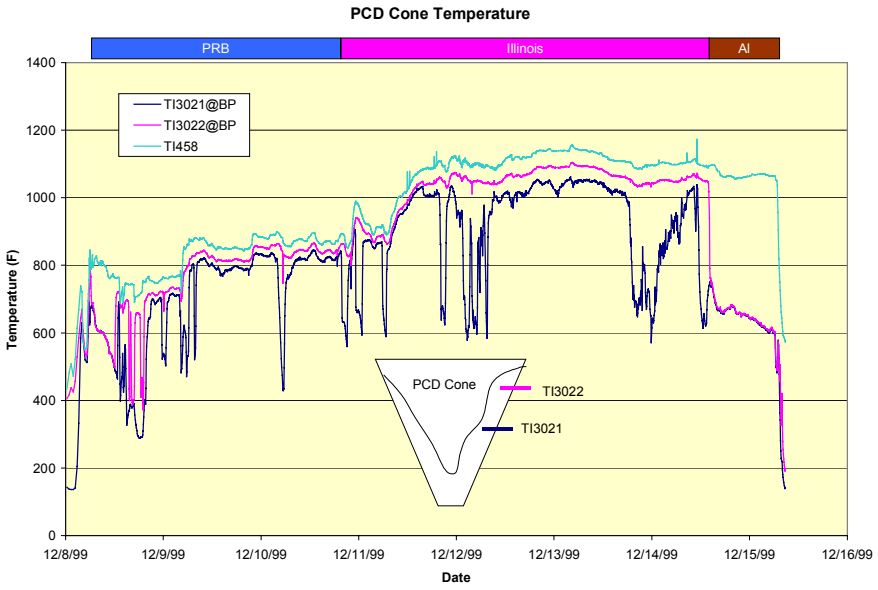

Figure 3.5-6 PCD-Cone Temperature Profile

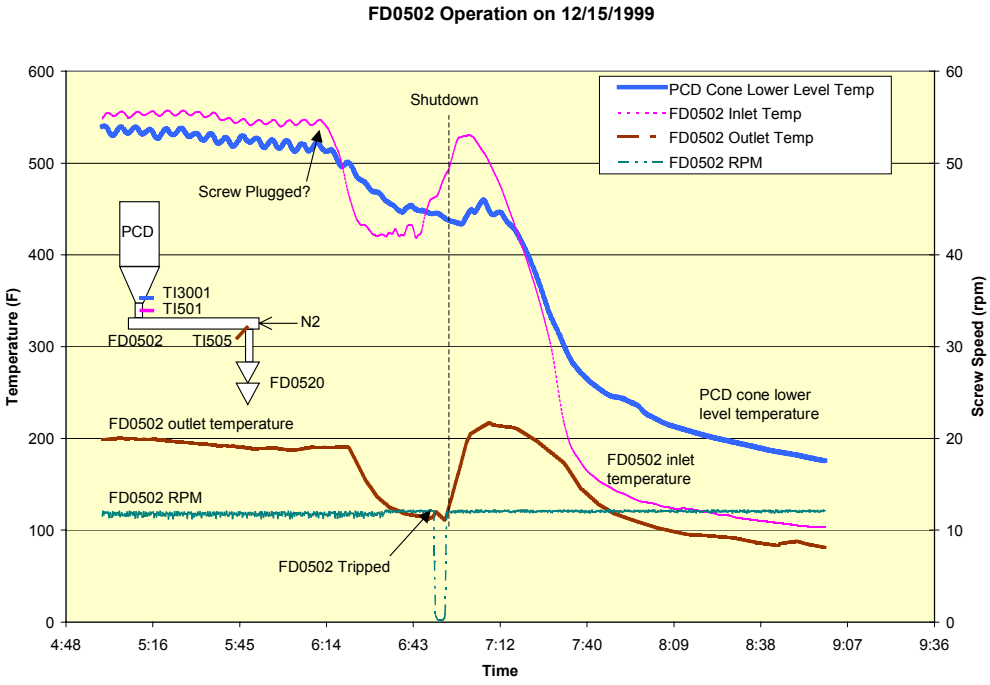

Figure 3.5-7 Ash Removal System Operation

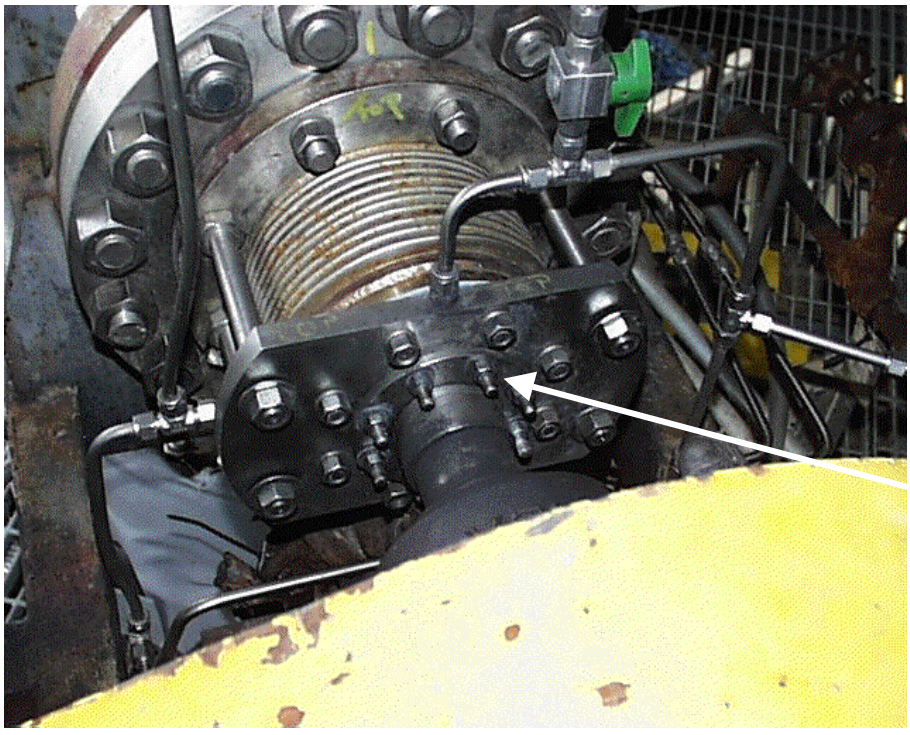

Eight-Bolt Design

Figure 3.5-8 Drive-Side Seal-Packing Follower (Eight-Bolt)

4.0 TRANSPORT REACTOR

4.1 GCT1 RUN SUMMARY

Test run GCT1 was started on September 9 (coal feed started on September 11) and continued through September 15, 1999, for GCT1A. Operations resumed on December 7 (coal feed started on December 8) and ended on December 15, 1999, with 233.1 hours on coal feed (63.4 hours for GCT1A and 169.7 hours for GCT1B through GCT1D-1). The mode of operation was gasification. See Table 4.1-1 for GCT1 operating conditions.

Both the transport reactor and the process were characterized for limits on operational parameter variations. Due to the short-time duration of the test run the tests were exploratory in nature and the results of some of the test objectives outlined below will be qualitative.

- Transport Reactor Commissioning – Complete precommissioning mechanical checks of process modifications and functional checks of safety interlocks and subsystems. Demonstrate stable and safe reactor, PCD, and other process operations using a Powder River Basin (subbituminous) coal and Plum Run dolomite sorbent.

- Sulfator Commissioning – Commission the sulfator preheat system, sorbent addition system, and solids removal and transport systems. Demonstrate stable operation of sulfator with char feed. Evaluate maintainability of operating temperature in the sulfator with varying char content in the feed, extent of sulfation, and SO_2 emissions.

- Other Subsystems Commissioning – Commission the flare and demonstrate stable reactor-start-up burner operations with low-excess air. Demonstrate complete incineration of syngas in the thermal oxidizer.

- Start-Up and Transition to Coal – Vary start-up procedures as necessary to minimize oxygen concentration in the process gas to PCD during heatup with the reactor start-up burner and during transition to coal gasification.

- Operational Stability – Characterize reactor loop and PCD operations with short-term tests by varying coal feed, air/coal ratio, riser velocity, solids circulation rate, system pressure, and air distribution.

- Reactor Operations – Devolatilization and tar cracking effects from transient conditions during transition from start-up burner to coal, effect of process operations on heat release, heat-transfer and accelerated-fuel-particle heat-up rates, and effect of changes in reactor conditions on transient temperature profiles, pressure balance, and product gas composition.

- Effects of Reactor Conditions on Syngas Composition – Vary air distribution, steam/coal ratio, and solids-circulation rate. (Effect of reactor temperature on CO/CO_2 ratio, gasification rates, carbon conversion, and cold- and hot-gas efficiencies.)

- Effects of Reactor Conditions on H_2S Emissions – Vary Ca/S molar ratio, riser velocity, and solids-circulation rate. Effects on limits of sulfur-capture dynamics in relation to CaS-H_2O-H_2S-CaO-reaction approach to equilibrium.

- Forms of Sulfur From Reactor Operations – Determine the effect of reactor operations on forms of sulfur (CaS, $CaSO_4$, FeS) in the reactor-standpipe solids and the fines from PCD. Quantify the reactive-sulfide concentration in these solids streams and at the sulfator-solids outlet.

- Bituminous Coal Feedstock – Characterize stable operations using Calumet Mine coal from Mary Lee seam in Alabama and Plum Run dolomite sorbent.

- Inspection – Upon shutdown, perform thorough inspections of start-up burner, complete reactor loop, disengager, primary cyclone, primary gas cooler, sulfator cooling coils, and other process equipment for any signs of corrosion due to H_2S and acid gases, deposit formation, and refractory and mechanical stability.

Activities during the outage after completing the TC05 combustion test campaign were focused on preparation for gasification. Spool pieces and spectacle blinds were changed to use nitrogen for char transport. Air can enter the reactor only through FV201 (the primary-combustion air nozzles), through FV680 (disconnected heat exchanger J-leg), and through the start-up burner air valves FV365 and FV386. During initial reactor heating the flow-through valves FV201 and FV680 are switched to nitrogen. The bottom of the combustion-heat exchanger was sealed and the heat exchanger was filled with sand. The top of the combustion heat exchanger remained connected to the standpipe since the combustion heat exchanger-to-standpipe spool piece was difficult to remove.

Preliminary work included pressure check of the reactor and repair of leaks, pressure balance of the PDTs, and filling the reactor and heat exchanger with 122 μm mmd sand. During the heat-up period the start-up burner tripped several times due to several reasons which were subsequently addressed. The GCT1A test period was from September 11 to September 15, 1999. The start-up coal was PRB coal with dolomite as sorbent. Coal feed started at 20:21 on September 11, 1999. The percent oxygen went to zero.

There were problems with steady-steam flow to the sulfator due to the large flow requirement (the condensate valves did not work well together to remove the water, resulting in condenser high pressure and multiple lifting of steam safety valves). These problems were corrected.

On September 12, 1999, at 15:13 the coal feeder stopped on a high-oxygen alarm created by calibration of the oxygen analyzer without deactivation of the alarm. An unsuccessful attempt was made to get coal feed back. The reactor was shut down and restarted on coal on September 13, 1999, at 10:54. A small amount of air was leaking through FV337 causing a high temperature on TI328 in the riser. The block valves were subsequently closed. Char was fed to the sulfator with a maximum operation temperature of 1,200°F. Coal-feed rate was about 2,100 pph with a reactor temperature of 1,450 to 1,550°F and pressure of 100 psig. On September 14, 1999, at 06:28 there was a total power failure. The coal fed system was shut down and minimum reactor and process operations were safely maintained for 2.5 hours before power was restored to the

facility. Coal feed was reestablished at 15:43. Sand was fed to the reactor to increase standpipe level. Reactor pressure was increased in steps to 180 psig. Since the PCD temperature was too high for metal candles in the presence of H_2S, the reactor was shut down on September 15, 1999, at 16:41.

After multiple piping revisions, restart of the gasification commissioning tests resumed at the end of November 1999. The diesel-fuel injection for the sulfator was tested. After addition of sand to the reactor on November 28, 1999, a heat-transfer fluid leak was found. The leak was through the internal shell of the inlet to the standpipe solids-removal screw (FD0206). The leak was through a weld crack. During the reactor heatup there were many start-up burner trips due to low excess air operations. It appears that the purple peeper intensity drops to zero once in a while and if it stays at zero more than a few seconds it trips the propane flow.

Coal feed started on December 8, 1999, at 05:15 with PRB coal and dolomite as sorbent. Test period GCT1B-1 was from startup to 11:20 on December 10, 1999. (See Table 4.3-1 for test period start and end times.) This period was used to establish steady state.

- At 06:03 the dipleg upset.
- At 06:25 the PCD cone was full of solids.
- At 12:10 the PCD cone was uncovered.
- At 13:01 and 13:10 the coal feeder tripped but was restarted.
- At 17:00 the PCD ash removal feeder (FD0520) operated intermittently primarily due to the logic that stops FD0520 if the high-level switch is made on the FD0530 surge bin. The FD0530 surge drum was full.
- At 17:20 the gas-analysis lines were beginning to plug with tar. Since FD0530 was full the PCD filled with solids and the coal rate was reduced. The PCD cone was cleared of solids at 01:10 on December 9, 1999.
- At 04:05 the coal feeder tripped and was put back on at 04:20.
- At 06:15 the high-level probe in FD0530 indicated a high level (240 ft^3) with only 3,000 lb, which indicated that the level probes were giving false indications.
- At 07:30 the spheri valve (FD0520) was not working properly due to fouling of the shuttle valve.

The period for GCT1B-2 from 11:20 to 13:15 on December 10, 1999, represents a high coal-feed rate (~4,200 pph) with PRB coal and dolomite at 175 psig. The air rate could not be raised above 11,300 pph because of high-reactor temperatures (1,740°F) and decreasing standpipe level.

The period for GCT1B-3 from 13:15 to 16:00 on December 10, 1999, was with a decreased-air rate (10,600 pph) and a slightly low coal-feed rate. The coal and sorbent were PRB and dolomite.

The period for GCT1B-4 represents PRB coal with limestone. At 16:00 on December 10, 1999, Alabama Longview limestone was started as sorbent.

At 18:05 on December 10, 1999, the Illinois No. 6 coal broke through with some PRB still in the silo. For period GCT1C-1 from 18:05 on December 10 to 07:00 on December 11, 1999, there

was a mixture of coal feeds with Alabama limestone. At 20:30 on December 10, 1999, the coal rate was reduced to 3,500 pph to reduce solids carryover to the PCD with the Illinois No. 6 coal.

A steady-state period with Illinois No. 6 coal and Alabama limestone was obtained between 07:00 on December 11 and 08:30 on December 12, 1999 (period GCT1C-2). The reactor pressure was increased to 192 psig. The highest temperature was 1,775°F in the midmixing zone. The coal rate was about 2,800 pph. There were several minor dipleg upsets and reactor pressure was increased from 190 to 200 psig during this period.

Ohio Bucyrus limestone was started at 08:30 on December 12, 1999 (period GCT1C-3). Nitrogen was leaking through the ball valves into the limestone feeder causing it to pressure up and blow more sorbent than was necessary for sulfur capture.

The auxiliary boiler stopped working due to loose wires at 14:15 on December 12, 1999, and was put back in service at 17:20. In test GCT1C-4 the reactor operation and performance evaluations were monitored in the absence of any steam flow.

With Illinois coal and Ohio limestone in use during the period of 17:20 on December 12 to 17:00 on December 14, 1999 (period GCT1C-5), the coal rate had to be reduced to 2,950 pph or solids accumulation would increase in the PCD. At 04:30 on December 13, 1999, the reactor pressure was increased to 210 psig. Tar was plugging the second-floor sample lines and there was a strong smell of naphthalene. The PCD baseline was increasing. Several thermocouples in the riser were fluctuating and had intermittent readings. TI360 was intermittent. TI367 was variable. TI329 was reading low and TI356 was reading wrong. Inspection of riser thermowells after the runs showed that the hardened end of TI356 in the crossover was totally eroded away. Part of the hardened end of TI360 near the top of riser was eroded and exposed the thermocouple. Other thermowells on TI352, TI351, TI328, TI368, TI329, and TI367 were highly eroded. TI328 and 329 were new thermowells at the start of the gasification tests. At 16:15 on December 13, 1999, coal feed was changed to the SI0112 silo, which contained 62 tons of Illinois No. 6 coal with Alabama coal on top.

GCT1D-1 was the last test period, from 17:00 on December 14 to 06:56 on December 15, 1999, and was with Alabama coal and Ohio limestone. The PCD cone was covered most of the period with a decreasing coal rate from about 2,700 to 2,200 pph. Coal feed was stopped at 06:56 on December 15, 1999, due to the high level of solids in the PCD cone.

Post GCT1 Reactor Inspection

The transport reactor was inspected on Wednesday, January 5, 2000. The primary cyclone and the vertical section of the dipleg were inspected with the borescope. There was a deposit of loose material around the H_2 nozzle used for insertion of the borescope. Most of this was dislodged through the movement of the borescope during the inspection. The walls were covered in thin layers of loose material. No hard deposits were found. The slant section of the dipleg was inspected visually and with the borescope. The dipleg was clear.

The riser and the mixing zones were inspected with the borescope. The riser was generally clear. The mixing zone had some moderate deposits on the walls. The deposits appeared to be located a few feet below the coal-feed nozzle, with more material in the lower mixing zone. They appeared to be soft and to extend a few inches from the wall.

Only a small amount of loose, granular material was observed in the riser crossover.

The standpipe was relatively clear although there were increasing signs of wear on the refractory — a number of small cracks could be seen and there were a few missing small refractory pieces as well.

The primary gas cooler (HX0202) was inspected by removing the spool piece above the heat exchanger. Only three tubes were completely unblocked with three more tubes partially obstructed. The remaining tubes were covered in a layer of loose material. Some of the material had formed agglomerates approaching 1- to 2-in. diameter.

The small bottom flange was removed from the secondary gas cooler (HX0402). Immediately above the flange was a layer of brown and yellow "mud." Six to eight inches above the flange was a very hard deposit of tar.

The small bottom flange on the sulfator heat exchanger (HX0601) was removed. A large amount of very fine material was removed from the heat exchanger. It was unclear whether any tubes were actually blocked.

Nozzle R on the reactor start-up burner (BR0201) J-leg was opened. A significant amount of granular char was removed along with several large 1- to 2-in. agglomerates, some smaller (less than 1 in.) clinkers, and some small refractory pieces.

Table 4.1-1

GCT1 Operating Conditions

Start-Up Bed Material	Sand
Fuel Type	Powder River Basin Coal Illinois No. 6 Coal Alabama Calumet Mine Bituminous Coal
Fuel Particle Size (mmd)	300 to 350 μm
Average Fuel-Feed Rate	1,500 to 4,000 lb/hr
Sorbent Type	Plum Run Dolomite Ohio Bucyrus Alabama Limestone
Sorbent Particle Size	15 to 140 μm
Average Sorbent-Feed Rate	100 to 700 lb/hr
Ca/S Molar Ratio	Ratio Required for 90%+ Sulfur Capture
Reactor Temperature	1,600 to 1,800°F
Reactor Pressure	150 to 215 psig
Riser-Gas Velocity (fps)	Design – 1.5 x Design
Solids-Circulation Rate (lb/hr)	0.3 x Design – 1.1 x Design
Primary Gas-Cooler Bypass	0%
PCD Temperature	700°F
Total Gas-Flow Rate	19,000 to 22,000 lb/hr
Air/Coal Ratio	2.0 to 3.5
Primary Air Split ($1^{st}/2^{nd}$ Levels)	90/10
Steam/Coal Ratio	0.2 to 0.5
Sulfator Operating Temperature	800 to 1,600°F
Planned Duration of Coal Feed	Nominally 150 Hours

Table 4.1-2

Coal Analyses as Fed[1]

	Alabama	Illinois No. 6	PRB
Moisture	2.2	4.2	15.4
Ash	16.9	11.8	8.5
Sulfur	0.9	2.9	0.6
C	66.4	67.0	58.6
H	4.3	4.4	4.0
N	1.6	1.4	1.0
O	7.8	8.3	11.9
Vol	31.2	38.3	36.1
Fix C	49.5	45.7	40.1
Calculated Heating Value(Btu/lb)	11,911	11,947	10,091

1. Data from TC05 test run.

Table 4.1-3

Sorbent Analyses[1]

	Plum Run Dolomite From Ohio	Bucyrus Limestone From Ohio	Longview Limestone From Alabama
$CaCO_3$ (wt %)	49.7	73.0	88.7
$MgCO_3$ (wt %)	41.9	15.8	5.5
Inerts (wt %)	8.4	11.2	5.8

1. Data from TC05 test run.

4.2 HEAT BALANCE

To gain a better understanding of the transport reactor operations a heat balance was performed for the reactor mixing zone and riser. Each thermocouple was taken as an independent control volume. Assumptions were made as to the amount of gas and feed solids heated within the control volume based on gas and solids velocities and on orientation of nozzles and thermocouples. The actual gas analysis was used to calculate heat-release rates based on CO and CO_2 production. Figures 4.2-1 and -2 show plots of actual and predicted temperatures for GCT1B through D. The plots show a good agreement between the actual and predicted balance.

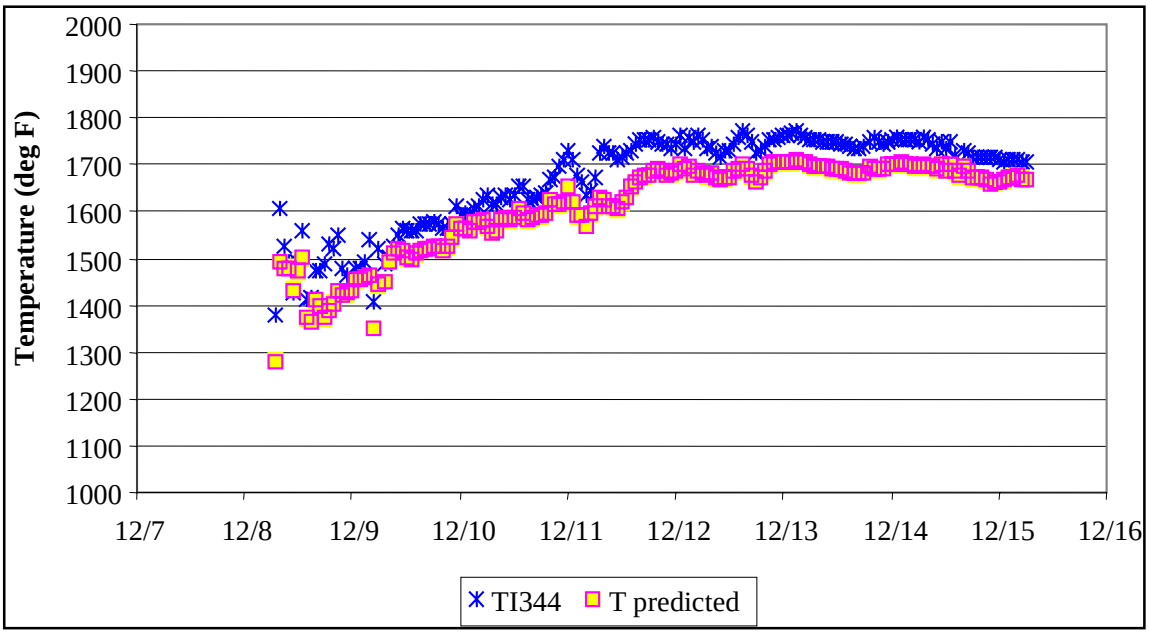

Figure 4.2-1 Mixing Zone Temperature (TI344) Actual Vs. Predicted

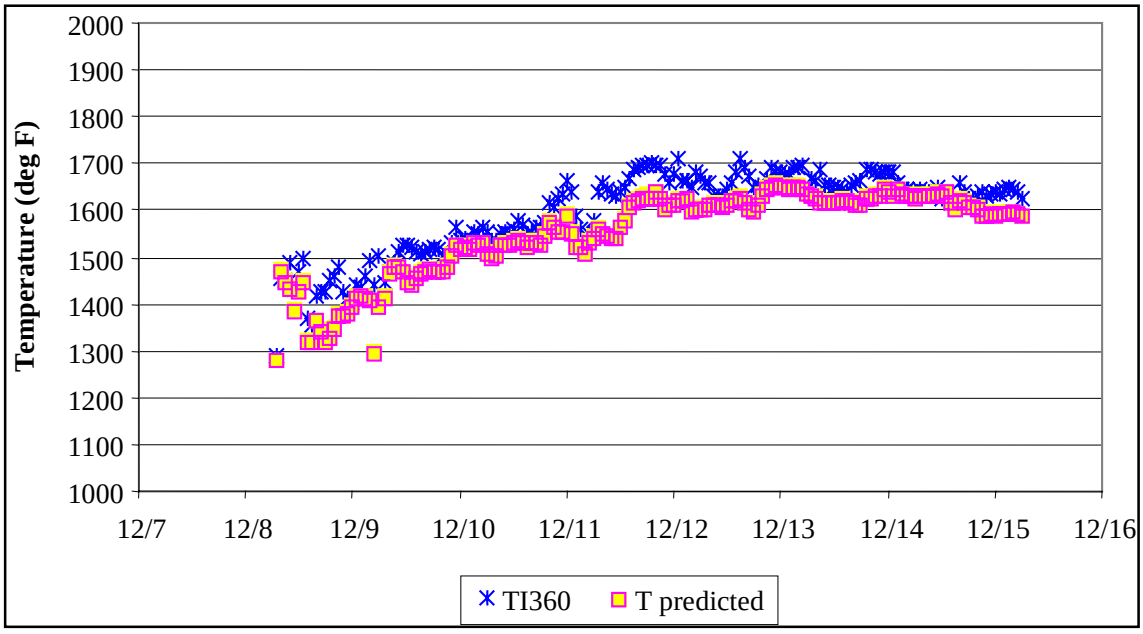

Figure 4.2-2 Riser Temperature (TI360) Actual Vs. Predicted

4.3 GAS ANALYSIS

During GCT1 fuel gas and combusted fuel gas composition analyses were continuously measured and recorded by the plant information system (PI). This section will use the gas analyzer data to show:

- Fuel gas-heating value.
- Fuel gas-molecular weight.
- Fuel gas compositions, including CO, H_2, CO_2, H_2O, N_2, CH_4, and C_2H_6.
- Fuel gas-sulfur levels.

Run GCT1 began on September 11 and ended on December 15, 1999, and consisted of four separate test periods (A through D) distinguished by the fuel used. The start and end time of each test as well as the fuel and sorbent are shown in Table 4.3-1. Test A consisted of three separate runs of 19 to 25 hours separated by a shutdown and restart. This section will ignore analysis of test GCT1A due to the lack of steady-state data during the short periods of operations. Test period GCT1C-1 was a transition period when Powder River Basin (PRB) and Illinois No. 6 coals were both fed to the reactor. No sorbent was added during test GCT1D due to operational problems. The exact test-start and -end times are a bit arbitrary because each new fuel and sorbent was placed on top of the previous fuel or sorbent in the bin system. There was some rat holing and backmixing of solids which resulted in solids not arriving at the time expected. The several transitions from PRB to Illinois No. 6 coal were clearly marked by their different reactivity and sulfur content. The sorbent transitions could not be clearly marked.

The fuels used during GCT1 were:

- PRB coal (a mixture of four different PRB coals) (tests A and B).
- Illinois No. 6 coal from the Pattiki Mine owned by the White County Coal Corporation (test C).
- Alabama Calumet Mine bituminous coal (test D).

Figure 4.3-1 shows hourly averages for the mixing zone temperatures, PCD (FL0301) inlet temperatures, and reactor pressures for GCT1B, C, and D. The first day of operation on PRB coal (test B) was characterized by fairly unsteady temperature at 1,400 to 1,600°F, 100 psig reactor pressure, and 800°F PCD temperature. At noon on December 12 the rector pressure was increased to 150 psig and the reactor temperature leveled out at 1,600°F. The reactor pressure was again increased to 175 psig early on the morning of December 10 and the reactor temperature slowly increased from 1,625 to 1,675°F until the PRB/Illinois coal transition. The PCD temperature remained constant at 875°F for several days until the PRB/Illinois coal transition. The PRB/Illinois coal transition is shown as a shaded area in Figure 4.3-1 (and all

other figures) since that was an unsteady period of reactor operation due to the sudden switching of two fuels that react at different rates. When the Illinois coal broke through at about 18:00 on December 10 the reactor temperature suddenly decreased. Once the reactor temperatures were stabilized a slug of PRB coal broke through at around 00:00 on December 11 and the reactor temperature suddenly increased. The last batch of PRB coal was finally fed at around 07:00 on December 11 when the reactor temperatures again dropped. (Note in Figure 4.3-1 that the PCD temperature swung up 100°F to 975°F and back down again during the coal-transition period.)

Once only Illinois No. 6 (test GCT1C-2) was fed to the reactor the temperatures were held constant at 1,800°F for several days. On the last day of operation on Illinois coal and Alabama coal the temperature dropped to 1,760°F. The reactor pressure was slowly increased during the Illinois operation from 190 to 215 psig. The PCD temperature slowly increased from 1,100 to 1,140°F during the first several days of Illinois coal operation. On December 13 the PCD temperature slowly decreased back to 1,100°F where it remained constant until late December 14. The PCD temperature decreased again on December 14 to 1,060°F and remained there for the Alabama coal test. The decreases in PCD temperature were caused by decreases in coal-feed rate (see Figure 4.3-2) to decrease the PCD-solids rate (see Figure 4.5-3).

Hourly averages for the coal-feed and air rates are shown in Figures 4.3-2. The fuel feed rate was calculated from the coal feeder speed and a correlation from the FD0210 weigh cells. The correlation is different for the PRB and the Illinois and Alabama coals. The air rate was obtained from FI205.

The coal and air rates varied a lot during the first day of PRB operation (December 8). During the morning of December 9 the coal and air rates were stabilized at 2,500 and 8,000 lb per hour, respectively. To increase the gas-heating value the coal rate was increased to the maximum rate of about 4,000 lb per hour late on December 9. The best gas-heating value was achieved at this coal-feed rate. During the transition period between PRB and Illinois coals the coal and air rates were varied to try to stabilize the reactor.

The coal rate was set at 2,800 lb per hour for the first day of Illinois operation. The coal rate was then decreased to 2,500 lb per hour on December 12 to decrease the solids rate to the PCD. The air rate was generally decreased to follow the coal rate and maintain a constant air-to-coal ratio (see Figure 4.3-13). The coal rate was increased to 3,000 lb per hour late on December 12 and then was slowly decreased to 2,700 lb per hour and maintained constant until the start of the Alabama coal test where it was decreased to 2,500 lb per hour. During the Alabama coal test the coal-feed rate was slowly decreased from 2,500 lb per hour to 2,300 lb per hour at the end of the test. Again, the air rate tracked the coal rate during the Alabama coal test.

The gas-analyzer system analyzed for the following gases during GCT1 using the analyzer tags beside each gas listed below:

H_2	AI464G
CO	AI425, AI453G, AI464C
CO_2	AI464D
CH_4	AI464E

C_2H_6+	AI464F
N_2	AI464B

The AI464B-G analyzers are from a single gas chromatograph and typically have about a 6-minute delay. The two other CO analyzers (AI425 and AI464C) are IR, which give more real-time measurements. All analyzers require that the gas sample be conditioned to remove water vapor so all the analyzers report gas compositions on a dry basis.

During the run the gas-analyzer conditioning system frequently plugged with tar and naphthalene which required analyzer technicians to clean the gas-analyzer conditioning systems. Around noon on December 13 the gas-analyzer system could not be cleaned of these plugs so no gas analyzer data was available for the rest of GCT1. The gas analyzers were off-line for the following periods:

- 22:00 December 8 to 07:00 December 9.
- 01:00 to 15:00 December 12.
- 11:00 December 13 to the end of the run.

The raw-gas analyzer data was adjusted in four steps to produce the best estimate of the actual gas composition:

- Choice of CO analyzers.
- Correction of GC H_2 data.
- Normalization of gas compositions (force to 100 percent total).
- Conversion of dry compositions to wet compositions.

With three CO analyzers there is a measure of consistency when all, or two of three, analyzers read the same value. There is also the choice of which analyzer to believe when none of the three analyzers agree. Hourly averages for the three CO analyzers raw data are shown in Figure 4.3-3. On the first day of operation there were only a few hours where the three analyzers agreed. On December 9, 1999, AI425 read higher than the other two analyzers, plus the GC analyzer AI464C did not follow the trends of the other two very well. From 08:00 on December 9 to 13:00 on December 10, 1999, AI425 was used. During the morning of December 10 all three analyzers were reading different values but at 12:00 all three analyzers were reading the same value and continued to agree with each other until the analyzers went off-line on December 13. The nonconforming points in the afternoon of December 11 are probably due to analyzer calibrations.

During the test run the sum of the raw-gas concentrations were consistently less than 100 percent at around 96 percent. When the sum of the concentrations went below about 95 percent this was a good indication that the analyzer sampling system was plugged. During the

next gasification run (GCT2) the analyzer technician noticed that the H_2 peak was overlapping another peak. Once the H_2 peak was correctly resolved the H_2 concentration increased to about three times its previous value. The CO and H_2 concentrations were correlated using post recalibration data to predict the correct H_2 concentration prior to the recalibration. The result of this calibration is shown on Figure 4.3-4 (GCT2 data). All GCT1 H_2 concentration data were calculated from the following correlation:

$$H_2 = CO \times 0.7318 + 1.5361 \quad (1)$$

This correlation is only valid for PRB coal at the beginning of operating conditions of GCT2 but will be used for GCT1. The use of the correlation produces sums of fuel gas mole percents that are closer to 100 percent, and it is certain that some of the missing gas was in fact H_2. Figure 4.3-5 provides the sum of the gas compositions for GCT1. For most of the PRB run the sum of gas compositions was above 100 percent by about 1.0 to 2.0 percent, indicating that the H_2 content was possibly overcorrected. After the PRB/Illinois coal transition the sum of compositions went down to 100 percent and seemed to stay there.

All gas compositions were normalized by dividing each gas composition by the sum of the mole fractions. This forces the dry-gas compositions to add up to 100 percent.

The fuel-gas water vapor content was measured five times during GCT1. Since the KBR transport reactor does not have a working H_2O analyzer this is the only H_2O measurement of the fuel gas during GCT1. Water-gas-shift equilibrium constants were calculated for each moisture measurement using the wet normalized CO_2, H_2, and CO concentrations (shown in Table 4.3-2). The water-gas-shift reaction:

$$CO + H_2O \leftrightarrow H_2 + CO_2 \quad (2)$$

The water-gas-shift equilibrium constant:

$$Kp = \frac{(H_2)(CO_2)}{(H_2O)(CO)} \quad (3)$$

() = partial pressure, mole per cent, or mole fraction

The water-gas-shift equilibrium temperatures for a given gas composition can be determined from literature thermodynamic data (see Table 4.3-2). Typically in design the water-gas-shift equilibrium is estimated from an approach to equilibrium temperature. The approach to equilibrium was determined from the riser inlet temperature. Note that the four equilibrium temperatures increase with increasing riser temperatures and that the H_2O content was larger for Illinois coal than for PRB coal, which is surprising since the PRB coal has a higher moisture and H_2 content than Illinois coal. The average approach to equilibrium temperature was -123°F. To estimate gas-moisture content in the fuel gas for times when the moisture content was not

measured, an average approach temperature of -123°F was used. The measured and calculated H_2O concentrations are shown in Figure 4.3-6.

The normalized fuel gas compositions (corrected for water vapor) for CO_2, H_2, CO, CH_4^+, and C_2H_6+ are plotted in Figure 4.3-7. The compositions varied a lot during the first day of operation. The H_2 and CO concentrations follow each other quite closely as forced by the use of equation (1). Note the sudden dip and recovery of the H_2 and CO concentrations during December 9. The CO_2 slowly increased during the run from 8 to 10 percent. The CO and H_2 rose to 8 percent at the end of the PRB run.

The transition from PRB to Illinois coal was not smooth, which can be tracked by the CO and H_2 concentrations during the transition period. The CO and H_2 suddenly dropped to 5.5 percent (at 23:00) from 9.0 percent (at 18:00) on December 10 when the Illinois coal broke through. The CO and H_2 peak at 04:00 and 05:00 on December 11 was caused by a slug of PRB coal that came through the FD0210 system. Then the Illinois coal came back at 07:00 on December 11 and the CO and H_2 dropped back to about 5.0 percent. For the remainder of the Illinois coal testing the gas concentrations were fairly constant.

The gas molecular weight and N_2 concentrations are plotted in Figure 4.3-8. The gas molecular weight and N_2 concentration were scattered during the first day of operation. On December 9 the molecular weight leveled out at 27.2 lb/lbmole and the N_2 leveled out at 74 percent. The increase in coal-feed rate on December 9 lowered the molecular weight to 26.6 lb/lb mole and the N_2 concentration to 66 percent. During the transition period from PRB to Illinois coal there were wide swings in both the molecular weight and the N_2 percent. The gas molecular weight leveled off at 27.1 lb/lbmole and the N_2 percent leveled off at 70 percent for the remainder the Illinois coal run when the gas analyzers were operating. The FI465 transmitter molecular weight was not changed from the combustion value of 30 lb/lbmole so a correction factor was developed using a thermal oxidizer oxygen balance. The correction was to multiply the measured FI465 reading by 1.11, which increased the flow rate and produced a better thermal oxidizer oxygen balance. This is shown in Figure 4.3-9.

The PSDF transport reactor adds more N_2 per pound of fuel gas than a commercial reactor because of the additional PSDF sampling purges, additional PSDF instrument purges, and the need to aerate the lower portion of the reactor J-legs. A commercial reactor would have no sample purges, fewer instruments, and relatively less aeration to J-legs. Any instrument purges would be proportionally smaller in a commercial design due to the scale factor (instruments stay the same size as plant size increases). Any additional N_2 added to the riser also requires additional fuel to bring the additional N_2 up to operating temperature; this additional fuel would go to fuel gas-heating value in a commercial reactor. It is proposed in a commercial reactor that significant quantities of N_2 for aeration would only be used for startup. To determine a commercial fuel gas the N_2 that comes in as FI609 (medium-pressure nitorgen flow) is taken out of the fuel-gas rate and then the fuel-gas concentrations and heating values are calculated using the remaining gas.

The lower gas-heating (LHV) value was calculated from the wet-normalized-gas compositions using the formula:

$$\mathrm{LHV(Btu/SCF)} = \left\{ \begin{matrix} 275\times(\mathrm{H_2\%}) + 322\times(\mathrm{CO\%}) + \\ 913\times(\mathrm{CH_4\%}) + 1641\times(\mathrm{C_2H_6\%}) \end{matrix} \right\} /100 \qquad (4)$$

The PCD exit LHV and the N_2-addition-corrected LHV of the fuel gas are plotted in Figure 4.3-10. The corrected LHV was at about 55 Btu/SCF at the start of the run, then slowly increased to 95 Btu/SCF by the end of the PRB testing on December 10. The increase seemed to precede the sudden coal-rate increase late on December 9 (see Figure 4.3-2) and follow the pressure increase on December 9 (see Figure 4.3-1). With the introduction of Illinois coal the LHV steadily decreased back to 55 Btu/SCF except for the short reintroduction of PRB on December 11 at 04:00 and 05:00. Again the rapid switching of coals during the PRB/Illinois coal transition shows up as wide swings in gas LHV.

Data obtained from the thermal oxidizer BR0401 (atmospheric syngas combustor) can be used to determine:

- Consistency check of the fuel-gas composition and flow rate with the thermal oxidizer data.
- The approximate heating value of the fuel gas when the gas analyzers were not operating.

The thermal oxidizer can be used as a large calorimeter to determine the fuel-gas-heating value since all the flows into the analyzer are measured, including fuel gas, propane, and air. The thermal oxidizer is not part of the commercial flow sheet. In a commercial plant the fuel gas would be burned in a combustion gas turbine.

To calculate the heating value of the fuel gas using the thermal oxidizer and the available data the thermal oxidizer heat loss must be known. For these calculations the thermal oxidizer heat loss was used as an adjustable parameter to "fit" the thermal oxidizer heating values with the gas analyzer heating values. The heat loss forcing agreement between the thermal-oxidizer LHV and the gas analyzer heating value was then plotted against the thermal oxidizer exit temperature as shown in Figure 4.3-11. The heat loss required varies from zero to 7.0 x 10^6 Btu/hr when the thermal oxidizer exit temperature was above 1,600°F. While the required heat loss varies a lot, the heat loss is just being used as a correlating parameter. A comparison of the gas analyzer and thermal-oxidizer-heating values is shown in Figure 4.3-12. The fit is not too good during the first day of operation and in the middle of December 9. It is good from the end of December 9 to the end of PRB and through the PRB/Illinois coal transition. The comparison is not very good for December 11 at the start of the Illinois coal operation but is good for the final day of Illinois coal operation when the gas analyzers were operating.

The heating values calculated from the thermal-oxidizer-energy balance for the entire period of operation from December 8 to 15 are shown with the air-to-coal ratios in Figure 4.3-13. This

figure shows the fuel gas lower heating values when the gas analyzers were not in operation. About a day after startup the PRB LHV stabilized at about 75 Btu/SCF (corrected for N_2) and an air-to-coal ratio of 3.25. When the air-to-coal ratio decreased to 2.5 due to a coal-rate increase late on December 9 the LHV increased to about 90 Btu/SCF. The transition period had swings from 82 to nearly zero LHV and finally stabilized at about 60 Btu/SCF and 3.5 air-to-coal ratio. After December 13 the LHV decreased from 55 to 45 Btu/SCF for Illinois coal. The LHV then slowly increased to 50 Btu/SCF. The Alabama coal seemed to decrease slightly, to nearly 40 Btu/SCF at the end of the run. During both the Illinois and the Alabama coal test the coal-feed rate was decreased (air-to-coal ratio increased) to decrease the particulate loading on the PCD.

The H_2S analyzer was not working during GCT1 but the thermal-oxidizer-SO_2 analyzer was working so the concentration of gaseous sulfur compounds (H_2S, COS, CS_2) in the transport reactor could be calculated from the thermal oxidizer SO_2 analyzer reading and the thermal oxidizer data. The measured SO_2 data are plotted with the calculated gaseous sulfur data in Figure 4.3-14. As expected, the sulfur emissions are low at about 200 to 300 ppm for the PRB coal since the PRB sulfur content was about 0.3 percent (see Figure 4.4-1) while the Illinois coal sulfur emissions were much higher at 400 to 1,000 ppm. The sulfur emissions of the Illinois coal test varied significantly during the period of operation. In section 4.4 the sulfur removals will be determined from the coal-sulfur content and compared to the PCD calcium-to-sulfur ratio.

The equilibrium-H_2S concentration in coal gasification using limestone is governed by three reversible reactions:

Reaction

$$CaCO_3 \leftrightarrow CaO + CO_2 \quad (5)$$

$$H_2S + CaO \leftrightarrow CaS + H_2O \quad (6)$$

$$H_2S + CaCO_3 \leftrightarrow CaS + H_2O + CO_2 \quad (7)$$

Reaction (5) is the limestone-calcination reaction. At thermodynamic equilibrium, according to the equilibrium constant, the CO_2 partial pressure should be a function of only system temperature as long as both $CaCO_3$ and CaO are present:

$$K_1 = P^O_{CO_2} \quad (8)$$

P^O_{CO2} is the partial pressure of CO_2. A plot of the partial pressure of CO_2 and temperature is shown in Figure 4.3-15.

At thermodynamic equilibrium, $CaCO_3$ and CaO only coexist on the equilibrium curve, while above the curve only $CaCO_3$ exists and below the curve only CaO exists. Typically there are both $CaCO_3$ and CaO in the PCD solids. This is because of kinetic limitations and the quick cooling down of the solids in the fuel gas from the reactor temperatures to PCD temperatures. This quick cooling down tends to "freeze" reactions at higher equilibrium temperatures than

would be indicated by the actual system exit temperature. In GCT1 the CO_2 partial pressures were typically around 20 psia. This curve was generated by curve fitting the results from Aspen simulations.

The H_2S equilibrium is governed by reactions (6) and (7) with the associated equilibrium constants:

$$K_2 = \frac{P^O_{H_2O}}{P^O_{H_2S}} \tag{9}$$

$$K_3 = \frac{P^O_{H_2O} P^O_{CO_2}}{P^O_{H_2S}} \tag{10}$$

Equations (5) through (7) state that the equilibrium H_2S concentrations in the $CaCO_3$-CaO-CaS system is a function of the system temperature and the CO_2 and H_2O partial pressures. As the CO_2 and H_2O partial pressures increase so would the H_2S partial pressures. The equilibrium constants are all functions of temperature and can be determined using thermodynamic data with Aspen simulations.

The H_2S equilibrium concentrations as a function of temperature are shown in Figure 4.3-16 for the average conditions for a 4-hr period (13:30 to17:30 on December 10, 1999) when the unit was operating on PRB coal and dolomite.

The H_2S-equilibrium curve was determined from Aspen simulations. The average partial pressure of CO_2 was 17 psia (175 psig system pressure, 9.5-percent CO_2) which means that the CO_2 partial pressure shown in Figure 4.3-16 crosses the CO_2 equilibrium partial pressure curve at 1,642°F. This means at equilibrium for 17 psia CO_2 partial pressure, 1,642°F is the only temperature at which CaO and $CaCO_3$ can coexist. At equilibrium calcium is only present as CaO or CaS above 1,642°F, and below 1,642°F all calcium is present as $CaCO_3$ or CaS. In Figure 4.3-16 the heavy vertical line divides the graph into a $CaCO_3$ region (left-hand side) and CaO region (right-hand side).

The temperature dictates which H_2S reaction will be used for sulfur removal, either (6) or (7), since (6) contains CaO and (7) contains $CaCO_3$. Thermodynamic data for equation (7) indicates that H_2S concentration decreases with temperature increase, while thermodynamic data for equation (6) indicates that H_2S concentration increases with temperature increase. Both curves meet at the equilibrium temperature for $CaCO_3$ calcination (1,642°F determined by the CO_2 partial pressure), which also determines the minimum equilibrium H_2S concentration (160 ppm H_2S) possible for the measured partial pressures of H_2O and CO_2. This minimum equilibrium concentration is independent of the amount of excess sorbent that is added to the system.

The main sulfur species in coal gasification are considered to be H_2S and carbon oxysulfide (COS). There should also be only a minor amount of carbon disulfide (CS_2). KRW data indicate that the majority of the gaseous sulfur is present as H_2S with the balance COS. The

KRW COS-concentration data were fairly constant at 100 to 300 ppm COS for 1.0- to 5.0-percent sulfur fuels.[1] To estimate the H_2S concentration, the COS concentration was assumed to be 100 ppm for the PRB coal testing and 200 ppm for the Illinois coal testing.

The measured sulfur concentrations and the maximum coal-sulfur emissions (calculated from the coal sulfur assuming that all coal sulfur is released as sulfur species to the fuel gas) are shown as horizontal lines in Figure 4.3-16. The measured sulfur emissions and coal-sulfur emissions indicate 45-percent sulfur capture. Both horizontal sulfur emission lines end at the maximum temperature measured in the reactor (1,666°F), which was barely above the calcination temperature. The measured sulfur emissions were 251 ppm. Using the estimated COS concentration of 100 ppm for PRB coal the estimated H_2S emissions were 151 ppm, which is 9 ppm less than thermodynamic minimum H_2S. The theoretical H_2S removal is defined as the percentage of H_2S actually captured out of the maximum H_2S capture assuming that the equilibrium H_2S concentration is the minimum H_2S concentration. Since the minimum-H_2S concentration achievable was 160 ppm the theoretical H_2S removal was 100 percent.

The PCD solids had about 40-percent calcination during this period, which indicates that the solids got above the calcination temperature long enough to calcine and then were cooled rapidly enough to prevent complete recarbonation. Calcination is defined as the mole-percent CaO divided by the sum of the moles percent of CaO and $CaCO_3$. Reaction (5) should go forward quickly since it is a decomposition reaction while the reverse of reaction (5) should be slowed by kinetics and mass transfer of a solid-gas reaction. Similarly, the solids reached the minimum equilibrium H_2S temperature of 1,642°F (160 ppm H_2S), removed 100 percent of the H_2S, and were cooled quickly enough to prevent the reversal of reaction (7).

Figure 4.3-17 shows the equilibrium H_2S concentration and temperature for operation with Illinois No. 6 coal and limestone for the average conditions between 17:30 and 20:30 on December 11, 1999.

The equilibrium calcination temperature is about the same as in Figure 4.3-16 (1,645°F) since the CO_2 partial pressures are the same. The minimum equilibrium H_2S concentration is higher than in Figure 4.3-16 at 219 ppm since the H_2O partial pressure is higher. The sulfur removal was 78 percent and the theoretical H_2S removal compared to minimum H_2S ppm was 94 percent. The higher removals for this case were due to the much higher maximum coal-sulfur concentrations. Since the maximum temperature reached was higher it would be expected to have a higher level of calcination than in Figure 4.3-16 but there was less calcination during this period, which is likely due to the inaccuracies in solids sampling.

Figure 4.3-18 is a plot of the equilibrium-H_2S concentration and temperature operation with Illinois coal and limestone for the average conditions between 17:30 and 20:30 on December 12, 1999.

The equilibrium calcination temperature (1,663°F) is higher than for the two previous periods because the CO_2 partial pressure is higher (24 psia). The minimum equilibrium H_2S concentration is higher (246 ppm) since both the H_2O partial pressure and the CO_2 partial pressure are higher than in Figures 4.3-15 and -16. The sulfur removal for this case is about

the same as shown in Figure 4.3-16. The measured calcination during this period was 20 percent.

Information itemized in Table 4.3-3 summarizes the calculations and results. This type of analysis was used by KRW in a 1988 DOE report[2]. This KRW report also gives equations for the three equilibrium constants (K_1, K_2, and K_3) as a function of temperature from a 1973 EPA Report[3].

References

1. Katta, Satyan, KBR, personal communication, July 13, 2000.

2. KRW Energy Systems Inc., "A 32-Month Gasifier Mechanistic Study and Downstream Unit Process Development Program for the Pressurized Ash-Agglomerating Fluidized-Bed Gasification System," Report No. DE-AC21-84MC21063, March 1988.

3. Curran, G. P., et al., "Production of Clean Fuel Gas for Bituminous Coal," Consolidation Coal Co., EPA-650/2-73-049, December 1973.

Table 4.3-1

Test Periods

Test Run No.	Start Time	End Time	Fuel	Sorbent
GCT1A-1	09/11/99 20:21	09/12/99 15:13	PRB	Dolomite
GCT1A-2	09/13/99 10:55	09/14/99 06:28	PRB	Dolomite
GCT1A-3	09/14/99 15:42	09/15/99 16:42	PRB	Dolomite
GCT1B-1	12/08/99 05:15	12/10/99 11:20	PRB	Dolomite
GCT1B-2	12/10/99 11:20	12/10/99 13:15	PRB	None
GCT1B-3	12/10/99 13:15	12/10/99 16:00	PRB	None
GCT1B-4	12/10/99 16:00	12/10/99 18:05	PRB	None
GCT1C-1	12/10/99 18:05	12/11/99 07:00	Illinois No. 6/PRB	None
GCT1C-2	12/11/99 07:00	12/12/99 08:30	Illinois No. 6	Alabama Limestone
GCT1C-3	12/12/99 08:30	12/12/99 14:15	Illinois No. 6	Ohio Limestone
GCT1C-4	12/12/99 14:15	12/12/99 17:10	Illinois No. 6	Ohio Limestone
GCT1C-5	12/12/99 17:10	12/14/99 17:00	Illinois No. 6	Ohio Limestone
GCT1D-1	12/14/99 17:00	12/15/99 06:56	Alabama Calumet	None

Table 4.3-2

Water-Gas-Shift Equilibrium

Date	Meas. H_2O (%)	Wet, Normalized H_2 Wet (%)	Wet, Normalized CO Wet (%)	Wet, Normalized CO_2 Wet (%)	Kp	Equilibrium Temperature (°F)	Riser Inlet (°F)	Approach Temperature (°F)
12/08/99	6.4	4.19	3.79	7.62	1.33	1,342	1,423	-82
12/09/99	6.5	5.03	4.90	8.50	1.34	1,337	1,515	-177
12/10/99	7.1	7.26	8.05	8.80	1.12	1,426	1.551	-125
12/13/99	11.8	3.89	3.41	9.27	0.90	1,546	1,654	-108
12/14/99	10.6	(1)						
							Average	-123

Note: No gas-analyzer data on 12/14/99.

Table 4.3-3

H_2S Removal

Coal	PRB	Illinois #6	Illinois #6
Sorbent	Dolomite	Limestone	Limestone
Date	12/10/99	12/11/99	12/12/99
Time Start	13:30	17:30	17:30
Time End	17:30	20:30	20:30
Pressure, psig	175	190	200
CO_2 mole fraction	0.087	0.083	0.092
H_2O mole fraction	0.078	0.106	0.112
CO_2 partial pressure, psia	17	17	20
H_2O partial pressure, psia	15	22	24
CO_2 calcination temperature, ^{O}F	1642	1645	1663
Maximum Coal Sulfur Emissions, ppm	454	2585	2725
Measured Sulfur Emissions, ppm	251	558	522
Estimated COS, ppm	100	200	200
Estimated H_2S, ppm	151	358	322
Thermodynamic minimum H_2S, ppm	160	219	246
Sulfur removal, %	45	78	81
Theoretical H_2S removal, %[1]	103	94	97
Solids calcination, %[2]	40	5	20

Notes:

1. Theoretical H_2S removal is the H_2S removal assuming that the H_2S level cannot be below the equilibrium H_2S level.
2. Solids calcination is the CaO mole percent divided by the sum of the CaO and $CaCO_3$ mole percent.

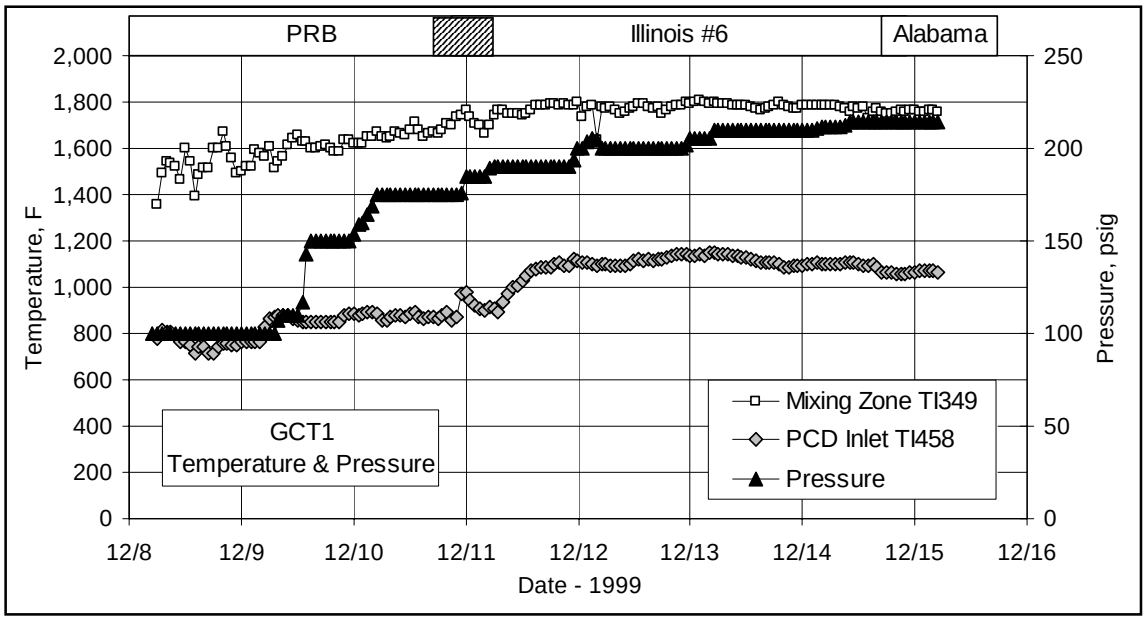

Figure 4.3-1 Temperatures and Pressures

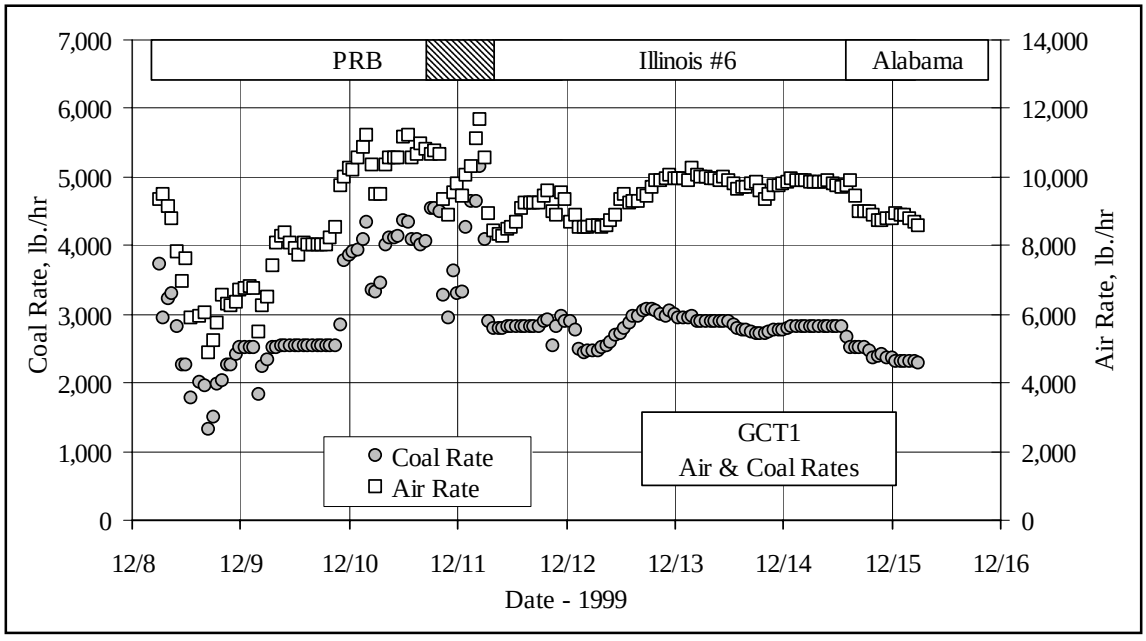

Figure 4.3-2 Air and Coal Rates

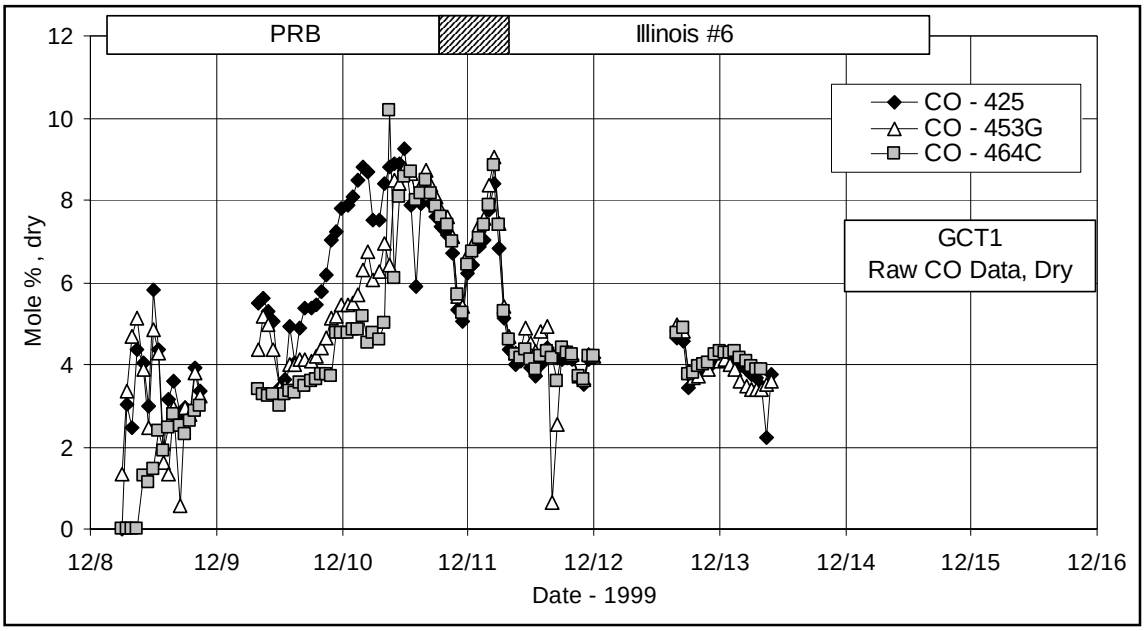

Figure 4.3-3 Dry, Raw Carbon Monoxide Gas Analyses

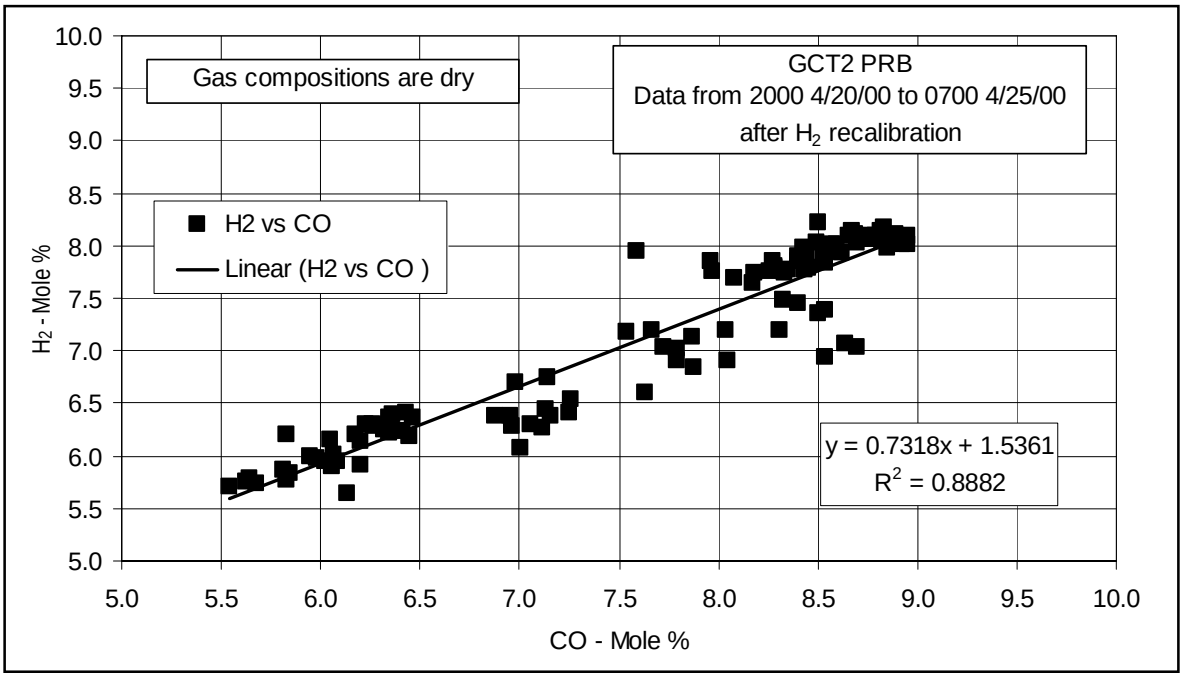

Figure 4.3-4 GCT2 Hydrogen-Carbon Monoxide Correlation

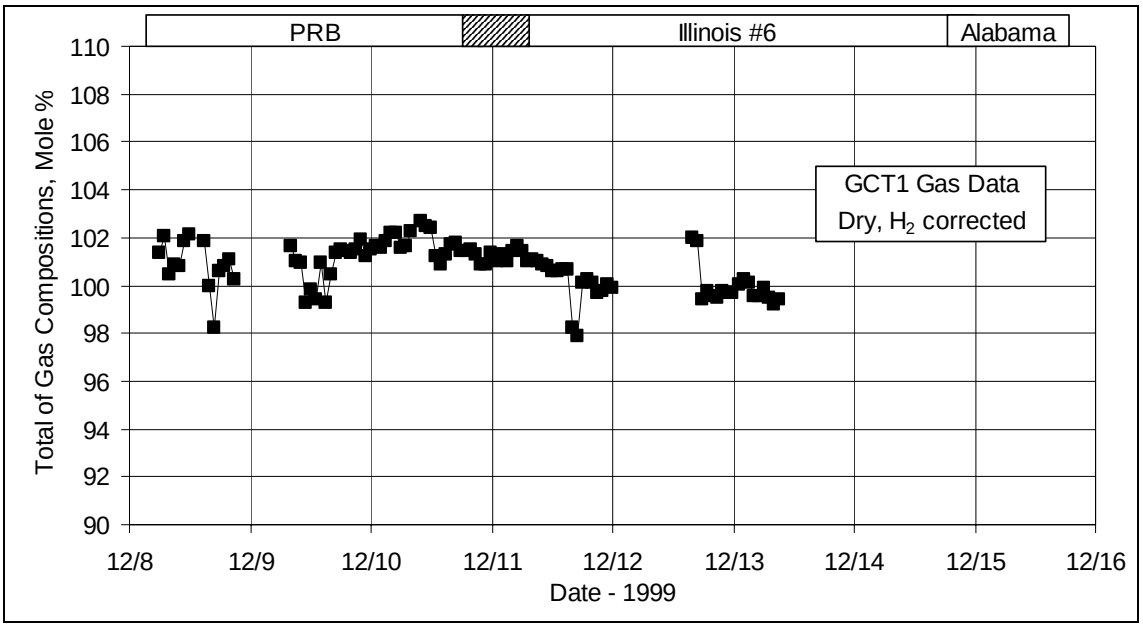

Figure 4.3-5 Sum of Gas Compositions After H_2 Correction

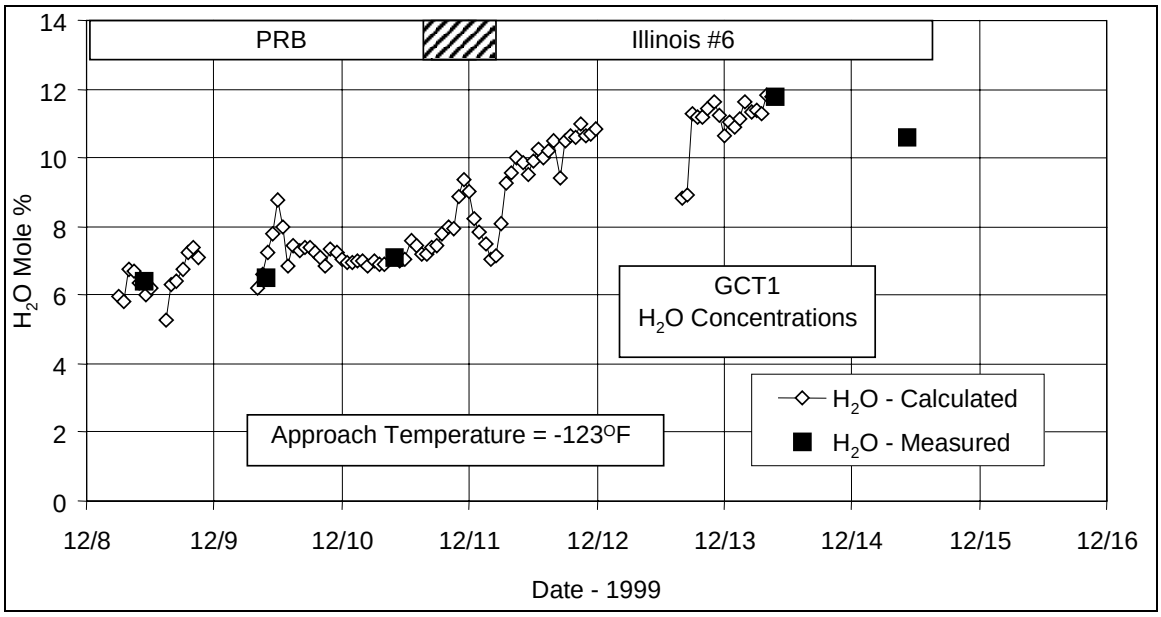

Figure 4.3-6 Measured and Calculated Water Vapor Mole Percents

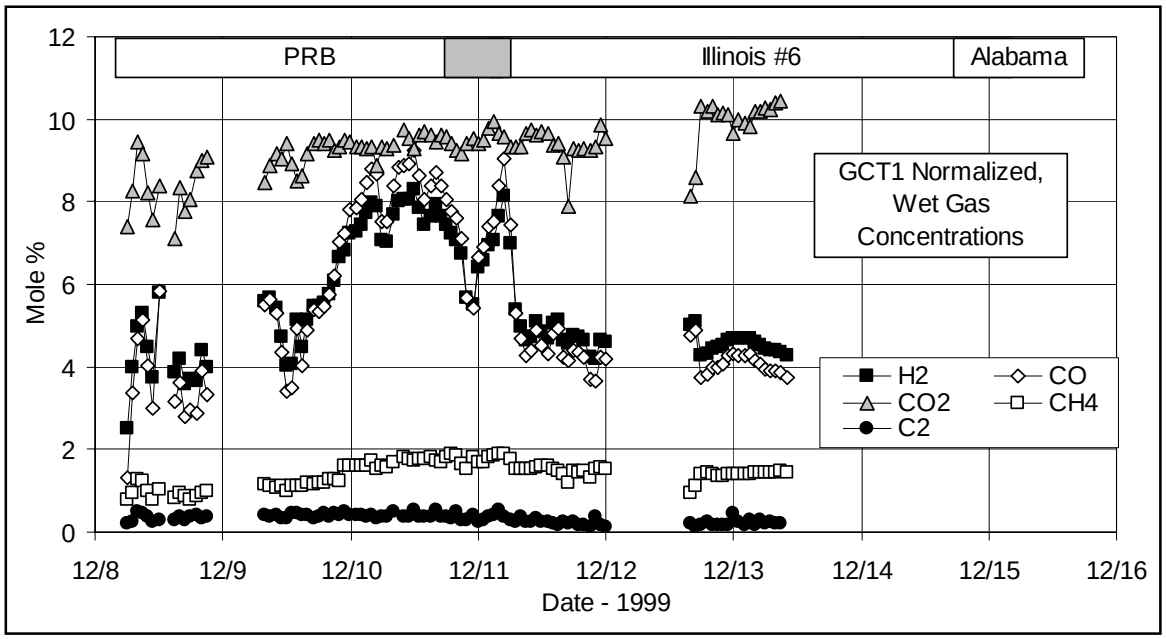

Figure 4.3-7 Fuel Gas Concentrations

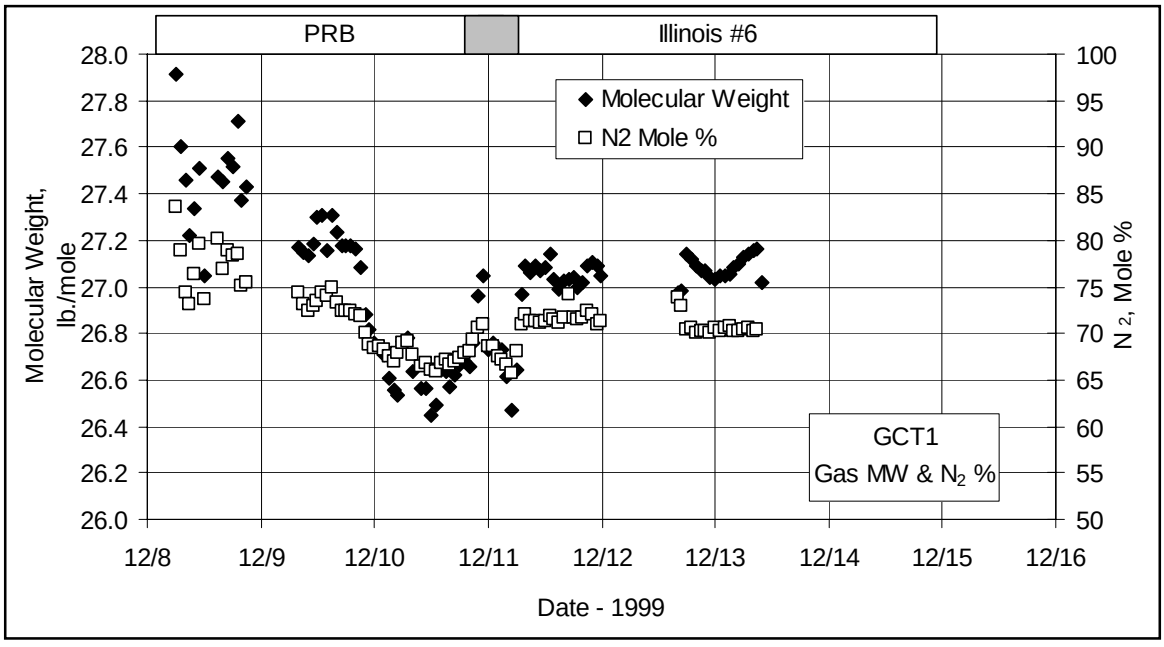

Figure 4.3-8 Fuel Gas Molecular Weights and Nitrogen Mole Percents

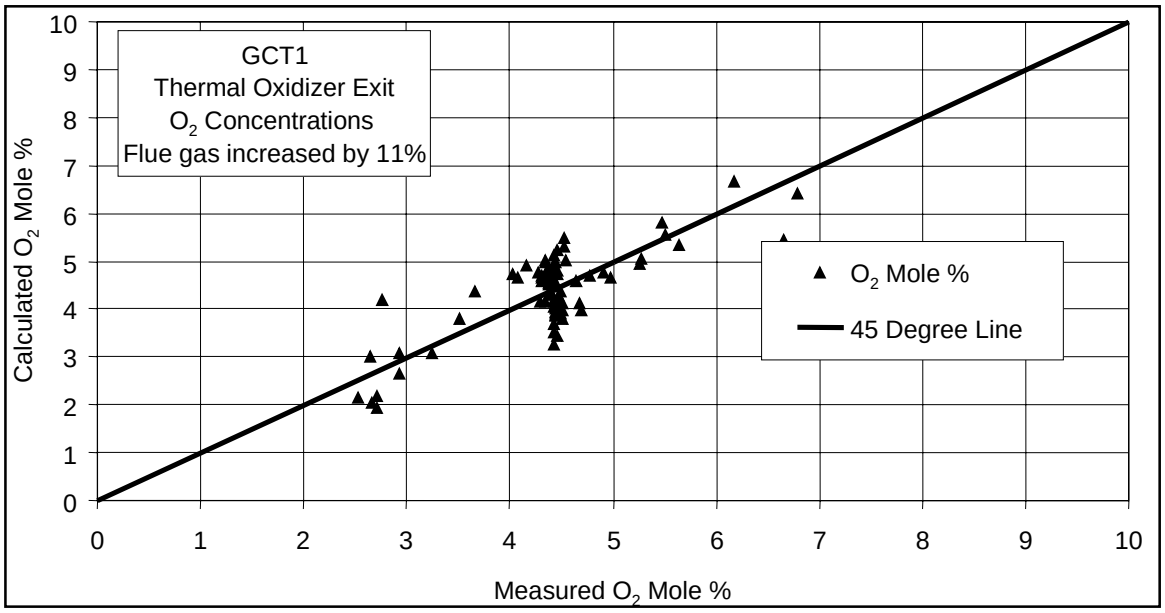

Figure 4.3-9 Measured and Calculated Thermal Oxidizer O_2 Mole Percents

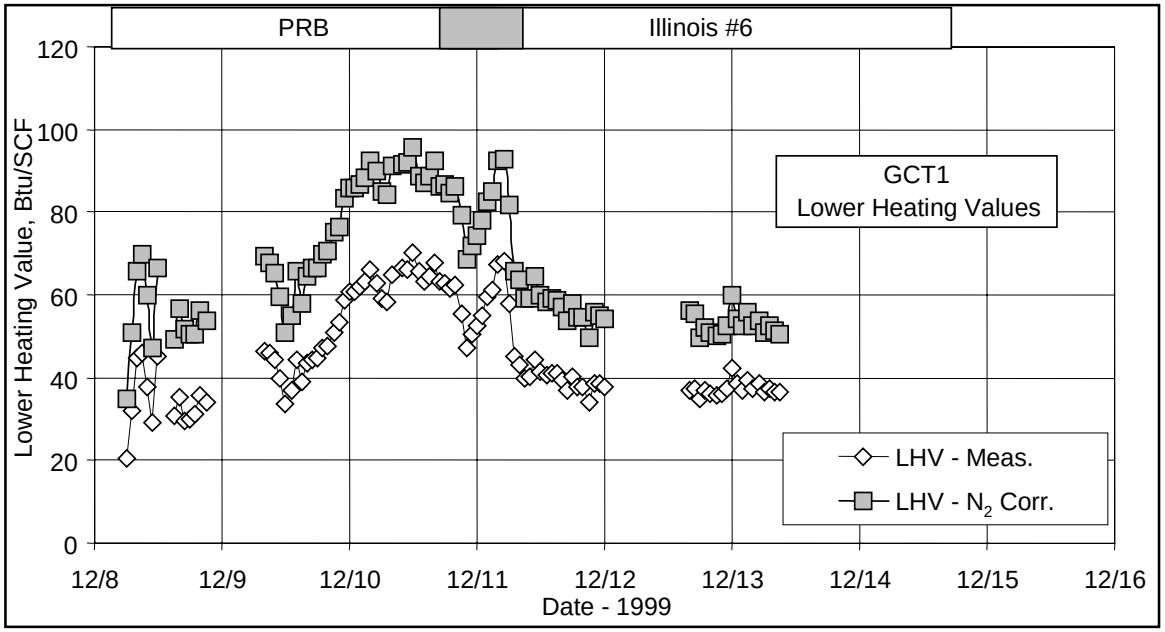

Figure 4.3-10 Actual- and N_2-Corrected-Fuel-Gas Lower Heating Values

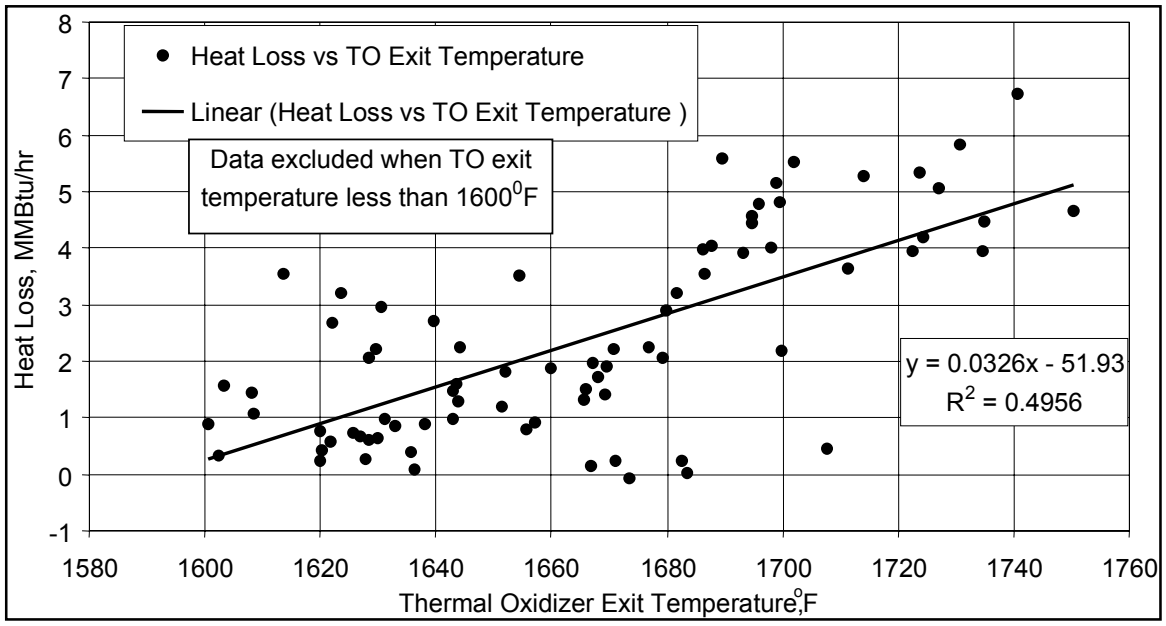

Figure 4.3-11 Thermal Oxidizer Heat Loss - Exit Temperature

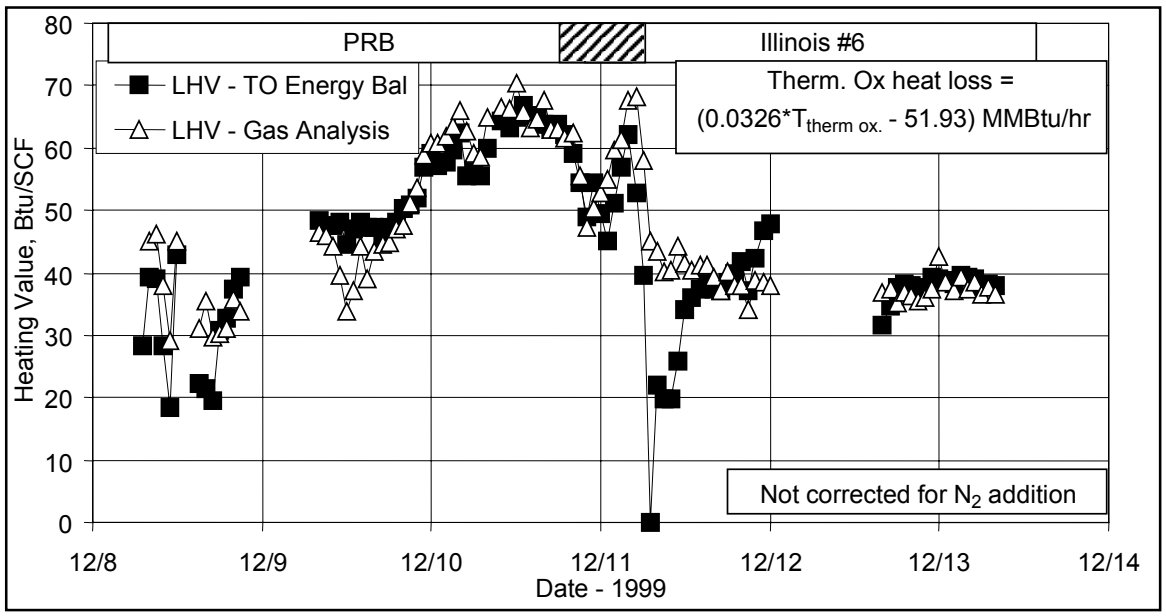

Figure 4.3-12 Fuel Gas Lower Heating Value by Gas Analyzers and Thermal Oxidizer Energy Balance

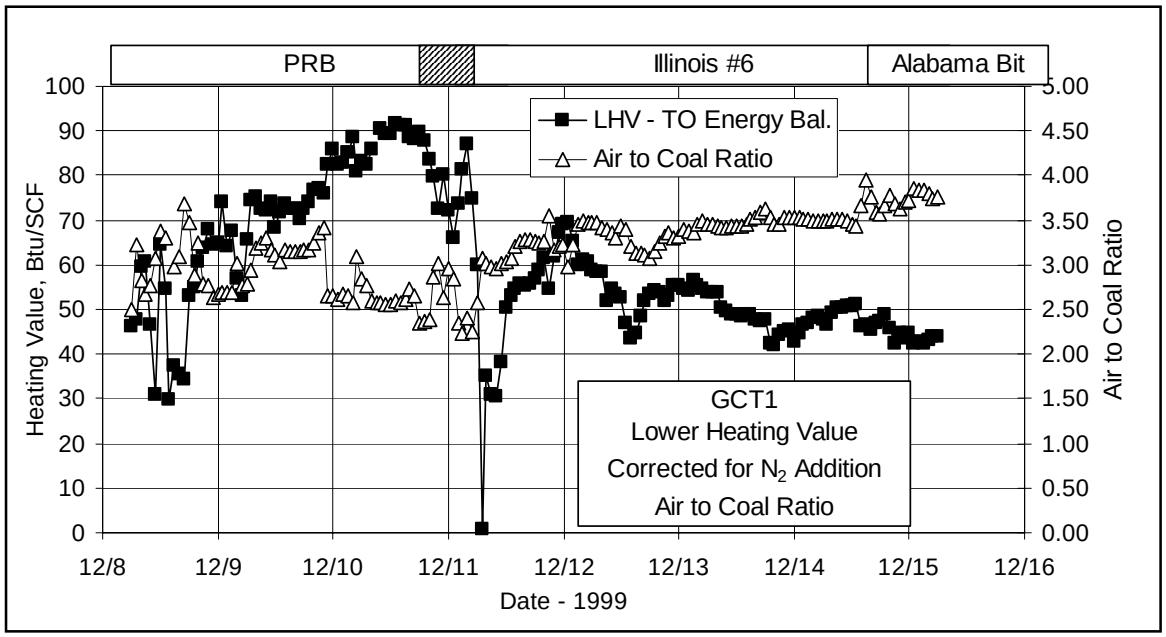

Figure 4.3-13 Fuel Gas Lower Heating by Thermal-Oxidizer-Energy Balance, Corrected for N_2 Addition and Air-to-Coal Ratio

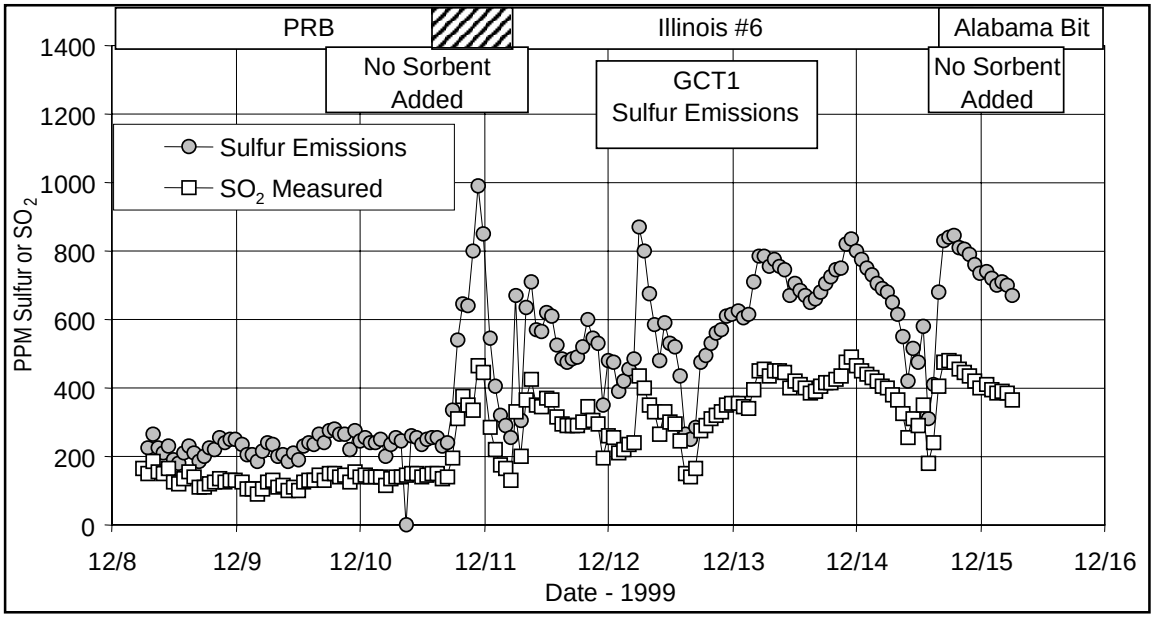

Figure 4.3-14 Thermal Oxidizer SO_2 Emissions and Transport Reactor Sulfur Emissions

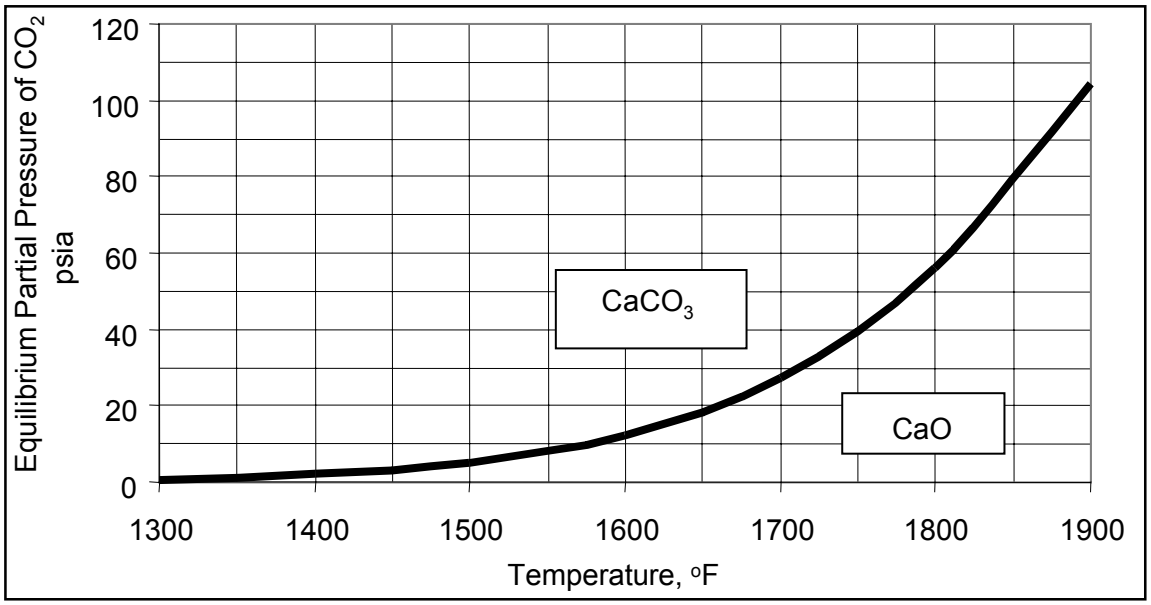

Figure 4.3-15 $CaCO_3$ - CaO - CO_2 Equilibrium

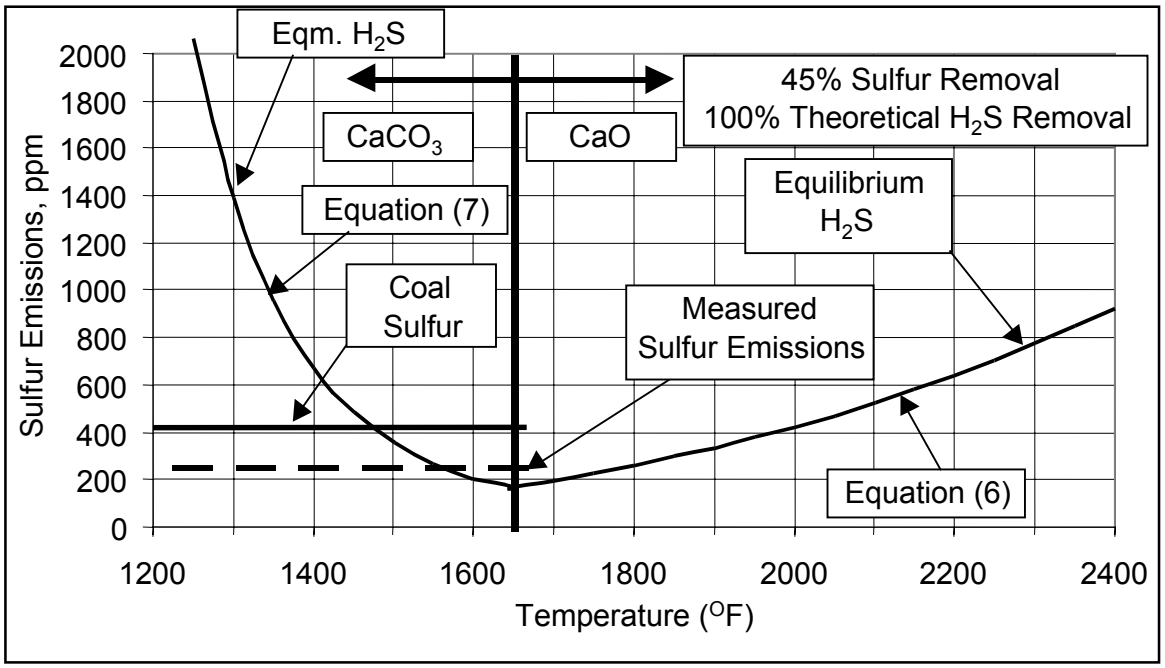

Figure 4.3-16 H_2S Equilibrium, December 10, 1999, 13:30 - 17:30
(15 psia P^o H_2O, 17 psia P^o CO_2)

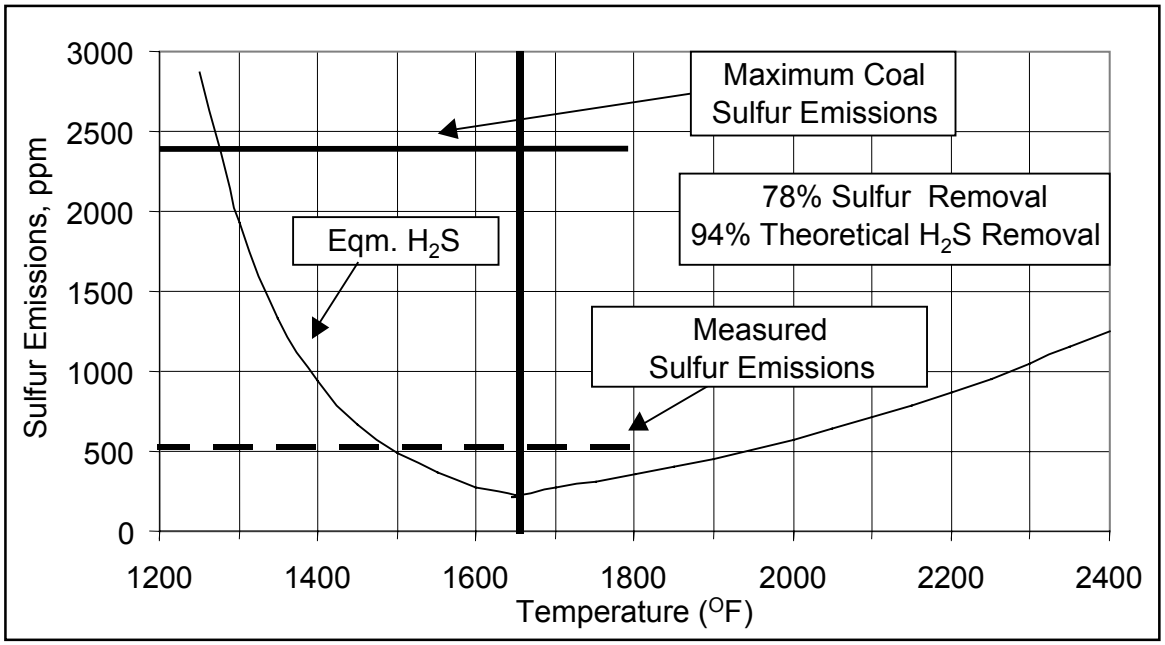

Figure 4.3-17 Illinois No. 6 - LS, December11, 1999, 17:30 - 20:30
(22 psia P^0 H_2O, 17 psia P^0 CO_2)

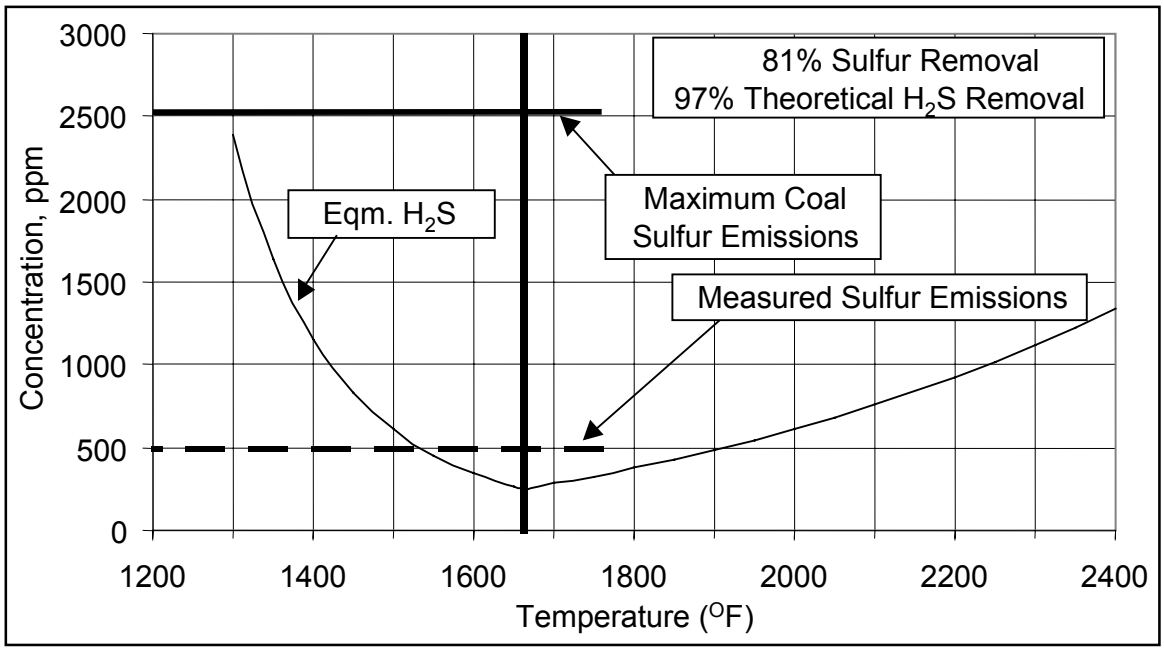

Figure 4.3-18 Illinois No. 6 - LS, December 12, 1999, 17:30 - 20:30
(24 psia P^0 H_2O, 20 psia P^0 CO_2)

4.4 SOLIDS ANALYSES

During GCT1 solids were collected from the fuel feed system (FD0210), the sorbent feed system (FD0220), the standpipe spent solids transport system (FD0510), and the PCD fine solids transport system (FD0520). These solids were analyzed for chemical composition and particle size. This section will use the chemical analysis data to show:

- Chemical composition changes.
- The effect of sorbent on sulfur removal.
- Particle size and solids bulk density changes.

Figure 4.4-1 shows the fuel sulfur and ash as sampled from the fuel feed system during GCT1. The Powder River Basin (PRB) coal had about 0.3-percent sulfur and 6-percent ash while the Illinois No. 6 had about 2.5-percent sulfur and 10-percent ash.

The data points out a problem in FD0210 sample collection. The samples are collected from the side of the FD0210 hopper. If there is rat holing of a new coal past an old coal during coal sampling, old coal will be sampled and the actual coal being fed will not be sampled. The Figure 4.4-1 data for the coal transition between PRB and Illinois coals indicates that the Illinois coal broke through on December 11 or 12 by the sulfur content or on December 11 by the ash content. Operating data including coal reactivity, fuel gas-heating value, thermal oxidizer SO_2 levels, and reactor temperatures (see Figures 4.3-1, -3, -7, -10, -12, -13, and -14) all indicate that:

1. Illinois coal broke through at 18:00 December 10.
2. A slug of PRB broke through for a few hours at 02:00 December 11.
3. Illinois coal came back at 07:00 December 11.

Much of the data for the period 18:00 December 10 to 07:00 December 11 have a "lazy S" shapes. The reactor temperatures, gas LHV, and thermal oxidizer SO_2 concentrations all have this shape.

The Sauter mean diameter (SMD) and mass mean diameter (D_{50}) particle size of the coal feed in GCT1 are shown in Figure 4.4-2. The general trend was of increasing SMD and D_{50} during the test. The PRB SMD diameter was from 300 to 400 microns while the Illinois coal was larger at 400 to 500 microns. The PRB D_{50} diameter was fairly constant at 300 microns while the Illinois coal was larger at 325 to 400 microns.

FD0220 was used during GCT1 to feed:

- Ohio Bucyrus limestone.
- Alabama Longview limestone.

- Ohio Plum Run dolomite.
- Wisconsin sand.

The SMD and D_{50} of the solids sampled from the sorbent feeder FD0220 are plotted in Figure 4.4-3. The SMD for the Alabama and Ohio limestones was 10 to 20 microns and the D_{50} for the Alabama and Ohio limestones is 20 to 40 microns. The first data point was probably a mixture of dolomite and 100-micron sand.

Only four sorbent samples from FD0220 were analyzed and were not plotted. During GCT1 sand was used to maintain bed heights and there were long periods when no sorbent was added to the reactor.

The Sauter mean diameter (SMD) particle size, mass mean diameter (D_{50}), and bulk density for the reactor solids sampled from FD0510 are provided in Figure 4.4-4. The SMD was constant for the PRB coal testing at 150 to 160 microns while the D_{50} was constant at 130 to 140 microns. Midway through the Illinois coal test the SMD increased to 200 microns and the D_{50} increased to 170 microns at 00:00 December 13. The SMD decreased down to 170 microns (D_{50} = 155 microns) early on December 13, then increased back up to 200 microns (D_{50} = 180 microns) by the end of December 13.

The reactor solids bulk density was constant at 90 lb/ft^3 for the first four samples, then dropped down to 70 lb/ft^3 early on December 12 during the Illinois coal test. The remainder of the Illinois coal test had a reactor solids bulk density of 70 to 80 lb/ft^3.

The constancy of the first four data points could indicate that the solids were just sitting in FD0510 from December 9 to 12 since FD0510 was minimally operated during that time. These solids could have just been from the start of the run and are not representative of the reactor solids at the time sampled.

Figure 4.4-5 shows the plot of the SMD, D_{50} and bulk density for the PCD solids sampled from FD0520. The PRB testing showed an increase from 10 to 20 microns SMD (15 to 40 microns D_{50}) during the first day of testing. The SMD then leveled out at 20 microns (D_{50} at 30 microns) until the transition to Illinois coal at on December 10. The best gasification during GCT1 occurred while the SMD of the PCD solids was about 15 to 20 microns and the D_{50} was 30 microns. During the Illinois coal testing the SMD decreased from 20 microns to 10 to 15 microns (20 to 25 microns D_{50}) on December 11 and remained nearly constant until December 14. The SMD increased to 20 microns during the last 12 hours of Illinois coal operation while the D_{50} stayed constant at 25 microns. Alabama coal operation had a SMD of 20 microns and a D_{50} of 25 microns.

The PCD solids bulk density started the PRB test at 25 to 30 lb/ft^3, then increased up to 40 lb/ft^3 at 00:00 December 9. The bulk density then dropped back down to 28 lb/ft^3 and then during December 9 the bulk density rose to 42 lb/ft^3. A sudden increase in coal feed (see Figure 4.3-2) dropped the bulk density down to 25 to 30 lb/ft^3 for the remainder of the PRB testing. The Illinois coal test bulk density started at 20 to 25 lb/ft^3 and slowly rose to 25 to 30 on December 12 where the bulk density held steady until the transition to Alabama coal. The bulk

density during Alabama coal operation decreased steadily to 20 to 25 lb/ft^3 until shutdown probably due to the cessation of sorbent feed on December 14.

GCT1 was the first KBR test that the solids were analyzed for sulfide sulfur and sulfate sulfur. Theoretically there should be very little sulfate sulfur in the reactor or PCD solids due to the reducing conditions in the reactor which would tend to push all the sulfur in the solids to CaS. The sulfator solids should have significant sulfate sulfur. The solid compounds produced by the reactor were determined using the solids analysis and the following assumptions.

1. All carbon dioxide measured came from $CaCO_3$; hence moles CO_2 = moles $CaCO_3$.
2. All sulfide sulfur measured came from CaS.
3. All sulfate sulfur measured came from $CaSO_4$.
4. All calcium not taken by CaS, $CaSO_4$, and $CaCO_3$ came from CaO.
5. All magnesium came from MgO.
6. Carbon measured includes organic carbon and inorganic carbon (as CO_2). Organic carbon is measured carbon minus CO_2 carbon..
7. Inerts are the sum of the Al_2O_3, Fe_2O_3, P_2O_5, K_2O, SiO_3, Na_2O, and TiO_2 contents.

Only FD0510 solids samples taken during the Illinois coal were analyzed and plotted. A few samples were taken during the PRB coal but due to the infrequent operation of FD0510 the solids are not representative of the reactor solids and, therefore, these solids were not analyzed. No FD0510 samples were taken during Alabama bituminous operation.

Figure 4.4-6 shows the plot of the organic carbon, $CaSO_4$, and CaS weight percent in reactor solids for GCT1C (Illinois No. 6 coal operation). The carbon levels are too low to produce good gasification (<5 percent carbon). This indicates that minimal carbon is being recycled back to the mixing zone. The CaS levels also seem low for the high-sulfur Illinois coal that was being run. Most of the CaS produced is not being retained in the reactor, possibly because it is produced as a fine particulate and is being lost to the PCD. If the solids were at thermodynamic equilibrium with the gas there should be no $CaSO_4$ in the solids. This level of $CaSO_4$ (zero to 3 percent) is either due to analytical inaccuracies (the difficulty of analyzing sulfate at the 3-percent or lower range) or due to partial oxidation in the mixing zone and incomplete reduction in the riser.

Figure 4.4-7 shows the plot of the reactor solids containing in $CaCO_3$ and CaO as well as the MgO. During the Illinois coal operation, the $CaCO_3$ and MgO were fairly constant at 6 and 3 percent while the CaO increased from near zero up to 25 percent. The high level of CaO in the reactor indicates that the reactor solids were well calcined.

Figure 4.4-8 shows the plot of the reactor ash or inerts. The inerts are from the start-up sand, coal ash, and sorbent inerts. The data on December 12 starts with the reactor nearly full of

inerts and then slowly decreasing to 60 percent inerts. The inerts were replaced by CaO. This data would imply that large amounts of sand were added to the reactor on December 11, which was not the case. Several shots of sand were added at 05:00 to 07:30 on December 12. The slowly decreasing inerts content on December 12 is due to the addition of limestone. This may be due to the time delay in sampling solids from the reactor (that is, the data actually reflect data that was valid for a day or so before the reported sampling date and time).

The limited reactor-solids data available indicates that planned standpipe solids sampler will greatly assist in understanding reactor performance.

Figure 4.4-9 shows the plot of the inorganic carbon (total carbon minus CO_2 carbon) for the PCD solids sampled from FD0520 and the coal-feed rate. Also included in Figure 4.4-9 is organic carbon determined from the in situ solid samples. Inorganic carbon was estimated from FD0520 solids samples and then deducted from the in situ measured total carbon (shown in Table 3.4-3) to put on the same basis as the FD0520 solids organic carbon. There was excellent agreement between the carbon contents of the in situ solids and the solids sampled from FD0520. Since FD0520 ran continuously during GCT1 samples were taken much more frequently than FD0510 with a goal of one every 2 hours.

During PRB coal operation the organic carbon content started out at about 50 percent, then dropped to 28 to 38 percent. The carbon content jumped up to 50 to 60 percent after 00:00 December 10 when the coal feed rate was increased from 2,500 to 4,000 lb per hour on December 9. The increased carbon reflects the higher coal-feed rate. This increase in coal-feed rate increased the fuel gas lower heating value (LHV) from 75 Btu/SCF (corrected for N_2) to 90 Btu/SCF (see Figure 4.3-13).

The operation on Illinois No. 6 coal on December 11 ended the day with a PCD-solids-carbon content of 30 to 40 percent and a fuel-gas LHV of 60 to 70 Btu/SCF. The carbon content had a December 12 "hiccup" when the carbon increased to 48 percent and then decreased during the day to 25 percent. During the morning of December 12 the gas LHV dipped down to 42 Btu/SCF and then gradually increased to 55 Btu/SCF. The final period of Illinois coal operation had a constant carbon content of 30 to 33 percent, the LHV constant at 40 to 50 Btu/SCF, and a constant coal rate of 2,800 to 3,000 lb per hour.

The transition to Alabama coal had the carbon content increase from 32 to 50 percent while the coal rate decreased to 2,400 lb per hour and the LHV dropped to 45 Btu/SCF.

Figure 4.4-10 shows the amounts of $CaCO_3$, CaO, $CaSO_4$, and CaS in the PCD solids as sampled from FD0520. The CaS determined from the in situ samples are also shown. There was excellent agreement between the in situ solids and the solids sampled from FD0520. The run started with a large excess of $CaCO_3$ at 20 to 40 percent, small levels of CaO (zero to 5 percent), and minimal CaS and $CaSO_4$ using PRB coal. The low CaS and $CaSO_4$ levels were due to the very low sulfur level of PRB (0.3-percent sulfur). Turning the sorbent feed off on December 10 lowered the $CaCO_3$ content to 5 percent. The introduction of Illinois coal (2.5-percent sulfur) slowly increased the CaS level from near zero to nearly 15 percent on December 13. The CaS content then decreased from 14 to 6 percent during December 14 the day before the transition to Alabama coal (probably due to a decrease in sorbent rate). Once the sorbent

feed stopped on December 14 the $CaCO_3$ decreased rapidly. All four compounds ($CaCO_3$, CaO, $CaSO_4$, and CaS) were at very low levels during the Alabama test due to no sorbent being fed to the reactor. The low reactor levels of CaO during GCT1 indicated that the limestone was not being calcined.

Figure 4.4-11 shows the PCD solids inerts as sampled from FD0520. The inerts were fairly constant at 20 to 30 percent during the PRB and Illinois coal tests except for low start-up values of 15 and 18 percent and an increase to 42 percent during the Alabama coal testing after the sorbent was turned off. When the sorbent-feed rate was stopped the inerts content increased (as expected) as the calcium- and magnesium-compounds-solids contents decreased.

The molar ratio of calcium to sulfur (Ca/S) was calculated for each sample from the fine ash system (FD0520) and reactor solids from the standpipe (FD0510). For dolomite addition the Ca/S ratio is the measure of excess sorbent required for sulfur removal according to the equation:

$$H_2S + CaCO_3 \bullet MgCO_3 \rightarrow CaS + H_2O + MgO + 2CO_2 \quad (1)$$

While for limestone addition the equation is:

$$H_2S + CaCO_3 \rightarrow CaS + H_2O + CO_2 \quad (2)$$

To react, all the dolomite or limestone calcium requires an equal molar amount of calcium and H_2S, which would result in the same molar amount of calcium in the solids as sulfur (Ca/S = 1.0). Solids with the minimum amount of sorbent required would then have calcium only present as CaS and there would be neither $CaCO_3$ nor CaO•MgO present. The higher the Ca/S ratio the more excess sorbent is used than theoretically required for 100 percent H_2S capture.

Using the coal sulfur analyses and the thermal oxidizer SO_2 analyzer data, the reactor sulfur removal can be calculated as in section 4.3. The sulfur removal and PCD solids Ca/S ratio are plotted in Figure 4.4-12. The in situ Ca/S ratios are also given as Figure 4.4-12 and agree well with the Ca/S ratios from the FD0520 samples. The sulfur removals were fairly constant for PRB coal at around 40 percent and very high Ca/S ratios. The slight dip in removal on December 12 was probably due to variations in the coal sulfur not picked up by the analyzed coal samples. The Ca/S ratios were above 6 before the sorbent feeder was turned off. Once the sorbent feeder was turned off the Ca/S ratio slowly dropped to 3.5 during the transition to Illinois coal. The Illinois coal has about 8 times the sulfur as the PRB. Note that even though the Ca/S ratio is less the removal is higher. The sulfur removal for Illinois coal was constant for a day after the transition at 80 percent at Ca/S ratios from 1.5 to 3.5. There was a dip in sulfur removal after the coal rate was decreased on December 12. The sulfur removal recovered up to 90 percent on December 12 then slowly decreased to 55 percent by midnight December 13 at a Ca/S ratio of 2.0. On December 14 the sulfur removal increased back up to 80 percent as the PCD solids Ca/S ratio increased from 2.0 to 3.5. Once the Alabama coal was introduced the sorbent feed was also stopped due to operational problems. The sulfur removal plunged to 10 percent due to the lack of sorbent. Because the sorbent feed was turned off there was no sudden change in thermal oxidizer SO_2 concentration for the Illinois-Alabama transition as there was for the PRB-Illinois transition. The PCD solids Ca/S ratio also decreased from 3.5 to 1.5 after the sorbent feed was turned off.

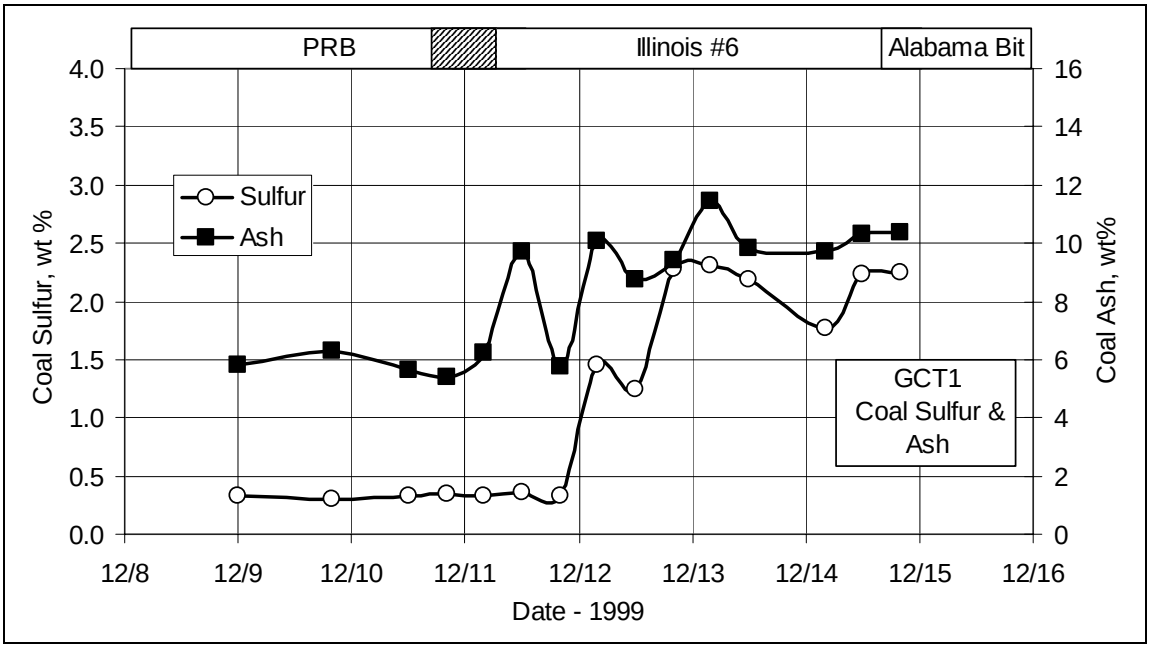

Figure 4.4-1 Coal Sulfur and Ash Contents

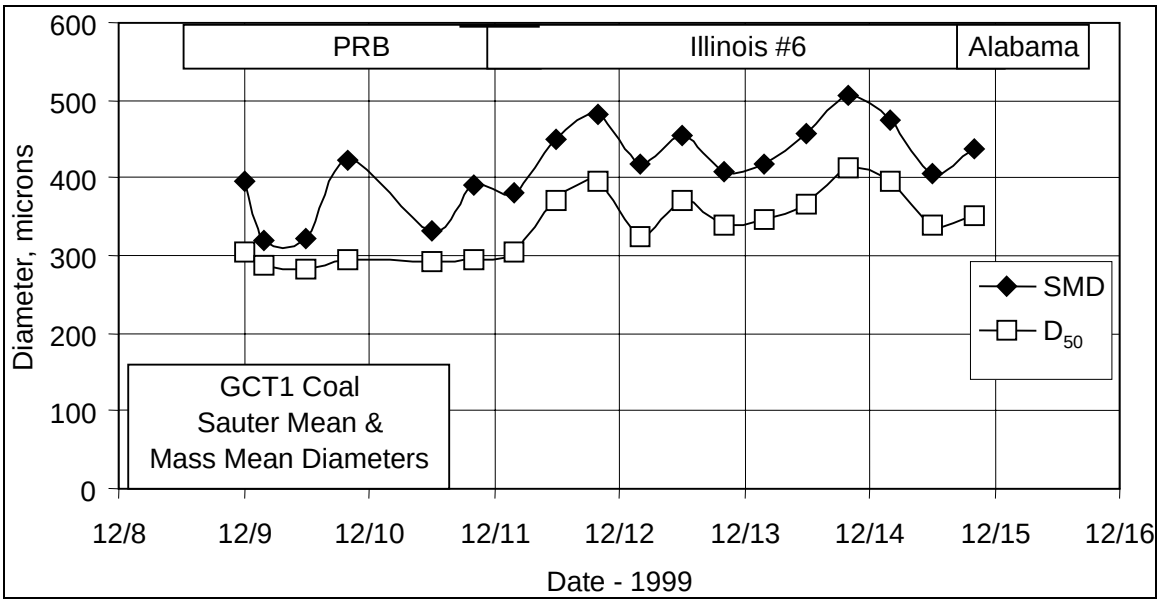

Figure 4.4-2 Coal Mass Mean and Sauter Mean Diameters

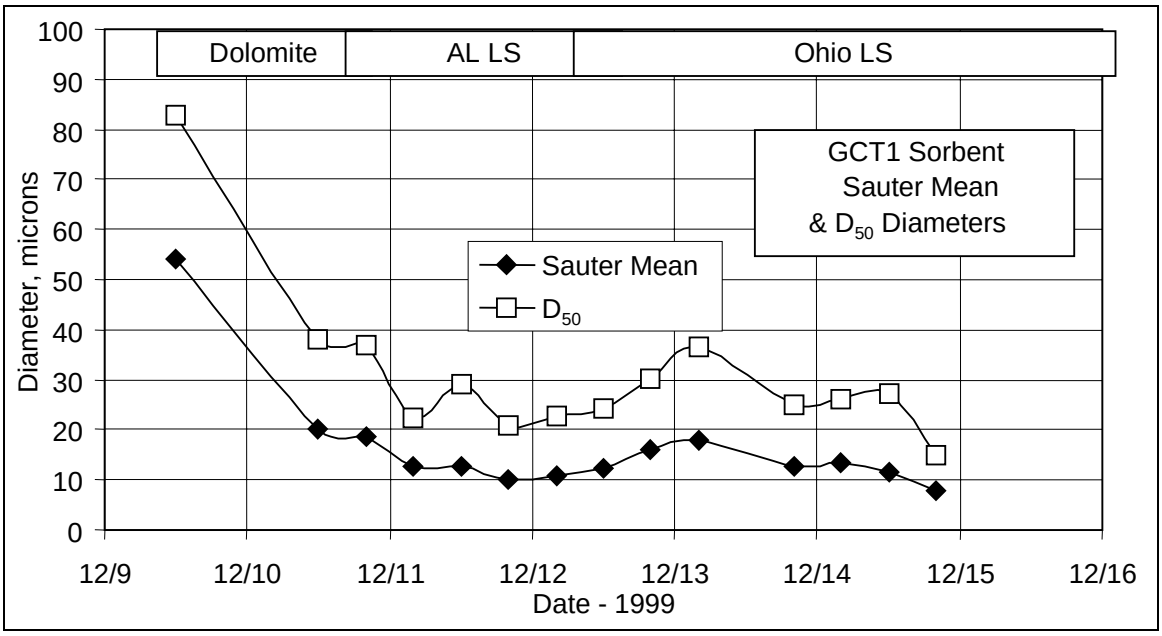

Figure 4.4-3 Sorbent Mass Mean and Sauter Mean Diameters

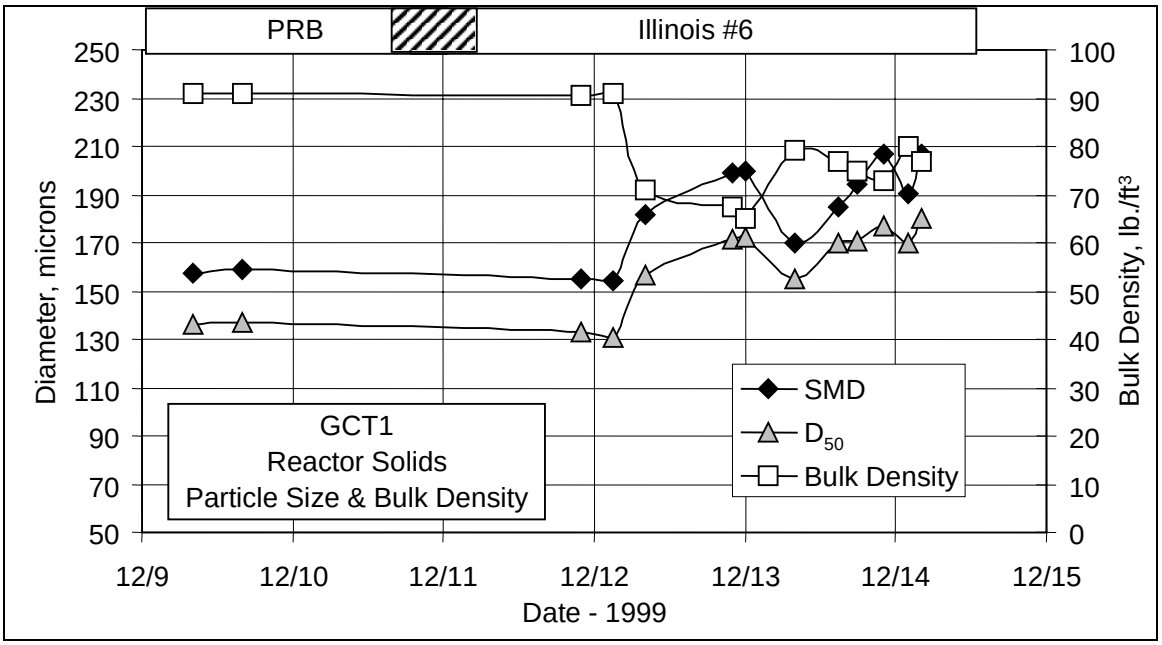

Figure 4.4-4 Reactor Sauter Mean and Mass Mean Diameters

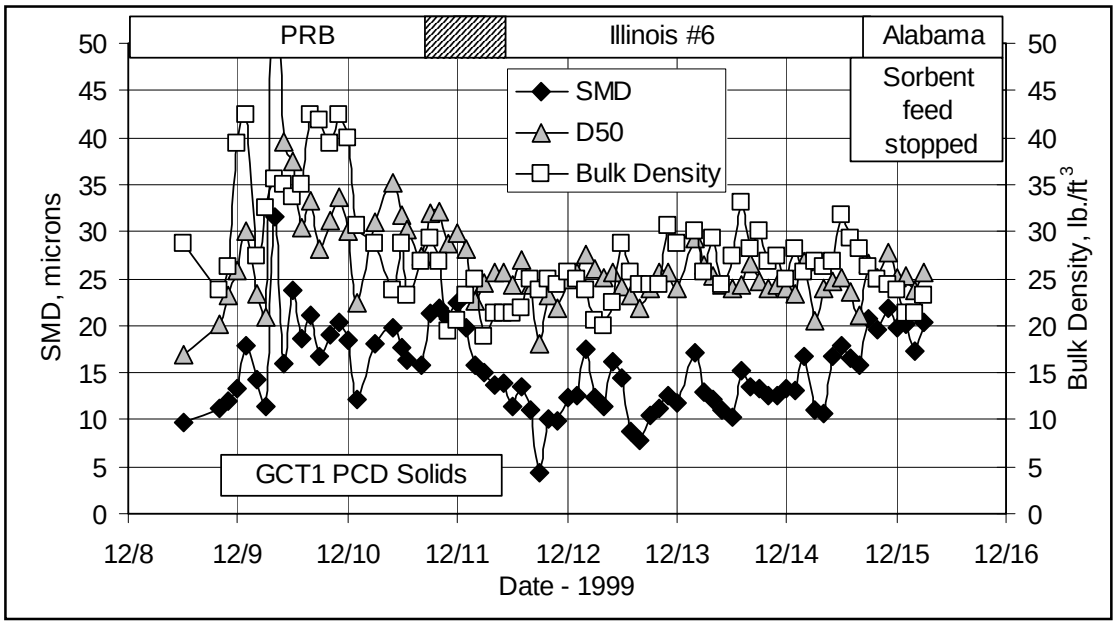

Figure 4.4-5 PCD Solids SMD, D_{50}, and Bulk Density

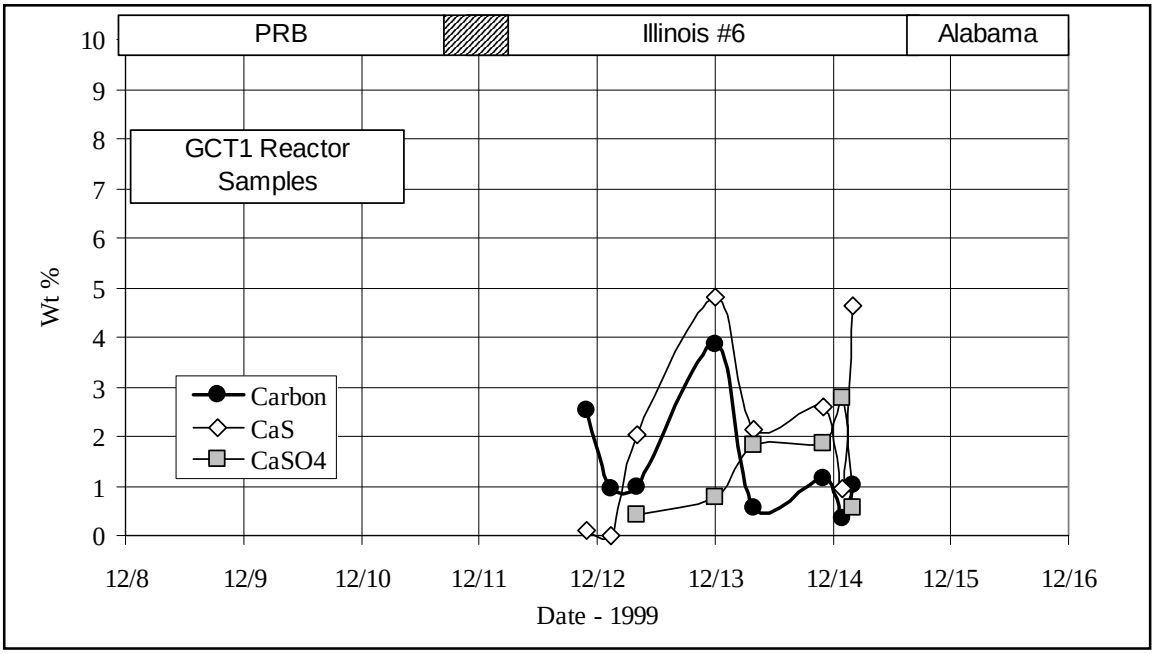

Figure 4.4-6 Reactor Solids Carbon, CaS, and $CaSO_4$

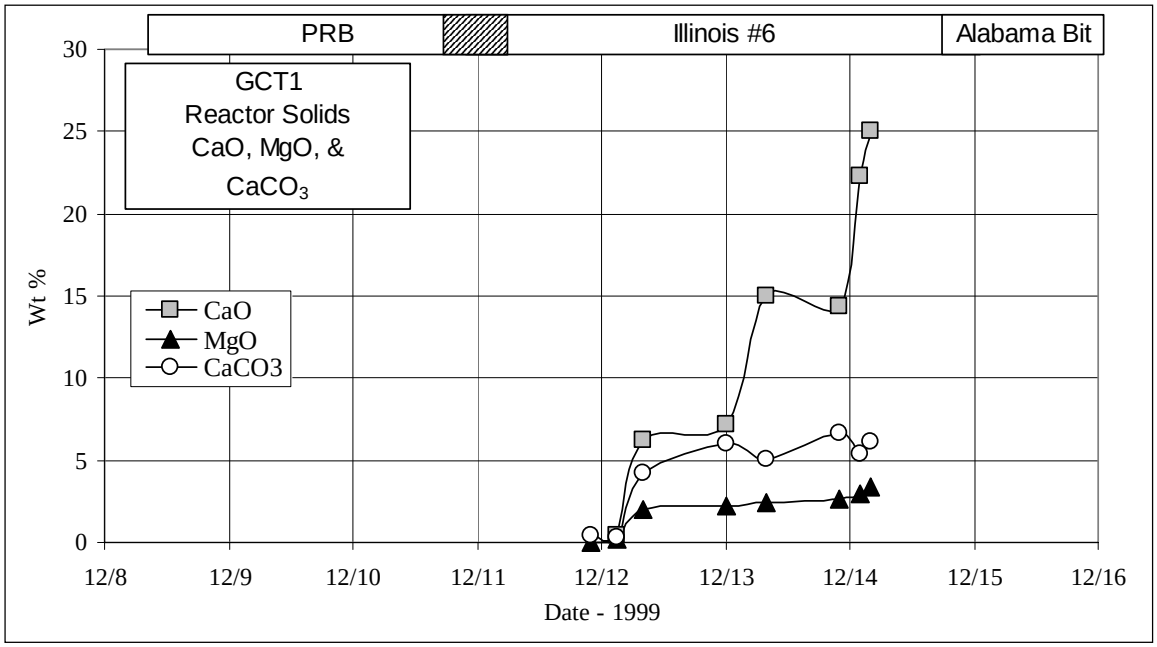

Figure 4.4-7 Reactor Solids CaO, MgO, and $CaCO_3$

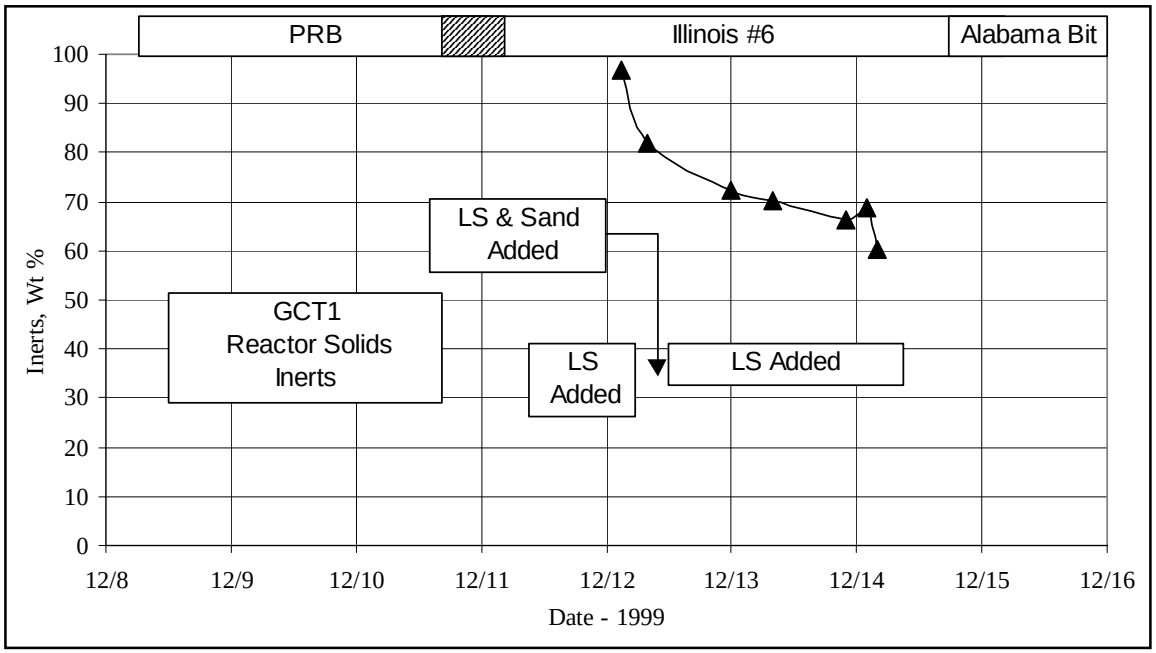

Figure 4.4-8 Reactor Solids Inerts

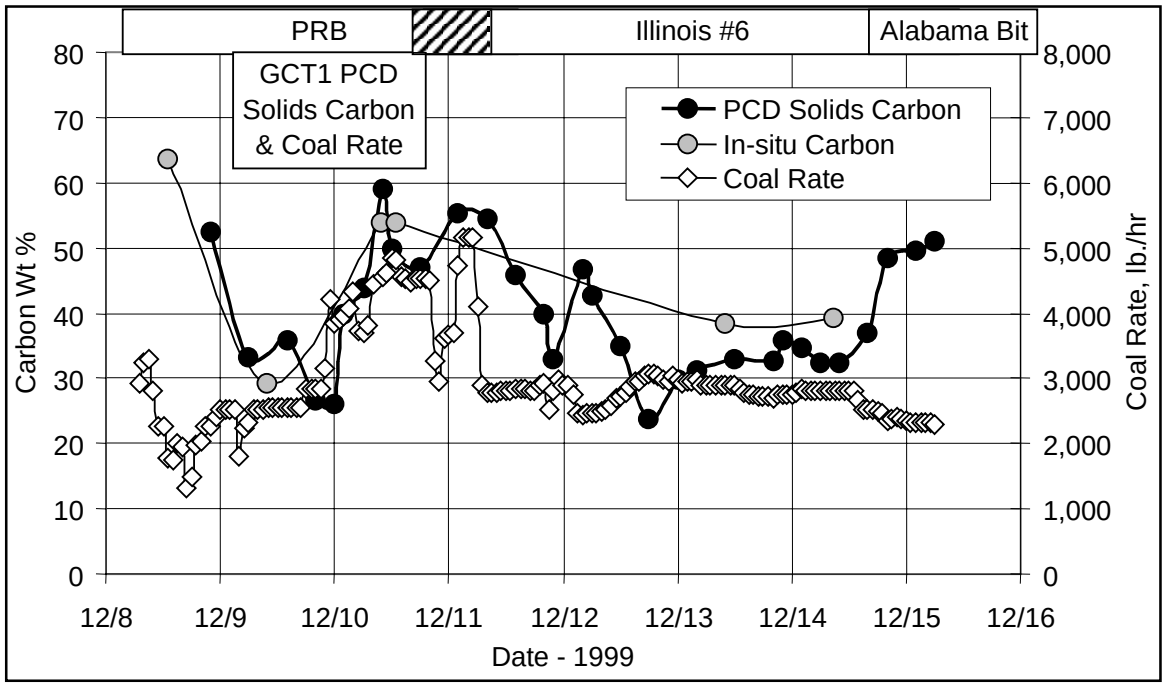

Figure 4.4-9 PCD Solids Carbon Content and Coal Feed Rate

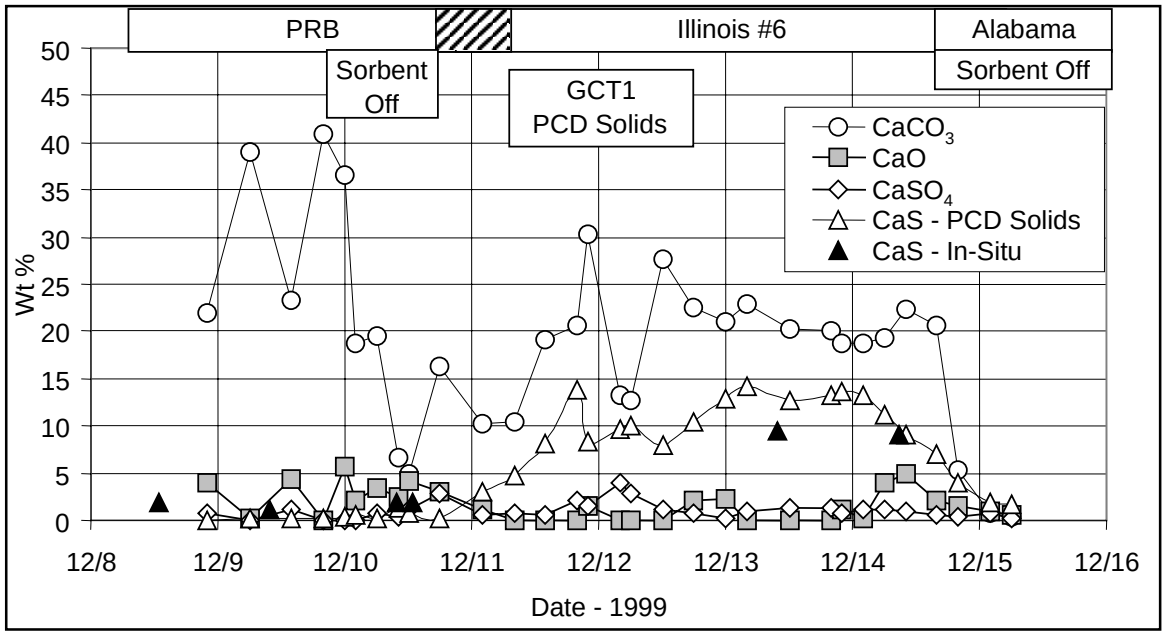

Figure 4.4-10 PCD Solids $CaCO_3$, CaS, CaO, and $CaSO_4$

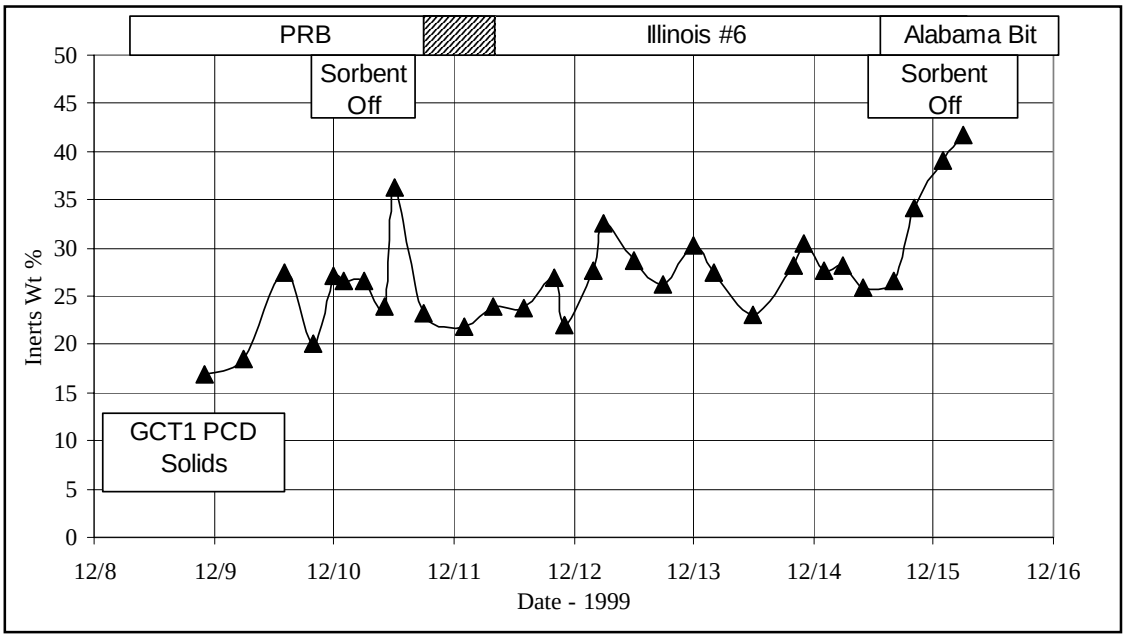

Figure 4.4-11 PCD Solids Inerts

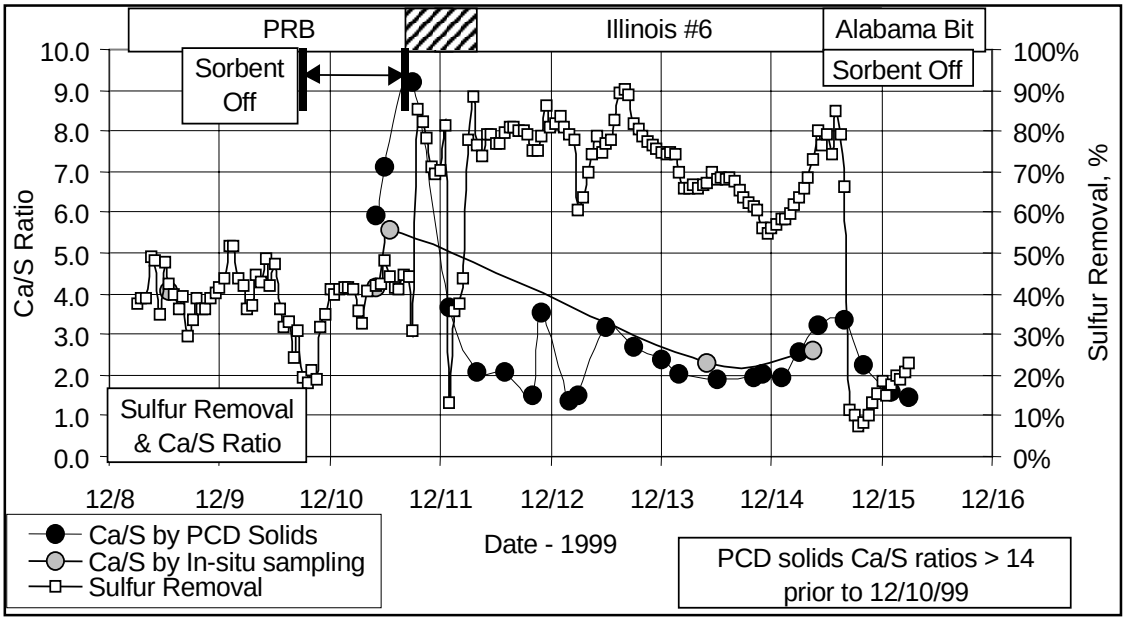

Figure 4.4-12 PCD Solids Ca/S Ratio and Sulfur Removal

4.5 MASS BALANCES

The carbon utilization and mass balance determinations were made using the gas analyses, solids analyses, and process flows entering and leaving the KBR transport reactor.

The process flows into the KBR transport reactor are:

- Coal flow through FD0210.
- Sorbent flow through FD0220.
- Air flow measured by FI205.
- Nitrogen flow measured by FI609.
- Steam flow measured by FIC204.

Typically the sorbent-flow rate is determined similar to the coal-feed rate (that is, by a correlation of weight cell and feeder speed data). In GCT1 the feeder leaked through and the feeder dumps could not be correlated with the feeder speed. The operator log of FD0220 fills was used to develop an estimate of the sorbent-flow rate. There were times when the sorbent and sand were both added to FD0220.

The estimated FD0220-feed rates are provided in Figure 4.5-1. Note the wide variations in sorbent-feed rate on December 8 and 9 with flows from 200 to 1,900 lb per hr. There was no sorbent fed during December 10 (the last day of PRB coal testing and the beginning of Illinois coal testing). The Illinois coal testing started with intermittent feeding at 400 lb per hr, then increased to 800 lb per hr and then decreased to 400 lb per hr prior to the end of sorbent feed. During the first four hours of December 12 sorbent was added to the feed bin but all blew through the feeder in a few minutes, then there was no feed until the next fill. The flow varied from 1,000 to zero lb per hr very quickly. Once the sorbent feeder was repaired the sorbent-feed rate was at 700 lb per hr early on December 12. The sorbent rate then decreased to 400 to 500 lb per hr through the end of the Illinois coal test. Sorbent feed was stopped just prior to the Alabama coal testing due to operational problems.

The process flows from the KBR transport reactor are:

- Fuel-gas-flow rate from the PCD measured by FI465.
- PCD solids flow through FD0520.
- Reactor solids through FD0510.

Since FD0510 was rarely used during GCT1 it will be neglected in the determination of the mass balances and carbon conversion.

The solids flow from the PCD can be determined by three different methods:

- In situ solids sampling upstream of the PCD.
- FD0530 weight cell data.
- A compound mass balance using a compound that is present as a solid in the PCD inlet.

The best measurement of the solids flow to the PCD is the in situ PCD inlet solids determination. The solids flow to the PCD can be determined using the fuel gas-flow rate since the PCD is capturing all of the solids.

The FD0530 weigh cell data can be used to determine the PCD solids flow only if both the FD0530 feeder and the FD0510 feeder (standpipe solids) are off because FD0520 and FD0510 both feed into FD0530 and FD0530 feeds the sulfator. This method assumes that the PCD solids level in the PCD and FD0502 screw cooler are constant (that is, the PCD solids level is neither increasing nor decreasing). The results for the first two methods are compared in Figure 4.5-2.

The in situ and weigh cell data generally compare well. Operation on December 8 was complicated by a dipleg upset during a high coal-feed rate which sent a large amount of solids to the PCD. The high weigh cell solids loading and flow rates are a result of clearing the PCD cone of excess solids. The in situ and weigh cell data agree well except for the one point on December 9, 1999. That data was taken the second day of operation during a period when the solids circulation was decreasing rapidly. Both techniques show an increasing PCD solids rate from the end of the Powder River Basin coal testing on December 10 to end of the run.

The third method to determine the PCD solids flow would be to use a mass balance using one of the components of the PCD solids as a 'tie' compound. The inerts was selected as the tie compound thus forcing the inerts mass balance. All the inerts in the coal and sorbent should exit with the PCD solids. This calculation assumes that FD0510 is not running. FD0510 was not run during the PRB testing and operated intermittently during the Illinois coal and Alabama testing.

The addition of the sorbent and coal inerts less any inerts accumulation in the standpipe results in the rate of inerts out of the transport reactor since there are no solids is the air, nitrogen, steam, or fuel gas streams. Coal inerts are not the same as coal ash since coal ash contains CaO, MgO, and SO_3, which are counted in the ash but not the inerts. All three sorbents had a very low inerts content and did not effect the total inerts much.

The mass balance PCD solids are plotted in Figure 4.5-3 along with the PCD solids from the in situ sampling and the FD0530 weigh cell data. While there is a lot of scatter in mass balance calculations there is some agreement with the in situ and weight cell data. The values from all three calculations have been 'smoothed' to represent all three methods of PCD solids flow determinations. The in situ determinations were given first priority and the weight cell determinations were given second priority for the data smoothing. The mass balance calculation

provides an indication of the PCD solids flow in between the in situ and weigh cell determinations. Some of the scatter in the mass balance PCD solids calculation was due to the varying level of standpipe solids during the run. This effected the calculation by subtracting solids that accumulated in the standpipe and adding solids to the PCD solids when the standpipe level was decreasing. The varying standpipe level added scatter of about ± 100 lb per hr to the PCD solids-flow rate calculation. Added error was that limited standpipe solids analyses are available. When there were no standpipe analyses available it was assumed that there were 75-percent inerts in the standpipe. There were also some errors in the time lag between the time that the sample was collected on the PCD filter elements and the time that it was actually sampled at FD0520.

The PCD solids-flow rate shows the clearing of the PCD cone of solids on December 8. During the PRB coal testing on December 9 the PCD solids-flow rate decreased from 900 to 200 lb per hr. The sudden increase in coal rate on December 9 increased the PCD solids rate up to 750 lb per hr. On December 10 the PCD solids rate seemed to hold steady at 600 to 700 lb per hr during the period of highest gas heating value. The transition period had a wide scatter of PCD solids rate. Operation on Illinois coal on December 11 had a steady increase of PCD solids rate to 1,000 lb per hr from 600 lb per hr. The decrease in coal and sorbent rate early on December 12 resulted in a decrease in PCD solids rate from 1,300 to 600 lb per hr. The PCD solids rate then slowly increased back up to 1,200 lb per hr by the middle of December 13. The remainder of the Illinois coal testing varied between 800 and 1,200 lb per hr until the switch to Alabama coal. The Alabama coal testing had steadily decreasing PCD solids probably due to no sorbent being fed to the reactor and decreased coal-feed rates. The sudden rise at the PCD solids mass balance rate at the transition from Illinois to Alabama coal was probably caused by the assumed sudden change in higher ash coal properties (Illinois No. 6 coal, 10-percent ash to Alabama coal, 17-percent ash). Actually, the "true" coal transition point is not known.

Carbon conversion is defined as the per cent fuel carbon that is gasified to CO, CO_2, CH_4, C_2H_6, and higher hydrocarbons. The commercial goal is 90 percent or greater carbon conversion to minimize/eliminate the potential need for a combustion train. Carbon conversion can be calculated two ways:

- From gas analysis using the fuel-feed rate, fuel-carbon content, fuel-gas rate, and fuel-gas composition.

- From solids analysis using the fuel-feed rate, fuel-carbon content, PCD solids-flow rate, PCD solids-carbon content, standpipe solids-accumulation rate, and standpipe solids-carbon content.

The results for the gas analysis and solid analysis are shown in Figure 4.5-4. The gas compositions used are determined using procedures wherein they are "normalized" and contain moisture (wet) (see section 4.3). The coal-feed rates were determined by a correlation between FD0210 weigh cell dumps and feeder speed. There are no gas analysis results for the periods when the gas analyzers were not in operation. The fuel-gas rate was increased by 11 percent to be consistent with the thermal oxidizer oxygen balance.

On the first day of PRB coal operation (December 8) the gas analysis carbon conversion was scattered between 65 and 90 percent. In the afternoon on the second day of operation (December 9) the gas carbon conversion increased from 80 percent to just below 100 percent. The large increase in coal rate around midnight December 9 decreased the carbon conversion from 95 to 85 percent. The highest gas heating value was measured at the end of the PRB testing on December 10 while the gas carbon conversion was at 85 percent. The transition period between PRB and Illinois coal produced a scattering of data due the unsteady operating conditions when alternating coals were fed to the reactor. For the initial Illinois coal testing the gas analyzers produced a carbon conversion of about 90 percent. Prior to when the gas analyzers conditioning system plugged for the last time on December 13, the gas analysis carbon conversion was increasing from 77 to 93 percent due to decreasing coal-flow rate and increasing fuel-gas rate.

The results for the solids analysis are shown in Figure 4.5-4. The solids analysis-based carbon conversion was between 65 and 85 percent for the first day of PRB coal. During the December 9 the solids carbon conversion increased from 75 to 98 percent just before the large coal-feed rate increase on December 9. The large coal-feed rate increase late on December 9 decreased the carbon conversion down to 85 percent. The coal conversion was 85 to 90 percent during the PRB operation with the highest heating value. During the transition from PRB to Illinois coal there was a scatter in the carbon conversions. After the first day of operation on Illinois coal (December 11) the solids coal conversion leveled out at 70 percent. The coal conversion then quickly increased to 82 percent due to a decrease in both coal-flow rate and PCD solids rate. The carbon conversion then slowly rose for the most of December 12 up to 88 percent, then slowly decreased to 78 percent by midday December 13. The carbon conversion followed the PCD solids rate for the remainder of the Illinois coal run with an increase in PCD solids rate decreasing the carbon conversion and vice-versa. The transition to Alabama coal on December 14 suddenly dropped the carbon conversions to 60 percent due to the sudden change in Alabama coal-ash content. Again this is probably a calculated result based on the assumed transition from Illinois to Alabama coal. The Alabama coal-carbon conversion slowly increased to 66 percent at the end of GCT1 due to the decrease in PCD solids flow.

The carbon conversions for the solids and gas analyses agreed well for the PRB testing, while not agreeing well for the Illinois coal testing. The gas analysis method should be more accurate than the solids analysis method since it has fewer assumptions and relies on continuous gas analyzers rather than grab-solids analyses, which have more variations, a potential for sampling errors, and have a time lag of probably several hours. There seemed to be no good reason why the two methods should be in consistently poor agreement for Illinois No. 6. Part of the reason is the unsteady conditions of the transport reactor in PCD solids flow and the internal solids circulation. The greatest error is in the determination of the PCD solids rate on an hourly basis.

Material balances are useful in checking the accuracy and consistency of the data obtained as well as determining periods of steady operation where the data is suitable for model development or design. GCT1 did not have many periods of stable operation, as evidenced by wide swings in both riser velocity and standpipe solids inventory.

The two most inaccurate flows were the steam flow and PCD solids flow. Errors in the PCD-solids-flow rate has been discussed earlier in this section. For most of the run the steam flow

rate indicator (FI204) was reading negative or was varying widely. The steam flow was assumed to read the following values for different time intervals:

- Start of test to 10:00 December 9, 1999 – 700 lb per hr.
- 11:00 December 9, 1999, to 18:00 December 11, 1999 – FIC204 readings varied from 201 to 888 lb per hr.
- 19:00 December 1, 1999, to end of test – 1,035 lb per hr.

Hourly, overall material balances are provided in Figure 4.5-5 showing the relative difference between feeds and products {(feeds - products)/feeds} or {(in - out)/in} and the absolute difference between feeds and products (in - out). The fuel-gas rate was not increased by 11 percent as in previous calculations. The overall material balance was quite good for the PRB coal testing, consistently between ±3 percent relative difference and ±500 lb per hr absolute difference. The Illinois coal testing had relative differences at -3 to 7 percent (-700 to -1,200 lb per hr) for December 11 and 12 and -5 to -10 percent relative difference (-1,000 to -2,000 lb per hr absolute difference) for the last 3 days of testing. Some value for two 1-hr total mass balances is provided in Table 4.5-1. The air, nitrogen, and fuel rate dominate the "in" streams while the fuel gas dominates the "out" streams.

Hourly nitrogen balances are provided in Figure 4.5-6. Balances are only calculated for times when the gas analyzers were in operation. The nitrogen balance was acceptable at zero to -8 percent relative difference (zero to -1,000 pounds per hour nitrogen absolute difference) for the periods when the gas analyzers were in operation. The run started at -7 percent relative difference (-500 pounds per hour nitrogen), then decreased to nearly perfect agreement during December 10 in PBR coal operation while the fuel gas heating value was maximized. Once the coal feed was changed to Illinois coal on December 11 the absolute difference slowly increased to -8 percent (-1,000 pounds per hour nitrogen). Table 4.5-1 provides details of the nitrogen balance for two 1-hr periods. Major flows for nitrogen are the inlet air and aeration nitrogen and the outlet fuel gas.

The carbon balances were not good for GCT1. The carbon balance was off over +10 percent (300 lb per hour of carbon). Typical carbon balance values are provided in Table 4.5-1.

The sulfur balance was not good for GCT1. The sulfur balance was off by ±10 to 40 percent for the PRB coal testing and by -150 to +80 percent for the Illinois coal testing. Table 4.5-2 provides details of the sulfur balance for two 1-hr periods. Note the low flows of sulfur in the PRB coal testing. The two coal periods selected in Table 4.5-2 were two of the few periods where there was an excellent sulfur balance.

The hydrogen balance was not very good in that there was significantly more hydrogen entering the system than leaving. Typical flows for the hourly hydrogen balance are shown in Table 4.5-2. Note the higher amount of fuel hydrogen in PRB due to the higher moisture content of PRB

coal. Although the PRB and Illinois coal had the same hydrogen output in these two cases the PRB fuel gas had a higher molecular hydrogen while the Illinois No. 6 fuel gas has a higher moisture content (see Figures 4.3-6 and -7).

The oxygen balance was poor with relative balances between -5 and -15 percent for most of the run. Since both the nitrogen and oxygen are feeding less in than out this could indicate that the measured air rate is lower than the actual air rate. Since the hydrogen and oxygen balances are not "off" in the same direction, changing the steam will not improve both hydrogen and oxygen balances. Two oxygen balances are provided in Table 4.5-2. Note that the fuel oxygen is higher for the PRB than for the Illinois No. 6 coal due to the higher moisture content of the PRB coal.

The calcium balances were poor for the entire test. Two calcium balances are provided in Table 4.5-3. Note the much lower calcium flows for the PRB coal balance. The PRB operation is characterized by very low flow rates of calcium due to the lack of sorbent feed to the reactor during this time. The poor calcium balances highlight inaccuracies in the sorbent-feed rate and PCD-solids rate determinations.

Table 4.5-1

Total, Nitrogen, and Carbon Balances

Mass Balance Type	Total		Nitrogen		Carbon	
Date	12/10/99	12/13/99	12/10/99	12/13/99	12/10/99	12/13/99
Time Start	12:30	3:30	13:30	3:30	13:30	3:30
Time End	13:30	4:30	14:30	4:30	14:30	4:30
Fuel	PRB	Illinois #6	PRB	Illinois #6	PRB	Illinois #6
Sorbent	Dolomite	OH LS	Dolomite	OH LS	Dolomite	OH LS
Mixing Zone Temperature, F	1,714	1,800	1,682	1,800	1,682	1,800
Pressure, psig	175	205	175	205	175	205
In, pounds/hr						
Fuel	4,328	2,949	66	65	2,502	1,856
Sorbent	0	532			0	47
Air	11,208	9,916	7,936	7,708		
Nitrogen	6,892	7,584	6,951	7,604		
Steam	468	1,035				
Total	22,897	22,015	14,953	15,377	2,502	1,903
Out, pounds/hr						
Fuel Gas	22,229	21,885	15,247	16,437	1,806	1,439
PCD Solids	605	1,086			304	374
Total	22,834	22,971	15,247	16,437	2,110	1,813
Accumulation	-31	26				
(In - Out)/In, %	0.41	-4.46	-1.97	-6.89	15.67	4.72
(In-Out), pounds per hour	94	-982	-295	-1,060	392	90

Table 4.5-2

Sulfur, Hydrogen, and Oxygen Balances

Mass Balance Type	Sulfur		Hydrogen		Oxygen	
Date	12/10/99	12/12/99	12/10/99	12/13/99	12/10/99	12/13/99
Time Start	13:30	20:30	14:30	3:30	15:30	3:30
Time End	14:30	21:30	15:30	4:30	16:30	4:30
Fuel	PRB	Illinois #6	PRB	Illinois #6	PRB	Illinois #6
Sorbent	Dolomite	OH LS	Dolomite	OH LS	Dolomite	OH LS
Mixing Zone Temperature, F	1,682	1,789	1,651	1,794	1,664	1,794
Pressure, psig	175	200	175	205	175	205
In, pounds/hr						
Fuel	12	69	393	275	1,065	525
Sorbent					42	194
Air			15	15	2,510	2,342
Nitrogen						
Steam			51	115	392	920
Total	12	69	459	405	4,010	3,980
Out, pounds/hr						
Fuel Gas	7	16	303	314	4,364	4,463
PCD Solids	4	53			58	146
Total	11	68	303	314	4,422	4,609
Accumulation						
(In - Out)/In, %	9.01	0.52	33.95	22.48	-10.27	-15.80
(In-Out), pounds per hour	1	0	156	91	-412	-629

Table 4.5-3

Calcium Balance

Mass Balance Type	Calcium	
Date	12/10/99	12/12/99
Time Start	13:30	22:30
Time End	14:30	23:30
Fuel	PRB	Illinois #6
Sorbent	Dolomite	OH LS
Mixing Zone Temperature, F	1,682	1,797
Pressure, psig	175	202
In, pounds/hr		
Fuel	38	19
Sorbent	0	153
Air		
Nitrogen		
Steam		
Total	38	172
Out, pounds/hr		
Fuel Gas		
PCD Solids	40	174
Total	40	174
Accumulation	0	-3
(In - Out)/In, %	-5.76	-1.30
(In-Out), pounds per hour	-2	-2

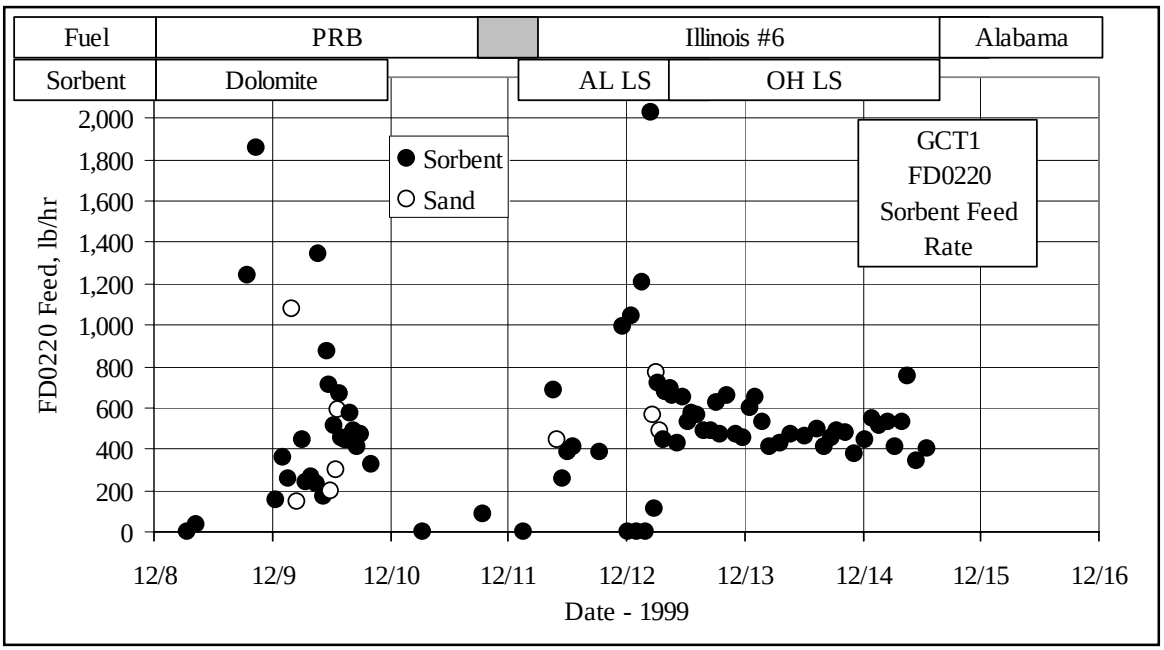

Figure 4.5-1 FD0220 Sorbent Feed Rate

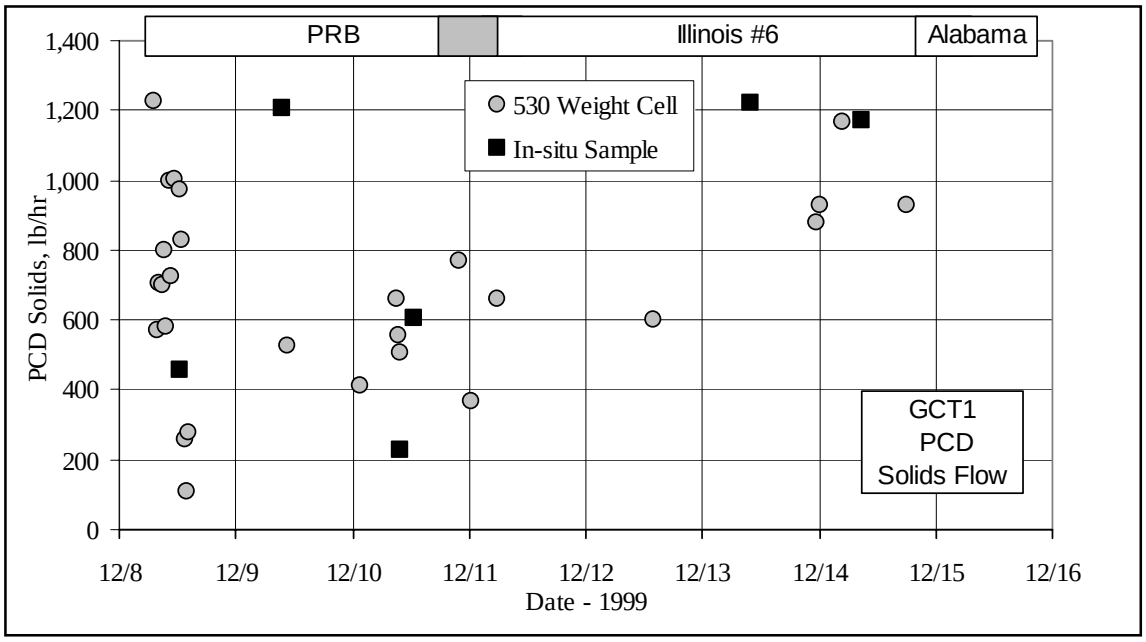

Figure 4.5-2 PCD Solids Rate

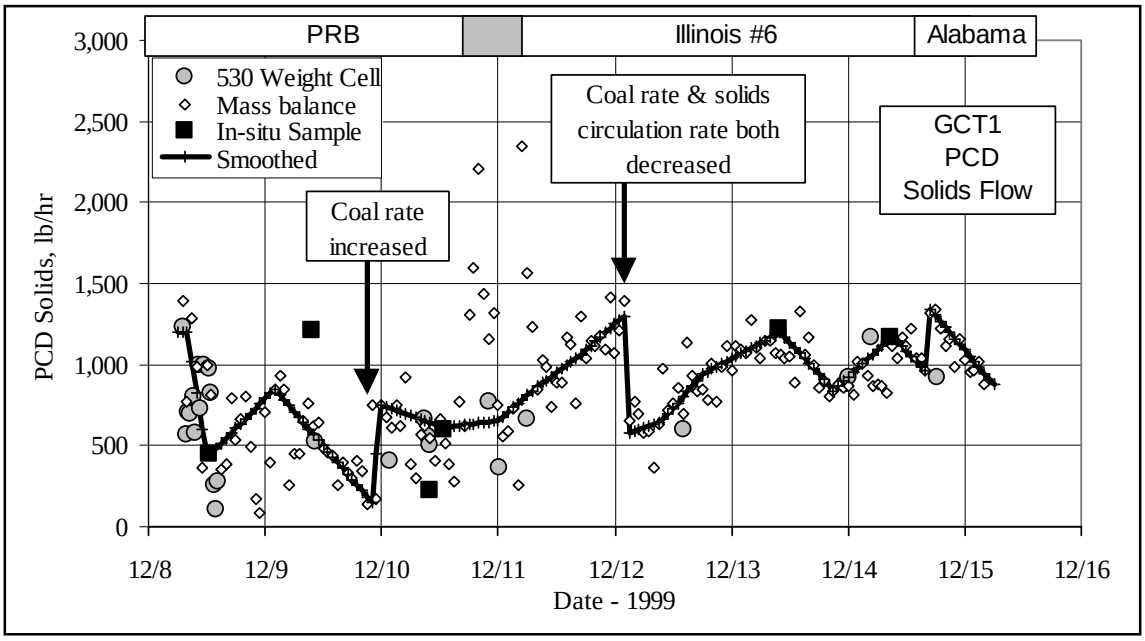

Figure 4.5-3 PCD Solids Rate

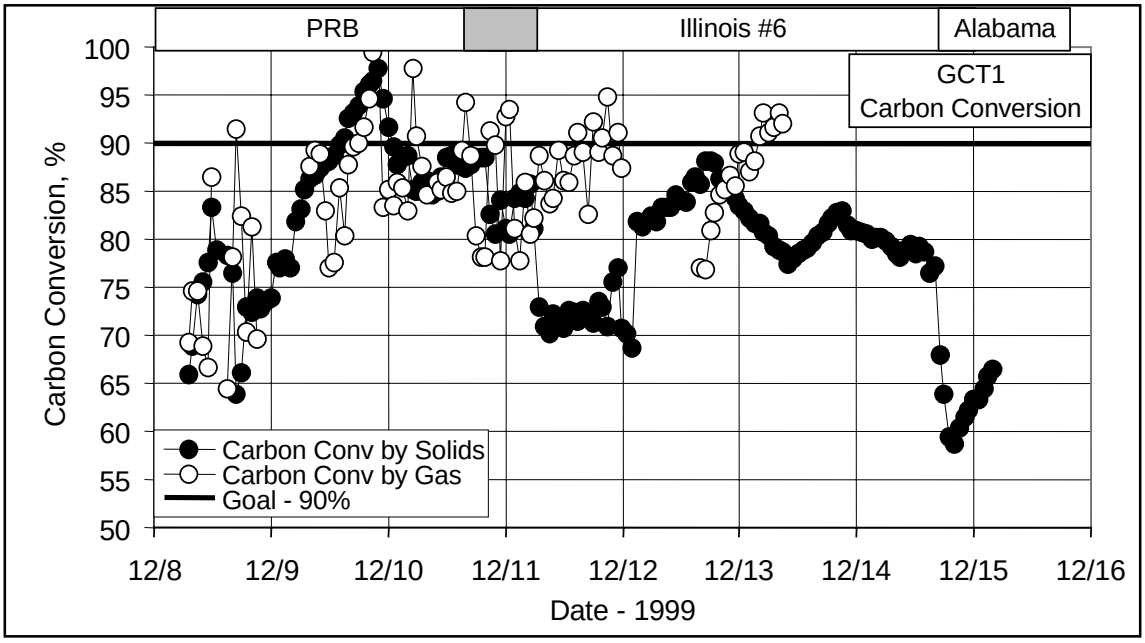

Figure 4.5-4 Carbon Conversion by Gas Analyses and Solids Analyses

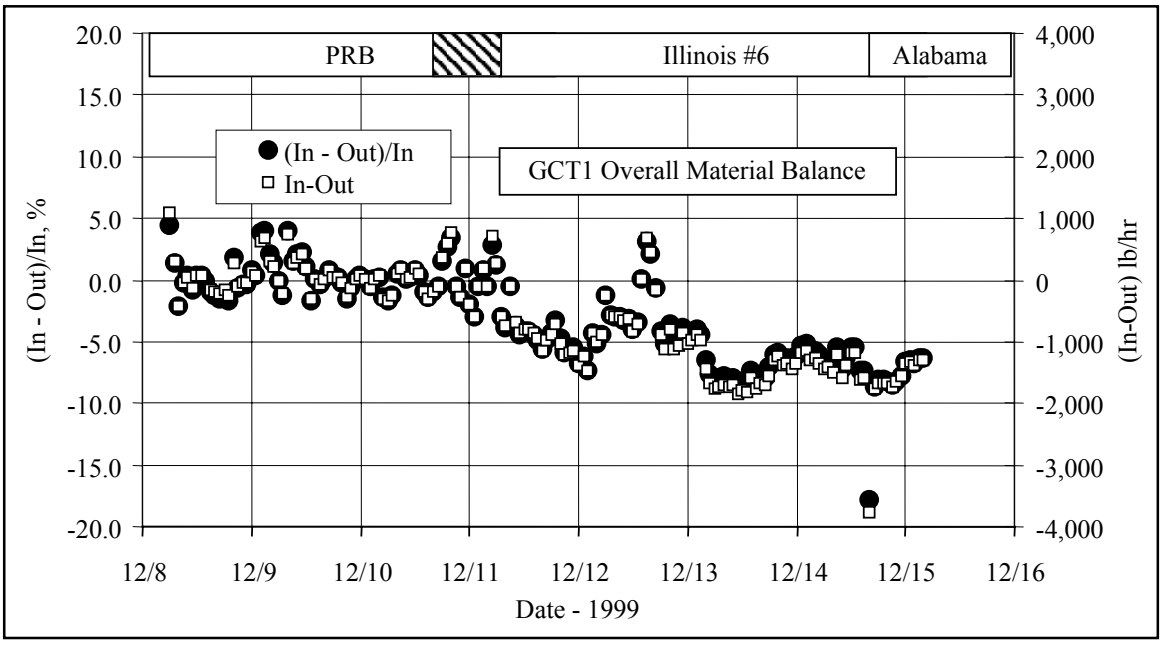

Figure 4.5-5 Total Material Balance

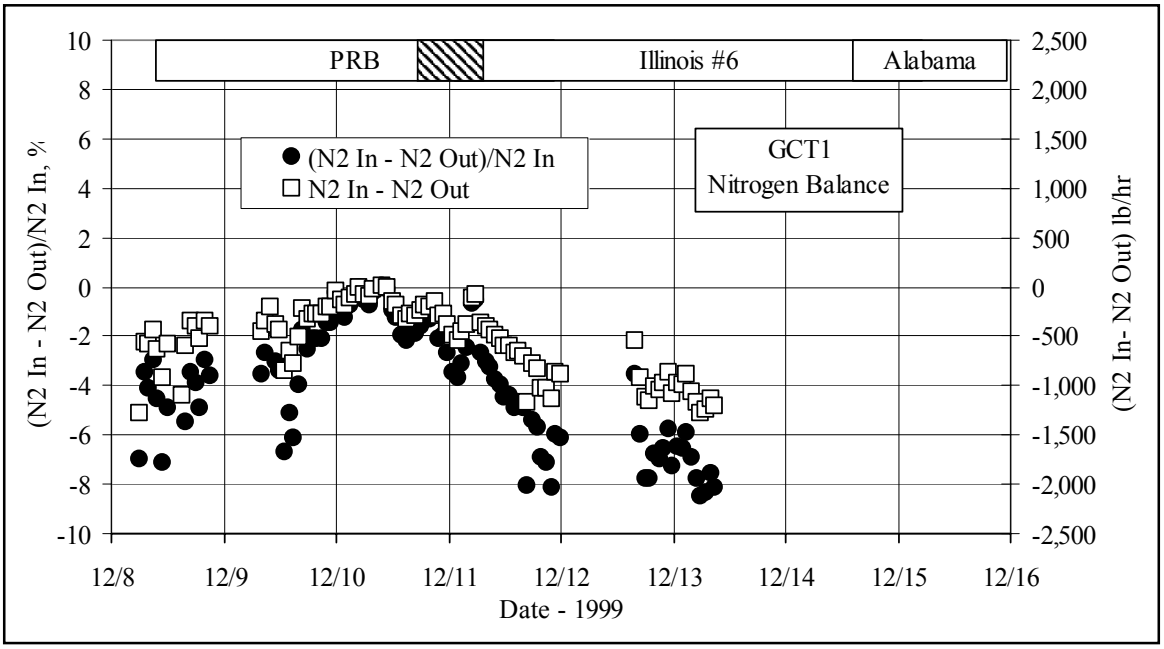

Figure 4.5-6 Nitrogen Balance

4.6 FUEL NITROGEN ANALYSIS

The fuel nitrogen released as volatile HCN or NH_3 during GCT1B through D was evaluated. Since there is no direct HCN or NH_3 measurement the NO measurement downstream of the thermal oxidizer was used to calculate the nitrogen that was released as volatile HCN or NH_3, assuming that 100 percent of the HCN and NH_3 is converted to NO in the thermal oxidizer. Thus, the actual HCN and NH_3 concentrations could be higher with some HCN and NH_3 converted to N_2 in the thermal oxidizer.

Figure 4.6-1 shows the combined HCN and NH_3 concentration versus time. During the first day of operation with the Powder River Basin coal the concentrations of HCN and NH_3 were close to design at 300 ppm. However, HCN and NH_3 concentrations increased to 900 ppm before transitioning to Illinois No. 6 coal. With Illinois No. 6 bituminous coal the concentrations of HCN and NH_3 varied from 300 to 500 ppm, which was slightly higher than design. The HCN and NH_3 concentrations with the Alabama coal averaged around 400 ppm. Multiple plots were created to correlate the HCN/NH_3 concentrations with other reactor parameters. The best correlation was achieved by comparing the HCN/NH_3 concentrations to the CO concentration in the syngas (see Figure 4.6-2). The plot shows an almost linear relationship between the HCN/NH_3 and CO concentrations.

During future test runs gas bomb samples will be analyzed to evaluate the actual HCN and NH_3 concentrations in the syngas stream.

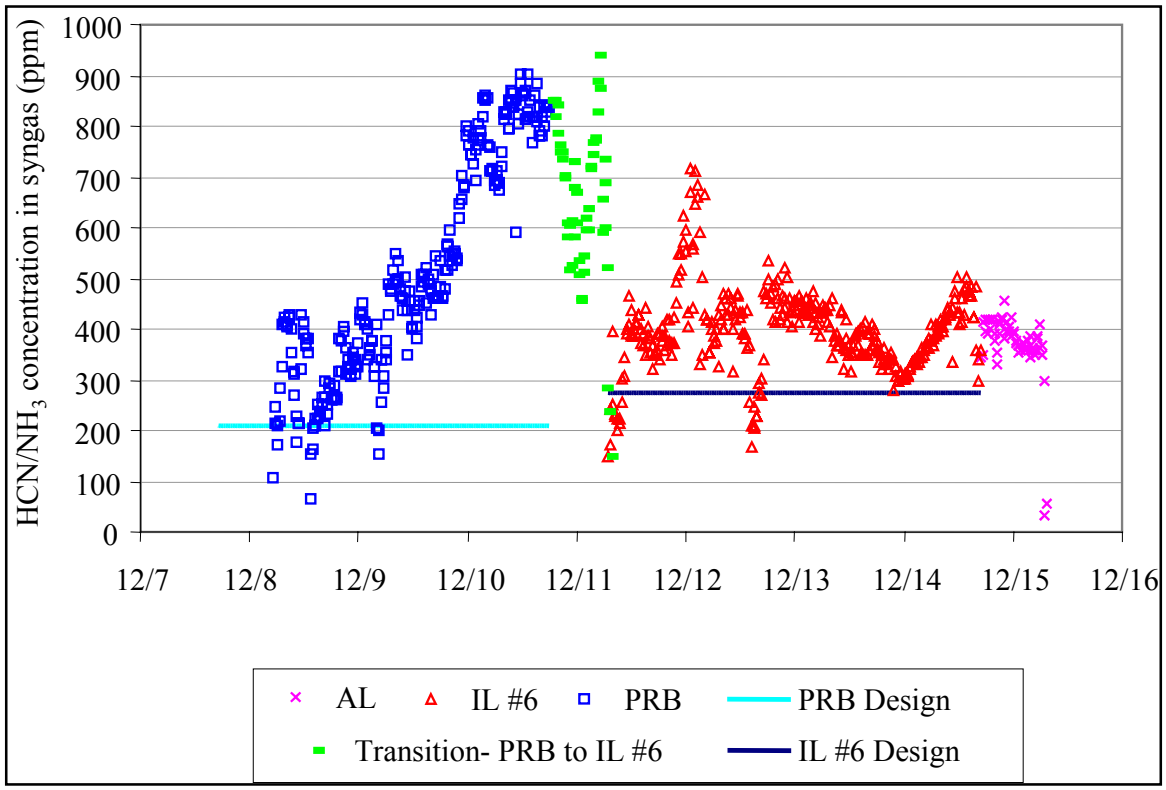

Figure 4.6-1 HCN/NH3 Concentration Versus Time

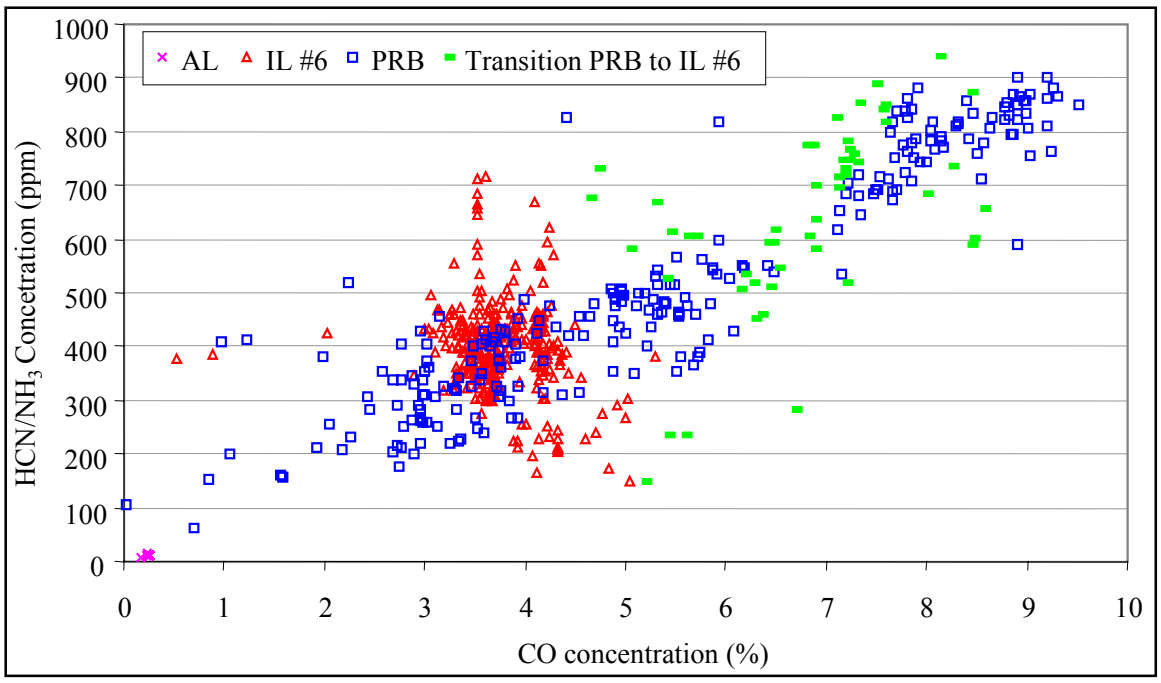

Figure 4.6-2 HCN/NH3 Concentration (ppm) Versus CO Concentration (%)

4.7 PROCESS GAS COOLERS

Heat transfer calculations were done on the primary gas cooler (HX0202) and the secondary gas cooler (HX0402) to determine if their performance had deteriorated during GCT1 due to tar or other compounds depositing on the tubes.

At the conclusion of GCT1 there was an accumulation of dust on top of the tubes in the primary gas cooler. After the dust was removed it was noted that several of the tubes were crusted over; the tubes were fairly clean. During GCT1 there was also tar plugging of the gas analyzer sampling system. Heat transfer and pressure drop calculations were done around HX0202 to determine if there was any deterioration in HX0202 performance that might appear when the dust accumulation occurred. The primary gas cooler is between the transport reactor cyclone (CY0201) and the PCD (FL0301). During GCT1, HX0202 was not bypassed and took the full gas flow from the transport reactor.

The primary gas cooler is a single-flow heat exchanger with hot gas from the transport reactor flowing through the tubes with the shell side operating with the plant steam system. The pertinent equations are:

$$Q = UA\Delta T_{LM} \tag{1}$$

$$Q = c_p M(T_1 - T_2) \tag{2}$$

$$\Delta T_{LM} = \frac{(T_1 - t_2) - (T_2 - t_1)}{\ln \frac{(T_1 - t_2)}{(T_2 - t_1)}} \tag{3}$$

Q = Heat transferred, Btu/hour
U = Heat transfer coefficient, Btu/hr/ft^2/°F
A = Heat exchanger area, ft^2
ΔT_{LM} = Log mean temperature difference, °F
c_p = Gas heat capacity, Btu/lb/°F
M = Mass flow of gas through heat exchanger, lb/hr
T_1 = Gas inlet temperature, °F
T_2 = Gas outlet temperature, °F
$t_1 = t_2$ = Steam temperature, °F

Using equations (1), (2), and (3) and the process data the product of the heat transfer coefficient and the heat exchanger area (UA) can be calculated. The UA for GCT1B through D is shown in Figure 4.7-1 as hourly averages along with the design UA and the pressure drop across HX0202. If HX0202 is plugging the UA should decrease and the pressure drop should increase. The UA deterioration is a better indication of heat exchanger plugging because the pressure drop is calculated by the difference of two numbers of about the same size (usually from 160 to 220 psig) resulting in pressure drops of 0.5 to 6 psig.

The UA decreased during the first day of Powder River Basin (PRB) coal testing from nearly the design value of 5,200 Btu/hr/°F to 3,500 Btu/hr/°F. The pressure drop followed this trend from 4.5 psi down to 3.5 psi, likely due to unsteady-state operation at the start of the test run. The gas analyzer system plugged with tar at 21:00 December 8. This tar formation appeared to cause some plugging of HX0202 at 05:00 December 9 as UA decreased and the pressure drop increased. This condition corrected itself by 13:00 December 9 and the heat exchanger performance improved for the rest of December 9. For the last day of PRB coal testing UA increased from 3,700 to 4,500 Btu/hr/°F and the pressure drop leveled out at 3.7 psi.

The transition from PRB to Illinois coal showed up as wide swings in UA caused by the wide swings in reactor temperature. The coal-transition-pressure drops bounced around a bit during the transition but remained between 3 and 4 psi. During the operation on Illinois coal the UA values quickly decreased from 4,500 Btu/hr/°F to 2,500 Btu/hr/°F on December 11.

The heat exchanger pressure drop increased from 09:00 December 11 just after the last PRB coal was fed to the reactor. The analyzer system plugged with tar around 03:00 December 12. The pressure drop leveled off on December 13 at 6 psi on Illinois coal. The gas analyzers plugged with tar at 08:00 December 13 and remained out of service through the end of the run. There was a slight pressure decrease early on December 13 where the pressure drop decreased to 5.3 for 6 hours and then returned to 6.0 psi. This was during a system pressure increase of 10 psig. These strange swings in pressure drop indicate that the small pressure drop changes are a poor indicator of heat exchanger plugging. At 15:00 December 13 the pressure drop slowly started decreasing to 3.5 psi which was reached at 00:00 December 14. At 13:00 December 14 the pressure drop suddenly jumped up to 4.8 psi at the same time the sorbent feed was turned off for 30 minutes. The pressure drop then remained at 4.5 psi through the transition to Alabama coal and the end of the test.

The heat exchanger UA remained steady at 2,500 Btu/hr/°F for several days after the start of Illinois coal. On December 13 the UA began slowly rising to 3,000 Btu/hr/°F and remained there through the transition to Alabama coal and the end of the test. Based on the UA and pressure drop results most of the heat exchanger plugging occurred during the transition from PRB to Illinois coal on December 11.

HX0202 data from two other periods are included for comparison with the GCT1B through D data. Figure 4.7-2 shows the plot of the HX0202 UA and pressure drop combustion for tests TC05F and G when the transport reactor was in combustion mode firing petroleum coke. This was the only time during TC05 that the full flow from the transport reactor was sent to HX0202. Other TC05 testing was operated either at total or partial heat exchanger bypass. The UA was at

7,000 to 7,800 Btu/hr/°F, above the design value of 5,200 Btu/hr/°F. The pressure drop was at about 2.5 psi and constant for the testing. Comparing the GCT1B through D data with the TC05F and G data it is clear that there was some plugging in HX0202 during gasification in that the gasification UA was below the combustion UA and the gasification pressure drop was above the combustion pressure drop for the gasification Illinois No. 6 testing.

Figure 4.7-3 shows the plot of the HX0202 UA and pressure drop for the gasification run GCT1A. The heat transfer coefficient was less than design values, generally decreasing during the entire run, which indicates some plugging. The pressure drop was fairly constant during the first two periods of operation at 1 to 2 psi. The third-period pressure drop was very constant but then suddenly increased from 2 to 15 psi and then started decreasing to 12 psi at the end of the run. The higher pressure drop was caused by the downstream PI (PI300) plugging (and reading low). PI300 decreased while the system pressure increased and seemed to lose the response to the PCD back pulsing. The PI downstream of PI300 (PI301) did not indicate the pressure decrease/pressure drop increase that PI300 indicated. This higher pressure drop on September 15 is a false reading and is not an indication of HX0202 plugging. Note the UA slightly increased during the apparent pressure drop increase.

At the conclusion of GCT1, 675 lb of black, shiny solids were found in the bottom of the secondary gas cooler (HX0402). The secondary gas cooler is a single-flow heat exchanger with hot gas from the PCD flowing through the tubes and the shell side operating with plant steam system. Some heat transfer and pressure drop calculations were done around HX0402 to determine if there were any clues to when the solids were formed. The solids are probably solidified coal tar that was in the gas phase at the PCD temperatures which then condensed out at the lower HX0402 temperatures. HX0402 is not part of the commercial flow sheet. In the commercial flow sheet the hot-fuel gas from the PCD would be sent to a combustion gas turbine.

Using equations (1), (2), and (3) and the process data, the product of the heat-transfer coefficient and the heat exchanger area (UA) can be calculated. The UA for the GCT1B through D testing is shown in Figure 4.7-4 as hourly averages along with the design UA and the pressure drop across HX0402. If HX0402 is plugging the UA should decrease and the pressure drop should increase. The UA was steady during the PRB coal testing, slightly increasing from 8,000 to 9,000 Btu/hr/°F (design 13,100 Btu/hr/°F). The HX0402 pressure drop was also very constant at around 2 psi.

The transition from PRB to Illinois coal was uneventful in the pressure drop while the UA showed a slight increase, then a decrease. During the operation on Illinois coal the UA values slowly increased from 9,000 Btu/hr/°F at 05:00 December 11 to the design value of 13,000 Btu/hr/°F at 00:00 December 13 where they remained until the transition to Alabama coal.

The heat exchanger pressure drop suddenly started increasing at 10:00 December 14 near the end of the Illinois coal testing. At this time the sorbent feed was turned off for 30 minutes. The HX0402 pressure drop increased over several hours from 2 to nearly 10 psi at 15:00 December 14. The sorbent was then turned off for good at 14:20 on December 14 and the HX0402 pressure leveled out at around 10 psi for a few hours. The Alabama coal broke through at 17:00

December 14, which seemed to slightly decrease the HX0402 pressure drop to 8 psi, where it remained until shutdown. The pressure drop data would indicate that the heat exchanger started plugging when the sorbent was turned off. Since the tar was collected at the bottom of the heat exchanger it could be coincidence in that the heat exchanger bottom was slowly filling up during the testing and just happened to start blocking the gas path when the sorbent was turned off.

HX0402 data from two other periods are included for comparison with the GCT1B through D data. Figure 4.7-5 shows the plot of the HX0402 UA for test TC05C when the transport reactor was in combustion mode firing Illinois No. 6 coal. The heat-transfer coefficient was at the design values and the pressure drop was at about 1.75 psi and slowly rising during the run. Figure 4.7-6 shows the plot of the data for the GCT1A gasification run. A small amount of solid tar was found at the bottom of HX0402 at the end of GCT1A. The heat-transfer coefficient was less than design values, generally decreasing during each testing period, which indicates some potential for plugging. Each period was really too brief to permit HX0402 to reach the design heat-transfer coefficient. The pressure drop was fairly constant during the first two periods of operation at 1 to 2 psi, and then increased for the third period of operation. At the end of each period the pressure drop was slightly increasing. The last 10 hours of operation on September 15 seemed to show some heat exchanger plugging as shown by the increase in heat-exchanger pressure drop.

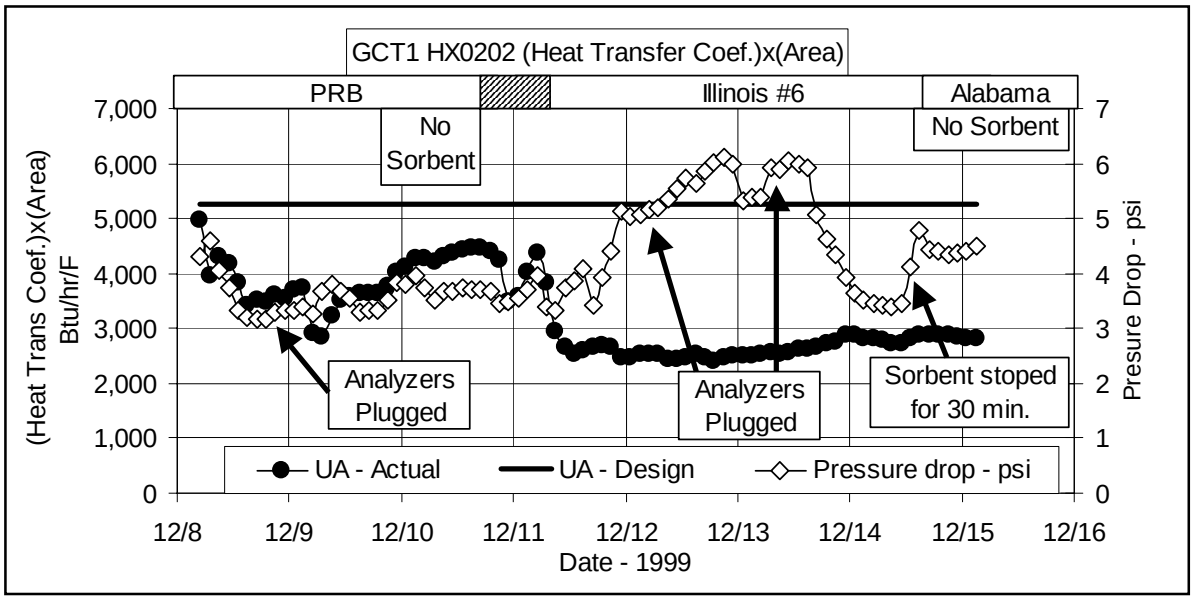

Figure 4.7-1 GCT1 HX0202 Heat-Transfer Coefficient - Area and Pressure Drop

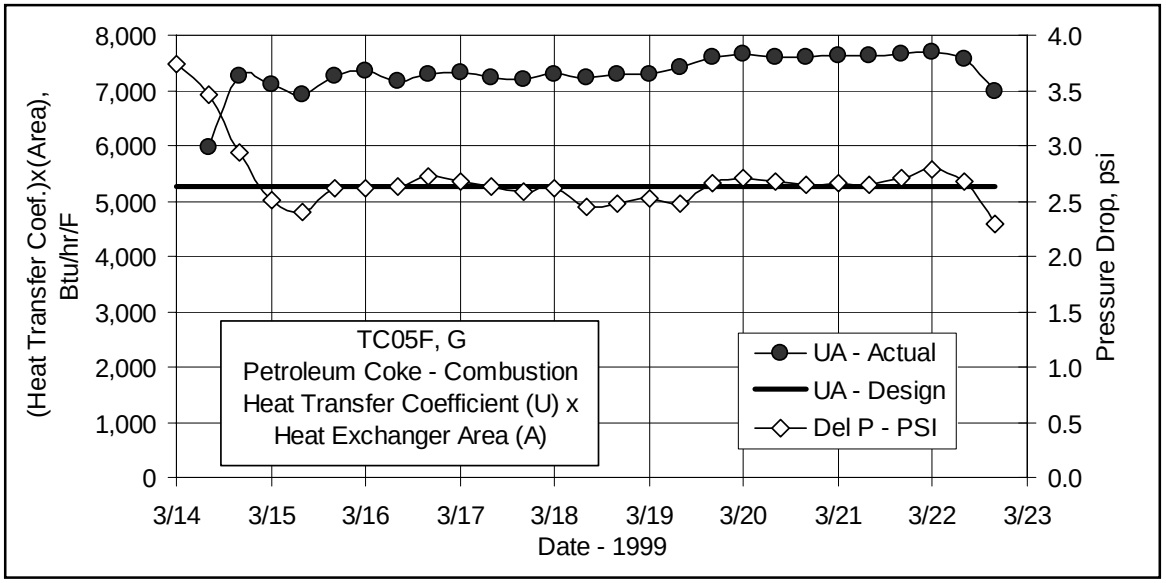

Figure 4.7-2 TC05F/G HX0202 Heat-Transfer Coefficient - Area and Pressure Drop

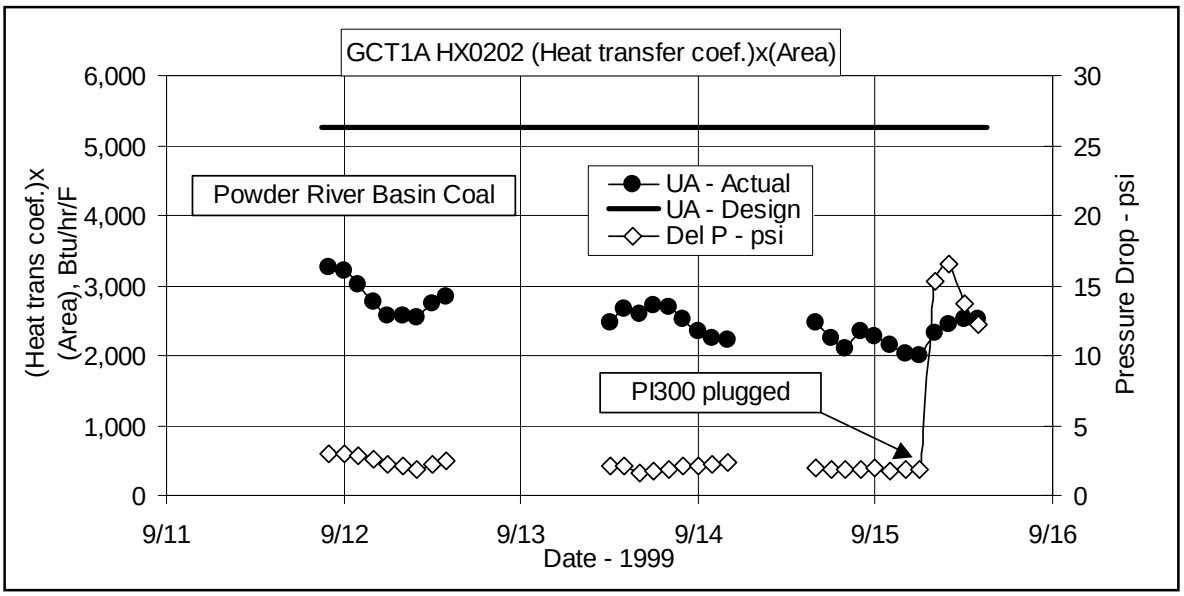

Figure 4.7-3 HX0202 GCT1A Heat-Transfer Coefficient - Area and Pressure Drop

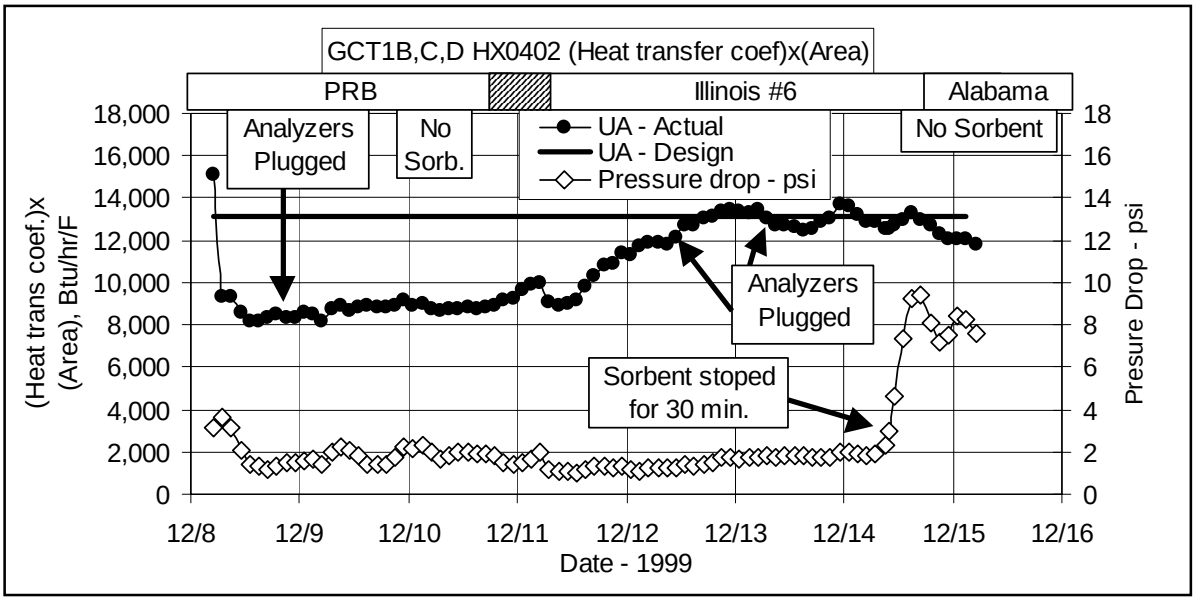

Figure 4.7-4 HX0402 GCT1B Through D Heat-Transfer Coefficient - Area and Pressure Drop

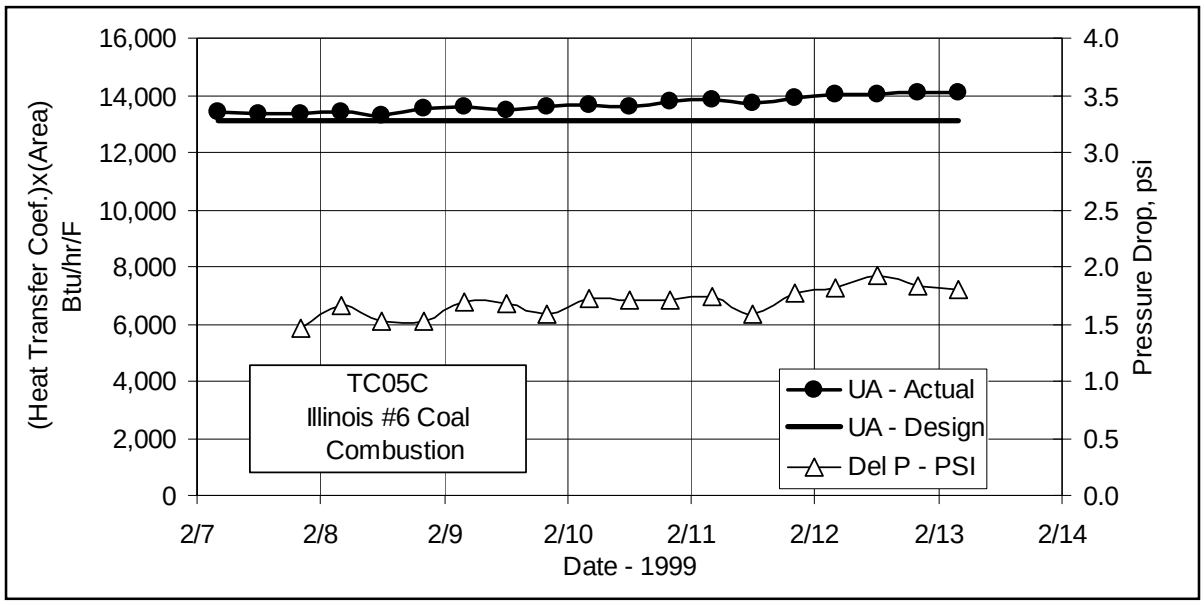

Figure 4.7-5 HX0402 TC05C Heat-Transfer Coefficient - Area and Pressure Drop

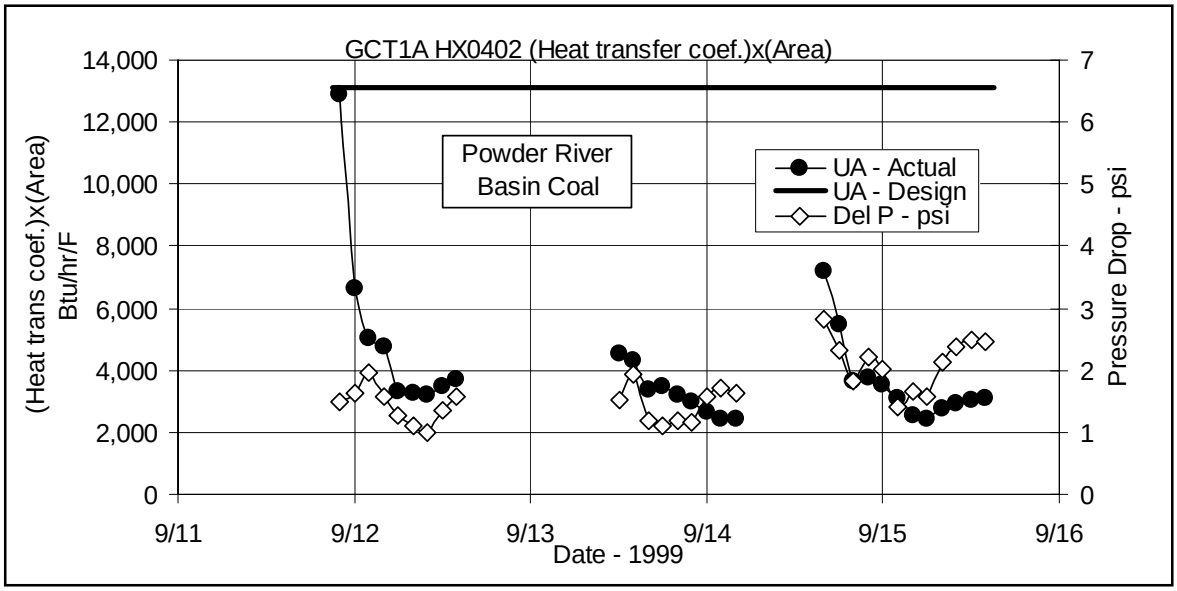

Figure 4.7-6 HX0402 GCT1A Heat-Transfer Coefficient - Area and Pressure Drop

4.8 SULFATOR OPERATIONS

From September 12 through September 16, 1999, the sulfator operated for 38 hours on char from the transport reactor and from December 8 through December 15, 1999, for 157 hours on char. The run did not encounter major mechanical problems but there were several areas of operation that should be addressed. Table 4.8-1 shows the operating conditions for the sulfator during GCT1.

Sulfator accomplishments from GCT1 include:

- Experienced 195 hours on char without any char-feeder problems.
- Increased bed temperature during the second half of the test run (accomplished by removing excess-steam-coil surface area).
- Operated at normal levels with excess solids overflowing into the sulfator screw cooler and the sulfator ash transport system.
- Tested limestone-feed system to the sulfator.
- Improved the operation of the cyclone dipleg during the course of the test by adjusting the aeration rate.
- Successfully checked out fuel-oil system and identified needed modifications.

During the September portion of GCT1A the bed temperature was generally around 1,100°F. The design-operating temperature is 1,600 to 1,650°F to ensure complete conversion of CaS to $CaSO_4$. The GCT1A temperature was less than that designed to meet the objective of sulfating CaS but the coals gasified during GCT1A did not produce char with a significant level of CaS. The cause of the low temperature was determined to be an excessive-heat-transfer area in the steam-superheating coils. This was also causing the superheated-steam temperature to be higher than expected, even at the low-bed temperatures. The high steam temperature prevented the steam flow from being reduced due to a system trip that occurs if the steam temperature exceeds 750°F.

Before the start of GCT1B about 35 percent of the surface of the coils was removed in order to raise the sulfator-bed temperature and to lower the superheated-steam temperature. During the first 3 days of GCT1B this modification allowed the sulfator to operate with a bed temperature of 1,500 to 1,625°F. After 3 days of operation the bed level became sufficient to cover the upper set of superheating coils and the bed temperature dropped to 1,250 to 1,450°F for the remainder of the run. Figure 4.8-1 shows the bed temperature and char feed to the sulfator versus lb of carbon per hour for GCT1A before the modification, GCT1B when only the lower set of superheating-steam coils were covered, and for GCT1B through D when both the upper- and lower-superheating coils were covered. The bed temperature that could be achieved for a given char feed is shown to increase appreciably as the surface area of the coils exposed to the sulfator bed decreases.

The design-heat removal from the sulfator is 2.4 to 3.4 MBtu/hr. During GCT1B through D the actual heat-removal rate was 3 to 4 MBtu/hr before the top coils were covered and 4.5 to 5.0 MBtu/hr after the top coils were covered. Because of the extra-heat transfer, high-steam flows were necessary to prevent tripping the sulfator due to high-superheated-steam temperature. Once the upper steam coils were covered the sulfator required 23,000 to 27,000 lb per hr of steam to keep the steam-exit temperature below 750°F. The design-steam flow is 15,000 to 18,500 lb per hr. The high-steam flows during GCT1 were often greater than the total steam being generated by the gasification process, which led to declining steam-drum pressures.

The sulfator-temperature profile shows that the bed was well mixed initially; however, it became less mixed as the run progressed. During September testing the sulfator did not operate enough hours to show any problems with poor bed mixing. During December the sulfator bed began to show evidence of poor mixing after 30 to 40 hours of operation. By the end of GCT1 the two lowest thermocouples in the bed indicated temperatures at least 600°F lower than the other bed temperatures. (Figure 4.8-2 shows the bed temperatures for runs GCT1B, C, and D.) The most likely cause is segregation of the bed. The start-up bed material is sand with a mean particle size of over 100 μm. The feed from the PCD has a mean particle size of around 25 μm. In lab scale testing the PCD material did not fluidize well and segregated when mixed with sand.

The sulfator waste-heat-recovery boiler does not remove as much heat as designed (it may be undersized). The design gas-exit temperature is 490°F while the actual gas-exit temperatures during GCT1 were 410 to 900°F. The period of time where exit temperatures were below design was after the top superheating coils were covered and the sulfator was operating well below normal-bed temperatures. The performance of the heat exchanger was decreased because of a higher-than-design gas flow of 8,000 to 9,000 lb per hr. Design-gas flow is 6,000 lb per hr. Figure 4.8-3 shows the heat-duty and the overall heat-transfer coefficient for the heat exchanger during GCT1B through D. Even with the additional gas flow the actual values were below the design values for most of the run, as indicated by the solid, horizontal lines in Figure 4.8-3. During GCT1A the heat exchanger also suffered from plugged tubes due to ash collecting in the cone until a large number of the tubes were filled with ash. (For GCT2 the exit piping will be reconfigured to prevent ash from settling by moving the flue gas exit to the bottom of the cone from the existing side exit.)

By using the two differential pressure gauges in the sulfator bed it is possible to calculate the bed density once the level achieves sufficient height to cover the high-pressure leg of the upper gauge. Figure 4.8-4 shows the sulfator-bed density for much of GCT1. The bed density ranges from 50 to 60 lb/ft^3. The density declines with time, indicating that some of the higher density sand that was used as a start-up bed was being lost and replaced with lighter ash from the char.

Prior to run GCT1 the ability to inject fuel oil was added to raise the temperature of the bed at startup. Using the start-up burner the maximum attainable bed temperature is 650 to 700°F. To raise the start-up bed temperature the fuel-oil system will allow about 20 gal per hr of fuel oil to be injected directly into the bed. The fuel is steam atomized and nitrogen is provided for purging of the fuel nozzles when the system is not in service. The first commissioning tests of GCT1 revealed some limitations in the sizing of the fuel lines. The control scheme for the system was successfully commissioned and proved to be acceptable. The fuel lines were undersized and failed to deliver adequate fuel to the sulfator due to higher than expected

pressure drop. The problem was exacerbated by nozzles plugging from failure to open the nitrogen purges before the sulfator was charged with bed material. The problems led to only 5 gal per hr of fuel oil being injected into the bed. For GCT2, modifications are being made which are expected to solve the problems. The fuel-oil-line size is being increased. Steam traps are being installed on the atomizing lines and a source of higher temperature steam will be used. The spray nozzles are being replaced with larger nozzles to further increase capacity and to provide a larger opening to blow away any bed material that may get into the nozzle.

Table 4.8-1

Range of Sulfator Operating Conditions During GCT1

	September	December
Bed Temp (ºF)	1,000 to 1,300	1,350 to 1,625
Air Flow (pph)	7,000 to 8,500	6,500 to 8,500
Total Feed (pph)	550 to 1,100	1,250 to 1,650
Carbon Feed (pph)	200 to 500	500 to 650
Steam Flow (pph)	13,000 to 23,000	18,000 to 27,000

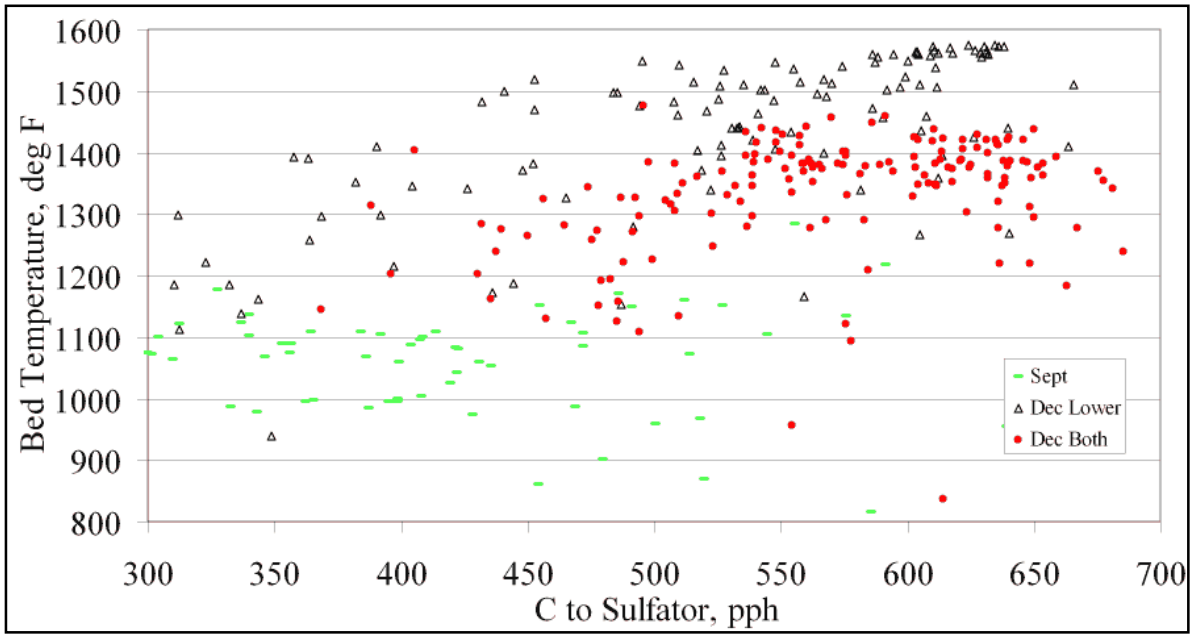

Figure 4.8-1 Changes in Bed Temperature as Various Surface Areas of Superheating Coils Are Covered

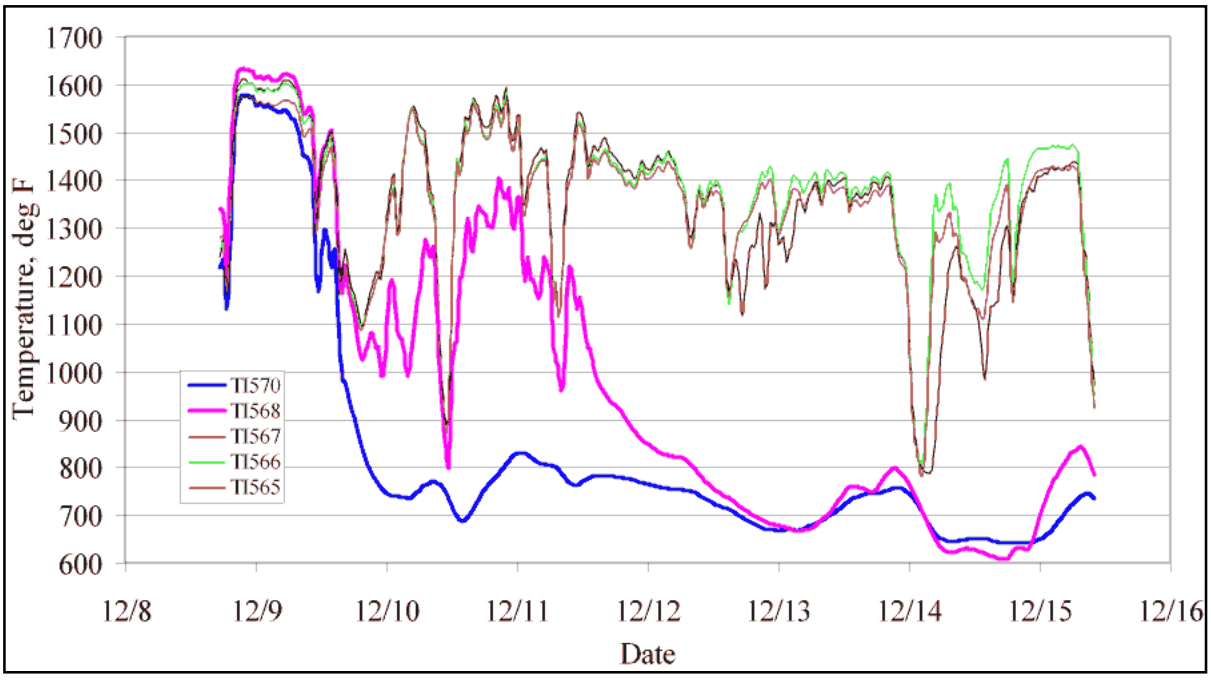

Figure 4.8-2 Bed Temperatures During GCT1 Showing Segregation of the Bed

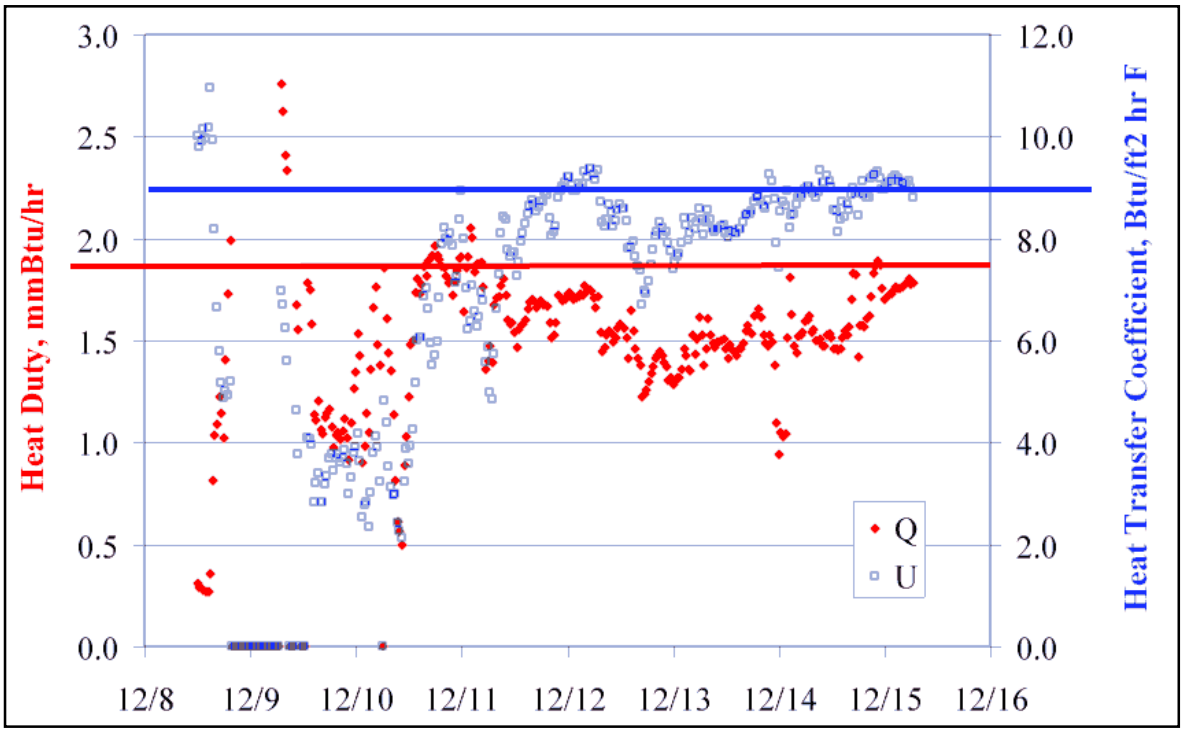

Figure 4.8-3 Heat-Duty and Overall-Heat-Transfer Coefficient of the Sulfator-Heat-Recovery Exchanger are Lower Than Normal

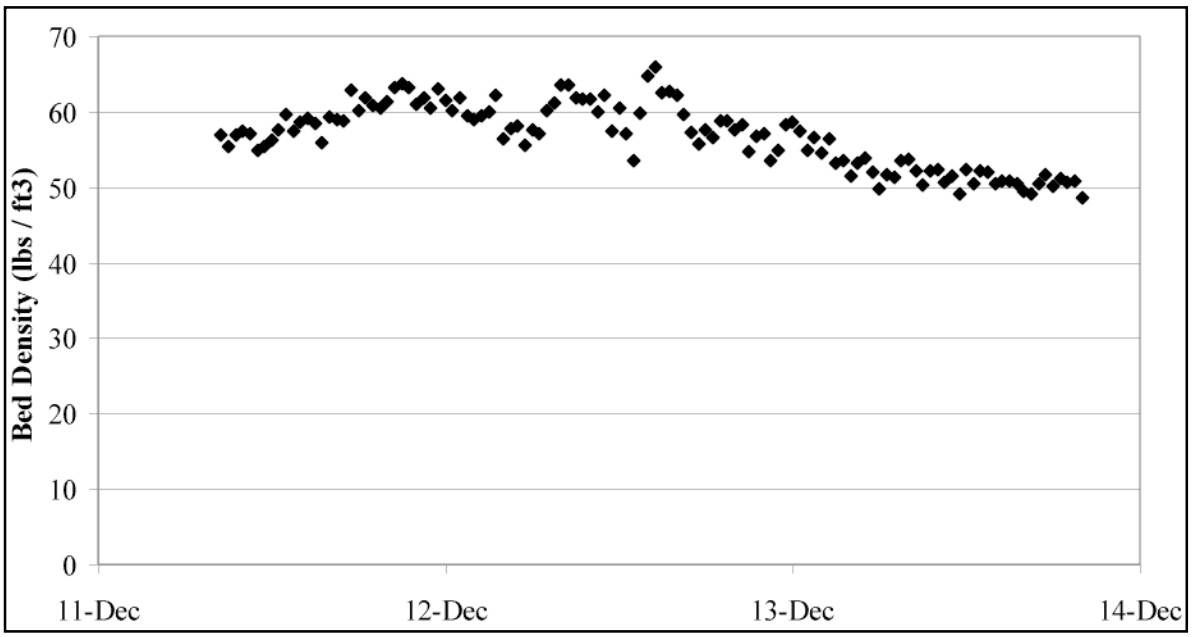

Figure 4.8-4 Density of the Sulfator Bed During GCT1

TERMS

Listing of Abbreviations

AAS	Automated Analytical Solutions
ADEM	Alabama Department of Environmental Management
APC	Alabama Power Company
APFBC	Advance Pressurized Fluidized-Bed Combustion
ASME	American Society of Mechanical Engineers
AW	Application Workstation
BFI	Browning-Ferris Industries
BFW	Boiler Feed Water
BMS	Burner Management System
BOC	BOC Gases
BOP	Balance-of-Plant
BPIR	Ball Pass Inner Race, Frequencies
BPOR	Ball Pass Outer Race, Frequencies
BSF	Ball Spin Frequency
CAD	Computer-Aided Design
CEM	Continuous Emissions Monitor
CFB	Circulating Fluidized Bed
CFR	Code of Federal Regulations
CHE	Combustor Heat Exchanger
COV	Coefficient of Variation (Standard Deviation/Average)
CPC	Combustion Power Compay
CPR	Cardiopulmonary Resuscitation
CTE	Coefficient of Thermal Expansion
DC	Direct Current
DCS	Distributed Control System
DOE	U.S. Department of Energy
E & I	Electrical and Instrumentation
EERC	Energy and Environmental Research Center
EPRI	Electric Power Research Institute
EDX	Energy-Dispersive X-Ray
ESCA	Electron Spectroscopy for Chemical Analysis
FCC	Fluidized Catalytic Cracker
FCP	Flow-Compacted Porosity
FETC	Federal Energy Technology Center
FFG	Flame Front Generator
FI	Flow Indicator
FIC	Flow Indicator Controller
FOAK	First-of-a-Kind
FTF	Fundamental Train Frequency
FW	Foster Wheeler
GBF	Granular Bed Filter
GC	Gas Chromatograph
GEESI	General Electric Environmental Services, Inc.

HP	High Pressure
HRSG	Heat Recovery Steam Generator
HTF	Heat Transfer Fluid
HTHP	High-Temperature, High-Pressure
I/O	Inputs/Outputs
ID	Inside Diameter
IF&P	Industrial Filter & Pump
IGV	Inlet Guide Vanes
IR	Infrared
KBR	Kellogg Brown & Root
LAN	Local Area Network
LIMS	Laboratory Information Management System
LOC	Limiting Oxygen Concentration
LOI	Loss on Ignition
LPG	Liquefied Propane Gas
LSLL	Level Switch, Low Level
MAC	Main Air Compressor
MCC	Motor Control Center
MS	Microsoft Corporation
NDIR	Nondestructive Infrared
NFPA	National Fire Protection Association
NOx	Nitrogen Oxides
NPDES	National Pollutant Discharge Elimination System
NPS	Nominal Pipe Size
OD	Outside Diameter
OSHA	Occupational Safety Health Administration
OSI	OSI Software, Inc.
P&IDs	Piping and Instrumentation Diagrams
PC	Pulverized Coal
PCD	Particulate Control Device
PDI	Pressure Differential Indicator
PDT	Pressure Differential Transmitter
PFBC	Pressurized Fluidized-Bed Combustion
PI	Plant Information
PLC	Programmable Logic Controller
PPE	Personal Protection Equipment
PRB	Powder River Basin
PSD	Particle Size Distribution
PSDF	Power Systems Development Facility
ΔP	Pressure Drop
PT	Pressure Transmitter
RFQ	Request for Quotation
RO	Restriction Orifice
RSSE	Reactor Solid Separation Efficiency
RT	Room Temperature
SCS	Southern Company Services, Inc.
SEM	Scanning Electron Microscopy

SMD	Sauter Mean Diameter
SRI	Southern Research Institute
SUB	Start-up Burner
TCLP	Toxicity Characteristic Leaching Procedure
TR	Transport Reactor
TRDU	Transport Reactor Demonstration Unit
TSS	Total Suspended Solids
UA	Product of heat transfer coefficient, U, and heat exchange area, AU, (Btu/hr ft² °F) x A (ft²) = UA (Btu/hr °F)
UBP	Uncompacted Bulk Porosity
UND	University of North Dakota
UPS	Uninterruptible Power Supply
UV	Ultraviolet
VFD	Variable Frequency Drive
VOCs	Volatile Organic Compounds
WPC	William's Patent Crusher
XRD	X-Ray Diffraction
XXS	Extra, Extra Strong

Listing of Units

acfm	actual cubic feet per minute
Btu	British thermal units
°C	degrees celsius or centigrade
°F	degrees fahrenheit
ft	feet
FPS	feet per second
gpm	gallons per minute
g/cm^3	grams per cubic centimeter
g	grams
GPa	gigapascals
hp	horsepower
hr	hour
in.	inches
inWg	inches, water gauge
°K	degrees kelvin
kg	kilograms
kJ	kilojoules
kPa	kilopascals
ksi	thousand pounds per square inch
m	meters
MB	megabytes
mm	millimeters
MPa	megapascals
msi	million pounds per square inch
MW	megawatts
m/s	meters per second
MBtu	Million British thermal units
m^2/g	square meters per gram
μ or μm	microns or micrometers
dp_{50}	particle size distribution at 50 percentile
ppm	parts per million
ppm (v)	parts per million (volume)
ppm (w)	parts per million (weight)
lb	pounds
pph	pounds per hour
psia	pounds per square inch
psig	pounds per square inch gauge
ΔP	pressure drop
rpm	revolutions per minute
s or sec	seconds
scf	standard cubic feet
scfm	standard cubic feet per minute
V	volts
W	watts